UNIVERSIDADE FEDERAL DE SANTA CATARINA

CENTRO TECNOLÓGICO

PROGRAMA DE PÓS-GRADUAÇÃO EM ENGENHARIA MECÂNICA

DIMITRI OLIVEIRA E SILVA

VARIABLE SPEED DIGITAL ELECTRO-HYDRAULIC ACTUATOR FOR AIRCRAFT APPLICATION

Florianópolis

2023

Dimitri Oliveira e Silva

VARIABLE SPEED DIGITAL ELECTRO-HYDRAULIC ACTUATOR FOR AIRCRAFT APPLICATION

Tese submetida ao Programa de Pós-Graduação em Engenharia Mecânica da Universidade Federal de Santa Catarina para a obtenção do título de Doutor em Engenharia.
Orientador: Prof. Victor Juliano De Negri, Dr.
Coorientador: Prof. Gierri Waltrich, Dr.

Florianópolis

2023

Dimitri Oliveira e Silva

Variable Speed Digital Electro-Hydraulic Actuator for Aircraft Application

O presente trabalho em nível de doutorado foi avaliado e aprovado por banca examinadora composta pelos seguintes membros:

Profa. Emilia Villani, Dra.
Instituto Tecnológico de Aeronáutica

Prof. Jean Vianei Leite, Dr.
Universidade Federal de Santa Catarina

Prof. Antonio Carlos Valdiero, Dr.
Universidade Federal de Santa Catarina

Certificamos que esta é a **versão original e final** do trabalho de conclusão que foi julgado adequado para obtenção do título de doutor em Engenharia Mecânica obtido pelo Programa de Pós-Graduação em Engenharia Mecânica.

_____

Coordenação do Programa de Pós-Graduação

_____

Prof. Victor Juliano De Negri, Dr.
Orientador

_____

Prof. Gierri Waltrich, Dr.
Coorientador

Florianópolis, 2023.

A minha esposa e a minha mãe (*in memoriam*).

AGRADECIMENTOS

"Se eu vi mais longe, foi por estar sobre ombros de gigantes" (Newton, 1675).

RESUMO

O desenvolvimento de equipamentos, produtos e sistemas mais eficientes é um dos principais focos de pesquisa na atualidade. Em muitos casos, o estudo para obter sistemas mais eficientes está relacionado à redução do consumo de combustível e à redução da emissão de poluentes, como ocorre nos meios de transporte utilizados atualmente, sejam eles terrestres, aquáticos ou aéreos. A hidráulica é uma tecnologia extensivamente utilizada em setores industriais, de máquinas pesadas e sistemas de atuação para controle de superfícies de aeronaves. Esta tecnologia destaca-se pela sua elevada densidade de potência, robustez, confiabilidade e dinâmica. Porém, é também conhecida por sua baixa eficiência energética devido, principalmente, ao uso de controle dissipativo e por vazamentos internos de componentes. Uma das formas de melhorar a eficiência energética de um sistema é através da redução do desperdício de energia. Nessa vertente, a hidráulica digital vem sendo estudada ao longo dos últimos anos no intuito de reduzir a utilização do controle dissipativo, amplamente utilizado em sistemas hidráulicos controlados por servo válvulas ou válvulas proporcionais. Esta tese de doutorado propõe uma nova topologia de atuador hidráulico digital denominado de *Variable Speed Digital Electro-Hydraulic Actuator – VSDEHA,* com ênfase na aplicação para superfícies de controle de aeronaves e foi realizada em colaboração com a Universidade de Linköping e a Saab AB. A solução proposta utiliza uma bomba hidráulica digital acoplada a um motor elétrico de velocidade variável para suprir um cilindro simétrico, de acordo com a demanda de vazão. Através do emprego do conceito de hidráulica digital, o controle de posição do cilindro é realizado utilizando válvulas on/off de assento, no intuito de reduzir a dissipação de energia do sistema e evitar o vazamento interno. Um método para o projeto de uma bomba hidráulica digital de velocidade variável é proposto. A aplicação do método gera informações úteis para a seleção de motores elétricos, como torque e velocidade, além da combinação de bombas sugerida para atender cada ponto de operação do atuador. A utilização da rotação variável possibilitou um controle suave e contínuo do cilindro, apresentando boa resposta ao controle de posição. Uma das vantagens dessa topologia é o reduzido número de válvulas, em relação a outras topologias de atuadores hidráulicos digitais. A implementação do sistema hidráulico foi feita utilizando os softwares MatLab/Simulink® e Hopsan. Um modelo de motor elétrico foi utilizado para avaliar o consumo energético da solução. Lógica Fuzzy foi utilizada para criar um identificador de esforços e direção de movimento, utilizado na estratégia de controle do atuador. Experimentos foram realizados em uma bancada construída para prova de conceito. A avaliação energética realizada apresentou uma eficiência de até 58% na conversão da energia hidráulica para saída de energia útil no cilindro. Foram realizadas simulações para comparar o VSDEHA como outros atuadores. Em comparação com um atuador eletro-hidrostático (EHA), foi possível atingir o dobro da eficiência na conversão de energia hidráulica. Em comparação com um atuador servo hidráulico (SHA), em uma simulação de voo, o VSDEHA precisou de cerca de 22 vezes menos energia para a execução do mesmo trabalho. Finalmente, foi concluído que o VSDEHA apresenta um grande potencial para o desenvolvimento de atuadores hidráulicos mais eficientes e com boa controlabilidade, podendo ser aplicado também em outras áreas como indústria e máquinas móveis, com a vantagem de utilizar componentes mais baratos, simples e robustos, reduzindo custo de implementação e manutenção.

Palavras-chave: Hidráulica Digital. Atuador Hidráulico Digital de Velocidade Variável. Bomba Hidráulica Digital. Superfícies de controle de aeronaves.

RESUMO EXPANDIDO

Introdução

A crescente conscientização sobre o meio ambiente e as mudanças climáticas trouxeram novos desafios para a engenharia nas últimas décadas. Um desses desafios está relacionado a mitigação das mudanças climáticas por meio do desenvolvimento de novas tecnologias, mais eficientes e menos prejudiciais ao planeta. Diante das novas regulamentações e acordos internacionais para redução de emissão de poluentes, pesquisas visando atender as novas normas ambientais, para obtenção de produtos mais sustentáveis, passaram a ser incentivadas (QAZI *et al.*, 2019; SCHÄFER *et al.*, 2019; ZAPOROZHETS *et al.*, 2020).

Embora os sistemas de atuação hidráulicos sejam conhecidos por possuírem baixa eficiência energética, devido ao controle dissipativo utilizado, eles ainda são a tecnologia mais empregada no controle de superfícies de aeronaves, devido ao seu alto nível de maturidade, confiabilidade, alta densidade de potência e outras características secundárias, como amortecimento e troca de calor (MARÉ, 2016; MARÉ; FU, 2017; MOIR; SEABRIDGE, 2008). Na indústria aeroespacial, os conceitos de aeronave mais elétrica (*More Electric Aircraft* – MEA) e de transmissão de potência via cabos (*Power-by-Wire*) foram encorajados desde a década de 90, no intuito de gradualmente substituir subsistemas de acionamentos hidráulicos, pneumáticos e mecânicos, por elétricos. Dentre os potenciais benefícios obtidos por essa substituição destacam-se a redução de peso, redução do tempo e do custo de manutenção, além da utilização de sistemas com maior eficiência (CHAKRABORTY *et al.*, 2013b; MARÉ; FU, 2017; NAAYAGI, 2013; ROSERO *et al.*, 2007). Neste contexto, destacam-se os atuadores eletro-hidrostáticos (EHA), aplicados em superfícies de controle secundárias e como *backup* para superfícies de controle primárias em aeronaves mais modernas, e os atuadores eletro-mecânicos (EMA), utilizados em aplicações menos críticas. No entanto, considera-se que tanto o EHA quanto o EMA ainda não possuem a mesma confiabilidade e densidade de potência que os atuadores hidráulicos convencionais (MARÉ, 2017; MARÉ; FU, 2017; QIAO *et al.*, 2018).

Em paralelo, as pesquisas relacionadas à obtenção de sistemas hidráulicos mais eficientes também evoluíram e uma das mais recentes linhas de pesquisa envolve o uso do conceito de hidráulica digital (*Digital Fluid Power*). Linjama (2011), define um sistema hidráulico digital como um sistema que possui componentes discretos capazes de controlar ativamente sua saída, onde a principal característica é o controle inteligente. As pesquisas em hidráulica digital têm apresentado resultados significativos de melhoria de eficiência energética em relação aos sistemas hidráulicos convencionais, onde é possível reduzir a dissipação de

energia entre 20 a 90% aplicando o conceito de hidráulica digital (BELAN, 2018; BELAN *et al.*, 2014; DONKOV *et al.*, 2020; LINJAMA, 2011; LOPES *et al.*, 2022; NOSTRANI, 2020; SCHEIDL *et al.*, 2012; SILVA *et al.*, 2022; ZHANG *et al.*, 2020).

Neste contexto, a presente tese propõe uma nova configuração de um atuador hidráulico, combinando os benefícios do conceito MEA com a hidráulica digital, no intuito de obter um sistema de acionamento descentralizado, utilizando um motor elétrico com controle de velocidade variável e uma bomba hidráulica digital para mover um atuador simétrico. Esta configuração visa substituir o uso de servoválvulas por válvulas direcionais do tipo on/off, no intuito de obter um sistema capaz de apresentar boa eficiência e bom desempenho em diferentes condições de operação.

Objetivos

O principal objetivo desta tese de doutorado é desenvolver uma nova concepção de atuador hidráulico digital, onde uma bomba hidráulica digital é acoplada a um motor elétrico com controle da frequência rotacional, no intuito de obter um atuador hidráulico descentralizado, alimentado por energia elétrica, que apresente boa controlabilidade, movimentação suave e boa eficiência energética, para atender as demandas das superfícies de controle de aeronaves.

Como objetivos específicos tem-se: desenvolvimento da arquitetura do sistema hidráulico proposto; desenvolvimento de um método para o projeto de bombas hidráulicas digitais (*Digital Hydraulic Pump* – DHP); pesquisa e implementação do modelo de um motor elétrico; modelagem e implementação do sistema hidráulico proposto utilizando os *softwares* Hopsan e MatLab/Simulink®; implementação do sistema proposto em bancada de testes experimentais, testes para validação do modelo e comparação com outras soluções.

Como contribuições e justificativa da tese tem-se a proposta da utilização de um atuador hidráulico digital para mitigar o uso de controle dissipativo realizado em sistemas hidráulicos convencionais. O resultado dessa topologia é a obtenção de um sistema hidráulico com consumo reduzido de energia, empregando o conceito de potência sob demanda para melhorar a eficiência energética. Além da eficiência, a controlabilidade do cilindro também é avaliada, no intuito de suavizar a movimentação do cilindro, reduzindo o típico movimento de passo discreto observado em sistemas hidráulicos digitais. Do ponto de vista econômico, o uso da hidráulica digital visa a utilização de componentes mais simples, como as válvulas direcionais on/off, para controlar o sistema. Essa abordagem reduz os custos de implementação e manutenção onde, mesmo que o sistema possua um número maior de válvulas, as válvulas

on/off são cerca de 10 a 40 vezes mais baratas que as servoválvulas proporcionais, comumente empregadas em sistemas hidráulicos de controle de posição.

Metodologia

Inicialmente, foi realizada uma revisão bibliográfica direcionada para sistemas hidráulicos utilizados em superfícies de controle de aeronaves, incluindo soluções utilizando o conceito MEA, onde foram observadas as principais vantagens e desvantagens das principais arquiteturas utilizadas atualmente. Em seguida, foi realizada uma revisão bibliográfica no intuito de verificar os tipos de motores elétricos que são mais adequados para aplicações aeronáuticas. Neste ponto, foi visto que os motores elétricos de imãs permanentes se destacam por apresentarem elevada eficiência. Porém, devido a limitações de custos o motor de indução trifásico foi a alternativa utilizada no presente trabalho. Na sequência, foi realizada revisão bibliográfica sobre hidráulica digital, destacando as principais vantagens apresentadas pela tecnologia, as pesquisas realizadas e os desafios encontrados. Neste contexto, percebeu-se que não há um método bem definido para o dimensionamento de bombas hidráulicas digitais, o qual se tornou uma proposta a ser desenvolvida na tese.

Assim, um método para o dimensionamento de bombas hidráulicas digitais foi proposto a partir da utilização de relações matemáticas e de um algoritmo de otimização, visando auxiliar o projetista na definição da quantidade de unidades de bombas e seus respectivos deslocamentos volumétricos.

Na sequência, o conceito do atuador eletro-hidráulico digital utilizando bomba hidráulica digital com velocidade variável é apresentado. Para a implementação da modelagem matemática do sistema hidráulico proposto, foram utilizados os softwares Hopsan e MatLab/Simulink®. O Hopsan foi usado para implementar o circuito hidráulico do sistema, enquanto o motor elétrico e o controle do atuador foram implementados no MatLab/Simulink®. Além disso, um identificador de carga assistiva utilizando lógica Fuzzy foi desenvolvido para auxiliar no controle do cilindro hidráulico.

O sistema foi implementado em uma bancada de testes onde experimentos foram realizados para parametrizar os componentes do sistema. Dentre eles, ensaios para obter as curvas de vazão das bombas, ensaios para obter os parâmetros utilizados no modelo de atrito de LuGre e ensaios para obter os parâmetros do motor elétrico. Após a parametrização dos componentes da bancada, ensaios foram realizados para validar o modelo do sistema proposto. O método de dimensionamento de bombas hidráulicas digitais foi aplicado para obter o mapa

de seleção de unidades de bombas da bomba digital utilizada. O mesmo, foi utilizado na criação da estratégia de controle do atuador, assim como o mapa de velocidade angular da bomba, de onde é obtido o comando de rotação para o motor elétrico, de acordo com a demanda de vazão do sistema e da combinação de bombas utilizada.

Resultados e discussões

O atuador eletro-hidráulico digital com bomba digital de velocidade variável (*Variable Speed Digital Electro-Hydraulic Actuator* – VSDEHA) apresentou boa capacidade de seguir as referências de posição utilizadas, dentro do tempo de acomodação desejado. Através do controle de rotação do motor elétrico, foi possível reduzir o efeito de movimentação discreta do cilindro, obtendo movimentos contínuos. A utilização do identificador de carga assistiva desenvolvido melhorou a controlabilidade do cilindro e reduziu o consumo de energia em 3% em relação ao mesmo sistema operando sem o identificador.

Os resultados de simulação apresentaram boa representatividade em relação aos resultados experimentais, obtendo praticamente os mesmos comportamentos. Devido a não linearidades presentes no sistema real, que não são completamente representadas pelo modelo, os valores de pressões nas câmaras do cilindro e nas bombas apresentaram pequenas diferenças. O modelo do motor elétrico foi utilizado para estimar o consumo de energia do atuador. Para o mesmo ciclo de avaliação o modelo do motor elétrico apresentou um consumo 8% maior que o obtido no experimento.

Um modelo do VSDEHA foi configurado para ser comparado com o um modelo de EHA, sendo empregadas diferentes entradas em degrau para avaliar o controle de posição, tempo de resposta e energia consumida. Dentre os resultados, notou-se que, em condições de espera sobre efeito de carregamento externo, o VSDEHA tem a vantagem de bloquear as câmaras do cilindro utilizando as válvulas on/off, enquanto o EHA precisa manter uma determinada rotação para equilibrar o carregamento externo e os vazamentos internos dos componentes, aumentando o consumo energético. Os tempos de assentamento para ambos atuadores foram similares.

Finalmente, são apresentadas considerações para aplicação em aeronaves, onde considera-se que o atuador atinge o nível de prontidão tecnológica 3 (*Technology Readiness Level* – TRL 3), sendo um protótipo construído para prova de conceito que apresenta um bom potencial para desenvolvimento. No entanto, dado ao nível tecnológico dos componentes utilizados, ainda não é possível fazer uma estima de peso e volume. No intuito de aplicar o atuador em um ambiente de aeronave, simulações foram realizadas utilizando o modelo de

aeronave denominado ADMIRE (*Aero-Data Model in a Research Environment*), para comparar o desempenho do VSDEHA e de outras arquiteturas de atuadores digitais desenvolvidas no LASHIP, como o atuador hidráulico digital (Digital Hydraulic Actuator – DHA), o atuador eletro hidrostático digital (Digital Electro Hydrostatic Actuator – DEHA) e um modelo de atuador servo hidráulico (SHA), utilizado como benchmark para avaliação energética dos atuadores. Na comparação, todos os atuadores digitais foram capazes de cumprir o objetivo da manobra executada pela aeronave. As principais diferenças foram percebidas no desempenho dinâmico, onde os atuadores apresentaram diferentes sobre passagens e tempos de acomodação. No quesito energia, os atuadores digitais apresentaram uma superioridade em relação ao SHA, enquanto que, na média geral, o VSDEHA apresentou a melhor eficiência energética dentre os atuadores digitais, apresentando um consumo de energia 22 vezes menor que o SHA. Destaca-se que a influência do comportamento dinâmico do atuador na aeronave deve ser estudada mais a fundo para verificar o impacto nas características de qualidade de voo e manobrabilidade da aeronave. Estudos abordando análise de modo de falha, confiabilidade e redundância do sistema proposto também deverão ser realizados.

Considerações finais

A presente tese teve como objetivo principal desenvolver uma proposta de atuador hidráulico digital visando aplicações aeronáuticas, combinado com os conceitos de aeronave mais elétrica e de transmissão de potência via cabos elétricos, para a obtenção de um atuador hidráulico descentralizado e eficiente.

O resultado da tese foi a proposta do VSDEHA, que combinou características do EHA, como o controle de rotação variável, com a hidráulica digital, para controle de direção do movimento do atuador com reduzida dissipação de energia. Nessa configuração, a velocidade do cilindro passou a ser definida pela combinação de unidade de bombas utilizadas, juntamente com a rotação do motor elétrico, o que permite o controle fino da vazão, no intuito de utilizar a combinação de bombas e a rotação mais eficiente para atender o sistema.

Em comparação com outras soluções de atuadores hidráulicos digitais, o VSDEHA não necessita que haja combinações de áreas de câmaras especificas do atuador com a DHP para alterar a velocidade do cilindro. Portanto, não é necessário utilizar um cilindro multicâmaras, o que resulta na redução do número de válvulas necessárias para implementar o sistema.

Dessa forma, observa-se que o atuador proposto apresenta elevado potencial para utilização em sistemas hidráulicos de controle de posição, voltados não somente para indústria aeronáutica, mas também, para outras aplicações como máquinas pesadas e equipamentos industriais. A baixa complexidade dos componentes necessários para construção do atuador faz com que ele apresente um baixo custo relativo, se comparado a sistemas servo-hidráulicos.

Ressalta-se que o atuador apresentado está em estágio inicial de desenvolvimento, o modelo validado e os resultados da bancada de testes podem ser considerados como nível de prontidão tecnológica 3 (*Technology Readiness Level* 3), onde a prova de conceito foi realizada. Estudos avaliando a solução sob outras perspectivas são necessários antes de propor um produto final para aplicações aeronáuticas, visto o alto nível de segurança e confiabilidade exigido nesta área. Além disso, melhorias tecnológicas nos componentes são necessárias para atingir todo o potencial da solução.

Palavras-chave: Hidráulica digital, Atuador hidráulico digital com velocidade variável, Bomba hidráulica digital com velocidade variável, Bomba hidráulica digital.

ABSTRACT

The development of more efficient equipment, products, and systems is one of the main focuses of research today. In most cases, the study to obtain more efficient systems is related to reducing fuel consumption and reducing the emission of pollutants, as it occurs in the currently used means of transport, whether land, water, or air. Fluid power is a technology extensively used in industrial sectors, heavy machinery, and actuation systems for controlling aircraft surfaces. This technology stands out for its high power density, robustness, reliability, and dynamics. However, it is also known for its relative low energy efficiency, mainly due to the use of dissipative control and internal leakage in components. One of the ways to improve the energy efficiency of a system is to reduce energy waste. In this sense, digital hydraulics has been studied in recent years in order to reduce the use of dissipative control, widely used in hydraulic systems controlled by servo valves or proportional valves. This doctoral thesis proposes a new digital hydraulic actuator topology called Variable Speed Digital Electro-Hydraulic Actuator – VSDEHA, with emphasis on application to aircraft control surfaces and was carried out in collaboration with the Linköping University and Saab AB. The proposed solution uses a digital hydraulic pump coupled to a variable-speed electric motor to supply a symmetrical cylinder, according to the flow demand. Through the use of the concept of digital hydraulics, the cylinder position control is carried out using the seat on/off valves, in order to avoid throttling control and internal leakage. A method for designing a variable-speed digital hydraulic pump is proposed. The application of the method generates useful information for the selection of electric motors, such as torque and speed, in addition to the suggested combination of pumping units to meet each actuator operating point. The use of the variable rotational frequency enables a smoother and more continuous control of the cylinder, presenting a good response to the position control. One of the advantages of this topology is the reduced number of valves, compared to other topologies of digital hydraulic actuators. The hydraulic system was implemented using MatLab/Simulink® and Hopsan software. An electric motor model was used to evaluate the energy consumption of the solution. Fuzzy logic was used to create an identifier of efforts and movement direction, used in the actuator control strategy. Experimental tests were performed on a test bench built for proof of concept. The energy evaluation carried out showed an efficiency of up to 58% in the conversion of hydraulic energy to useful energy output in the cylinder. Simulations were performed to compare the VSDEHA with other actuators. Compared to an electro hydrostatic actuator (EHA), it was possible to achieve twice the efficiency in converting hydraulic energy. Compared to a servo hydraulic actuator (SHA) in a flight simulation, the VSDEHA needed about 22 times less energy to perform the same work. Finally, it was concluded that VSDEHA has great potential for the development of more efficient hydraulic actuators with good controllability, and can also be applied in other areas such as industry and mobile machinery, with the advantage of using cheaper, simpler, and more robust components, reducing implementation and maintenance costs.

Keywords: Digital Hydraulics. Variable Speed Digital Hydraulic Actuator. Digital Hydraulic Pump. Aircraft Control Surfaces.

LIST OF FIGURES

LIST OF TABLES

LIST OF ABBREVIATIONS

ABNT	Associação Brasileira de Normas Técnicas
ADMIRE	Aero Data Model in a Research Environment
DEHA	Digital Electro Hydrostatic Actuator
DFCU	Digital Fluid Control Unit
DFP	Digital Fluid Power
DHA	Digital Hydraulic Actuator
DHP	Digital Hydraulic Pump
DHPMS	Digital Hydraulic Power Management System
D-IMV	Digital Independent Metering Valve
EHA	Electro Hydrostatic Actuator
EAHA	Electro Assisted Hydrostatic Actuator
EBHA	Electrical Backup Hydrostatic Actuator
EBMA	Electro Backup Mechanical Actuator
EMA	Electro Mechanical Actuator
FLUMES	Fluid and Mechatronic Systems
FPVM	Fixed Pump Variable Motor
GRUCAD	Grupo de Concepção e Análise de Dispositivos Eletromagnéticos
HPU	Hydraulic Power Unit
IGBT	Insulated Gate Bipolar Transistors
IM	Induction Motor
LABMAQ	Laboratório de Maquinas Elétricas
LASHIP	Laboratório de Sistemas Hidráulicos e Pneumáticos
MEA	More Electric Aircraft
PbW	Power-by-Wire
PMSM	Permanent Magnet Synchronous Motor
PWM	Pulse Width Modulation
SHA	Servo Hydraulic Actuator
SRM	Switched Reluctance Motor
SyncRel	Synchronous Reluctance Motor
TRL	Technology Readiness Level
VPFM	Variable Pump Fixed Motor
VPVM	Variable Pump Variable Motor

VSDEHA   Variable Speed Digital Electro-Hydraulic Actuator

LIST OF SYMBOLS
GREEK ALPHABET

α	Empiric friction parameter	[1]
β_e	Equivalent Buck modulus	[Pa]
ξ	Damping factor	[1]
λ_{ds}	Stator magnetic flux d axis	[Wb]
λ_{qs}	Stator magnetic flux q axis	[Wb]
λ_{0s}	Stator magnetic flux 0 axis	[Wb]
λ_{dr}	Rotor magnetic flux d axis	[Wb]
λ_{qr}	Rotor magnetic flux q axis	[Wb]
λ_{0r}	Rotor magnetic flux 0 axis	[Wb]
ρ	Specific mass	[kg/m^3]
σ_0	Bristle stiffness coefficient	[N/m^2]
σ_1	Bristle damping coefficient	[Ns/m]
σ_2	Viscous coefficient	[Ns/m]
η_g	Global efficiency	[1]
η_m	Mechanical efficiency	[1]
η_v	Volumetric efficiency	[1]
η_v^*	Estimated volumetric efficiency	[1]
η	Energy efficiency	[1]
ω	Angular velocity	[rad/s]
ω_b	Base electrical angular velocity	[rad/s]
ω_{puc}	Angular velocity of pump unit combination	[rad/s]
ω_{cmd}	Angular velocity command	[rad/s]
ω_{c_max}	Maximum angular velocity calculated	[rad/s]
ω_{c_min}	Minimum angular velocity calculated	[rad/s]
ω_{max}	Maximum angular velocity	[rad/s]
ω_{min}	Minimum angular velocity	[rad/s]
ω_n	Natural frequency	[rad/s]
ω_r	Rotor angular velocity	[rad/s]

LATIN ALPHABET

a_{max}	Maximum cylinder acceleration	[m/s²]
A	Cylinder area	[m²]
A_A	Area of the chamber A	[m²]
A_B	Area of the chamber B	[m²]
A_C	Area of the chamber C	[m²]
A_D	Area of the chamber D	[m²]
A_v	Area of passage of the hydraulic fluid	[m²]
B	Viscous friction coefficient	[kg/s]
c_d	Discharge coefficient	[1]
dT_{min}	Minimum time interval for a valve combination change	[s]
dT_s	Sample time interval	[s]
d	Closing element diameter	[m]
D	Volumetric displacement of the pump	[m³/rad]
D_1	Volumetric displacement of the pump 1	[m³/rad]
D_2	Volumetric displacement of the pump 2	[m³/rad]
D_3	Volumetric displacement of the pump 3	[m³/rad]
D_{max}	Maximum volumetric displacement	[m³/rad]
e	Error signal	[m/s]
E_{s_DEHA}	Supplied energy for the DEHA	[J]
E_{s_SHA}	Supplied energy for the SHA	[J]
E_{s_DHA}	Supplied energy for the EHA	[J]
E_{o_DEHA}	Output energy for the DEHA	[J]
E_{o_SHA}	Output energy for the SHA	[J]
E_{o_EHA}	Output energy for the EHA	[J]
$E_{supplied}$	Supplied energy	[J]
$E_{dissipated}$	Dissipated energy	[J]
E_{output}	Output energy	[J]
f	Closing element diameter fraction coefficient	[1]
F_C	Coulomb friction	[N]
F_S	Static friction	[N]

F_{fric}	Friction force	[N]
F_L	Load force	[N]
f_{obj}	Objective function	[1]
F_u	Useful force	[N]
i_{ds}	Direct axis stator current	[A]
i_{qs}	Quadrature axis stator current	[A]
i_{0s}	Zero axis stator current	[A]
i'_{dr}	Direct axis rotor current referred to stator current	[A]
i'_{qr}	Quadrature axis rotor current referred to stator current	[A]
i'_{or}	Zero axis rotor current referred to stator current	[A]
K	Load stiffness	[N/ms]
k_{vin}	Internal leakage coefficient	[m^3/(sPa$^{0.5}$)]
l	Actuator length	[m]
L_{ls}	Self inductance	[H]
L_M	Mutual inductance	[H]
M_t	Total mass	[kg]
n_d	Number of digital hydraulic pumps	[1]
$n_{u(i)}$	Number of pump units in a digital hydraulic pump	[1]
q_V	Flow rate	[m^3/s]
q_{Ve}	Effective flow rate	[m^3/s]
q_{Vleak}	Leakage flow rate	[m^3/s]
q_{Vt}	Theoretical flow rate	[m^3/s]
q_{V_max}	Maximum flow rate	[m^3/s]
q_{V_min}	Minimum flow rate	[m^3/s]
q_{Vc_max}	Calculated maximum flow rate	[m^3/s]
q_{Vc_min}	Calculated minimum flow rate	[m^3/s]
q_{V_puc}	Flow rate of pump unit combination	[m^3/s]
q_{Vloss}	Pump internal leakage	[m^3/s]
q_{vreal}	Real pump flow rate	[m^3/s]
p	Pressure	[Pa]
p_A	Pressure in the chamber A	[Pa]
p_B	Pressure in the chamber B	[Pa]

p_C	Pressure in the chamber C	[Pa]
p_D	Pressure in the chamber D	[Pa]
p_l	Load pressure	[Pa]
p_{max}	Maximum system pressure	[Pa]
p_{sys}	System pressure	[Pa]
p_T	Reservoir pressure	[Pa]
puc	Pump unit combination	[1]
r_r	Rotor resistance	[Ohm]
r_s	Stator resistance	[Ohm]
T	Torque	[Nm]
T_e	Effective torque	[Nm]
T_t	Theoretical torque	[Nm]
T_{puc}	Torque of pump unit combination	[Nm]
t_{ds}	Time delay	[s]
tol	Tolerance	[1]
t_s	Settling time	[s]
t_{SCD}	Spool closing delay time	[s]
t_{SCR}	Spool close response time	[s]
t_{SOD}	Spool opening delay time	[s]
t_{SOR}	Spool opening response time	[s]
U_{DHP}	Digital hydraulic pump valve command signal	[1]
U_{LCU}	Limitation and control unit valve command signal	[1]
U_{puc}	Selected pump unit combination	[1]
u_n	Input signal	[1]
v	Velocity	[m/s]
v_{max}	Maximum cylinder velocity	[m/s]
v_S	Stribeck velocity	[m/s]
V	Volume	[m³]
V_{ds}	Voltage on stator winding d axis	[V]
V_{qs}	Voltage on stator windings q axis	[V]
V_{0s}	Voltage on stator windings 0 axis	[V]

V'_{dr}	Rotor voltage related to stator d axis	[V]
V'_{qr}	Rotor voltage related to stator q axis	[V]
V'_{0r}	Rotor voltage related to stator 0 axis	[V]
X_M	Mutual inductive reactance	[Ohm]
X_{lr}	Referred rotor reactance	[Ohm]
X_{ls}	Stator reactance	[Ohm]
x_{A1}	Cylinder position signal	[m]
x_{max}	Cylinder steady-state displacement	[m]
x_{ref}	Reference signal	[m]
x_{vmax}	Maximum opening of the on/off valves spoon	[m]
Z	Deflection of rugosity	[m]

1 INTRODUCTION

Growing awareness about the environment and climate change has brought many challenges to engineering in recent decades. One of these challenges concerns the mitigation of climate change through the development of new technologies that are more efficient and less harmful to the planet (ZAPOROZHETS *et al.*, 2020).

Faced with this new global trend, research in several areas began to be carried out in order to meet the new standards of development and sustainable production. As an example, the use of recycled materials, aiming to reuse all or part of the discarded material, and the development of biodegradable materials, to reduce decomposition time and environmental contamination (WRÓBLEWSKA-KREPSZTUL *et al.*, 2018; ZHANG *et al.*, 2019; ZUO *et al.*, 2019).

The emission of greenhouse gases is one of the main points when it comes to climate change. This has driven the use of clean sources of energy to replace conventional ones, aiming to reduce fuel consumption and the emission of pollutants into the atmosphere (CANALS CASALS *et al.*, 2016; QAZI *et al.*, 2019; SCHÄFER *et al.*, 2019). The emission reduction trend is clearly observed in the automobile industry, where it is possible to distinguish 3 evolutionary stages.

The first is the replacement of large displacement engines with smaller and supercharged engines, which is also known as downsizing. The second is the use of hybrid cars where part of the energy is provided by an electric motor. And the third is the use of all- electric vehicles. Reducing fuel consumption, improving energy efficiency, reducing polluting emissions, reducing moving mechanical components, and, in some cases, completely eliminating some adjacent subsystems, such as lubrication and cooling, are mentioned as some of the results and benefits of this electrification trend (GRANOVSKII *et al.*, 2006; KARAGÖZ *et al.*, 2020; LEE *et al.*, 2016; NANAKI; KORONEOS, 2013).

In aircraft, the More Electric Aircraft – MEA and Power-by-Wire – PbW concepts have been encouraged since the 90s to gradually replace the hydraulic, pneumatic, and mechanical subsystems with electric ones (ROSERO *et al.*, 2007). Among the potential benefits that can be provided by this technological replacement, weight reduction, reduction of time and maintenance costs, and greater efficiency stand out (CHAKRABORTY *et al.*, 2013a; MARÉ; FU, 2017; NAAYAGI, 2013).

Although hydraulic actuation systems are known to have low energy efficiency, they are still the most widely used technology applied to aircraft control surfaces due to their high level of maturity, reliability, high power density, and other secondary features, such as damping and heat exchange (MARÉ, 2017; MOIR; SEABRIDGE, 2008).

Research is being carried out using the MEA concept to obtain new actuation systems to totally or partially replace the functions of servo-hydraulic actuators. In this context, the Electro-Hydrostatic Actuators (EHA) stand out, which are currently applied on secondary control surfaces in modern aircrafts, and the Electromechanical Actuators (EMA), which are applied to less critical applications (MARÉ; FU, 2017). However, such actuators still do not have the same reliability and power density as conventional hydraulic actuators (MARÉ, 2017; QIAO *et al.*, 2018).

According to Maré and Fu (2017), it is important to emphasize that concept of PbW/MEA actuators still needs to be improved in terms of cost, arrangement, mass, reliability, and lifecycle, with regard to the technologies of power electronics, electric motors, and mechanical transmission. Despite the state of maturity of these technologies, alternative solutions must be sought that combine the best of hydraulics and electrics.

Research related to obtaining more efficient hydraulic systems has also evolved and one of the most recent lines of research involves the use of the Digital Fluid Power concept. Linjama (2011) defines a digital hydraulic system as a system that has discrete components able to actively control its output, where the main feature of a digital system is intelligent control. The concept of Digital Hydraulics or Digital Fluid Power – DFP is relatively new, its characteristics, benefits, and challenges are under study and are not fully known (LINJAMA, 2011). Research in digital hydraulics has shown significant results of energy improvement in relation to conventional hydraulic systems, whereby using digital hydraulics it was possible to reduce energy dissipation between 20 to 90% (BELAN, 2018; BELAN *et al.*, 2014; LINJAMA, 2011; SCHEIDL *et al.*, 2012; ZHANG *et al.*, 2020).

Therefore, it is clear that current research indicates that the main challenges related to hydraulic systems to actuate the control surfaces of aircraft are moving towards reducing the use of systems controlled by servo valves and decentralization of hydraulic systems. This trend aims to reduce aircraft hydraulic piping, reducing weight, the risk of leaks, and time and maintenance costs (ALLE *et al.*, 2016; GARCIA *et al.*, 2008; MARÉ, 2017; MARÉ; FU, 2017; VAN DEN BOSSCHE, 2006).

Looking at the currently available technologies, it is possible to infer that in electro-hydrostatic systems, the challenges are related to how to improve efficiency under low load conditions; how to increase the power density and hydraulic stiffness, and how to avoid inversion of the high rotational frequency of the electric motor (ALLE *et al.*, 2016; MARÉ; FU, 2017; VAN DEN BOSSCHE, 2006). In electromechanical systems, the main risks are linked to jamming, mechanical resistance to overloads, and redundancy (GARCIA *et al.*, 2008; JIAN *et al.*, 2017; MARÉ; FU, 2017). In digital hydraulics, the main limiting factors are related to the development of valves with shorter response time and high flow rate capacity, reduction of pressure peaks due to switching, and how obtaining a system with smoother behavior (BELAN, 2018; MANTOVANI *et al.*, 2018)

In this context, the present thesis proposes a new configuration of a hydraulic actuator, combining the benefits of the MEA concept with Digital Hydraulics, in order to obtain a decentralized actuation system, using an electric motor with speed control and a digital hydraulic pump to move a symmetric actuator. This design aims to replace the use of servo valves with on/off valves, reduce the weight of the system and make it more flexible to new arrangements, obtaining a system able to present good efficiency and performance in different operating conditions.

1.1 OBJECTIVES

The main objective of this thesis is to propose a digital hydraulic actuator, composed of a digital hydraulic pump coupled to an electric motor to control the rotational frequency resulting in a power-on-demand system, aiming to improve the cylinder controllability, smooth operation, and better energy efficiency, meeting the demands of aircraft control surfaces.

In order to achieve the main objective, the following specific objectives were defined:

- Develop an actuator topology using a digital hydraulic pump with variable speed, focusing on controllability and energy efficiency;
- Develop a method to design a digital hydraulic pump using variable speed and its control strategy to optimize efficiency;
- Develop detailed modelling of system components, including electric motor;
- Implement the proposed digital hydraulic system model using Hopsan and MatLab/Simulink® to perform simulations;

- Design and install the necessary test bench modifications to implement the proposed digital hydraulic system;
- Perform experimental tests and analysis of the components and system;
- Compare the topology with other solutions.

1.2 JUSTIFICATIVE AND CONTRIBUTION

This thesis proposes the use of a digital hydraulic actuator to avoid the energy dissipation of the throttle control of conventional hydraulic systems. The result of this topology is to obtain a hydraulic system with reduced energy consumption, aiming at the concept of power on demand to improve the energy efficiency. In addition to efficiency, cylinder controllability is also evaluated to make cylinder movement smoother, reducing the typical stepping movement seen in digital hydraulic systems.

From an economical point of view, the use of digital hydraulics also aims into use simpler components such as directional on/off valves to control the system. This approach also reduces the implementation and maintenance costs where, even if the system has more valves, on/off valves are about 10 to 40 times cheaper than proportional valves or servo valves.

This work contributes to the dissemination and application of knowledge in digital hydraulics. A method, from the literature, for designing a cylinder for positioning control is applied to obtain the cylinder area and flow rate required to meet the system requirements. In addition, a method to design a digital hydraulic pump, using standard manufacturer pumps, is proposed. Together, the two methods can be used as a guide for other researchers to design a digital hydraulic actuator.

Furthermore, in Brazil, the use of digital hydraulics is quite new, with the Laboratory of Hydraulic and Pneumatic Systems (LASHIP) being a pioneer in the application of this technology. Based on this, the experimental results and models presented in the thesis contribute to increasing the available database for future research in digital hydraulics.

1.3 THESIS STRUCTURE

The thesis is divided into 8 chapters as follows. Chapter 2 presents a review of aircraft control surfaces, the main types of actuators applied in aircraft, and a review of electric motors suitable for aircraft applications. In Chapter 3, a review of digital hydraulics is presented, highlighting its main characteristics and studies carried out in Brazil. Chapter 4 presents a method for sizing a digital hydraulic pump with variable speed, where an algorithm is used to

configure different digital hydraulic pumps and, subsequently, evaluate the pumps to select the most efficient configuration. Chapter 5 presents the Variable Speed Digital Hydraulic Actuator, where to dimension the actuator the method proposed in Chapter 4 is used combined with a method to dimension a cylinder for positioning systems. Models of hydraulic components are presented, including the model of a three-phase induction motor used in the study. The chapter also presents the implementation of the hydraulic system in simulation software and the control of the system. Chapter 6 presents the test bench used to carry out the experiments for the proof of concept of the proposed actuator. The main components are presented by function. This chapter presents the list of components and parameters used in the simulation and test bench. Chapter 7 presents the simulation and experimental results. Chapter 8 presents the conclusions of the work and proposals for future works.

2 AIRCRAFT FLIGHT CONTROL AND ACTUATION SYSTEMS

One of the most well-known stories in the world is the myth of Icarus and Daedalus, who built wings to fly away from the island of Crete. Perhaps this is one of the oldest representations of the human desire to fly. Time passed, the first aircraft was built and the desire to fly was fulfilled. New challenges arise, such as increasing aircraft size to carry more cargo, achieving supersonic speeds, improving control systems, and improving aircraft efficiency. From an engineer's point of view, the myth of Icarus and Daedalus shows that solutions are not complete, there is always room for improvement. However, like Daedalus, we also have limited resources and technology for our time.

2.1 AIRCRAFT CONTROL SURFACES

On the begin of flight history, the flight control of the earliest aircraft was performed through the use of wires attached to the control surfaces in order to warp the wings. This rudimentary control technique was replaced by the use of articulated flight control surfaces controlled by the use of pulleys and wires, which was used for many years (MOIR; SEABRIDGE, 2008).

Currently, the flight control system can be mechanical or electrical and includes all the components necessary to transmit control command input to drive actuators in order to generate force and/or torque to move the aircraft control surfaces. In addition, flight control needs to realize some other control features such as the control of aircraft flight path, altitude, airspeed, aerodynamic configuration, ride, and structural modes, making it a complex and extremely important system for the aircraft (WANG *et al.*, 2016).

According to Moir & Seabridge (2008), aircraft motion is governed by the basic principle of flight control, which is defined in relation to a translational and rotational motion around a fixed set of axes. Rotational motion is related to the motion of the aircraft around three defined axes called pitch, roll, and yaw (Figure 2.1).

Control surfaces are used to control the aircraft maneuvers and, together with the flight control systems, allow the pilot to exercise control of the aircraft during the flight (MOIR; SEABRIDGE, 2008). Aircraft control surfaces can be classified according to their priority level as primary and secondary control surfaces. The purpose of the primary control surfaces is to control the aircraft trajectory while secondary control surfaces are concerned with modifying the aerodynamic configuration of the aircraft during specific phases of flight (MARÉ, 2016).

Figure 2.1 presents a generic commercial aircraft with its primary and secondary control surfaces highlighted. Primary control surfaces are structures capable of controlling the aircraft around the fixed set of axes described before. In this case, the ailerons, elevators, and rudder are responsible for controlling the aircraft around the roll, pitch, and yaw axes, respectively (MOIR; SEABRIDGE, 2008).

Flaps, slats, and spoilers, are examples of secondary flight control surfaces. In this case (Figure 2.1), flaps and slats are normally used during takeoff and landing to increase the lift effect, by increasing the aircraft wing area and camber (MOIR; SEABRIDGE, 2008).

Figure 2.1 – Flight control axes and surfaces of a generic commercial aircraft.
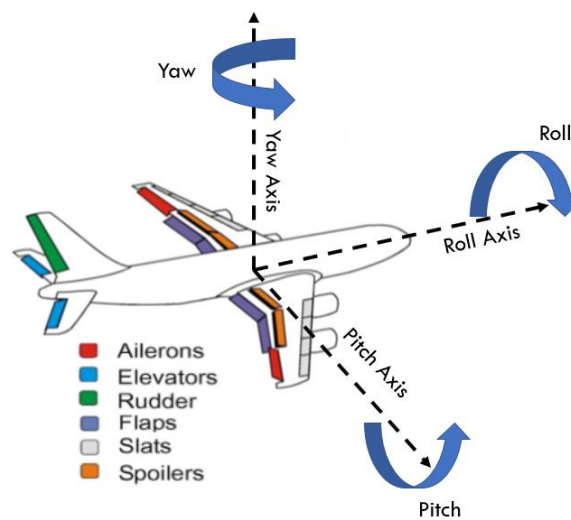
Source: Adapted from Cao *et al.*, 2012.

Control surfaces and their requirements can vary significantly between different aircraft types, sizes, maneuverability and applicability. The actuation system needed to move the control surfaces is developed to meet requirements such as controllability, power, dynamics, environment, service life, reliability and integration with the aircraft structure, which is related to the architecture, size and volume occupied by the solution (MARÉ, 2016). Table 2.1 present examples of typical power and dynamics needs for different types of aircraft.

This work is concerned with developing the topology of the solution and its proof of concept, while the integration with the aircraft structure is not evaluated since the components used are not at the high level of development to be applied in aircraft, which means that they are probably heavier and larger than the final solution.

Table 2.1 – Example of power and dynamics requirements for aircraft actuators.

Actuation function		Typical range	Aileron Airbus A320	Nose landing gear steering Airbus A320	Tiltrotor Boeing V22 Osprey Mode conversion	Thrust vector control Ariane V
Stroke	(mm)	20 – 700	44		1143	± 160
	(degree)			± 75		
Speed	(mm/s)	20 – 500	90 no-load		97	972 no-load
	(degree/s)	20 – 90		20		
Force	(kN)	20 – 350	44		80	347
	(Nm)			7000		
Bandwidth	(Hz)	1 – 20	≈ 1	≈ 1.5	3.2	7.9

Source: Maré (2016).

2.2 AIRCRAFT ACTUATOR SOLUTIONS

This section presents an overview of the technological solutions currently applied to aircraft, starting with the servo hydraulic actuator, which is the most mature solution, and therefore, considered as the conventional solution.

2.2.1 Servo Hydraulic Actuators (SHA)

Modern aircraft flight control actuator systems are predominantly dominated by hydraulic technology, a fact that has been shaped throughout aviation history, where the increase in flight speed made the load on the control surfaces higher, resulting in difficulty physically flying the aircraft. In order to overcome this difficulty, in 1950 the first servo-controlled hydraulic system applied to aircraft was built, which boosted the development and use of this technology in aircraft control surfaces (MARÉ, 2016).

Through the technological development of SHA, they have gained sufficient maturity, reliability, and security to serve aeronautical applications for decades. Among the advantages of using an SHA, the high power density, robustness, reliability, and high dynamic response stand out as the main advantages. In addition, SHA has secondary characteristics such as the ability to exchange heat through the hydraulic fluid, perform high forces at low speeds, withstand overloads without damage, and damping capability (MARÉ, 2016; MOIR; SEABRIDGE, 2008).

Figure 2.2 presents a simplified SHA, where a position reference signal is used to command the cylinder movement by servo valve control. The difference between the current cylinder position and the reference generates an error signal used to control the servo valve movement. The servo valve controls the flow direction to the cylinder chambers to move the cylinder to the reference position. A centralized power unit is used to supply the servo valve and cylinder. In this configuration, the hydraulic pump is normally driven by mechanical energy extracted from the main engines of the aircraft, through accessories such as a gearbox, and works by constantly pumping fluid to maintain the system pressure and to supply internal leaks of components (MARÉ, 2016; ROSERO *et al.*, 2007).

Figure 2.2 – A generic Servo Hydraulic Actuator.
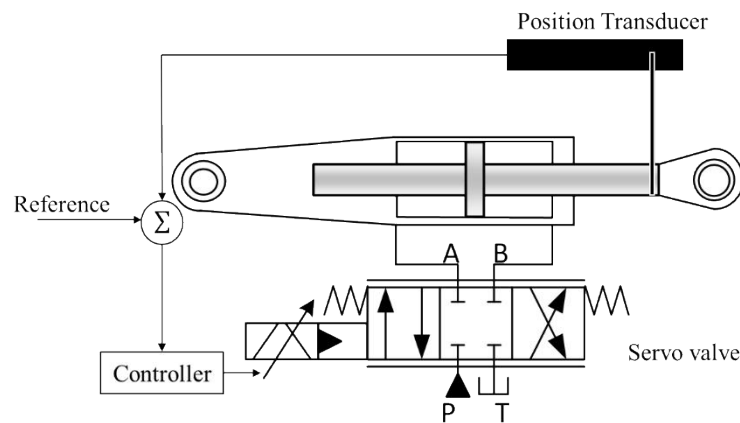
Source: Adapted from Wang *et al.* (2016).

In most cases, a centralized power unit implies that the SHA has a heavy and inflexible pipeline network used to transport the hydraulic fluid over long distances in the aircraft, which makes energy management difficult at the power distribution network level, increasing the risk of leakage and impacting system vulnerability (ROSERO *et al.*, 2007; WANG *et al.*, 2016). Another disadvantage of SHA systems is related to their relatively low energy efficiency due to the energy dissipation process imposed by throttling control and permanent internal leakage of the power management components in the limitation and control unit (DE NEGRI *et al.*, 2014; MARÉ & FU, 2017).

In parallel, with the development of the electronic systems, new concepts have emerged aimed to improve the energy efficiency, safety, and to reducing weight, such as the Power-by-Wire (PbW) and More Electric Aircraft (MEA) concepts (MARÉ; FU, 2017; RONGJIE *et al.*, 2009; ROSERO *et al.*, 2007). Using electrical power supplied by wires (PbW), the concepts aim to replace centralized hydraulic power units with localized units to avoid

transporting fluid over long distances inside the aircraft. Therefore, the MEA and PbW aircraft concepts aim to replace the SHA systems with systems such as the Electro-Hydrostatic Actuator (EHA) and Electro-Mechanical Actuator (EMA) (JIAN *et al.*, 2017; MARÉ; FU, 2017; RONGJIE *et al.*, 2009).

2.2.2 Electro-Hydrostatic Actuators (EHA)

The EHA is a decentralized and independent hydraulic system, usually comprising a bidirectional hydraulic pump coupled to an electric motor, in addition to other secondary elements such as pressure relief valves and accumulators, interconnected by a manifold block (ALLE *et al.*, 2016).

According to Rongjie *et al.* (2009), the EHA can be classified into three main configurations, regarding the hydraulic pump and electric motor control, such Fixed Pump Variable Motor – FPVM, Variable Pump Fixed Motor – VPFM, and Variable Pump Variable Motor – VPVM. Variable or fixed pump means the use of a variable or fixed volumetric displacement pump, and the use of variable or fixed motor means the use of variable o fixed rotational frequency of the electric motor.

According to Alle *et al.* (2016), the EHA using a fixed displacement pump coupled to a variable rotational frequency electric motor has a simpler structure and configuration, with better efficiency than the configuration using a variable pump and fixed motor.

Figure 2.3 shows a schematic of a generic FPVM – EHA, the reference command is compared with the current position of the cylinder, the controller uses the error signal to control the electric motor drive, which controls the direction and frequency of electric motor rotation. The electric motor is coupled to a bidirectional pump used to transfer energy to the hydraulic fluid to move the cylinder.

Figure 2.3 – A generic Electro Hydrostatic Actuator.
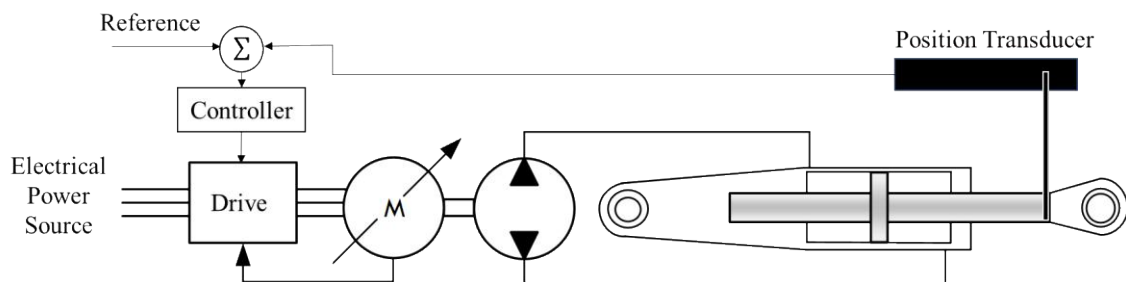
Source: Made by the author, based on (MARÉ, 2017).

The EHA follows the Power-by-Wire concept, which means that electrical energy is carried by wire to the actuator drive. The replacement of the centralized hydraulic system improves the flexibility of the aircraft layout as the pipelines are replaced by electric wire, which reduces the risk of hydraulic fluid leakage, pressure drop along the pipeline, the weight of the system, and increases the survivability of military aircraft (ALLE *et al.*, 2016; MARÉ, 2017).

According to MARÉ & FU (2017), another advantage of using decentralized PbW solutions is related to maintenance and production, as it is possible to design a plug-and-play integration in the airframe to reduce assembly time. The same author affirms that, from the point of view of energy efficiency, the EHA has the advantage of working according to the power-on-demand concept, being activated according to the needs of the system.

According to the authors Alle *et al.* (2016), Maré (2017), and Maré & Fu (2017), the main drawbacks of the EHA are related to:

- Heat dissipation: the compact design makes it more difficult for the system to dissipate heat to achieve a thermal balance;
- Pump work conditions: the pump must be able to operate in four power quadrants, a wide range of angular velocity and pressure differential, which means that they operate in much more severe conditions than SHA system pumps, these characteristics make it difficult to develop pumps capable of providing high efficiency across the entire operating range and long service life.
- Electromagnetic interferences: High-frequency switching of high currents generates electromagnetic interference that can affect other aircraft systems.

As an application of the EHA, the Airbus A380 was the first commercial aircraft model to implement electro-hydrostatic actuators to drive control surfaces, equipped with EHA (to command the aileron and elevator) and backup EHA (Electrical Back-up Hydrostatic Actuator – EBHA) used to command the rudder and spoiler (VAN DEN BOSSCHE, 2006).

2.2.3 Electro-Mechanical Actuators (EMA)

The EMA may represent the highest level of the PbW and MEA concept, in this configuration, the hydraulics is completely removed and the power generated by the electric motor is transmitted to the control surface through a mechanical transmission (GARCIA *et al.*, 2008; JIAN *et al.,* 2017; QIAO *et al.*, 2018).

Figure 2.4 shows a generic schematic of an EMA. Similar to the EHA, the command of the reference position is compared to the position of the rod and the controller uses the error signal to control the electric motor drive, which controls the direction and frequency of the electric motor rotation. The electric motor power is transmitted directly or through a gearbox to a screw mechanism (QIAO *et al.*, 2018).

Figure 2.4 – Generic scheme of an Electro Mechanical Actuator.
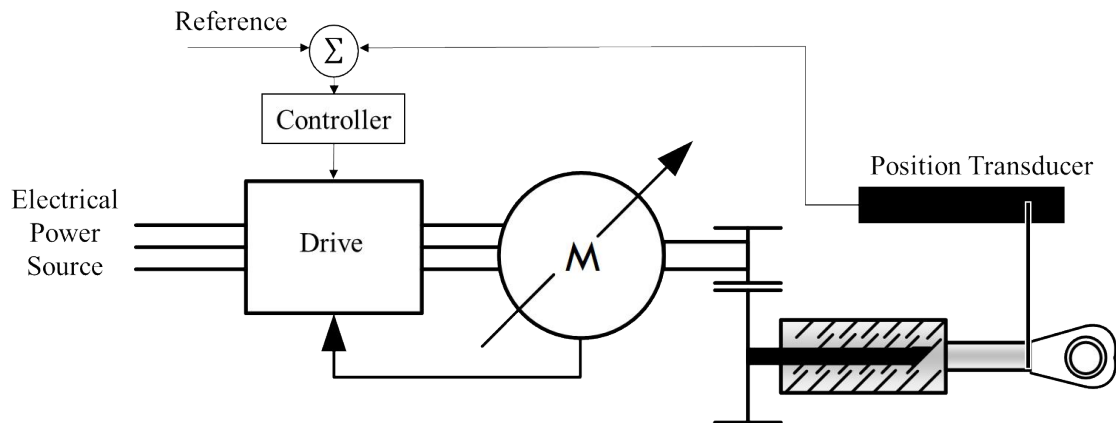
Source: Created by the author based on Maré (2017).

Van Den Bossche (2006) cites the EMA as a potentially attractive solution, instead of the EHA, to be applied in low power applications mainly due to its good characteristics regarding to complexity, weight, reliability, and maintenance. However, EMA is considered not to have sufficient technological maturity to replace the SHA in safety-critical functions such as primary flight control surfaces, due to the risk of failures by jamming, health monitoring and assessment, and thermal management (QIAO *et al.*, 2018).

On the secondary control surfaces, jamming is not as severe as on primary control surfaces, and a blocked failure is expected (MARÉ; FU, 2017; QIAO *et al.*, 2018). In this context, the EMA is currently applied on four of the 14 spoilers on the Boeing B787, in the slats of the Airbus A380, and in the horizontal stabilizers of Embraer KC390 and Airbus A350 (MARÉ, 2017).

Failure response is one of the criteria addressed by Jian *et al.* (2017), the authors highlight that for primary control surfaces the failure rate must be extremely low (about 10^{-9} per hour of flight), and to achieve this requirement redundant systems are implemented. Jian *et al.* (2017) mention that the implementation of bypass valves, restrictors, pilot-controlled check valves, and isolation valves can be adopted in SHA to provide a fail-safe response with low

mass and low cost. However, it is not easy to implement bypass at EMA where clutches, brakes, dampers, and torque limiters may be required.

According to Maré & Fu (2017), in addition to transmitting and transforming energy, it is desirable for actuators to perform some secondary functions such as damping, releasing or locking the load in position, and overload protection. The authors emphasize that such characteristics can be obtained through the EHA. However, they are more difficult to service with EMA, where the designer must find ways to perform these functions mechanically or electrically.

2.2.4 Fault tolerance and hybrid systems

According to Bennett *et al.* (2012), an important aspect of the flight control surface actuator system is fault tolerance, which in aircraft this task can be solved by the use of multiple surfaces driven by multiple actuators. The authors cite some methods used to obtain flight control redundancy such as surface redundancy, actuator redundancy, actuator with internal redundancy, and a combination of these methods (Figure 2.5).

Figure 2.5 – Redundancy schemes for aircraft control surfaces.

a)   b)

c)
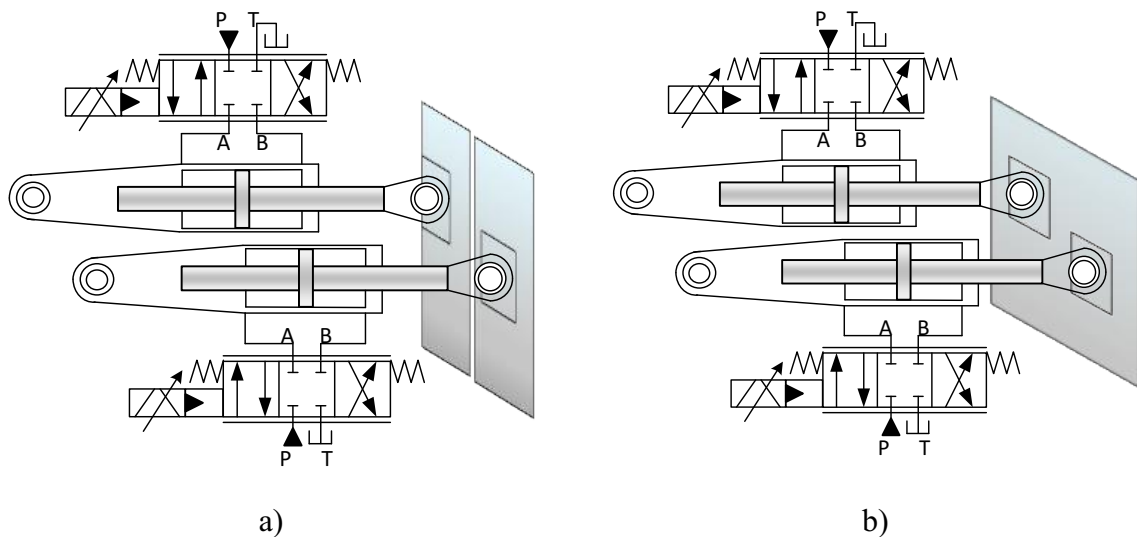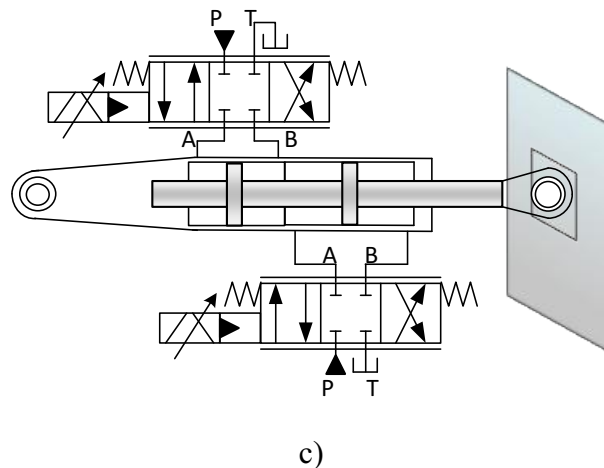
a) Surface redundancy, b) Actuator redundancy, and c) Internal actuator redundancy.
Source: By the author based on Bennett *et al.* (2012).

In the cases shown in Figure 2.5, by pass valves can be used between the servo valves and the cylinder to change the connection of the cylinder chambers in order to allow the cylinder to have different modes of operation such as locked or damped.

According to Maré & Fu (2017), hybrid systems can be used to improve the system reliability and fault tolerance, since different power sources are used to supply the system. In this case, hybrid systems are characterized by the combination of the concepts presented before (SHA, EHA, and EMA), in order to obtain more reliable actuation systems. Maré & Fu (2017) present some hybrid systems such as Electro-Hydrostatic Backup Actuator – EBHA, Electro-Assisted Hydrostatic Actuator – EAHA, and Electro-Backup Mechanical Actuator – EBMA.

In the EBHA configuration, the same cylinder shares two different power sources. When under normal conditions, the centralized power source is used as the main power source and the cylinder is in SHA mode. If necessary, an electro hydrostatic power source is used as a backup to supply the cylinder, which switches to EHA mode. In this case only one power source or mode can be activated at a time (MARÉ & FU, 2017) (Figure 2.6).

According to Maré & Fu (2017), the EAHA follows the same concept as the EBHA, where an EHA is combined with a SHA to supply the cylinder. However, the operational logic is modified to enable both active power sources simultaneously. With this arrangement, the flow rate from both sources is summed and the EHA can boost the SHA at peak power demands or in case of partial loss of hydraulic power, thereby increasing the capability of the actuator (Figure 2.7).

Figure 2.6 – Electro Hydrostatic Backup Actuator.
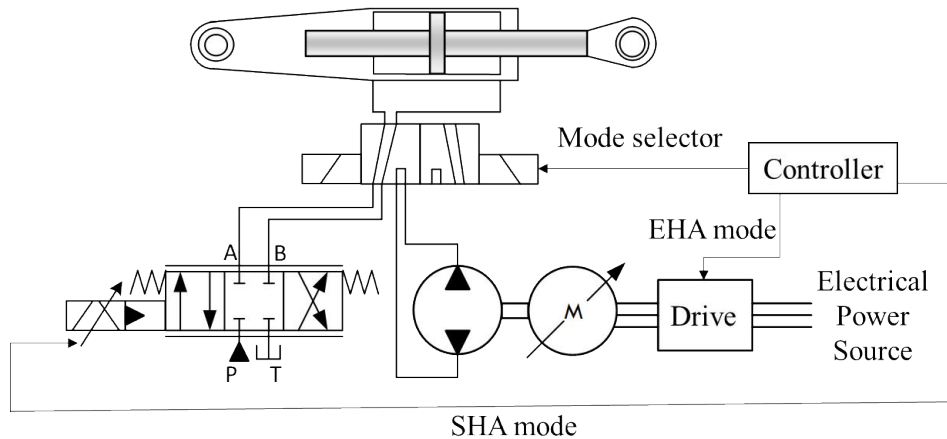
Source: Author adapted from Maré (2017).

Figure 2.7 – Electro Assisted Hydrostatic Actuator.
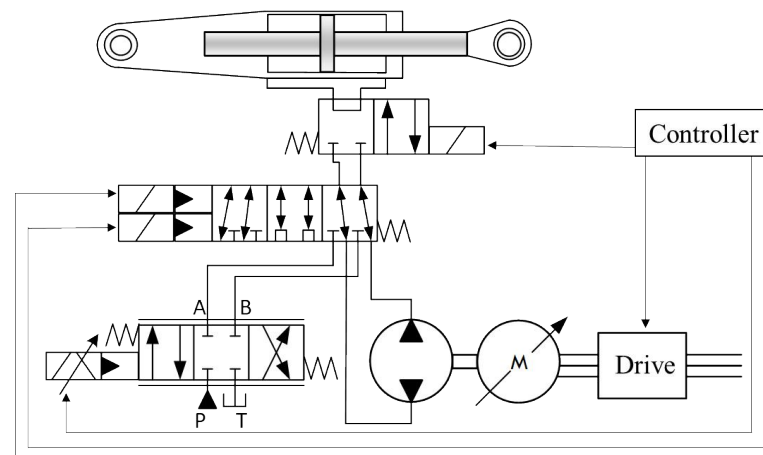
Source: Author, adapted from Maré (2017).

In the EBMA, an EMA is used as a backup power source for the servo hydraulic actuator, this concept is applied to the actuator of the landing gear doors of the Airbus A400M military transport (MARÉ & FU, 2017).

Table 2.2 presents the surfaces where the SHA, EHA and EBHA concepts are applied, in some aircraft currently in service.

Table 2.2 – Actuators solutions currently applied.

	Airbus A380	Airbus A400M	Airbus A350	Gulfstream G650
Ailerons	8/4/0	2/2/0	6/2/0	2/0/2
Elevator	4/4/0	2/2/0	2/2/0	2/0/2
Rudder	0/0/4	0/0/2	2/1/0	1/0/1
Spoilers	12/0/4	8/0/2	8/0/4	4/0/2
Total	24/8/8*	12/4/4	18/5/4	9/0/7

*The sequence number means the quantity of SHA/EHA/EBHA.
Source: Adapted from Maré (2017).

2.3 ELECTRIC MOTORS FOR AIRCRAFT APPLICATIONS

The trend of aircraft following the concept of more electric aircraft (MEA) with power carried via cables (PbW) has become a multidisciplinary challenge within aeronautical systems engineering. The search for more efficient solutions for aircraft is growing and it is natural to search for technologies that present good performance, good efficiency and high reliability. This section addresses technologies related to electrical machines that have the potential to be applied in actuation systems on aircraft control surfaces. An overview focusing on its main characteristics and limitations is presented. For more information, the author recommends reading the cited references.

2.3.1 Requirements

According to Elbuluk & Kankam (1995), the choice of an electric motor for a specific application depends on factors such as demanded power, operating speed, work environment, fault tolerance, reliability, performance requirements, thermal capacity, cost, weight and occupied volume, among others. These criteria will determine the characteristics of the power electronics circuits and controllers needed to drive the motor.

Due to the strict and specific reliability and power density requirements demanded in aerospace applications, electric motors play an important role in the electric drive system (CAO *et al.*, 2012). Boglietti *et al.* (2009) points out that a fault-tolerant electric motor for applications in EMAs must have the following characteristics:

- High torque/weight ratio;
- High torque/current ratio;

• High efficiency in the entire speed range;

• Electrical, thermal, magnetic and mechanical isolation between phases;

• High phase inductance, in order to limit short-circuit currents;

• Safe operation under fault conditions (loss of a phase).

Cao *et al*. (2012) considers that these criteria can be generalized for the development of machines aimed at critical safety applications. Therefore, according to him, electrical machines that have brushes or commutators do not meet these requirements due to the need for maintenance, low torque density and low reliability. Considering the restrictions mentioned above, the types of electrical machines most suitable for use in aircraft systems are induction, reluctance, and permanent magnet machines (CAO *et al.,* 2012; DUNKER *et al.*, 2013; ELBULUK & KANKAM, 1995). The next section presents a short resume of those three types of electric motors highlighting their main advantages and disadvantages according to the literature review.

2.3.2 Suitable Electric Motors

Currently, Induction Motors (IM) are considered the main means of converting electrical energy into mechanical work, cover a wide power range (from tens to thousands of Watt) and serve a wide variety of applications, including use in household appliances (air conditioners, refrigerators, electric gates, among others) and use in industrial equipment (overhead cranes, presses, hydraulic pumps, among others). This popularity of using induction machines is related to their low cost, simplicity, robustness and reliability (BIM, 2012; CAO *et al.*, 2012; KRAUSE *et al.*, 2013).

According to Cao *et al.* (2012), due to the characteristic of the machine being highly dependent on the existing magnetic couplings between the rotor and stator phases, performing the magnetic isolation between the motor elements becomes practically impossible. Cao *et al.* (2012) quotes also that to meet the fault tolerance characteristics, drivers for multiphase motors were developed in a modular way with the objective of reducing electrical and magnetic couplings between phases. However, such solutions involve more complex control techniques to be implemented.

Another type of electric motor is the Permanent Magnet Synchronous Machine (PMSM), which has gained ground in the market due to its good characteristics and performance, such as high power density, high efficiency, excellent dynamics, long service life, low noise, wide speed range, low operating temperature, shock and vibration resistance and

high torque/inertia, torque/current, and torque/volume ratios (BOLOGNANI *et al.*, 2000; CAO *et al.*, 2012; OBED & KADHIM, 2018; PATEL *et al.*, 2014).

According to Hughes & Drury (2013) when analyzing permanent magnet synchronous machines, it is clear that the approaches used in industry and academia ended up assigning a variety of different names to what is essentially the same machine. The following names are commonly found: brushless permanent magnet motor (Brushless AC and Brushless DC) and permanent magnet servo motor. According to the same authors, the main characteristic of permanent magnet machines is the presence of permanent magnets that replace the field winding of the rotor.

One of the limitations in the use of permanent magnet motors was linked to the technological development of power control drivers and control techniques. Matsuse *et al.* (2013) cite the example of the Pulse Width Modulation (PWM) control technique, which was initially applied only for harmonic reduction, it has become a technology for instantaneous voltage control due to the high voltage frequency switching of Insulated Gate Bipolar Transistors (IGBT). This feature explains how high-performance drivers provide fast response and low-ripple torque control.

The cost and availability of rare earth to manufacture magnets with better performance are considered limitations (YANG *et al.*, 2015). It is also observed the presence of thermal limitations during the operation of the PMSM due to the high temperature tolerance limit for the permanent magnets, which according to Jack *et al.* (1996) is not so critical since the windings are designed to have a peak temperature close to 220°C and a magnet is limited to a temperature of 180°, in the case of an Sm_2Co_{17} alloy.

The Switched Reluctance Motors (SRM) is the third type of motor pointed as an option to be used in aircraft applications. One of its advantages is its natural characteristic of fault tolerance due to the use of independent windings in each pole, which allows the motor to continue operating, with reduced capacity proportionally to the number of phases in fault. In addition, SRMs have less electromagnetic coupling between phases and lower rotor losses, which makes them preferable to induction motors (CAO *et al.*, 2012).

The main limitations of this type of machine are related to high noise, low power factor, high torque ripple, and vibration. Due to these aspects, the application of this type of machine in some areas is still very limited, requiring further development (BOSTANCI *et al.*, 2017; ISHIKAWA & DOHMEKI, 2012; KRISHNAN, 2001; YANG *et al.,* 2015).

Table 2.3 and Figure 2.8 presents a summary of the characteristics of the electric motors. Cao *et al.* (2012) present a generalist evaluative approach to the types of machines aimed at aircraft applications. Bostanci *et al.* (2017) present an evaluation addressing some sub-classifications of the types of machines presented, focusing on the point of view of motors aimed at vehicular traction, which have needs similar to the MEA concept.

Table 2.3 – Electric motors comparison.

Characteristics	IM	SRM	PMSM
Fault tolerance	low	low	medium
Power density	medium	medium	high
Robustness	high	high	high
Efficiency	medium	high	high
Cost	low	medium	high
Speed range	low	high	High
Open loop control	yes	no	no
Closed-loop control simplicity	medium	medium	medium
Torque ripple	low	high	medium
Noise	low	medium	low

Source: Adapted from Cao *et al.* (2012).

The sub-classifications discussed in Figure 2.8 refer to permanent magnet synchronous motors with magnets mounted on the surface of the rotor (SM-PMSM), permanent magnet synchronous motors with magnets mounted internally to the rotor (IPMSM), induction motors (IM), synchronous reluctance motors (SyncRel), synchronous reluctance motors assisted by ferrite magnets (SyncRel ferrite), synchronous reluctance motors assisted by neodymium magnets (SyncRel NbFeB) and reluctance motors (SRM).

Among the main aspects evaluated in electric machines, high power density, efficiency, and reliability stand out. Compared with hydraulic systems, the power density requirement is perhaps the most important factor in hydraulic technology. In this requirement, the electrical machines that present the best power density are permanent magnet synchronous machines (BOSTANCI *et al.*, 2017; CAO *et al.*, 2012; DUNKER *et al.*, 2013; ELBULUK & KANKAM, 1995).

In Cao *et al.* (2012), Dunker *et al.* (2013), and Elbuluk & Kankam (1995), the SRM is presented as a high-efficiency motor as well as the PMSM. However, evaluating the study presented by Bostanci *et al.* (2017), it is noticed that the SRM presents good efficiency, being positioned between the PMSM and the induction motor, the latter, due to the winding losses also present in the rotor, present the lowest efficiency among the motors evaluated by the authors.

Figure 2.8 – Electric motors comparison.
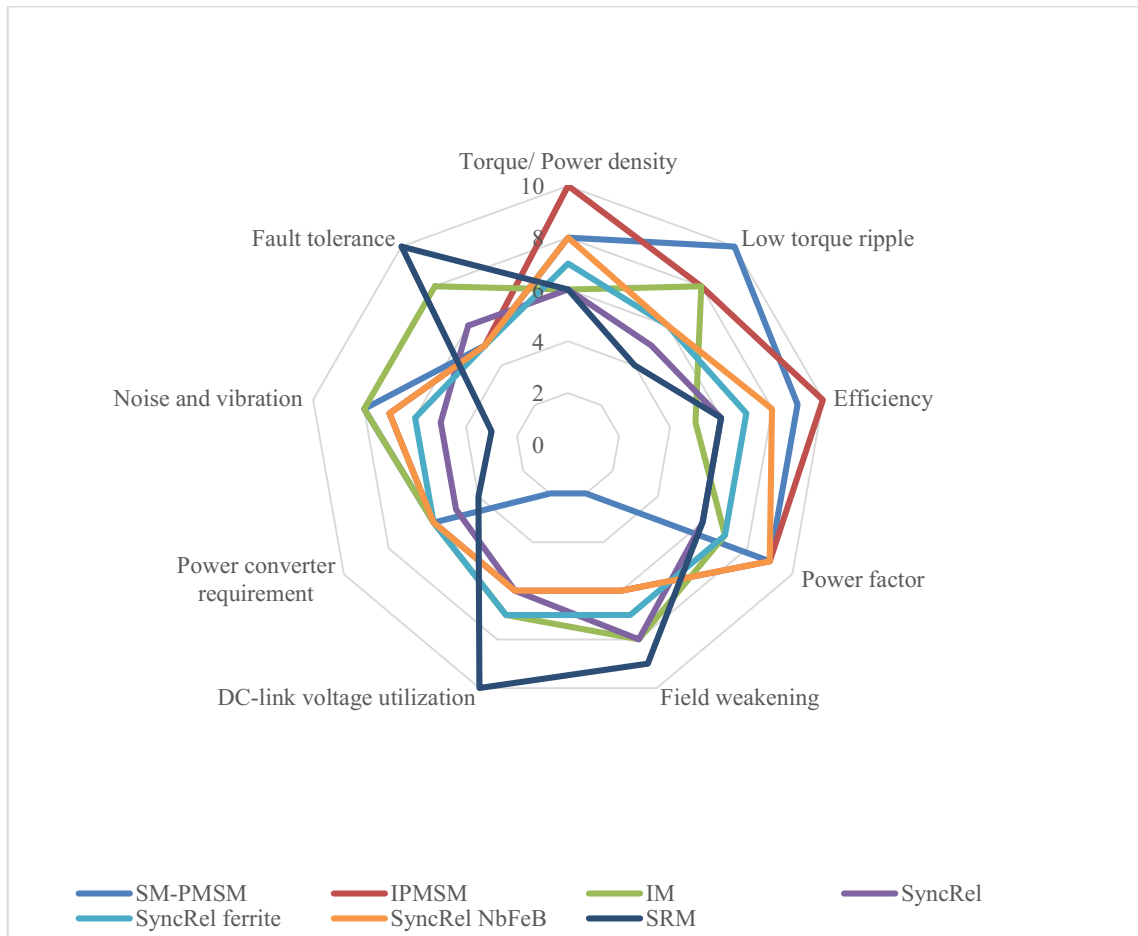
The reliability criterion in traditional hydraulic systems is linked to the maturation of technology over decades, which enabled the development of more robust and fault-tolerant components. In this regard, it is clear that the SRM has constructive characteristics that make them more fault tolerant than the PMSM and the IM (BOSTANCI *et al.*, 2017; CAO *et al.,* 2012; DUNKER *et al.*, 2013; ELBULUK & KANKAM, 1995). It is noticed that this fact is mainly related to the configuration of the windings used in each motor. The IM, PMSM, and SyncRel have windings distributed along the stator, while the SRM has windings separated by poles, in this configuration a failure in one of the phases of the SRM is less harmful than in motors that use physically and magnetically coupled phases to operate (BOSTANCI *et al.*, 2017).

Regarding robustness, it is considered that in addition to the distribution of windings mentioned above, the use of a less complex rotor increases the robustness of the machine. Therefore, by having a simpler rotor the SRM would be more robust than the IM, which in turn

would be more robust than the PMSM. Therefore, by having a simpler rotor, the SRM would be more robust than the IM, which in turn would be more robust than the PMSM, since the latter needs to have permanent magnets attached to its rotor that are susceptible to thermal cycling and demagnetization (JACK *et al.,* 1996; RADUN, 1992; YANG *et al.,* 2015).

Observing the criterion of use, it is clear that the PMSM is the most applied in solutions aimed at use in aircraft, being present in the activation of electro-hydrostatic and electromechanical actuators, and in applications in electric or hybrid vehicles (ISHIKAWA & DOHMEKI, 2012; MARÉ, 2017; MARÉ & FU, 2017; SARLIOGLU & MORRIS, 2015). The SRM, on the other hand, still needs to be improved in order to reduce the characteristics of torque ripple, noise, and vibration, for this reason, there are still few examples of its application (ISHIKAWA & DOHMEKI, 2012; MARÉ & FU, 2017).

Another important point is related to cost, Ishikawa & Dohmeki (2012) and Bostanci *et al*. (2017) recognize the superiority of PMSM using neodymium magnets. However, they also report that the cost of these machines is high, due to fluctuations in the price of rare earth, which is highly dependent on Chinese production, which accounts for approximately 90% of world production. In this sense, the authors point out that there is a growing tendency to improve machines that do not depend on magnets for operation, such as IM and SRM.

3 DIGITAL FLUID POWER

As previously presented, conventional hydraulic systems have relatively low energy efficiency, mainly due to the use throttling valves to control fluid power. According to Achten (2010), in comparison with mechanical and electrical transmission components, hydraulic pumps and motors are very inefficient, especially under part load conditions. In addition to inefficiency, Achten (2010) highlights that hydraulic components are expensive, costing almost three times more than mechanical transmission components. In this scenery, Zhang *et al.* (2020) quote that digital hydraulic technology is a feasible way to obtain high-efficiency and low-cost systems capable to survive the new trends of the industry.

This chapter introduces the concept of digital fluid power and the main features of this technology. An overview of digital hydraulics and application examples are presented to make the reader comfortable with the names used.

3.1 DIGITAL HYDRAULIC CONCEPT

According to Linjama (2011), Digital Fluid Power is defined as a hydraulic and/or pneumatic system composed of discrete components which are able to actively control the system output by the use of an intelligent control strategy in order to obtain different output levels.

The name digital has been used in recent years as a trend of the new developments in technology and industry. However, in a fluid power context, this name is sometimes not completely understood. Using the signal approach to analyze the digital name, it is possible to notice that the signals can be mathematically classified as a function of the independent and dependent variable (CASSANDRAS; LAFORTUNE, 2008). A variable is considered continuous if it can take on all values within an interval and discrete if only some values can be assumed. In many engineering applications, time is considered the independent variable, and the terms continuous-time variable and discrete-time variable are commonly used (CASSANDRAS; LAFORTUNE, 2008; DE NEGRI, 2006; OPPENHEIM; WILLSKY; NAWAB, 2003).

Considering time as an independent variable, the signals can be classified as an Analog signal if it has a continuous-time signal with continuous amplitude values of the dependent variable; Quantized signal if it has a continuous-time signal with discrete amplitude values of the dependent variable; Sampling signal if it has a discrete-time signal with continuous

amplitude values of the dependent variable; Discrete signal if it has a discrete-time signal with discrete values of the dependent variable, the Digital signal is a particular case of a Discrete signal (CASSANDRAS; LAFORTUNE, 2008; DE NEGRI, 2006; LATHI; GREEN, 2018; OPPENHEIM; WILLSKY; NAWAB, 2003).

Applying the signal approach in digital hydraulic systems, it can be concluded that the system has a continuous-time behavior since it can be activated at any time, being classified as a continuous-time signal system. On the other hand, the signal amplitude is the output of the on/off valves which have discrete values according to each input. Therefore, one can conclude that this type of hydraulic system is a quantized signal system or it can be called a continuous-time system with discrete outputs. Otherwise, a digital system means the system has discrete time with discrete outputs.

Therefore, it is noticed that the name digital is used mainly due to the popularization of the name linked to the technological development of electronic devices. The signal approach is not complete considered in this context, where the use of digital is sometimes justified by the discrete output used on the on/off valves and the intelligent control strategy adopted to control the on/off valves which have a binary signal of 0 or 1.

3.2 APPLICATION OF DIGITAL HYDRAULICS

In this section, the application of the digital hydraulic concept is presented following the main functions of the conventional hydraulic system (Figure 3.1), which are primary energy conversion, energy limitation and control, and secondary energy conversion (LINSINGEN, 2016). In this case, the digital hydraulic concept is not applicable to fluid storage and conditioning.

One of the goals of digital hydraulics is to increase hydraulic system efficiency by reducing energy losses caused mainly by resistive control strategies and internal leakage present in conventional hydraulic systems (LINJAMA *et al.*, 2011). In addition, through the use of digital hydraulics, it is possible to obtain a robust and fault tolerant system with good reliability (BELAN, *et al.*, 2014; LINJAMA, 2011; SCHEIDL; LINJAMA; SCHMIDT, 2012).

Digital hydraulics is divided into two main branches, the first concerns the technology of rapid switching of components (Switching Hydraulic Systems), and the second concerns the parallel connection of two or more components (Parallel Connection Systems) (LINJAMA, 2011). Examples explaining both branches are presented in the next subsections.

Figure 3.1 – Main functions of a conventional hydraulic system.

Secondary conversion unit

Limitation and control unit

Primary conversion unit

Storage and conditioning unit
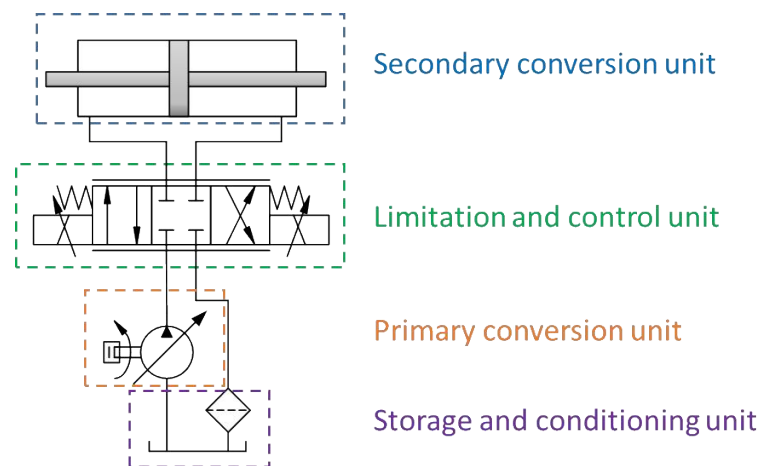
Source: Author.

3.2.1 Limitation and control unit

In the digital hydraulics concept, the system is mainly controlled by on/off valves (Figure 3.2a) which have two work positions, open and closed, represented by the two central squares of the symbol, where the square with an upward arrow represents the open valve and the no arrow square represent blocked port. The valve actuation elements are shown on each side of the symbol, on the left side a solenoid is represented by a rectangle with a diagonal line, and on the right side is represented the spring used to return the valve to its normal position, which can be normally open or closed. When the solenoid is activated, the spring is compressed and the valve changes from the closed state to the open state or vice versa. When the solenoid action ceases, the spring returns the valve element to its normal position. In Figure 3.2a, a solenoid control signal is represented above the solenoid.

In the Switching hydraulic approach only one valve is necessary to control the flow rate. The valve is opened and closed in a high frequency commutation to give an average flow rate which is obtained by control techniques such as Pulse-Width-Modulation – PWM. The output flow rate and control performance depends on the frequency and bandwidth of the pulses (BELAN, 2018; DONKOV *et al.*, 2020).

In the parallel connection approach (Figure 3.2b), the valve only switches to change its state, and the number of states of the system can be obtained by 2^N, where N is the number of valves. Each state has a combination of valves that result in an output flow rate, which is the sum of the flow rate of each open valve (BELAN, *et al.*, 2014; LINJAMA, 2011). In this

context, with the use of multiple on/off valves in parallel it is possible to obtain a variable control orifice.

As example, to control the flow rate in a digital hydraulic systems, Linjama (2011) proposes the use of a Digital Fluid Control Unit – DFCU (Figure 3.2b) where the on/off valves can have or not different sizes, which can be combined to obtain a certain numeric distribution of flow rate levels. According to Donkov *et al.* (2020), multiple DFCUs can be used to obtain a Digital Independent Metering Valve (D-IMV), which can be used to simulate a proportional valve.

Figure 3.2 – Digital hydraulic valves.

a)   b)

c)
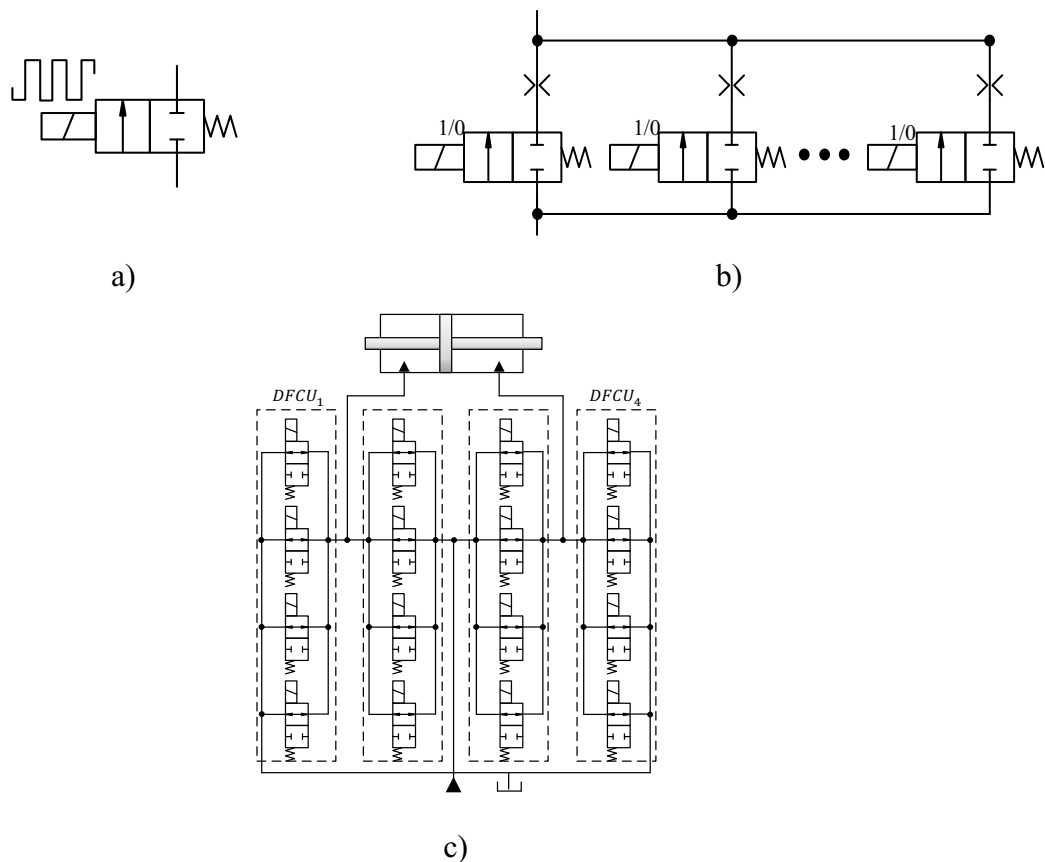
a) Fast switching b) Parallel connection c) D-IMV
Source: Adapted from Linjama (2011) and Donkov *et al.* (2020).

Mantovani (2019) mentions that one of the challenges in using the on/off valves is related to the delay time to open and close the valves, which have different dynamics to open and close, and also due to manufacturing process, two valves of the same model may have different delays.

Figure 3.3 shows a typical behavior of an on/off valve during the opening and closing movements, where t_{sod} is the spool opening delay time, which is the time to charge the solenoid

before the spool start to move; t_{sor} is the spool opening response time, which is the time to the valve spool open; t_{scd} is the spool closing delay time, which is the time to discharge the solenoid before the spool start to move; t_{scr} is the spool close response time, which is the time to the valve spool close (BELAN, 2018; MANTOVANI, 2019; ZHANG *et al.*, 2018).

The delay of the valves impacts the behavior of the system and allows the presence of hydraulic short circuits and cavitation, to avoid these phenomena Mantovani (2019) presents a way to synchronize the opening and closing time of the valves.

Figure 3.3 – Typical behavior of on/off valve opening and closing movements.
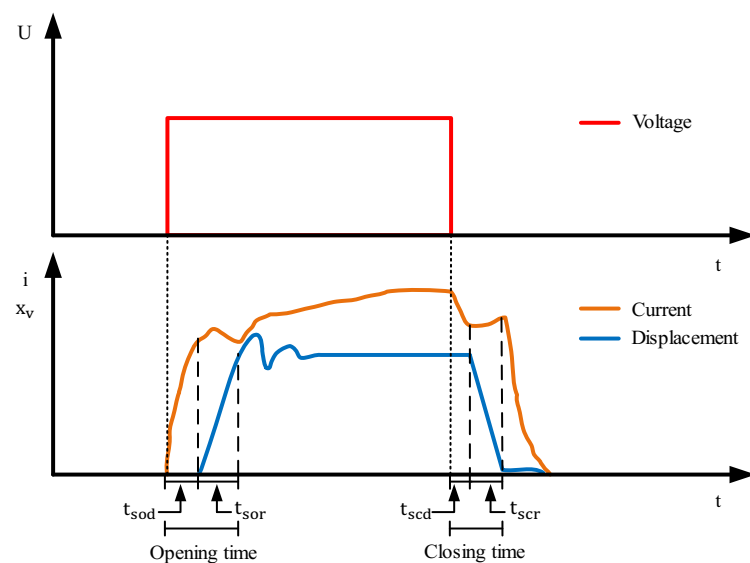
Source: Adapted from Zhang *et al.* (2018)

Nowadays, research is focused on the development of on/off valves for digital hydraulic applications in order to improve its dynamic characteristics and size limitations since obtaining a small valve with high flow rate capacities is still a challenge (ZHANG *et al.*, 2020)

3.2.2 Primary conversion unit

The Digital Hydraulic Pump (DHP) can follows the fast switching or the parallel connection approach. In the fast switching, the valve changes the flow rate direction to reservoir or to the system in high frequency to control the output flow rate to the system (Figure 3.4a)(LINJAMA, 2011). In the parallel connection (Figure 3.4b), two or more pumps can be connected in parallel through the a shaft to have the same angular speed source and each pump outlet can be controlled independently to send the flow rate to the system or reservoir. The total flow rate available is the sum of each pump outlet active to the system (LINJAMA, 2011).

Heikkilä *et al.* (2010) present the use of a digital hydraulic pump in a piston pump-motor configuration where each piston has its outlet controlled independently by an on/off valve to operate as a digital hydraulic pump or a digital hydraulic motor, called Digital Hydraulic Power Management System – DHPMS (Figure 3.5).

Figure 3.4 – Digital Hydraulic Pump.

a)   b)
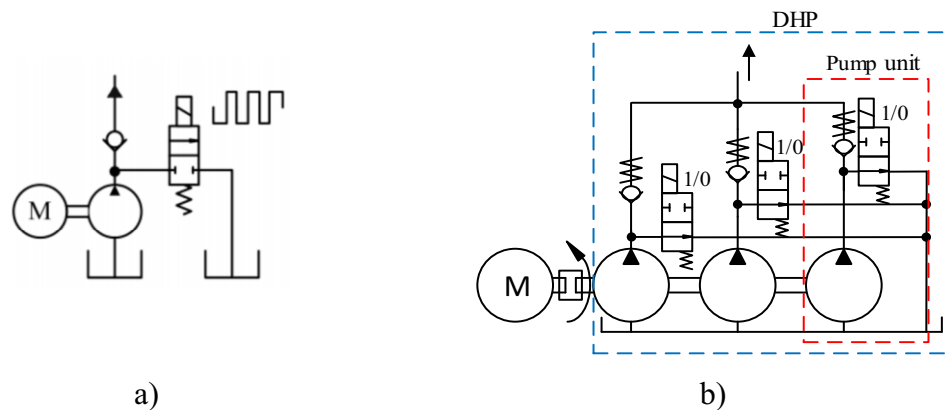
a) Fast switching, b) Parallel connection.
Source: Adapted from Linjama (2011).

Figure 3.5 – Digital Hydraulic Power Management System.
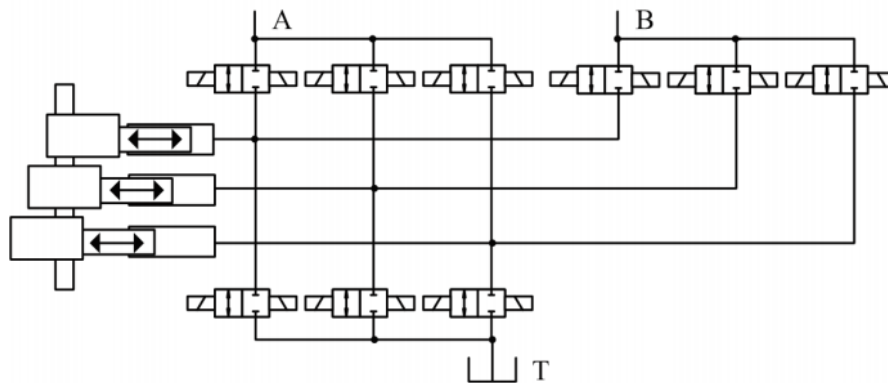
Source: Heikkilä *et al.* (2010).

Heikkila & Linjama (2013) evaluate the energy recovery possibility of the DHPMS applied to the model of an excavator arm actuator Figure 3.6a. Figure 3.6b, presents the possible configurations that the DHPMS can assume during operation, where the configurations a1, a2, and a3 represent the system in standby mode, where the fluid could only be recirculated within the system; in b1 and b2 configurations type the system works as a pump for outputs A and B; in the configuration type c1, and c2, the system works as a motor, and in configurations type d1 and d2 the hydraulic power is transferred between the outputs. In the configuration presented

by the authors, it is still possible to store the energy recovered through the use of an accumulator.

Figure 3.6 – DHPMS application example.
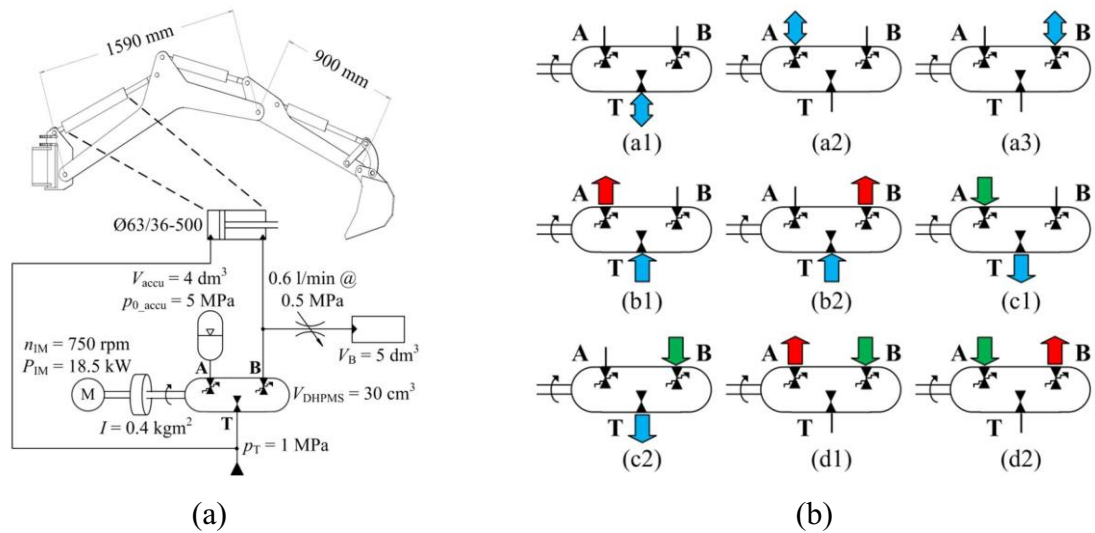
a) Application, b) Working modes.
Source: Heikkila & Linjama (2013).

Currently, the company Danfoss markets a digital hydraulic pump called the Digital Displacement Pump® (Figure 3.7). Each pump piston output is individually controlled to increase or decrease the output flow.

Figure 3.7 – Digital Displacement Pump® from Danfoss.

Source: https://www.danfoss.com/en/products/dps/pumps/digital-displacement-pumps/digital-displacement-single-and-multiple-outlet-pumps/#tab-overview.

3.2.3 Secondary conversion unit

The digital hydraulic concept can be applied to hydraulic actuators, whether rotary or linear, following the same operational logic. Figure 2.10a shows a digital hydraulic motor in a fast switching approach. In this configuration, the torque is alternated between zero and maximum, according to the bandwidth and frequency of the valve switching pulse (LINJAMA, 2011).

Figure 2.10b shows a digital hydraulic motor in the parallel connected approach. In this case, each motor can be activated independently, the torque output is the result of the sum of the torques of the active motors. Figure 2.10c shows a linear digital hydraulic actuator with four chambers that can be supplied independently, according to the activation of the on/off valves. The number of possible combinations will define the number of states of the digital hydraulic actuator and the possible output values of force or velocity (BELAN, 2018; NOSTRANI, 2021).

Figure 3.8 – Digital Hydraulic Actuators.

a)   b)   c)
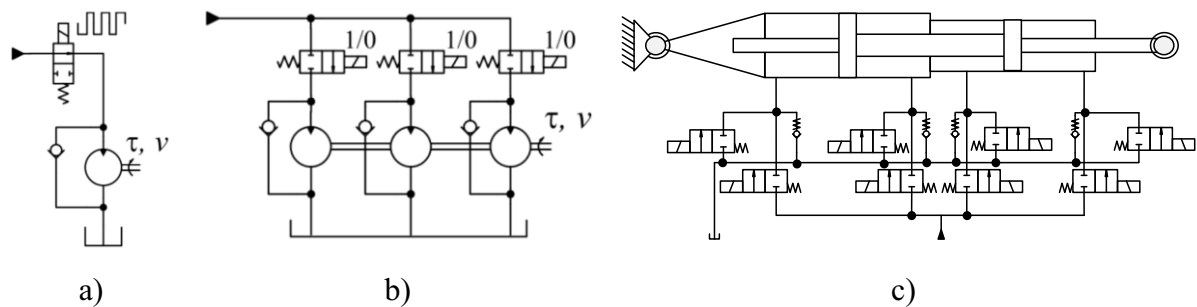
a) Fast switching configuration, b) Parallel configuration, c) Digital hydraulic cylinder
Source: Adapted from Linjama (2011) and Nostrani *et al.* (2019).

3.3 RESEARCH ON DIGITAL HYDRAULICS

The research on digital hydraulics is currently been carried out in countries as Bulgaria, Brazil, China, United Kingdom, Denmark, France, Germany, United State of America, Russia, and Finland, with emphasis on the latter, which has one of the pioneering research centers in digital hydraulics in Tampere University supervised by Matti Linjama (MANTOVANI *et al.*, 2018). Donkov *et al.* (2020) and Zhang *et al.* (2020) present a recent overview of the main research in digital hydraulics over the last ten years highlighting the applications and the necessities to develop new components.

In Brazil, the research on digital hydraulics has begun in 2012 through the partnership between the Laboratory of Hydraulic and Pneumatic Systems (LASHIP) from the Federal

University of Santa Catarina, with the Division of Fluid and Mechatronic Systems (FLUMES) from the Linköping University in Sweden, and the company Saab AB.

Focusing on the development of actuators for aircraft control surfaces, Belan (2018) proposed a Digital Hydraulic Actuator with three different pressure lines supplying a four-chamber cylinder with different chamber areas. In the system proposed by Belan (2018), the combination of chamber areas and pressure lines results in different discrete levels of forces that are used to move the cylinder in different directions controlled by combinations of on/off valves (Figure 3.9). In this case, the same pressure line can be connected to chambers with different areas to reduce or increase the output force and the position control is achieved by force control. This first topology studied at LASHIP was able to reduce energy dissipation by about 65 times in comparison with a conventional hydraulic system (BELAN, 2018).

Figure 3.9 – Digital Hydraulic Actuator.
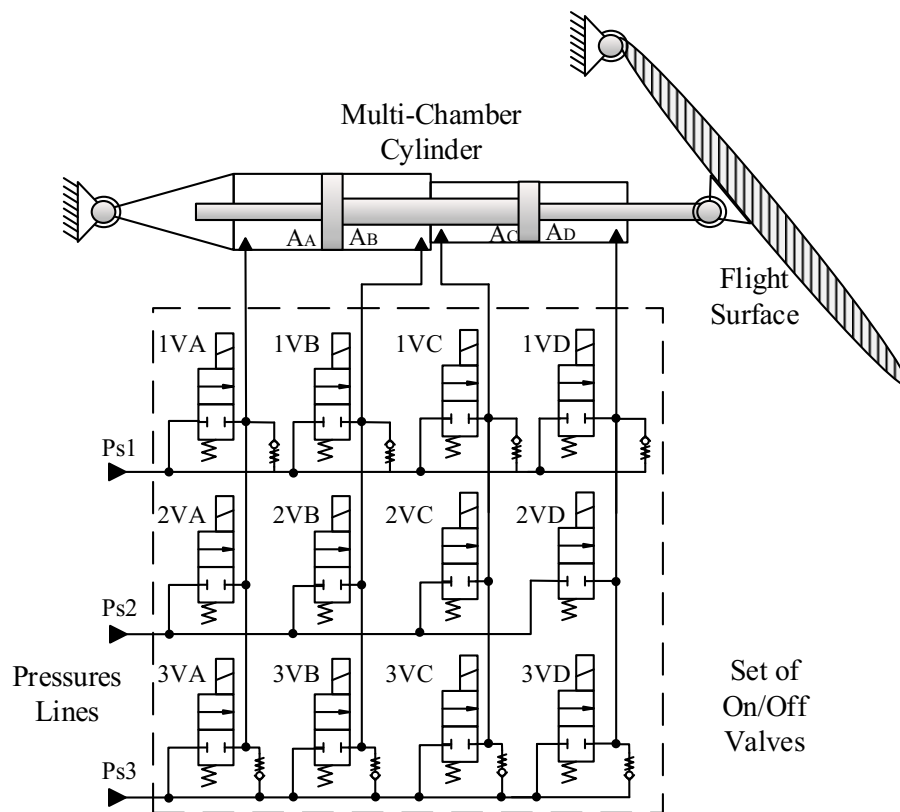
Source: Adapted from Belan (2018).

The second topology was a Digital Electro Hydrostatic Actuator (NOSTRANI, 2020), where a four-chamber cylinder supplied by a Digital Hydraulic Pump with three pump units running in a constant angular speed was used (Figure 3.10). In this case, the digital hydraulic pump is used to control the flow rate and to obtain different discrete cylinder velocities that are used to achieve the position control of the system, pressure is a consequence of the system

loads. To increase the number of discrete cylinder velocities, Nostrani (2021) proposed using the cylinder in regenerative mode, where by redirecting the flow between the cylinder chambers it is possible to increase the number of cylinder velocities available. By the use of this configuration, it was possible to reduce the energy dissipation by about 29 times than the conventional hydraulic system (NOSTRANI, 2021).

Figure 3.10 – Digital Electro Hydrostatic Actuator.
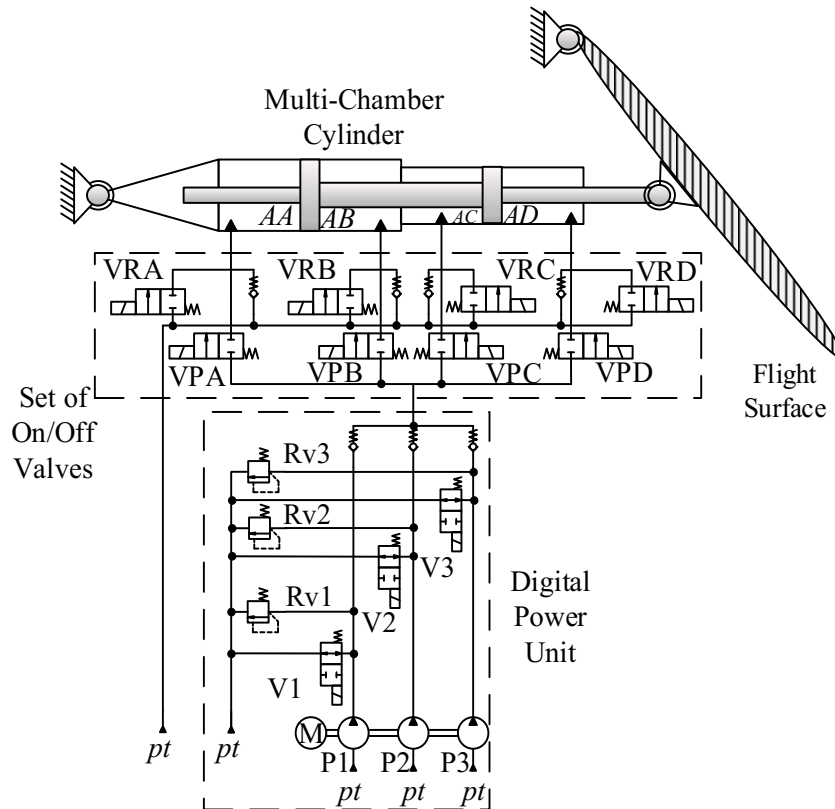
Source: Adapted from Nostrani (2021).

In parallel, researches were conducted at LASHIP to analyze the digital hydraulic systems from other perspectives, as example, the optimization of switching ON/OFF valves in digital hydraulic actuators (MANTOVANI, 2019) and to evaluate the dynamic behavior of a digital hydraulic actuator designed for flight control purposes under a failure condition (LOPES JUNIOR, 2021).

This thesis presents a third topology of a digital hydraulic actuator evaluated at LASHIP, where a variable speed digital hydraulic pump is used to supply a symmetric cylinder, which is called Variable Speed Digital Electro-Hydraulic Actuator (VSDEHA). Table 3.1 present a comparison of the main characteristics of the topologies developed in LASHIP.

Table 3.1 – Comparison of the characteristics of the digital hydraulic topologies.

Characteristic	DHA	DEHA	VSDEHA
Controlled hydraulic variable	Pressure	Flow rate	Flow rate
Controlled mechanical variable	Force	Velocity	Velocity
Hydraulic supply unit	Not considered	Digital hydraulic pump	Digital hydraulic pump
MEA concept	Not considered	Considered	Considered
Electric motor control	Not considered	Fixed angular speed	Variable angular speed
Cylinder valve commutation	To change force and direction	To change velocity and direction	To change direction
Pump valve commutation	Not considered	To change the pump unit combination	To change the pump unit combination
Number of forces or velocities	Discrete, Limited by the number of pressure lines and cylinder chambers	Discrete, Limited by the number of pump units and cylinder chambers	Continuous, but with minimum value limited by the angular speed range

Source: Author.

4 DESIGN OF DIGITAL HYDRAULIC PUMP WITH VARIABLE SPEED

This chapter presents a method for designing a variable-speed digital hydraulic pump using commercial pumps coupled in a parallel configuration. The method focuses on how to configure the digital hydraulic pump, choosing the number of pump units used and their respective volumetric displacements.

4.1 PROPOSAL AND JUSTIFICATION

A digital hydraulic pump (DHP) in parallel configuration is composed of two or more pumping units connected by the same shaft to an angular velocity source (Figure 3.4b). Typically, the volumetric displacement of the DHP is distributed among the pumping units in some numerical pattern (power of two, Fibonacci, etc.) to obtain different discrete output flow rates (Figure 4.1a).

Analyzing the Figure 4.1 it is possible to notice that a digital hydraulic pump operating with constant angular velocity has two limitations. The first is the number of different discrete output flow rates, which is limited by the number of pumps of the DHP. The second is the discrete flow values, where it is not possible to achieve values between two consecutive levels. However, if a variable angular velocity is used, a continuous flow rate can be achieved by overcoming both constant angular velocity limitations.

Figure 4.1 – Theoretical flow rate for different pump unit combinations.

a)   b)
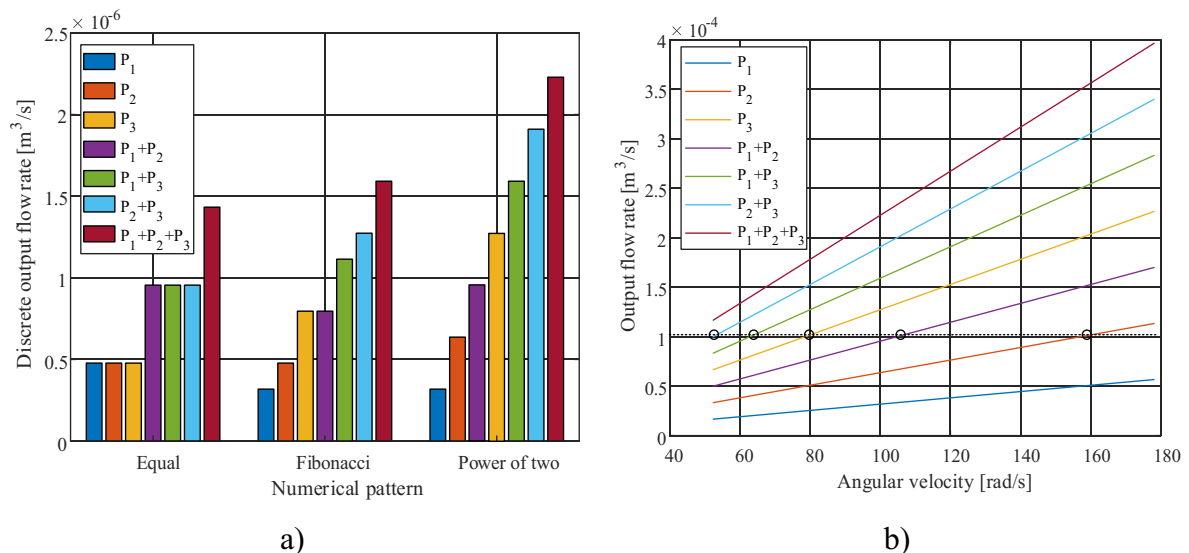
Output flow rate for a) Constant angular velocity, b) Variable angular velocity. Source: Silva *et al.* (2021).

The possibility of changing the angular speed of the DHP makes it necessary to define a criterion to choose which combination of pumping units should be used to supply a certain demand. In this context, it is possible to analyze the efficiency of each combination of pumping units at the desired operating point and choose the most efficient combination.

A comparison of DHP with fixed and variable angular velocity was presented in Silva *et al.* (2021), where the advantage of using the variable angular velocity configuration is related to the possibility of obtaining a continuous flow rate overcoming the limited number of discrete output flows. In this paper, a study comparing a variable displacement pump with a variable angular velocity DHP was presented, where it was observed that, in low-demand conditions, the DHP presented better efficiency than the variable displacement pump due to the possibility of using the combination of the pump unit and its respective angular velocity to meet the flow demand using the best efficiency available.

Therefore, using a digital hydraulic pump with a variable angular velocity source, it is possible to overcome the limitations of the fixed velocity configuration and obtain efficient systems. In the next sections, a method to design a digital hydraulic pump with variable angular velocity is presented.

4.2 A METHOD TO DESIGN A DIGITAL HYDRAULIC PUMP

In digital hydraulic pumps with variable velocity, it is possible to obtain energy-efficient combinations to supply the system in low and high-load conditions. However, the main doubts during the design of a DHP concern how to define the number of pumping units to be used and their respective volumetric displacements. Without a guide or a concise approach to defining these parameters, the task can become very time-consuming.

In this context, a method was developed to be used as a guideline for the design of digital hydraulic pumps. Based on design requirements, the approach combines different number of pumps with different volumetric displacements to configure different digital hydraulic pumps. Configured digital hydraulic pumps are evaluated within a range of pressures and flow rates and compared to each other. Overall average efficiency is used to rank the proposed digital hydraulic pumps. After this, specific analyses of the digital hydraulic pumps can be carried out considering secondary characteristics such as maximum torque, maximum power consumption, the efficiency at specific demand cycle, and also qualitative analysis as maximum volume and weight, to define the solution with the best balance.

The method is divided in three main phases, which one with steps as presented in Figure 4.2.

Figure 4.2 – The phases and steps of the method.
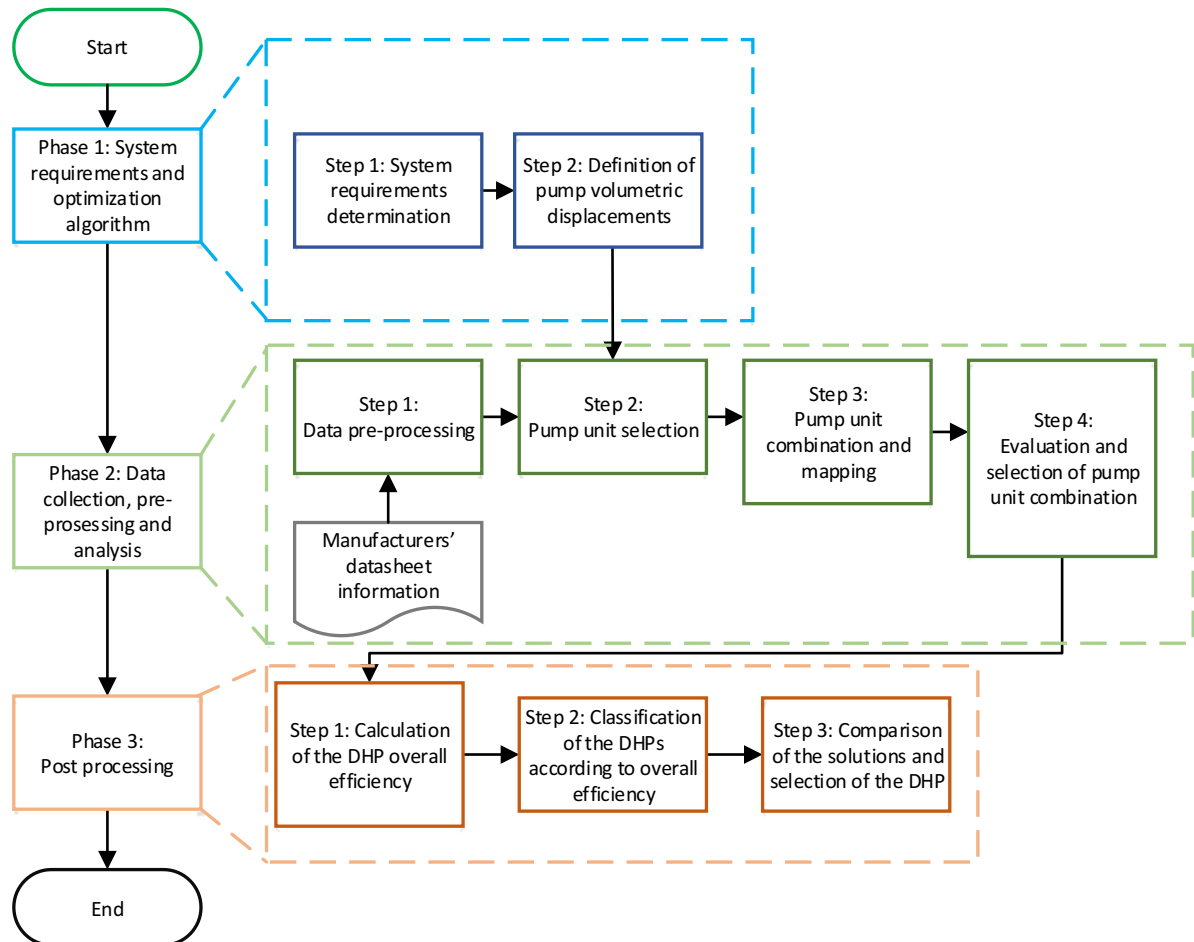
Source: Author.

4.2.1 Phase 1 – System requirements and optimization algorithm

4.2.1.1 Step 1 – System requirements determination

This step aims to collect the operating requirements of the digital hydraulic pump to be attending an application. The digital hydraulic pump has a digital variable volumetric displacement, which is defined by the number of pump units connected to the system in pumping mode. In order to design the pump unit sizes in a dynamic hydraulic system with variable flow rate demand, it is required to determine the maximum and minimum flow rates necessary to supply the system during work conditions.

In the present approach, the digital hydraulic pump is driven by a variable angular speed electric motor, which directly impact on the delivered flow rate of the DHP. Therefore, it is necessary to consider the range of angular velocities the pump will be operating. In addition, an estimated volumetric efficiency for the pump units will be used in this first phase of the design.

Therefore, the minimum and maximum flow rates (q_{V_min}, q_{V_max}), an estimated volumetric efficiency (η_V^*); the operating pressure range of the system (p_{max}); and the minimum and maximum angular velocities (ω_{min}, ω_{max}) must be specified by the system designer.

4.2.1.2 Step 2 – Definition of pump volumetric displacements

The first task is to define the number of DHP to be designed (n_d), the number of pump units used in each DHP ($n_{u(i)}$) where *i* is the index of the DHP, and the distribution pattern of the volumetric displacement for each DHP (Figure 4.3). This task is used to configure different DHP for further comparisons. The designer is free to choose the number of DHP, pump units and their numerical pattern distribution, and the constructive principle of the pump units that usually are among gear, vane or piston pumps.

Figure 4.3 – Configuration of DHP.
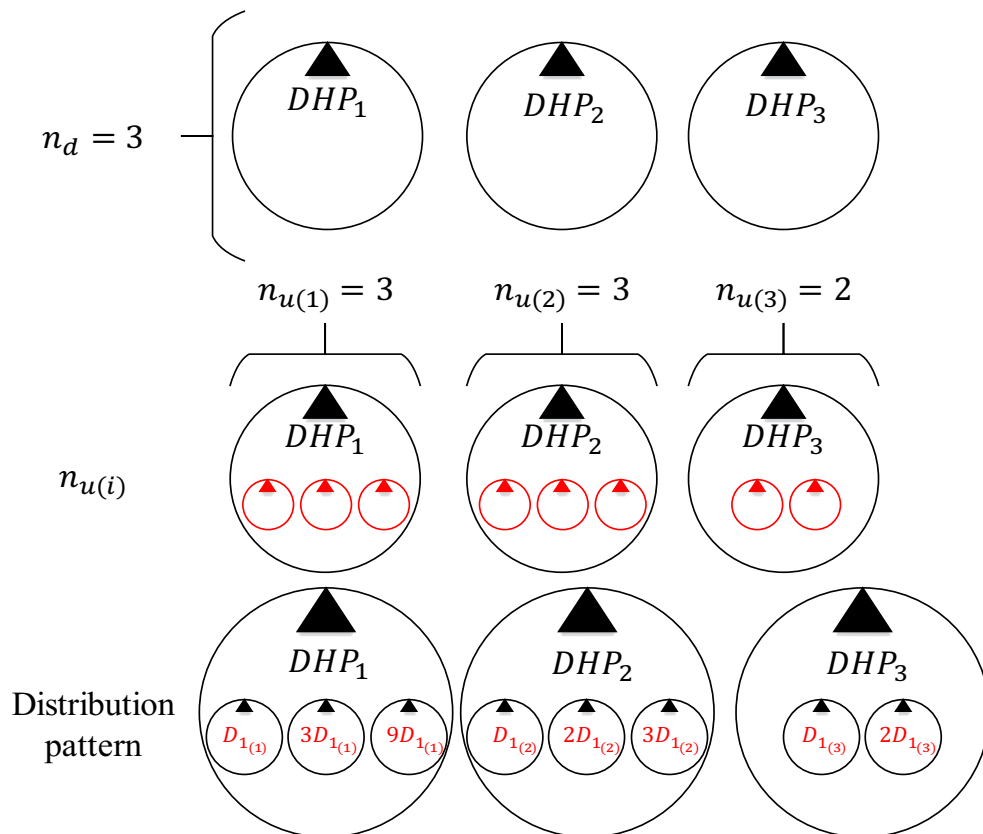
Source: Author.

Adopting a distribution pattern before starting the calculations is a strategy used to relate the volumetric displacements of the pump units of the same DHP. This strategy aims to reduce the computational cost avoiding calculating volumetric displacements that are not feasible and facilitating obtaining volumetric displacements close to those available in the market.

The next task in Step 2 is to calculate the volumetric displacements of the pump units for each DHP where numerical patterns are considered. This task includes the use of an optimization algorithm, called in MatLab as *fmincon* function, to find minimum of a constrained nonlinear multivariable function (Figure 4.4).

For the first iteration, the value of the calculated minimum and maximum angular velocities corresponds to the minimum and maximum angular velocities defined by the designer $(\omega_{c\_min} = \omega_{min})$ and $(\omega_{c\_max} = \omega_{max})$, respectively. Therefore, the volumetric displacement of the smallest pump unit is calculated by

$$D(i,j,k) = \frac{q_{V\_min}}{\omega_{c\_min}\eta_V^*} \tag{4.1}$$

where i = 1 to n_d corresponds to the number of DHP, j is an auxiliary variable used to count the optimization loop (j = 1…), k = 1 to $n_{u(i)}$ corresponds to the number of pump unit for each DHP, η_V^* is the estimated volumetric efficiency and q_{V_min} is the minimum flow rate of the system.

The next task is to calculate the volumetric displacements of the other pump units according to the distribution patter of the DHP under analysis. Considering the pump units in each DHP are indexed by $k = 1$ to $n_{u(i)}$, the volumetric displacements can be correlated as follows: For a power of two distribution, $D(i,j,k) = 2^{k-1}D(i,j,1)$; for power of three $D(i,j,k) = 3^{k-1}D(i,j,1)$; for equal distribution $D(i,j,k) = D(i,j,1)$; and for Fibonacci sequence distribution, $D(i,j,2) = D(i,j,1)$ and $D(i,j,k+2) = D(i,j,k+1) + D(i,j,k)$ for $k \geq 1$.

The maximum volumetric displacement is given by the sum of the volumetric displacements as

$$D_{max}(\text{i,j}) = \sum_{k=1}^{n_{u(i)}} D(i,j,k) \qquad (4.2)$$

Figure 4.4 – Flowchart of Phase 1 – Step 2.
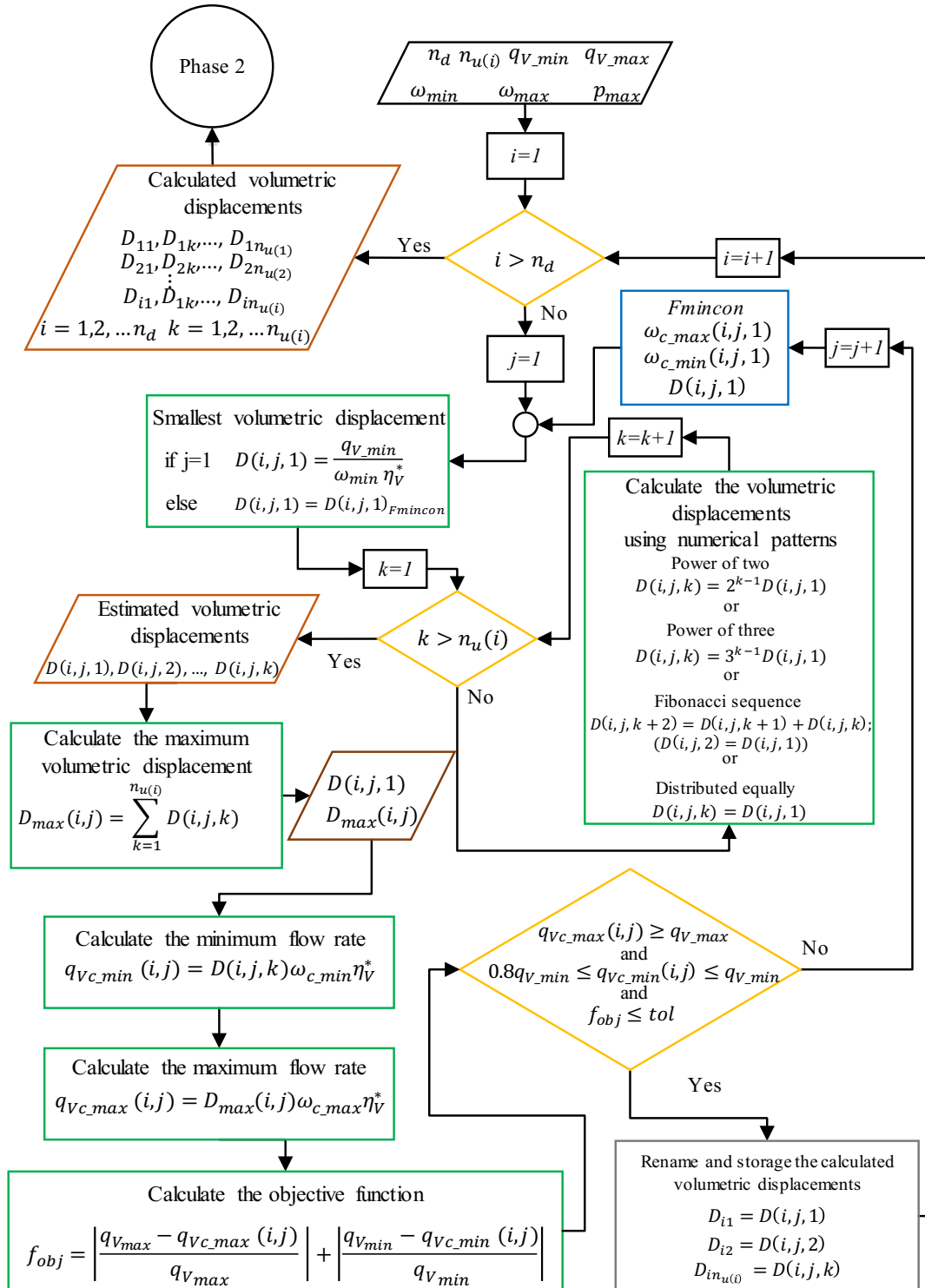
Source: Author.

After the volumetric displacements are determined, the calculated minimum and maximum flow rates (q_{Vc_min} and q_{Vc_max}, respectively) are estimated by

$$q_{Vc\_min}(i,j) = D(i,j,1)\omega_{c\_min}\eta_V^*$$ (4.3)

$$q_{Vc\_max}(i,j) = D_{\max}(i,j)\omega_{c\_max}\eta_V^*$$ (4.4)

The objective function (f_{obj}) expresses sum of the errors of the calculated flow rates in relation to the respective minimum and maximum values and are calculated by

$$f_{obj} = \left|\frac{q_{V\_max} - q_{Vc\_max}(i,j)}{q_{V\_max}}\right| + \left|\frac{q_{V\_min} - q_{Vc\_min}(i,j)}{q_{V\_min}}\right|$$ (4.5)

The constriction functions used in the optimization algorithm are given by

$$0.8q_{V\_min} \leq q_{Vc\_min}(i,j) \leq q_{V\_min}$$ (4.6)

$$q_{Vc\_max}(i,j) \geq q_{V\_max}$$ (4.7)

and
$$f_{obj} \leq tol$$ (4.8)

The objective function is minimized to a certain tolerance (tol). When the above conditions are achieved, the iteration of the optimization algorithm is finished and the last calculated volumetric displacements are determined for the ith DHP. The process is repeated until all n_d DHPs are designed. The optimized variables are the minimum and maximum angular velocities (ω_{c_min}, ω_{c_max}) and the smallest volumetric displacement of the DHP $\left(D(i,j,1)\right)$. Therefore, the optimization algorithm is used to select the volumetric displacements and angular speeds that best fit the objective function of each digital hydraulic pump.

4.2.2 Phase 2 – Data collection, pre-processing and analysis

This Phase comprises 4 steps that are carried out for each digital hydraulic pump configured in Phase 1.

4.2.2.1 Step 1 – Data collection and pre-processing

The first task of this step is to search for manufacturers' datasheets to obtain pumps with volumetric displacement sizes close to or equal to the calculated values obtained in Phase 1. Multiple datasheets can be used to provide a range of different pump sizes (Figure 4.5). Datasheet information is usually presented in a graphical format where it is necessary to pre-process it by capturing the points of the flow and torque curves. Using linear regression, it is possible to obtain the flow rate and torque curves of the pumps for each pressure condition as

$$q_V(p_x) = a_{(px)}\omega_{(px)} + b_{(px)} \tag{4.9}$$

$$T(p_x) = c_{(px)}\omega_{(px)} + d_{(px)} \tag{4.10}$$

where ω is the angular velocity, a, b, c, and d are the coefficients of the linear equations from the datasheets, the subscript p_x is related to the pressure level, q_V is the effective pump flow rate, and T is the effective torque.

Figure 4.5 – Example of manufacturer's datasheets.
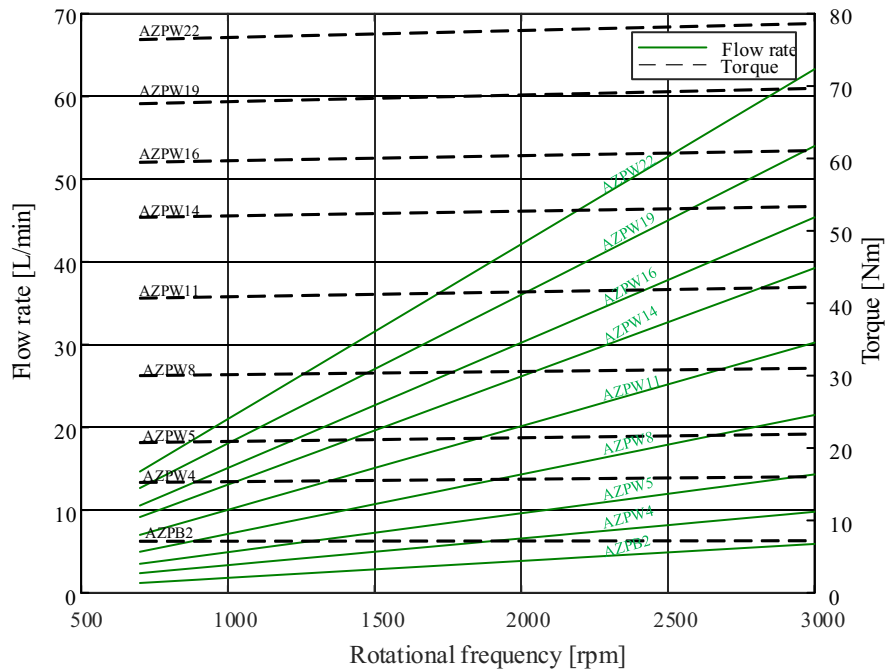
Datasheet information flow rates and torques at 21 MPa of pressure.
Source: Adapted from Bosch Rexroth external gear pump AZPW and AZPB datasheet (BOSCH REXROTH, 2013, 2016).

Normally, the flow and torque curves are presented only for few pressure values. To obtain points at intermediate pressure levels, a linear interpolation between two pressure values is applied, given by

$$f_j(x) = \frac{(x - x_{j+1})}{(x_j - x_{j+1})} y_j + \frac{(x - x_j)}{(x_{j+1} - x_j)} y_{j+1} \qquad (4.11)$$

where x is the point to be calculated, x_j, y_j and x_{j+1}, y_{j+1} are the points before and after the interpolated one, respectively.

With the pump datasheet information, for a given pressure and flow rate condition, the pump angular speed can be calculated using the result from Equation (4.9), as

$$\omega = (q_V - b)/a \qquad (4.12)$$

The volumetric efficiency and mechanical efficiency are given by

$$\eta_v = \frac{q_V}{D\omega} \qquad (4.13)$$

$$\eta_m = \frac{D\Delta p}{T} \qquad (4.14)$$

where Δp is the pressure differential at the pump, D is the volumetric displacement of the pump.

The pre-processed data are used to create a database with information on the pressure, torque, flow rate, angular speed, and mechanical and volumetric efficiencies of pumps.

4.2.2.2 Step 2 – Pump unit selection

In this step, the calculated volumetric displacements of the pump units obtained in Phase 1 are compared with the created database in Phase 2 – Step 1. Volumetric displacements equal to or near to the calculated are selected to be used in the next steps. Pressure, torque, flow rate, angular velocity, and mechanical and volumetric efficiencies are associated for each pump unit, which fully defines each designed digital hydraulic pump (Figure 4.6).

Figure 4.6 – Configuring the DHP with manufacturers' datasheet.
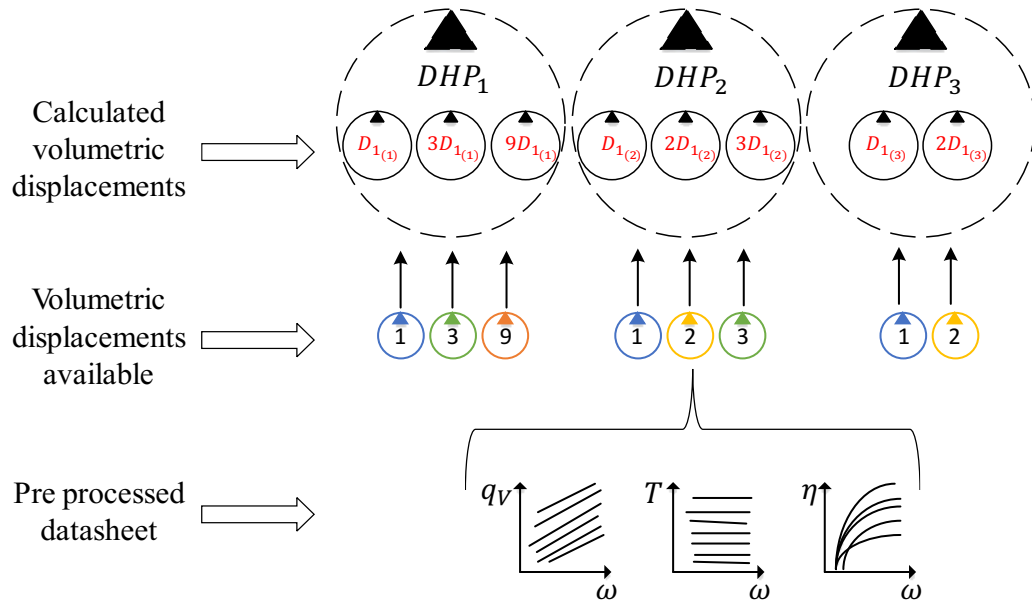
Source: Author.

4.2.2.3 Step 3 – Pump unit combination and mapping

As each DHP has two or more pump units, the number of different pump unit combination (n_{puc}) available to supply flow rate to the system can be described by $n_{puc} = 2^{n_{u(i)}} - 1$. The effective flow rate of the active pump unit combination is obtained summing the effective flow rate of each active pump unit. The flow rate map of each pump unit is obtained by evaluating the flow rate for different pressures and angular velocities within the operation range. Likewise, the effective torque of the pump combination is obtained by summing the individual effective torque (Figure 4.7).

Figure 4.7 – Combination and mapping of pump units.
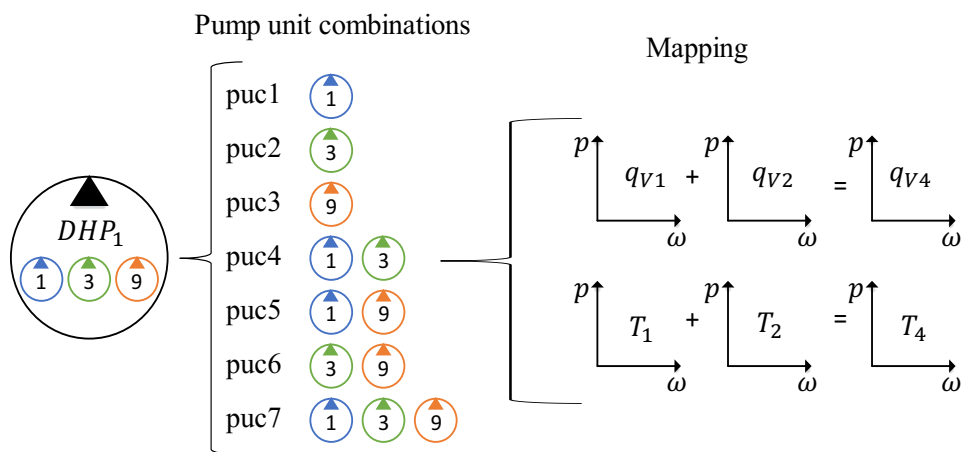
Source: Author.

The overall efficiency of each pump combination is calculated for each pressure and angular velocity condition within the operating range as follows

$$\eta_g = \eta_V \times \eta_m \tag{4.15}$$

$$\eta_v = \frac{q_{Ve}}{q_{Vt}} \tag{4.16}$$

$$\eta_m = \frac{T_t}{T_e} \tag{4.17}$$

where q_{Ve}, q_{Vt}, T_e, and T_t are the effective flow rate obtained from datasheet, theoretical flow rate $(q_{Vt} = \omega D)$, effective torque from datasheet $(T_t = \Delta p D)$, and theoretical torque, respectively.

At the end of this step, the pump unit combinations for each digital hydraulic pump are fully defined with the flow, torque, and overall efficiency maps obtained for the evaluated operating range.

4.2.2.4 Step 4 – Evaluation and selection of pump unit combination

This step aims to select a pump unit combination resulting on the higher overall efficiency for each operating point defined by the pair pressure and flow rate. The first task is to identify the combinations of pump unit capable of fulfilling the operating point within the angular velocity range, described by

$$\omega_{min} \leq \omega_{puc}(p, q_V) \leq \omega_{max} \tag{4.18}$$

where ω_{puc} is the angular velocity of the pump unit combination.

The next task is to compare and choose the pump unit combination that has the best overall efficiency for the assessed operating point, the result is used to create a selection map (Figure 4.8). The selection maps show the pump unit combination that has the best overall efficiency for a given operating condition. In addition, flow rate, pressure, and efficiency information for each pump unit combination is carried over to build the final flow, pressure, and efficiency maps of the digital hydraulic pump. The steps outlined in Phase 2 are carried out for each digital hydraulic pump configured in Phase 1.

Figure 4.8 – Pump unit selection map for a DHP.

DHP_1

p					
puc2	puc3	puc5	puc6	puc7	puc7
puc2	puc2	puc5	puc6	puc6	puc7
puc1	puc2	puc3	puc4	puc5	puc6
puc1	puc2	puc3	puc4	puc4	puc6
puc1	puc1	puc2	puc3	puc4	puc5
puc1	puc1	puc2	puc3	puc4	puc5

q_V
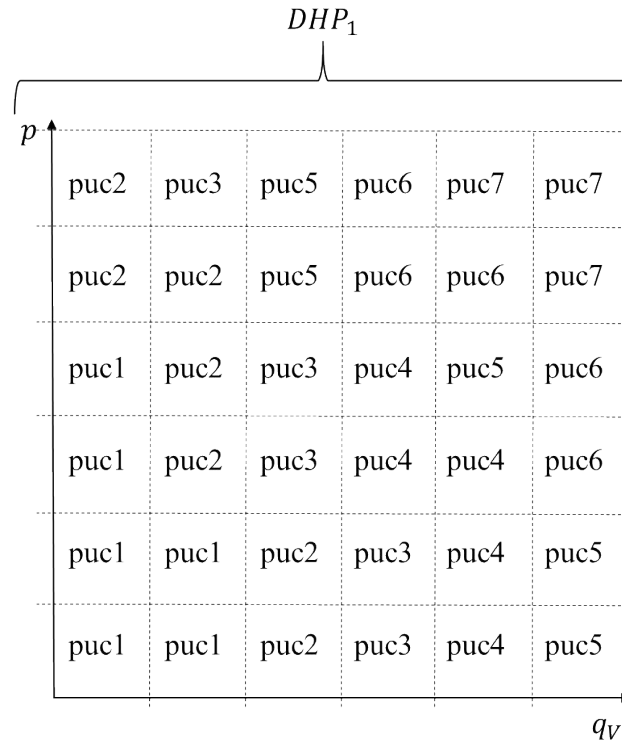
Source: Author.

4.2.3 Phase 3 – Post processing

As presented in Figure 4.2, in this phase, Step 1 consists of calculating the overall average efficiency over the entire operating range of each previously configured digital hydraulic pump, which is based on the efficiency map estimated for each DHP. In Step 2, a rank of the overall average efficiency is created to classify the digital hydraulic pump with the best average efficiency, which gives a quantitative value about the efficiency of the digital hydraulic pumps configured. In Step 3, a final analysis has to be performed, in order to verify other characteristics, such as maximum torque, estimated maximum energy consumption, efficiency at low flow demand, occupied volume, weight, and so on, which must be considered by the designer to define the DHP with the best balance, as the criteria for these characteristics are different for each application.

If necessary, the input data can be changed to obtain other pump settings. However, the database plays an essential role in this process, as the results are directly related to the available data.

4.3 CONCLUSION OF CHAPTER 4

Chapter 4 presented a method for designing a digital hydraulic pump with variable speed using standard pumps from manufacturers. In this approach, it is important to observe that the pumps considered must be connected to the same shaft, running at same speed. In addition, it is important to analyze the results in the post-processing phase to verify that all points in the working range have been met. An application example is presented in APPENDIX B – Design of DHP an example of application.

5 VARIABLE SPEED DIGITAL ELECTRO-HYDRAULIC ACTUATOR

This chapter presents the proposed digital hydraulic actuator, the inspiration to develop the topology, the system description, the design approach used, the component models, the implementation, and the control strategy.

5.1 SYSTEM CONCEPT AND DESCRIPTION

The proposed actuator is based on the application of two concepts. The first is the MEA concept, presented in the Chapter 2, which aims to improve energy savings and energy transport through the use of electrical components. Following this concept, in actuation systems for aircraft control surfaces, the electric motor is the main power source for EHA and EMA, where the control of the motor speed and direction of rotation are often used to control actuator movement. The second is related to the potential for reducing energy dissipation using digital hydraulic systems presented in Chapter 3. Based on this background, this work proposes the use of a digital hydraulic pump with variable speed to supply a symmetrical hydraulic cylinder, resulting in a Variable Speed Digital Electro-Hydraulic Actuator – VSDEHA.

The proposed system can be divided into four main subsystems which are called primary energy conversion, energy limitation and control, secondary energy conversion, and fluid storage and conditioning (LINSINGEN, 2016). The storage and conditioning unit is responsible for the storage, filtration, and heat exchange of the hydraulic fluid. The primary conversion unit is responsible for converting mechanical energy into hydraulic energy. In this case, a digital hydraulic pump (DHP) is used. A matrix of on/off valves is used as limitation and control unit, where the valves are responsible for directing the hydraulic fluid to the cylinder chambers or to the reservoir. A cylinder is used as a secondary conversion unit, which is responsible for converting hydraulic power into linear mechanical power. Figure 5.1 shows the hydraulic diagram of the system proposed.

In idle condition, each pump unit of the digital hydraulic pump is connected to the return line through the normally opened on/off valves 1V1, 1V2, and 1V3. To supply fluid to the cylinder, the on/off valves of the DHP can be actuated individually, closing the way to the reservoir and forcing hydraulic fluid through the check valves (1V4, 1V5, 1V6) toward the cylinder. In this case, to simulate a pressurized reservoir of an aircraft, the return line is pressurized (p_T).

Figure 5.1 – Variable Speed Digital Electro-Hydraulic Actuator.
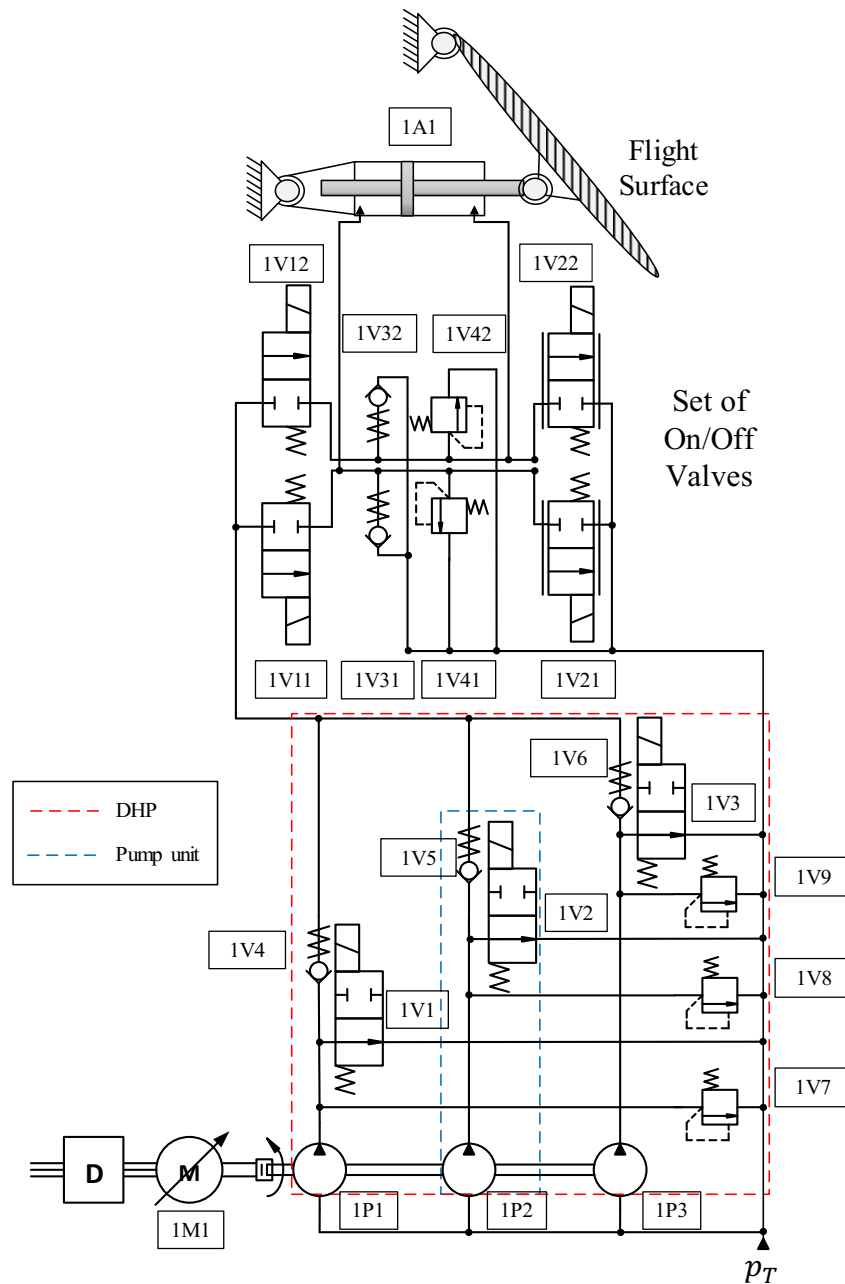
Source: Author.

Each cylinder chamber can be connected to the supply line through the normally closed on/off valves (1V11, 1V12) and to the return line (1V21, 1V22), independently. The direction of movement defines which valves must be actuated to connect the cylinder chambers with the supply or return lines. The cylinder velocity is defined by the pump unit combination of the

DHP and angular speed of the electric motor, which does not need to reverse to change the cylinder direction.

The valves 1V11, 1V12, 1V21, and 1V22, are normally closed directional seat valves. The valves 1V21 and 1V22 are also proportional, where they can work as fully opened or closed on/off valves, and also proportionally to improve system controllability during some conditions, discussed in Section 5.5.4.

The use of the variable speed digital hydraulic pump aims to control the hydraulic energy supplied to the system, applying the power-on-demand concept. The digital hydraulic pump increases the number of different flow rates provided at each rotational frequency, which based on the previous study presented in Chapter 4, it is possible to optimize the use of the pump through the use of more efficient combinations (SILVA *et al.*, 2021).

The main advantage of using a variable speed source is related to cylinder speed control. In earlier digital actuators developed in LASHIP, cylinder velocity was controlled by changing cylinder chamber combinations and the combination between flow source and cylinder chambers during the cylinder movement. In these cases, the number of different velocities is limited by the number of different chambers and flow combinations available, which requires a specific method to design the cylinder areas and the flow rate source to match the desired discrete velocity levels (NOSTRANI, 2021).

In the proposed system, the cylinder velocity is directly controlled by the flow provided by the digital hydraulic pump with variable speed. In this case, the valves of the limitation and control unit are used to direct the flow rate from the DHP to the cylinder chambers. They are not used to change the cylinder chamber combination to change the cylinder velocity. This implies less valve commutation during the cylinder movement since the valve is changed only to change the direction of the cylinder. Another characteristic observed is the reduced number of components, when using a cylinder with two chambers instead of four chambers, fewer valves are needed, making the system more compact.

However, due to technical limitations, it was not possible to implement the system shown in Figure 5.1 in the test bench used to validate the model and serve as a proof-of-concept. Instead, a similar configuration using a circuit assembly from a previous project was used to implement the proposed topology (Figure 5.2). A multi-chamber cylinder was used as a double-chamber cylinder where the chambers were connected in pairs. Following the digital hydraulic concept, each cylinder chamber can be connected to the supply line through the normally closed on/off valves (1V11, 1V12, 1V13, and 1V14) and to the return line (1V21, 1V22, 1V23, and

1V24), independently. A third set of on/off valves (1V31, 1V32, 1V33, and 1V14) is serially connected with a flow metering valve (1V50) to simulate the behavior of the on/off valves when in proportional mode (Section 5.5.4). In order to prevent cavitation in the cylinder chambers, check valves are used to connect the cylinder chambers with the pressurized return line. A relief valve was used to limit the maximum system pressure, for safety reasons.

Figure 5.2 – VSDEHA in a multi chamber cylinder approach.
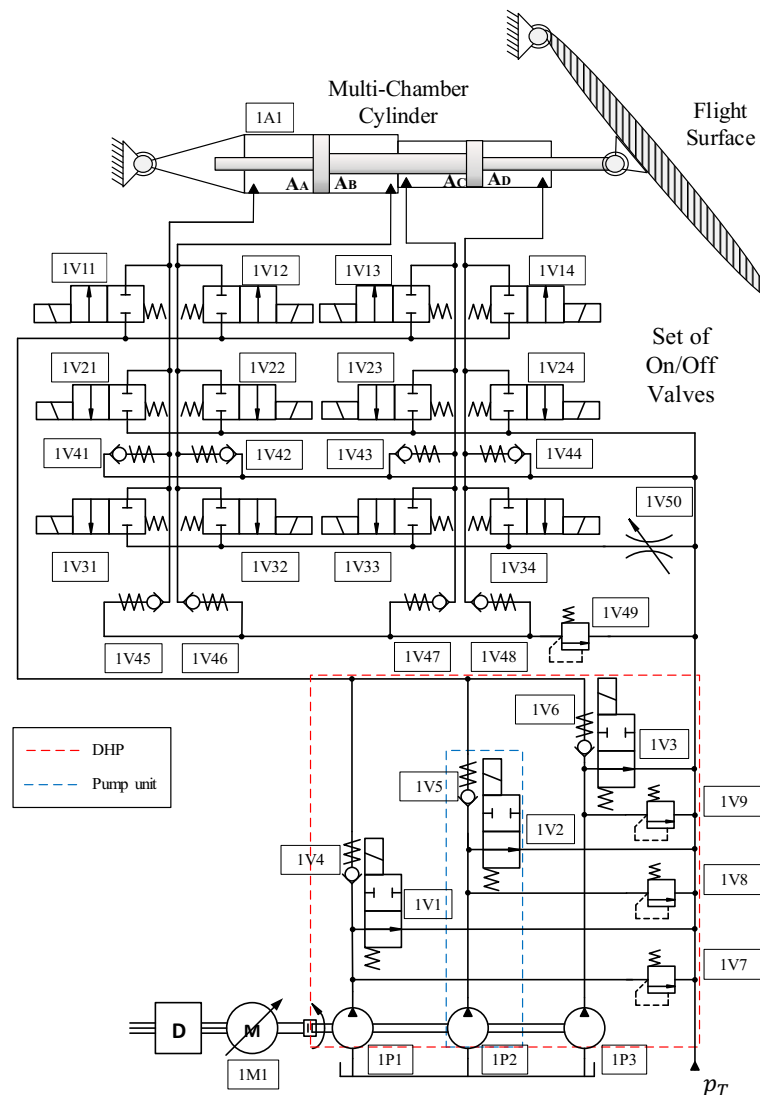
Source: Author.

5.2 DIGITAL HYDRAULIC ACTUATOR SIZING

Currently, at LASHIP, the methodology used to design hydraulic positioning systems is based on the paper "*A design method for hydraulic positioning systems*" (DE NEGRI *et al*.,

2008), where the static and dynamic requirements of the system are used to specify the cylinder and proportional valve. However, in case of digital hydraulic systems, this method is used just to specify the cylinder and the maximum flow rate required.

According to De Negri *et al.* (2008), considering a second-order system without overshooting (damping coefficient equals to 1), the undamped natural frequency is calculated by

$$\omega_n = \frac{6}{t_s} \tag{5.1}$$

where t_s is the desired system settling time.

The maximum acceleration and speed of the system are obtained respectively by

$$a_{max} = x_{max}\omega_n^2 \tag{5.2}$$

and

$$v_{max} = 0.37 x_{max}\omega_n \tag{5.3}$$

where x_{max} is the cylinder steady-state displacement.

Following the method, to define the cylinder area or the maximum load pressure, the system must be evaluated under three different conditions: maximum displacement, maximum speed, and maximum acceleration (De Negri *et al.*, 2008), which are estimated by

$$Ap_c = Kx_{max} + F_u \tag{5.4}$$

$$Ap_c = Bv_{max} + F_u \tag{5.5}$$

$$Ap_c = M_t a_{max} + F_u \tag{5.6}$$

where, F_u is the useful force applied to the load, K is the load stiffness, B is the viscous friction coefficient, M_t is the total mass moved by the actuator, and p_l is the load pressure ($p_A - p_B$).

After defining the cylinder areas, it is possible to estimate the maximum flow rate of the system by

$$q_{vmax} = v_{max}A \tag{5.7}$$

Following the method, the maximum flow rate is used to define the proportional valve, which is used as a limitation and control unit for the flow rate source. However, in the proposed digital hydraulic actuator design, the system is not controlled by a proportional valve. Therefore, from this point on, the method proposed by De Negri *et al.* (2008) is not followed.

The next step is to define the flow rate source for the proposed system. At this point, the maximum flow rate has already been determined and it is necessary to estimate a minimum flow rate based on the minimum cylinder velocity, by equation (5.7) changing it to v_{min} and q_{vmin}, respectively. Therefore, after obtaining the minimum and maximum flow rate of the actuator, the guideline proposed in Chapter 4 is used to design a digital hydraulic pump to be the flow rate source of the actuator.

The system design parameters were based on developing an actuator capable of moving a load of 20 kN, in a step of 0.05 m in a settling time of 1 s, without overshoot. The cylinder and the pumps used in this work were those installed in the test bench from a previous project, such that the design method presented was used to check if the pumps and cylinder were able to be used, the results are presented in the Section 6.1 and 6.3, respectively.

5.3 SYSTEM COMPONENT MODELS

In this section, models of the system components are presented. MatLab/Simulink and Hopsan software were used to implement the models.

5.3.1 Cylinder

In this study, a four-chamber cylinder is considered due to the cylinder available on the test bench. However, the cylinder chambers are connected in pairs to be used as symmetrical double-chamber cylinder. The cylinder is modeled using the equation of motion as

$$M_T \ddot{x} = p_A A_A - p_B A_B + p_c A_c - p_D A_D - F_{fric} - F_L \tag{5.8}$$

where M_T is the total mass moved, $\ddot{x}$ is the acceleration, $p_A, p_B, p_C, p_D, A_A, A_B, A_C$ and A_D are the chamber pressures and areas, respectively; F_{fric} and F_L are the friction and load forces, respectively.

Mapping the behavior caused by friction force is one of the main challenges in modelling hydraulic cylinders for positioning systems. As the friction force shows significant

nonlinearities influenced by system loading, speed, temperature, the direction of motion, lubrication, and surface conditions (VALDIERO, 2005). Tran; Hafizah; Yanada (2012), quotes that hydraulic cylinder friction is dominated by the friction caused between the piston/rod seals and contacting surfaces, the pressures acting on the seals affect the deformation of the seals and may also affect the friction characteristics. These characteristics influence the behavior of the actuator, causing positioning errors and inaccuracies in the system, and must be carefully observed to mitigate their effects.

Friction models can be categorized as static friction models and dynamic friction models. Static friction models are used to describe the steady-state relationship between the friction force and the relative velocity, while dynamic friction models are used to assess friction force based on actual contact state and contact history (AWREJCEWICZ; OLEJNIK, 2005; JAISWAL et al., 2021; MARQUES et al., 2016).

In this work, the LuGre model is used to model the friction forces of the cylinder. The LuGre model is a dynamic model capable of capturing the Stribeck effect, hysteresis, spring-like characteristics for stiction, and varying break-away force (DE WIT et al., 1995). The LuGre model is described in the ANNEX A – LuGre Model.

The continuity equation was applied for each chamber of the cylinder, which is given by

$$q_{V_{in}} - q_{V_{out}} = q_{Vleak} + Av + \frac{V}{\beta_e}\frac{dp}{dt} \tag{5.9}$$

where $q_{v_{in}}$, $q_{v_{out}}$, and q_{vleak} are the input, output and leakage flow rates, respectively, A is the chamber area, v is the cylinder velocity, V is the chamber volume, β_e is the effective bulk modulus, and p is the pressure.

5.3.2 On/Off valves

The on/off valves are the components used to control the direction of the hydraulic fluid in the system. The output of each pump unit is controlled by normally opened directional on/off valve, while the normally closed directional on/off valves are used to direct the flow rate to the cylinder chambers.

The on/off valves were modeled using a orifice equation (LINSINGEN, 2016) given by

$$q_v = c_d A_v \sqrt{\frac{2\Delta p}{\rho}} \tag{5.10}$$

where c_d is a discharge coefficient, A_v is the orifice passage area, Δp is the pressure differential across the valve, and ρ is the fluid density.

In Hopsan, the on/off seat valve is modeled as a leak-free spool (BELAN, 2018), where A_v is given by

$$A_v = \pi d x_{max} f \tag{5.11}$$

where d is the spool diameter, x_{max} is the maximum displacement of the spool, and f is the fraction of the perimeter of the orifice passage area.

According to Belan (2018), the on/off valves may have different dynamics for the opening and closing movement and due to the difficulty of measuring the displacement of the valve plug and obtaining the valve parameters such as plug mass, coefficient of viscous friction, and the stiffness coefficient, the valve dynamics can be modeled as a second order transfer function given by

$$x = \frac{\omega_n^2}{D^2 + 2\xi\omega_n D + \omega_n^2} u_n, \tag{5.12}$$

where x is the spool displacement, u_n is the input signal, ξ is the damping factor, ω_n is the valve natural frequency.

Belan (2018), based on a pre-existing on/off valve model from Hopsan, has implemented the transfer functions to create an on/off valve model with two different movement dynamics. The model also considers two different time delays to represent the solenoid charge and discharge dynamics and two different discharge coefficients, for each flow rate direction. The same model is used in this current work.

Figure 5.3 shows a block diagram of the model in Hopsan, a binary input signal (0 or 1) is used to change the valve position. A different solenoid time delay, blocks (1) and (2), are used according to the current input signal, which is selected by the block (3). Block (4) is the time delay block. Block (5) is used to limit the maximum spool displacement. Blocks (6) and (7) carry the second order transfer functions, which are selected by the flip flop block (8)

according to the position of the valve (9). Blocks (10) and (11) carry the discharge coefficients, which are selected by the block (12) according to the flow rate direction.

Figure 5.3 – On/off valve model in Hopsan.
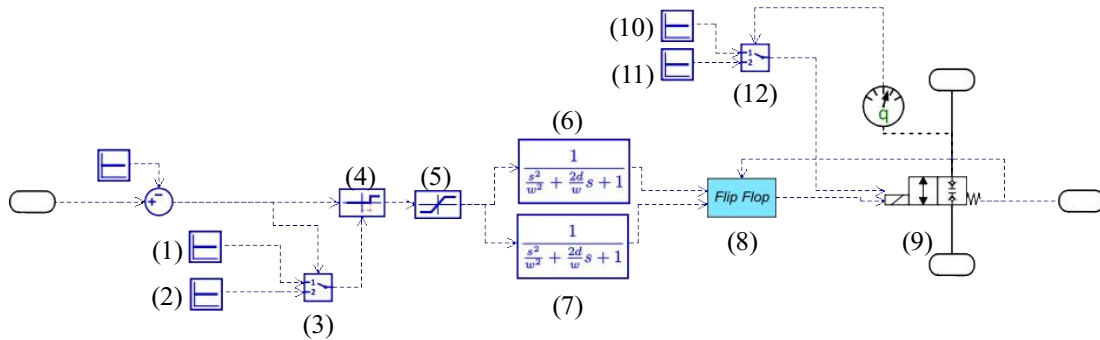
Source: Adapted from Belan (2018).

5.3.3 Check valves

In the proposed hydraulic system, check valves are used in three different positions. The first is to isolate each pumping unit, avoiding the return of the hydraulic fluid. Second, check valves are used in the on/off valve block to prevent cavitation by connecting the pressurized line to the cylinder chambers. Finally, they are also used in the valve block connecting the cylinder chambers with a safety line where the maximum block pressure is limited by a relief valve.

Check valve flows were modeled by the orifice equation (5.10) and their dynamics were modeled by Equation (5.12), where the fluid will only pass through the valves in one direction if there is a pressure difference capable of opening the valve.

Figure 5.4 – Generic check valve view.
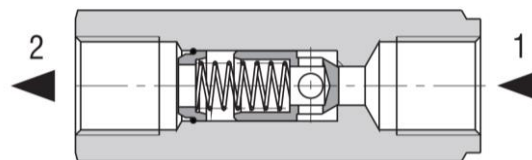
Source: Argo Hytos (2019).

5.3.4 Digital hydraulic pumps

The digital hydraulic pump model is based on the flow and torque maps of each pumping unit. The output flow for each pumping unit is a function of the angular velocity (ω),

pump volumetric displacement (D), and pressure differential across the pump (Δp). For each pump unit, the output flow rate is given by

$$q_{Vreal} = \omega D - q_{Vloss} \tag{5.13}$$

where q_{Vloss} is the pump internal leakage modeled as a laminar orifice equation given by

$$q_{Vloss} = k_{vin}\Delta p \tag{5.14}$$

where k_{vin} is the internal leakage coefficient and Δp is the pressure differential at the pump ports.

The q_{Vreal} is obtained from the flow rate map of each pump unit and the k_{vin} is calculated in real-time simulation by

$$k_{vin} = \frac{(\omega D - q_{Vreal})}{\Delta p} \tag{5.15}$$

The torque is obtained from the torque map of the pumps and it is used as input for the electric motor model according to the pressure variation in each pump unit. The torque and flow rate maps are used as lookup tables where the input variables are pressure and angular velocity.

5.3.5 Electric motor

The bibliographic review presented in Section 2.3 shows that the permanent magnet synchronous motor is the best choice among the electric machines available. However, a three-phase induction motor is more economically viable for developing a proof-of-concept test bench and, therefore, it was used as a power source for the implemented digital hydraulic pump. The three phase induction motor was modeled using the voltage equations following the model presented by Krause *et al.* (2013). Figure 5.5 presents an analogous electrical circuit of the motor where it is possible to apply the concepts of electrical circuits to express parameters such as voltage and flux linkage in terms of reactance, since the machine parameters are generally given in ohms or in per unit of a base impedance.

Figure 5.5 – Equivalent circuits for a three-phase symmetrical induction machine.
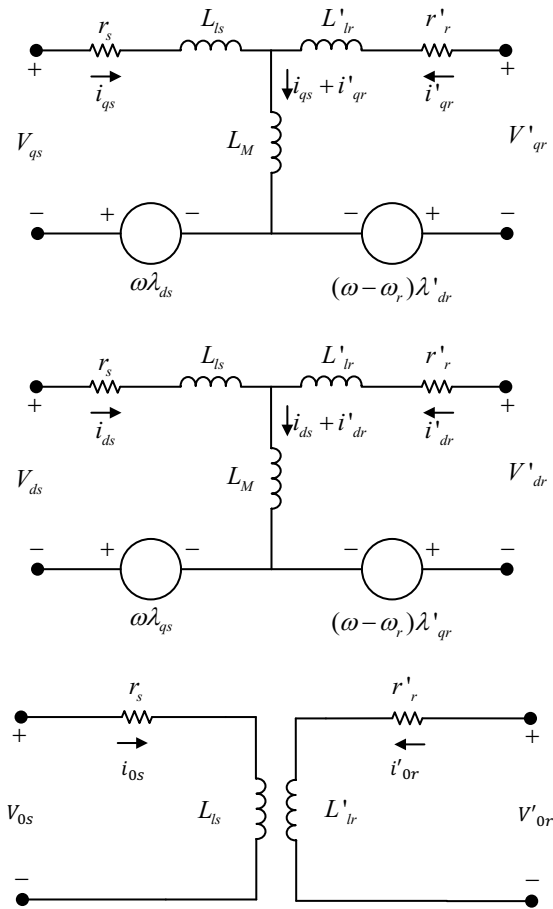
Based on the electrical circuit (Figure 5.5), the voltage equation for the stator and rotor in the quadrature axis (q-axis) can be written as

$$V_{qs} = r_s i_{qs} + \omega \lambda_{ds} + \frac{d}{dt} \lambda_{qs} \tag{5.16}$$

where V_{qs} is the stator voltage, r_s is the stator resistance, i_{qs} is the stator current on q-axis, ω is the electrical angular velocity, λ_{ds} and λ_{qs} are the stator flux linkages given by

$$\lambda_{qs} = \left(L_{ls} + \frac{3}{2}L_M\right) i_{qs} \tag{5.17}$$

and

$$\lambda_{ds} = \left(L_{ls} + \frac{3}{2}L_M\right) i_{ds} \tag{5.18}$$

where L_{ls} and L_M is the self and mutual inductances, respectively, i_{ds} is the stator current on direct axis (d-axis).

For the rotor side the voltage equation is given by

$$V'_{qr} = r'_r i'_{qr} + (\omega - \omega_r)\lambda'_{dr} + \frac{d}{dt}\lambda'_{qr} \qquad (5.19)$$

where V'_{qr} is the rotor voltage referred to the stator voltage, r'_r is the rotor resistance referred to the stator resistance, i'_{qr} is the rotor current referred to the stator current on q-axis, ω_r is the rotor angular velocity, and λ'_{dr} and λ'_{qr} are the rotor flux linkage referred to the stator.

After some mathematical manipulations, the voltage equations can be written as

$$\frac{d}{dt}\Psi_{qs} = \omega_b \left[V_{qs} - \frac{\omega}{\omega_b}\Psi_{ds} + \frac{r_s}{X_{ls}}\left(\Psi_{mq} - \Psi_{qs}\right) \right] \qquad (5.20)$$

$$\frac{d}{dt}\Psi_{ds} = \omega_b \left[V_{ds} + \frac{\omega}{\omega_b}\Psi_{qs} + \frac{r_s}{X_{ls}}\left(\Psi_{md} - \Psi_{ds}\right) \right] \qquad (5.21)$$

$$\frac{d}{dt}\Psi_{0s} = \omega_b \left[V_{0s} - \frac{r_s}{X_{ls}}\Psi_{0s} \right] \qquad (5.22)$$

$$\frac{d}{dt}\Psi'_{qr} = \omega_b \left[V'_{qr} - \left(\frac{\omega - \omega_r}{\omega_b}\right)\Psi'_{dr} + \frac{r'_r}{X'_{lr}}\left(\Psi_{mq} - \Psi'_{qr}\right) \right] \qquad (5.23)$$

$$\frac{d}{dt}\Psi'_{dr} = \omega_b \left[V'_{dr} + \left(\frac{\omega - \omega_r}{\omega_b}\right)\Psi'_{qr} + \frac{r'_r}{X'_{lr}}\left(\Psi_{md} - \Psi'_{dr}\right) \right] \qquad (5.24)$$

$$\frac{d}{dt}\Psi'_{0r} = \omega_b \left[V'_{0r} - \frac{r'_r}{X'_{lr}}\Psi'_{0r} \right] \qquad (5.25)$$

where $\Psi_{mq} = X_{mq}\left(\frac{\Psi_{qs}}{X_{ls}} + \frac{\Psi'_{qr}}{X'_{lr}}\right)$; $\Psi_{md} = X_{md}\left(\frac{\Psi_{ds}}{X_{ls}} + \frac{\Psi'_{dr}}{X'_{lr}}\right)$; $X_{mq} = X_{md} = \left(\frac{1}{X_M} + \frac{1}{X_{ls}} + \frac{1}{X'_{lr}}\right)^{-1}$;

$\Psi_{qs} = \omega_b\lambda_{qs}$; $\Psi_{ds} = \omega_b\lambda_{ds}$; $\Psi_{0s} = \omega_b\lambda_{0s}$; $\Psi'_{qr} = \omega_b\lambda'_{qr}$; $\Psi'_{dr} = \omega_b\lambda'_{dr}$; $\Psi'_{0r} = \omega_b\lambda'_{0r}$;

ω_b and ω_r are the base electrical angular velocity and rotor angular velocity, respectively;

V_{qs}, V_{ds} e V_{0s} are the voltages applied to stator windings; V'_{qr}, V'_{dr} e V'_{0r} are the rotor voltages related to the stator; $\lambda_{ds}, \lambda_{qs}$ e λ_{0s} are the stator flux linkages; $\lambda'_{dr}, \lambda'_{qr}$ e λ'_{0r} are the rotor flux linkages; r_s e r'_r are the stator and rotor resistances, respectively; X_{ls}, X'_{lr} e X_M are the stator reactance, referred rotor reactance, and mutual inductive reactance, respectively, and Ψ denote the flux linkages per second. The subscripts *d*, *q* e *0* are referred to the coordinate direct-quadrature-zero axis and the subscripts *s* e *r* are related to the stator and rotor, respectively.

The electromagnetic torque can be written as

$$T_e = \left(\frac{3}{4}P\right)\left(\lambda_{ds}i_{qs} - \lambda_{qs}i_{ds}\right) \tag{5.26}$$

where P is the pole pairs number, λ_{ds} and λ_{qs} are the flux linkages and i_{ds} and i_{qs} are the stator currents.

The model considers symmetrical phases, symmetrical windings, uniform air gap, linear magnetic circuit, and the mutual leakage between the windings is neglected. For more details about the development of the model, the author recommends the references Krause *et al.* (2013) and Bose (2002).

5.4 SIMULATION MODELS

5.4.1 Hydraulic system and components

The hydraulic system was implemented using Hopsan software. The software was developed by the Department of Fluid and Mechatronic Systems of Linköping University and it is an open-source software based on the Transmission Line Method to simulate the dynamics of the hydraulic systems (BRAUN; KRUS, 2014). Hopsan has a large library of components that make it easy to implement systems without creating components from scratch. However, it is possible to create custom components as the on/off valves used in this thesis. Another advantage of Hopsan is its use in co-simulation with MatLab/Simulink®.

Figure 5.6 shows the Variable Speed Digital Electro-Hydraulic Actuator implemented in Hopsan version 2.14.2, where the components have the same symbols used in hydraulic systems, which facilitates the interpretation of the system. After created, the system is exported as an S-function to be used in Simulink. Input and output ports are used to communicate the

system created in Hopsan with the Simulink environment. The parameters of the components are presented in the mask of the S-function block in Simulink.

The LuGre friction force model is implemented directly in the Simulink and the friction force generated is added to the input force to the cylinder. Table 5.1 presents the list of parameters of secondary components implemented in Hopsan (Figure 5.6). Parameters for check valves and relief valves are taken from the manufacturers' data sheets. Volumes are calculated based on the size of the ducts and manifolds needed to implement the solution, which in this case were sized to the test bench.

Table 5.1 – Parameters used in secondary components of the hydraulic circuit.

Parameters	Value	Unit
Bulk Modulus	1.5×10^9	Pa
Check valve restriction coef.	7.5×10^{-7}	$m^3/(s\text{Pa}^{0.5})$
Check valve crack pressure	2×10^5	Pa
Load mass	27	kg
Oil density	870	kg/m^3
Relief valve opening pressure	1.5×10^7	Pa
Relief valve nominal flow rate	1.667×10^{-3}	m^3/s
Reservoir pressure	1×10^6	Pa
Volume 1	1×10^{-6}	m^3
Volume 2	5×10^{-5}	m^3
Volume 3	3.5×10^{-4}	m^3
Volume 4	1×10^{-4}	m^3

Source: Author.

Figure 5.6 – Digital hydraulic system implemented in Hopsan.
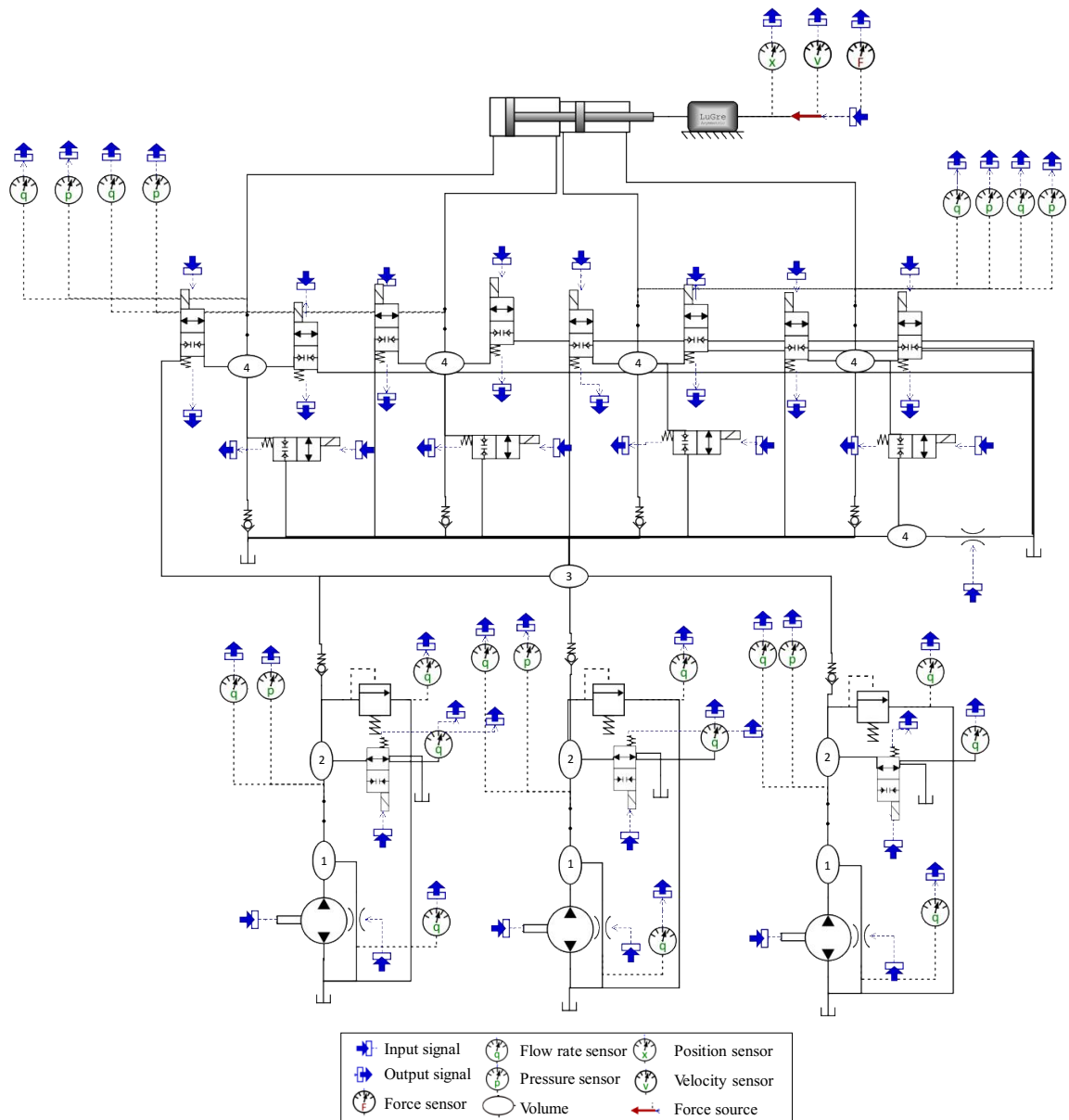
Source: Author.

5.4.2 Electric motor implementation

Firstly, the electric motor model was implemented in Simulink using the equations presented in section 5.3.5. However, the time step needed to simulate the dynamics of the electrical system is about 1×10^{-6} s while the time step used to simulate hydraulic system dynamics is about 1×10^{-3}s. As a consequence, when the two systems were put together the computational cost and time consumption were not feasible.

Another way found to implement the electric motor model was using the Simscape component library in Simulink (Figure 5.7). The MatLab/Simulink user guide and MathWorks help center were crucial in implementing the electric motor system, which was build adapting some parts of the example "Three phase asynchronous drive with sensor control" (MATHWORKS, 2021).

Even though using the Simscape model for the electric motor the computational cost to run the complete hydraulic and electric models together were still high due to the large number of variables that needed to be processed and saved. Consequently, the models where simulated separately.

To run the models separately, the electric motor model needed the rotational frequency command and the torque input from the hydraulic model, while the hydraulic model needed the rotational frequency of the electric motor model. During the development of the digital hydraulic system, to obtain a rotational frequency source, a second order transfer function was used to simulate the dynamics of the electric motor. The rotational frequency command for the transfer function and the calculated pump torque were used as input to the electric motor model. Therefore, the electric motor model is used to obtain the electric power input and to compare the response of the rotational frequency with the test bench and the transfer function used in the hydraulic model. The electric motor model parameters (Table 5.2) were obtained from tests on the electric motor of the digital hydraulic pump (ANNEX B – Electric motor report). The Indirect Field Oriented Control (IFOC) was used to control the electric motor model is presented in the Section 5.5.7.

Table 5.2 – Electric motor parameters.

Parameters	Value	Unit
Stator resistance	0.5538	Ohm
Stator reactance	0.8572	Ohm
Referred rotor resistance	0.5842	Ohm
Referred rotor reactance	1.261	Ohm
Magnetizing reactance	26.58	Ohm
Nominal power	5.5×10^3	W
Rated voltage	380	V
Rated frequency	60	Hz
Pole pairs	2	

Rotational inertia	0.0193955 kgm^2

Figure 5.7 – Electric motor model implemented in Simscape.
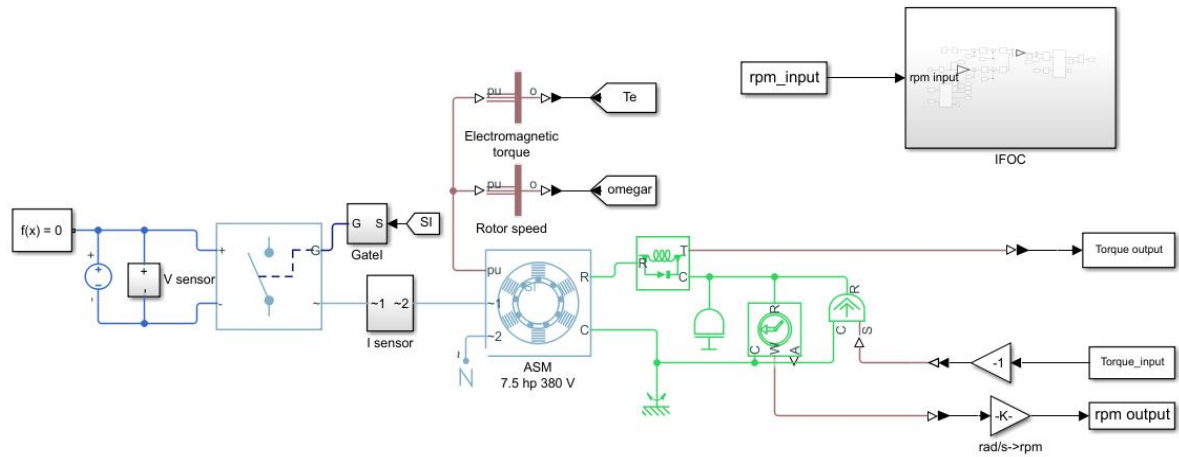
5.5 SYSTEM CONTROL

One of the main advantages of using the digital hydraulics concept is the flexibility to implement different control strategies to control the system due to individually controlled components. In this current work, the proposed system uses a four-chamber cylinder supplied by a variable angular speed Digital Hydraulic Pump. In this case, in addition to controlling the number of active pump units, there is also control of the angular speed of the electric motor, which is selected according to the system demand, in order to improve the overall efficiency of the system.

5.5.1 System control overview

Figure 5.8 presents a block diagram with an overview of the system control. The position reference signal (x_{ref}) is the input to the system, which is compared with the actual cylinder position signal (x_{A1}) resulting in an error signal (e). The error signal is used as input for a Proportional Integrative controller. The output of the controller is interpreted as a flow rate demand, which is the input signal (q_V) to the pump unit selector block. From the required flow rate and system pressure information, the pump unit combination (U_{puc}) and angular velocity command (ω_{cmd}) are chosen based on the digital hydraulic pump maps. In addition,

the torque map of the digital hydraulic pump is used to provide torque load feedback (T) to the electric motor and the flow maps are used to calculate the internal leakage coefficient (k_{vin}) for each pump unit.

Figure 5.8 – System control overview.
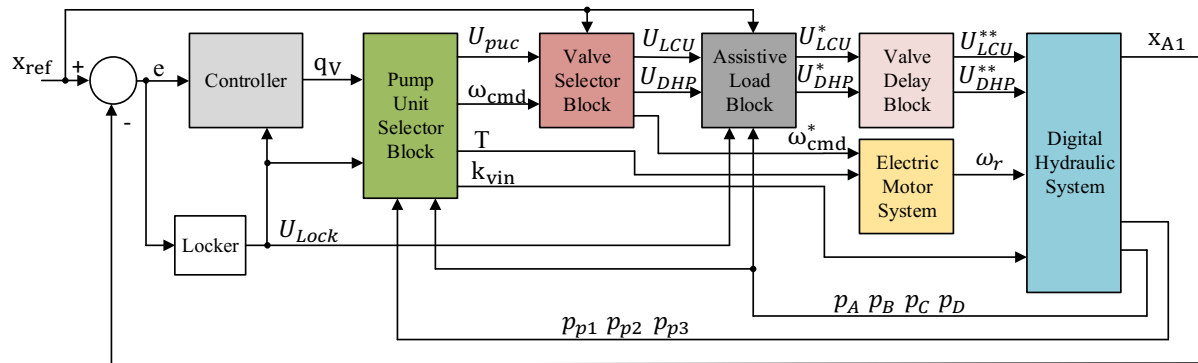
Source: Author.

The cylinder movement direction and the pump unit combination are the inputs to the valve selector block, which is responsible for choosing which on/off valves of the limitation and control unit (U_{LCU}) and digital hydraulic pump (U_{DHP}) should be activated. The valve signal commands are sent to the assistive load block, which is responsible for verifying whether the cylinder is in assisted load condition, changing the return line to be used, modifying the signal to U_{LCU}^*. Next, the valve signals are sent to the delay control block, which is used to control the time delay between the opening and closing movements, synchronizing the valves. Finally, the valve signals U_{LCU}^{**} and U_{DHP}^{**} are sent to the Digital Hydraulic System.

Parallel to the valve selection process, the angular velocity command obtained from the angular velocity map of the DHP is used as input for the Electric Motor System block, which has a speed controller to control the angular velocity of the pump. The system control was implemented in MatLab/Simulink® and more details about the blocks are provided in the next subsections.

5.5.2 Pump unit selector block

The pump unit selector block is based on the maps of the digital hydraulic pump obtained following the design approach presented in Chapter 4. The selection map is used to obtain the pump unit combination needed to achieve the required flow rate in each system pressure. The system pressure is defined by the maximum value of the pressure in the cylinder

chambers, which is supposed to be the pressure in the pump outlet when it is connected to the cylinder chambers.

In parallel to the pump unit selection map, the angular speed map is used to obtain the angular speed of the pump unit combination selected. The maps are implemented in look up tables in Simulink, where the output is related to the input information. In this case, pressure and flow rate are the inputs for the look up tables (Figure 5.9). During the simulation, the torque maps of the pumps are used to calculate the torque load to the electric motor model according to the pump pressures and angular speed. Besides, the flow rate maps of each pump unit are used to calculate the internal leakage coefficient of the pumps.

Figure 5.9 – Pump unit selector block.
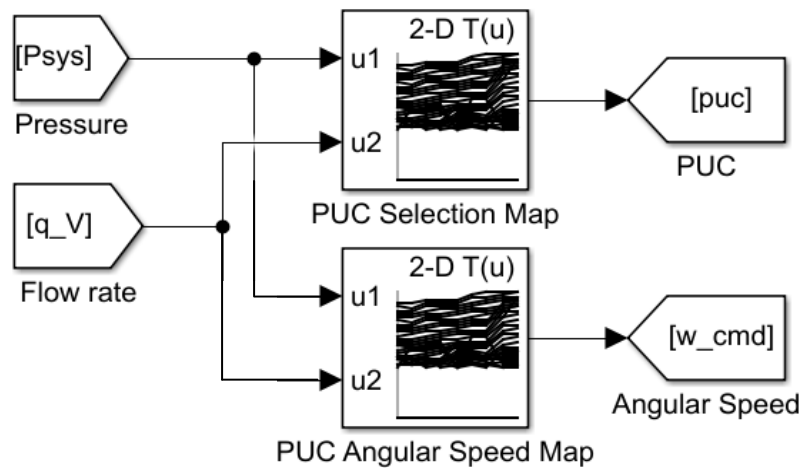
Source: Author.

5.5.3 Valve selector block

One of the advantages of using variable angular velocity is related to the reduction of complexity in valve selection compared to the fixed angular velocity. In the variable angular velocity, the on/off valves of the limitation and control unit are used only to direct the flow rate to the cylinder chambers, according to the direction of movement (Figure 5.10). In this configuration, it is not necessary to change the cylinder valve combination to change the cylinder velocity, which is done in the DHP.

Figure 5.10 – Cylinder movement and valve commutation.
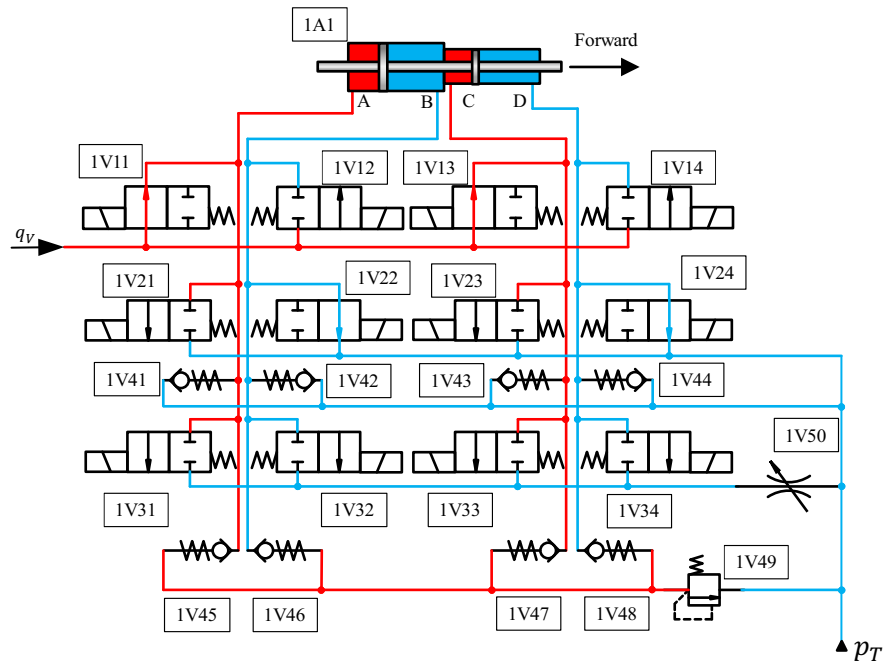
a)
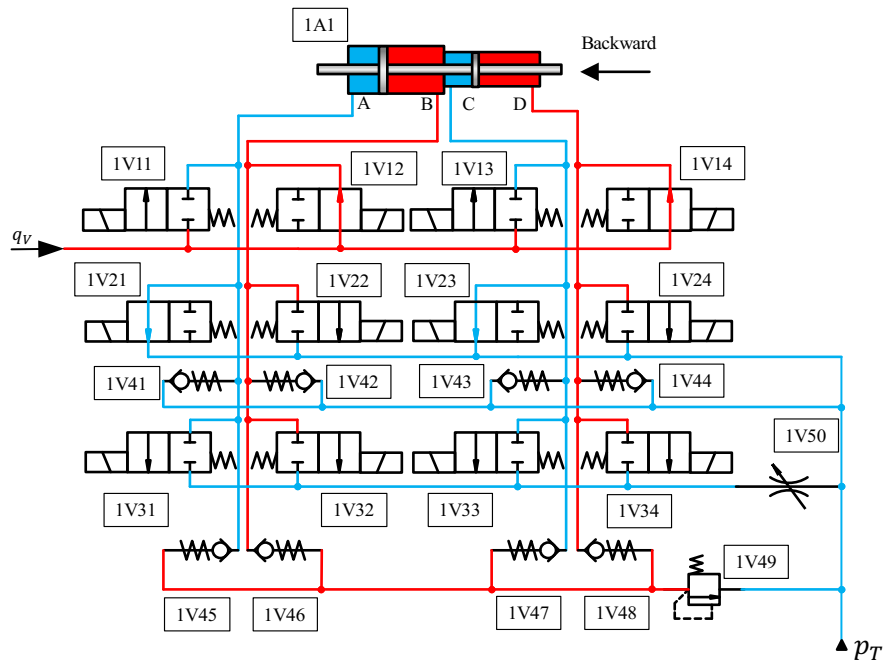
b)

Forward movement (a), backward movement (b).
Source: Author.

Inside the valve selector block a script is used to verify the direction of the movement, to choose the valves that should be turned on or off in the limitation and control unit, and the number of the pump unit combination, to activate the necessary pump units. Since the system

is dynamic, the inputs can be constantly changing. However, a minimum time interval (dT_{min}) is used for a valve combination change to ensure its complete movement due to its dynamics.

5.5.4 Assistive load block

The digital hydraulics is used to avoid the use of throttling control by the use of on/off valves, which are designed to work totally opened or closed. During the development of this work, it was noticed that this concept presents good results under resistive load conditions where the system is working against an external load. When the cylinder is under assistive load conditions, it means that the external load is in the same direction as the cylinder movement, the external load force may be able to increase the cylinder speed to the point where it exceeds the design speed limit.

When the cylinder speed is over the limit, the on/off valves are not able to close fast enough to track the position, which can result in a position overshoot error. In this case, more system energy is consumed to move the cylinder back to the desired position. The extra energy from the load must be managed in order to avoid the overshoot. However, the easiest way to manage the extra energy from the external load is using a dissipative control.

In this thesis, in order to keep using the digital hydraulic control and its characteristics, two return lines were used, where the first return line is a normal line to be used when the system is working under resistive external load while the second return line is used when the system is working under assistive external load. In the second line, the flow rate from the cylinder pass through a throttle valve, which is adjusted to keep the cylinder speed within the designed range.

The assistive load block is used to identify the presence of assistive external load acting in the cylinder, in order to choose the return line with the throttle valve to dissipate the extra external energy and to avoid the cylinder over speed. The cylinder displacement command and the pressures in the cylinder chambers are used to identify the external force acting on the system. The identification process is done using a Fuzzy Inference System – FIS.

Fuzzy logic has been used in a wide range of applications as a powerful tool for dealing with uncertainty, using words for knowledge-based calculations and vague information for decision-making (SIVANANDAM *et al.*, 2007). One of the common applications of Fuzzy is related to the control of systems. According to Ross (2010), unlike standard control systems, devices with Fuzzy controllers provide consumers with optimal settings that are closer to their perceptions and reactions.

In this case, the advantage of using the Fuzzy logic control is related to the range of the fluctuation of the variable values where it is not necessary to use a precise value to control the change of the configuration of the system.

For example, in a Boolean control, if a value is positive or negative, it is possible to set the output as 1 or 0 respectively. However, how positive or negative is the value is not observed by this type of control. If rapid fluctuations occur, the Boolean control may start to toggle between 0 and 1. By using the Fuzzy control, the uncertainty due to the fluctuation of the variable value is represented by a membership level, and the final result takes into account the sum of each membership function to obtain a control output result, avoiding undesired commutation due to fast fluctuations. Furthermore, using the knowledge of the system, it is possible to infer the conditions for obtaining the desired control output, since the behavior of the external load is unpredictable.

The membership functions were developed using the inference method following the analysis in Figure 5.11. When the cylinder is in a stationary condition, without external load force ($F_L = 0$), to move the cylinder forward it is necessary to increase the pressures in the cylinder chambers p_A, which implies a pressure differential ($p_A > p_B$), resulting in a positive hydraulic force (Figure 5.11a). To move the cylinder backward the resultant hydraulic force must be negative ($p_A < p_B$) (Figure 5.11d).

When an external load force acts on the cylinder, this results in a pressure differential to achieve balance. The direction of the external load can be estimated through the pressure differential and according to the movement command, it is possible to deduce whether the load is assistive or resistive. If the pressure differential is positive, it means that p_A is greater than p_B and the external load is compressing the cylinder chamber A. In this condition, if the system receives a command to move the cylinder forward, the external load will act against the movement as a resistive load force (Figure 5.11b). However, if the system receives a command to move the cylinder backward, the external load will act in favor of the movement as an assistive load force (Figure 5.11c). The same logic can be applied to the condition where the pressure differential is negative ($p_A < p_B$)((Figure 5.11e and Figure 5.11f).

Figure 5.11 – Assistive load analysis.

Forward	Forward	Backward
$\longrightarrow$	$\longrightarrow$	$\longleftarrow$
$p_A > p_B$	$p_A > p_B$	$p_A > p_B$
$F_L = 0$	$\longleftarrow F_L$	$\longleftarrow F_L$
	Resistive	Assistive
(a)	(b)	(c)
Backward	Backward	Forward
$\longleftarrow$	$\longleftarrow$	$\longrightarrow$
$p_A < p_B$	$p_A < p_B$	$p_A < p_B$
$F_L = 0$	$F_L \longrightarrow$	$F_L \longrightarrow$
	Resistive	Assistive
(d)	(e)	(f)
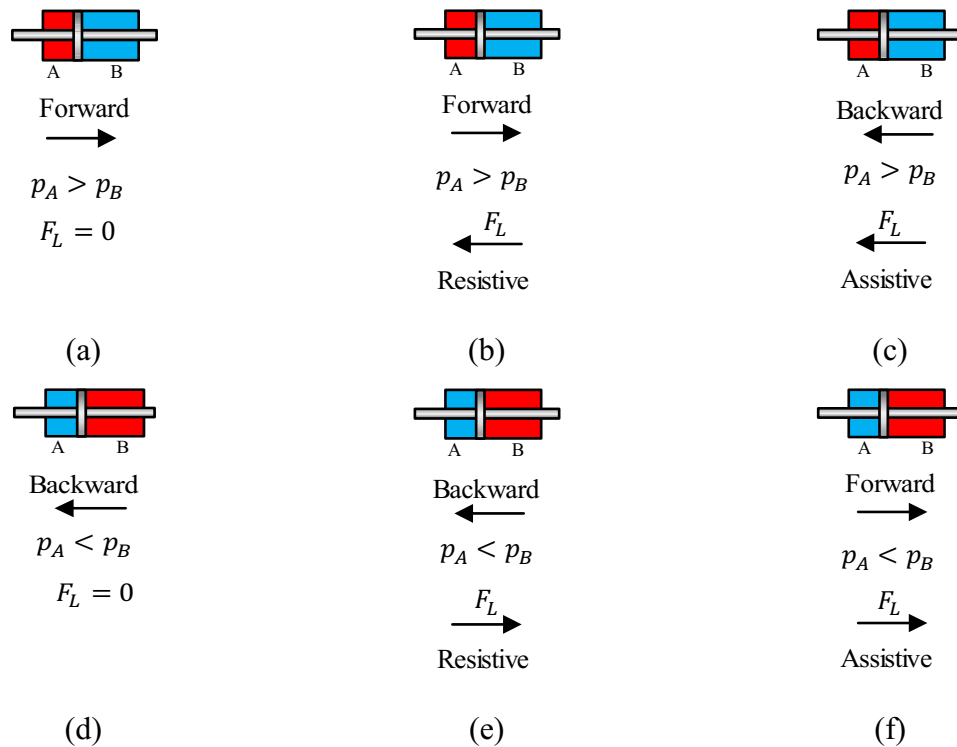
Source: Author.

From this analysis, the membership function of the inputs can be built based on the pressure differential to obtain the external load and its direction and the position reference command to obtain the movement direction information. The position reference command signal is derived to obtain the movement direction signal. A positive sign represents a forward command, while a negative sign represents a backward command.

Figure 5.12 presents the membership functions for the Fuzzy inputs (external load and direction signals) and Fuzzy output (Assistive Load signal). To calculate the effects of the external load, five membership functions were created to represent the information about the direction and intensity of the external load as High Positive (PH), Small Positive (PS), High Negative (NH), Small Negative (NS), and Dead Zone (DZ). For the movement direction, the membership functions created are Back, Front, and Dead Zone (DZ). In both cases, the Dead Zone member function is used to prevent command oscillations due to the noise effect of the sensors.

The output variable represents a value for the assistive load condition, which is represented by three membership functions given by Off (when there is no assistive load), On (when there is assistive load), and Dead Zone, as well as presented before. The membership functions for output signal were created using a spline-based Z-shaped membership function

from the Fuzzy toolbox of MatLab, which was used due to the rapid change in the value to represent the state on or off.

The parameters used to construct the membership functions are given in Table 5.3. Where due to the type of membership function adopted to the assistive load, only two parameters are needed to define the member function.

Figure 5.12 – FIS member functions.
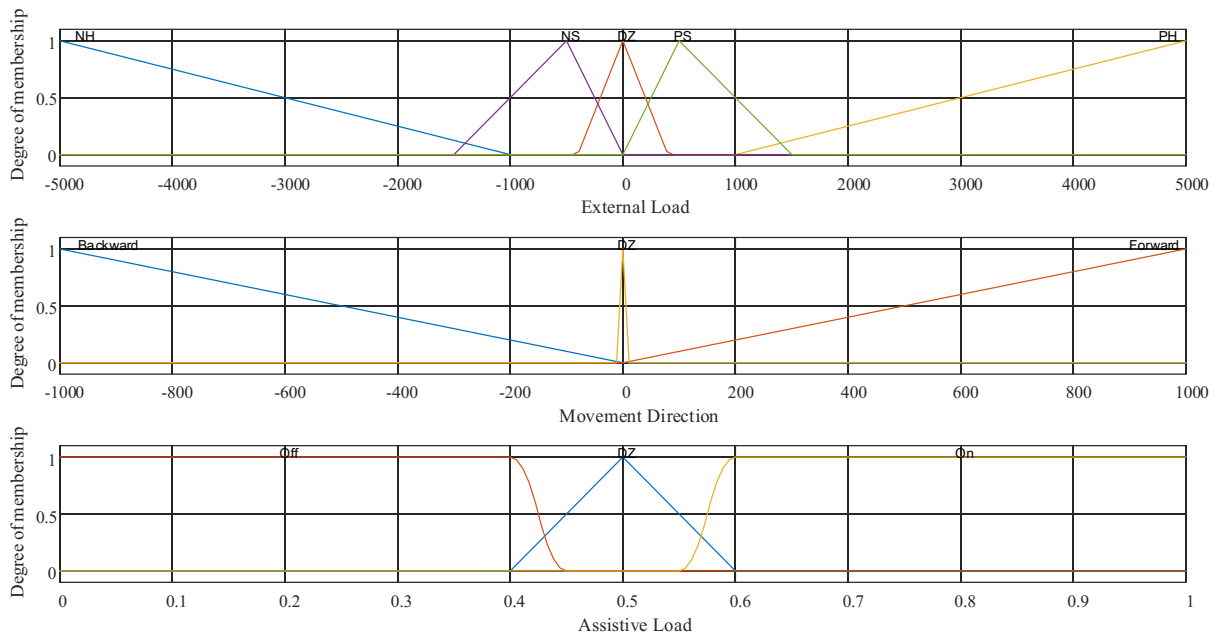
Source: Author.

Table 5.3 – Parameters of membership functions.

External Load				Movement Direction				Assistive Load		
NH	-9000	-5000	-1000	Backward	-1500	-1000	0	Off	0.4	0.45
NS	-1500	-500	0	DZ	-5	0	5	DZ	0.4	0.5	0.6
DZ	-400	0	400	Forward	0	1000	1500	On	0.55	0.6
PS	0	500	1500							
PH	1000	5000	9000							

Source: Author.

According to Ross (2010), in the field of artificial intelligence, the most common way to represent human knowledge is to transform it into natural language expressions, such as the "IF-THEN" type, which is a deductive form that expresses an inference in such a way that if one fact or hypothesis is known, then it is possible to infer another fact called a consequence or

conclusion. Based on this, the rules for the Fuzzy inference system were created using IF-THEN ruled based form as presented in Table 5.4.

Table 5.4 – Rules of the Fuzzy Inference System.

Rules		External Load		Direction		Assistive Load
Rule 1	If	PS	and	Forward	Then	Off
Rule 2	If	PH	and	Forward	Then	Off
Rule 3	If	NS	and	Forward	Then	On
Rule 4	If	NH	and	Forward	Then	On
Rule 5	If	NS	and	Backward	Then	Off
Rule 6	If	NH	and	Backward	Then	Off
Rule 7	If	PS	and	Backward	Then	On
Rule 8	If	PH	and	Backward	Then	On
Rule 9	If	DZ	and	DZ	Then	Off
Rule 10	If	DZ	and	Forward	Then	Off
Rule 11	If	DZ	and	Backward	Then	Off
Rule 12	If	PS	and	DZ	Then	Off
Rule 13	If	NS	and	DZ	Then	Off
Rule 14	If	PH	and	DZ	Then	DZ
Rule 15	If	NH	and	DZ	Then	DZ

Source: Author.

The Mamdani system was used as the deductive inference method, which is the most common in practice and in the literature (ROSS, 2010). The aggregation was performed by sum and the centroid was the defuzzification method adopted. The FIS was implemented using MatLab FIS toolbox. To obtain the valve command signal, the FIS output is filtered and values below 0.6 are interpreted as a low level command (0), which means that there is no Assistive Load, while values above 0.6 are interpreted as a high level command (1), which means the presence of Assistive Load.

5.5.5 Valve delay control block

The delay control block is used to synchronize the opening and closing movement of the on/off valves, according to their dynamic responses and the input command signal, before the command signal is sent to the valves. This synchronization is necessary due to the differences in the time response to open and to close the on/off valves, which can be influenced by the type of actuation used, such as solenoid or spring, and by deviation in the construction characteristics, such as dimensional tolerances, internal friction and so on.

According to Mantovani (2019), due to the dynamics of closing and opening the valves, during the switching of the valves of the same cylinder chamber, two phenomena may occur. The first one is called a short circuit, where during a short period of time the cylinder chamber is connected in two different lines, which can be a high-pressure line and a low-pressure line. When this occurs, part of the hydraulic energy from the high-pressure line is lost by the pressure difference to the low-pressure line. The second case is a blocked cylinder chamber, which occurs when the cylinder chamber is not connected to any lines during valve switching. As a consequence, it can cause cavitation, pressure spikes, or cylinder blockage (MANTOVANI, 2019).

To avoid blocking and short-circuit conditions, it is necessary to synchronize the opening and closing of the valves. When the valves are synchronized, the closing movement ends exactly when the opening movement begins, avoiding or reducing the risk of short circuits and blockage of the chambers (Figure 5.13).

Figure 5.13 – Valve synchronization.
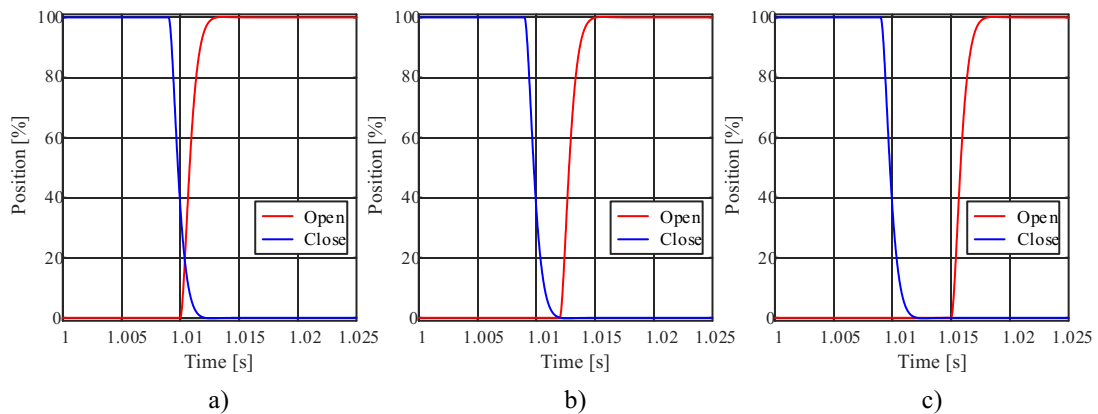
Cylinder chamber configuration: a) Short circuited, b) Synchronized and c) Blocked.
Source: Author.

For example, in Figure 5.13, the signals to open and close the valves are fired up at the same time (1s). Figure 5.13a shows the response of the valves without synchronization delay, which in this case, the time to close the valve is less than the time to open. Therefore, the signal to open the valve must be delayed to synchronize the valves (Figure 5.13b). However, by increasing the time delay, the blocking condition is reached (Figure 5.13c).

According to Mantovani (2019) the minimum time delay (t_{ds}) to synchronize the valves is given by

$$t_{ds} = t_{scd} + t_{scr} - t_{sod},\qquad(5.27)$$

where t_{sod} is the spool open time delay (time to the solenoid be charged), t_{scd} is the spool close time delay (time to the solenoid be discharged), t_{scr} is spool close response time, and t_{sor} is the spool open response time (Figure 5.14)

Figure 5.14 – Time delays of the valves.
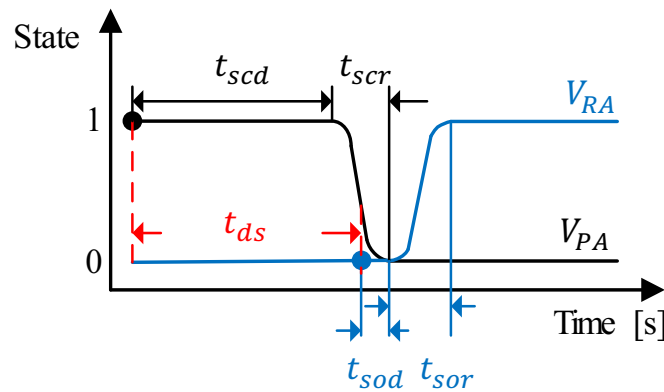
Source: Author, based on Mantovani (2019).

The valve delay block control is used to synchronize the valves during cylinder direction change. In the control of the digital hydraulic pump, it was observed that the short circuit condition is not a problem and it is used to keep the DHP sending flow to the system during the pumping unit commutations, to not stop the cylinder movement.

5.5.6 Locker block

The locker block is part of the adopted control strategy to avoid undesired actuator fluctuations caused by electromagnetic noise present in the position signal. The block compares position error to a certain tolerance. When the error is within the tolerance, the locker is activated and its signal is used in the PI controller to reset the integrator, in the pump unit selector block to change the required flow rate to zero, and it is used to reset the signal of the assistive load block. The tolerance value used to the experiments and simulation was 0.001 m.

$$\begin{cases} |e| \leq tol; locker = 1 \\ |e| > tol; locker = 0 \end{cases}$$

5.5.7 Electric motor control

In this case, electric motor angular speed is controlled using Indirect Field Oriented Control – IFOC. The IFOC estimates the magnetic flux from the applied voltage and the resulting current through the motor model. This makes system behavior highly dependent on machine parameters. However, it is the most common control method applied to induction machines in the industry, due to its good performance compared to the number of parameters required as information for the controller (REZAEI *et al.*, 2018).

Figure 5.15 presents the IFOC block diagram, whose implementation requires measuring the rotor angular velocity and the stator currents. The induction motor with field orientation control works similarly to the direct current motor, where the field orientation control converts the currents/voltages measured in the motor into two components related to field current (i_{ds}) and torque current (i_{qs}), which are decoupled and independently controlled (BOSE, 2002; KRAUSE *et al.*, 2013).

To decouple the currents, the IFOC considers that the magnetic flux and current in the rotor must be perpendicular to each other, which requires two conditions: the rotor magnetic flux on the quadrature axis and the rotor current on the direct axis must be both equal to zero $(\lambda_{qr} = 0; i_{dr} = 0)$. The first condition is met by directing all rotor flux to the direct axis and the second condition is met by keeping the stator current in the direct axis constant (BOSE, 2002; KRAUSE *et al.*, 2013).

Therefore, the magnetic flux (λ_{dr}^*) is kept constant, which in a steady state makes i_{ds}^e constant. Torque or angular speed control can be performed through an external loop, which generates a reference torque (T_e^*) and results in the command of the current i_{qs}^e. The rotor angular frequency information is used to calculate the rotor pole position with respect to the synchronous rotation frequency used in the Clarke and Park transformation to convert the current information from a three-phase reference to the direct and quadrature reference axis. A current control is used to control the stator currents.

Figure 5.15 – IFOC block diagram.
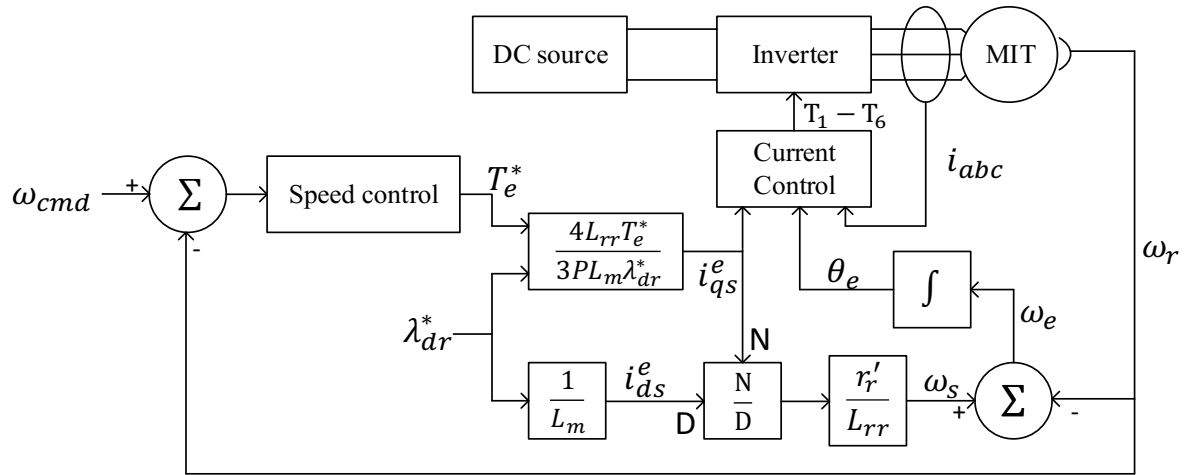
6 TEST BENCH

This chapter presents the test bench, its components, hardware, and software used to carry out the experimental tests. Figure 6.1 presents the hydraulic diagram of the test bench. The subsystems are detailed in the following subsections.

The test bench was built in partnership and collaboration with manufacturers Bosch Rexroth, Hydac, Medal, Nova Motores, and Wipro, which LASHIP is grateful for their support.

Figure 6.1 – Test bench hydraulic diagram.
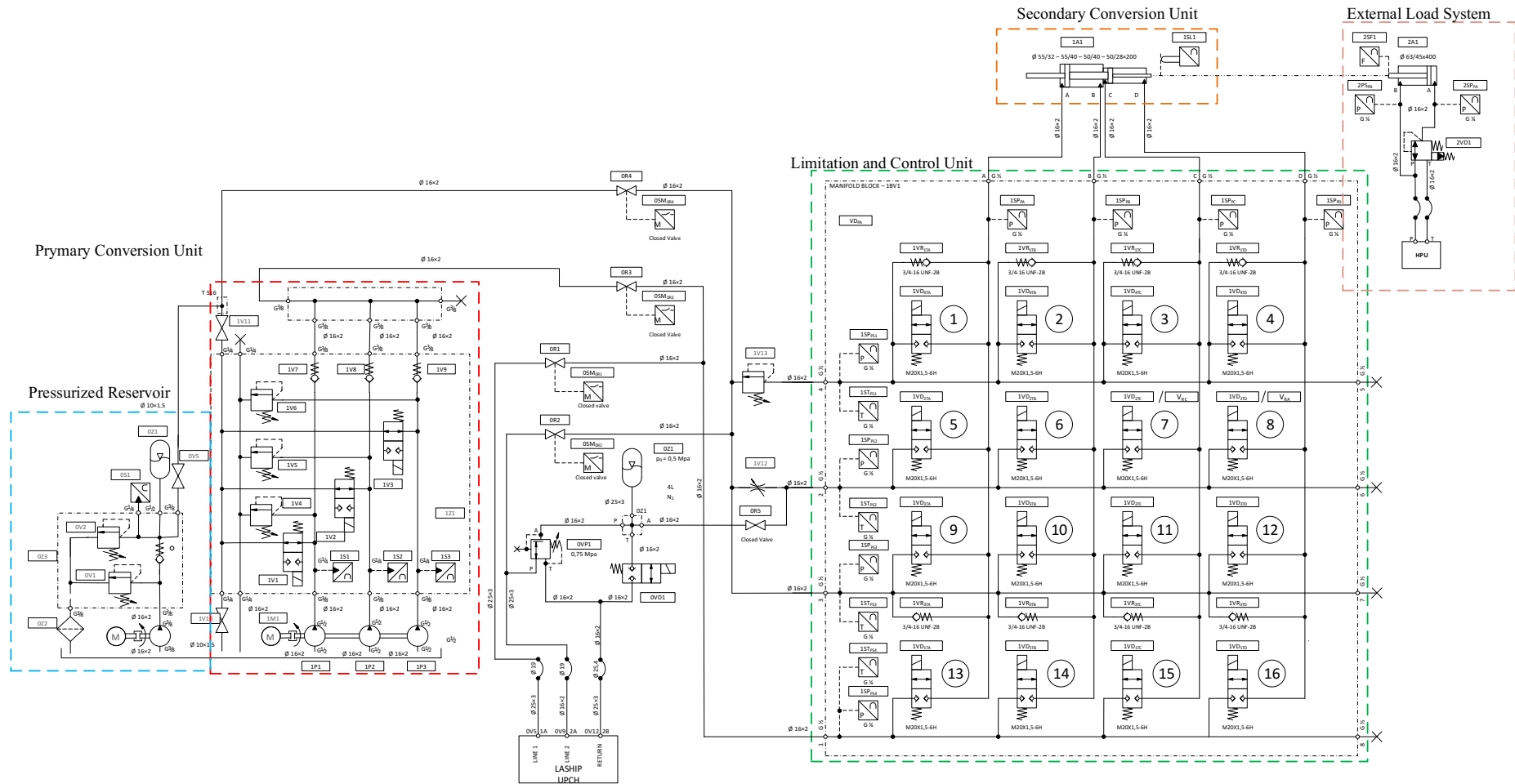
Source: Granted by LASHIP, updated by the author.

6.1 PRIMARY CONVERSION UNIT

In this thesis, the primary conversion unit is a digital hydraulic pump composed of three external gear pumps coupled to the same shaft (1P1, 1P2, 1P3), from the manufacturer Medal. The pumps are prototypes developed by Medal as one of the partners to support the project, they were made to special order as the required pump configuration was not available on the market. The external gear pumps are connected to a 5.5 kW three-phase induction motor (1M1) from Nova motors. The angular speed of the electric motor is controlled by a Siemens M440 frequency inverter, commanded by a signal from the dSPACE control board.

The pump units have different volumetric displacements distributed close to the power of two numerical pattern (2.5, 4, and 6 cm³/rev). However, the numerical distribution was designed for the working conditions presented in Nostrani (2021). On/off directional valves (1V1, 1V2, 1V3) used in each pump unit are from the manufacturer Hydac. The valves are normally opened, which means that, they connect the pump outlet to the reservoir when the valve is not active. Check valves (1V7, 1V8, 1V9) are used to isolate each pump unit individually, preventing backflow from other pump units. For safety, each pump unit line has a relief valve (1V4, 1V5, 1V6) connecting the lines to the reservoir. The pressure in each pump unit outlet is measured through pressure transmitters.

In order to reproduce a pressurized reservoir condition of an aircraft, a secondary hydraulic power unit (HPU) is connected to the return line to keep the line pressurized at 1 MPa (10 bar). The pressure is controlled by a relief valve, which discharges the flow rate to the reservoir. In this case, the pressurized line is also used to prevent cavitation in the cylinder chambers. The line is connected to each cylinder chamber through the check valves in the valve manifold ($1VR_{3TA}$, $1VR_{3TB}$, $1VR_{3TC}$, $1VR_{3TD}$). The digital hydraulic pump also discharges to this pressurized line when running in idle mode. The HPU consists of an external gear pump (0P1) with a volumetric displacement of 1.6 cm³/rev, connected to a 0.37 kW three-phase induction motor (0M1) running at a fixed electrical frequency of 60 Hz, two relief valves (0V1 and 0V2), a check valve (0V3), and an accumulator (0Z1). The pump runs constantly sending hydraulic fluid through a pressure limit valve back to the reservoir (0V2). The relief valve 0V1 is used for safety. The accumulator is used to prevent pressure fluctuations and maintain the pressure of the return line. Table 6.1 present the component list of the primary conversion unit presented in the Figure 6.1.

Table 6.1 – Primary conversion unit component list.

Component	Label	Code
Ball valve	0V4, 1V10, 1V11	Hydac KHB-10SR-1112-03X-A-SW09
Check valves	0V3, 1V7, 1V8, 1V9	Hydac RV08A-01-C-N-145
Electric Motor	0M1	Nova motores M751410A01Z
Electric Motor	1M1	Nova motores M753220A03Z
External gear pump	0P1	Hydac PGE101-160-RBQ1-N-3700
External gear pump prototipes	1P1, 1P2, 1P3	Medal pumps 2.5, 4, and 6 cm³/rev
Filter	0Z1	Hydac RFM 165 BD XX A
Membrane Accumulator	0Z2	Hydac SBO210-2E1/112U-210AB
Pressure transmitters	0S1, 1S1, 1S2, 1S3	Hydac HAD 844K-B-0250-000
Relief valves	1V4, 1V5, 1V6	Hydac DB06A-01-C-N-300F125
Relief valves	0V1, 0V2	Hydac DB4E-01X-100P
Reservoir	1Z2	NG70
Solenoid directional valves	1V1, 1V2, 1V3*	Hydac WSM06020V-01-C-N-0

Source: Author.

6.1.1 Electric motor characterization

To characterize the primary conversion unit, experiments were performed on the electric motor and frequency inverter to obtain the power consumption and power loss under different conditions of angular velocity and torque. The experiments were conducted by Prof. Dr. Carlos A. C. Wengerkievicz and Eng. Cristian F. Mazzola under supervision of the Prof. Dr. Nelson Jhoe Batistela in the LABMAQ/UFSC, which is part of the Grupo de Concepção e Análise de Dispositivos Eletromagnéticos – GRUCAD/UFSC. Figure 6.2 shows the electric power consumption map and the electric motor efficiency map related to the output shaft power of the electric motor and frequency inverter according to its angular speed and torque load condition using indirect field-oriented control mode (ANNEX B – Electric motor report).

Figure 6.2 – Power and efficiency maps of electric motor with frequency inverter.
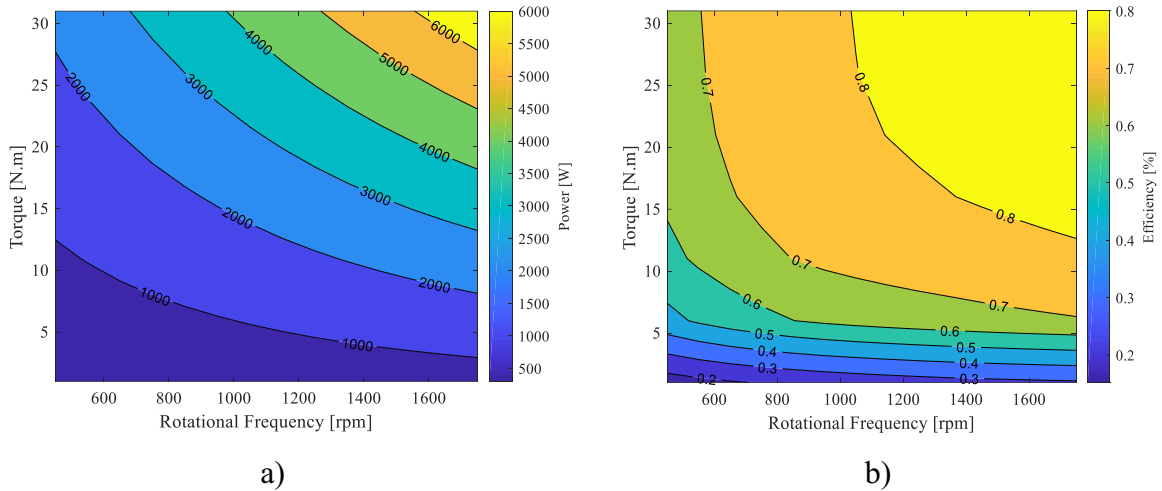
a) Electric power consumption map, b) Electric motor efficiency map.
Source: Author based on the experimental data from GRUCAD report (ANNEX B – Electric motor report)

6.1.2 Digital hydraulic pump characterization

To characterize the digital hydraulic pump, experiments varying the rotational frequency and pressure were performed to obtain the flow rate, electrical power, and torque curves for each pump unit combination of the DHP. Figure 6.3 and Figure 6.4 shows the hydraulic diagram and an image of the system installed at LASHIP, respectively.

During experiments, the DHP output is connected to flow rate and pressure transmitters 1S4 and 1S5, respectively. A relief valve (1V12) is used to adjust the pressure for each test. The experiments were carried out in the pressure range of 2 MPa (20 bar) to 10MPa (100 bar) and in the rotational frequency range of 600 rpm to 1500 rpm. The experimental points were taken at a steady state for each pressure and rotational frequency evaluated. The electrical power consumption was measured using a WEG multi-meter MMW02, connected to the electric lines to obtain the consumption of the DHP, including the inverter.

Using data from the experiments carried out in the characterization of the electric motor it was possible to calculate the torque of the DHP. Figure 6.5 and Figure 6.6 present the flow rate, electrical power and torque curves for each pump unit, respectively. Similar results were obtained to each pump unit combination of the DHP.

Figure 6.3 – DHP hydraulic diagram for flow rate curve experiments.
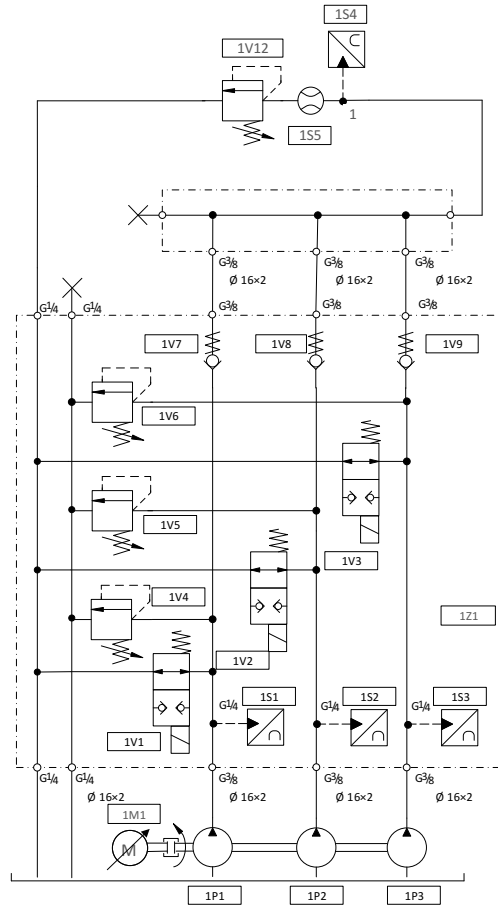
Source: Author

Figure 6.4 – Digital Hydraulic Pump.
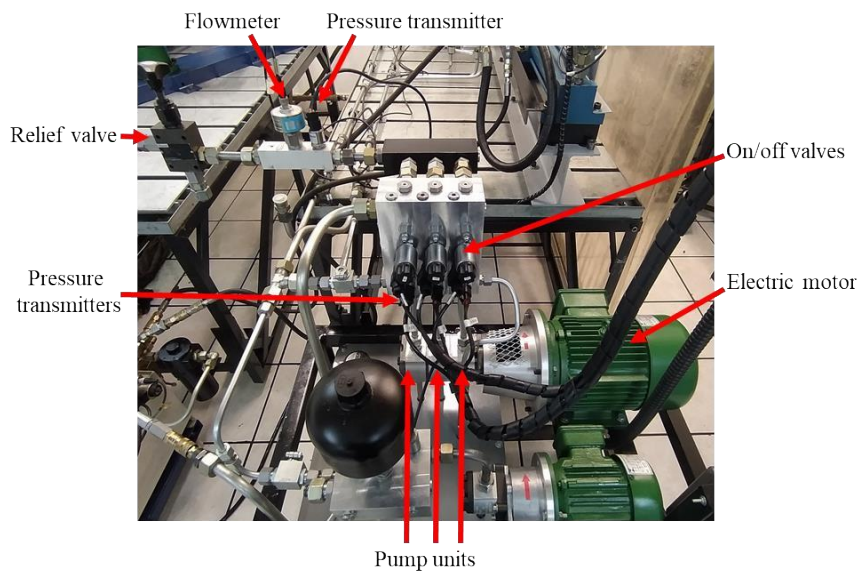
Source: Author.

Figure 6.5 – Pump units flow rate curves of the DHP.

$$y = 2.271 \times 10^{-3}x - 0.4875$$
$$y = 2.354 \times 10^{-3}x - 0.8458$$

a)

$$y = 3.818 \times 10^{-3}x - 0.6580$$
$$y = 3.814 \times 10^{-3}x - 0.8757$$

b)

$$y = 5.749 \times 10^{-3}x - 0.8186$$
$$y = 5.583 \times 10^{-3}x - 0.9095$$
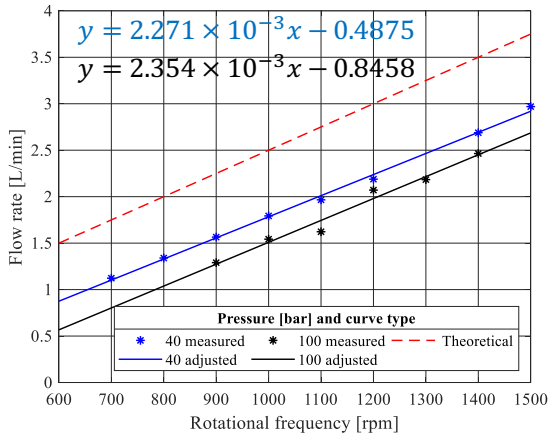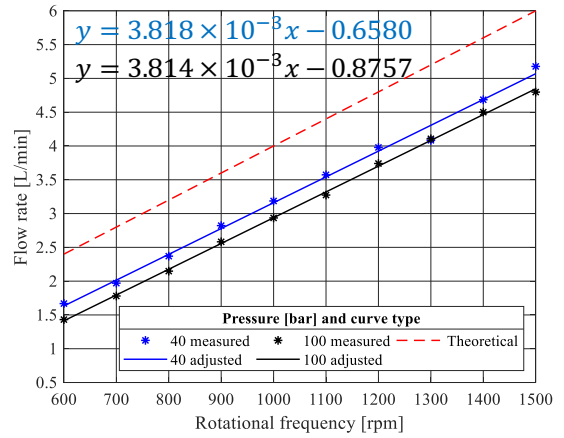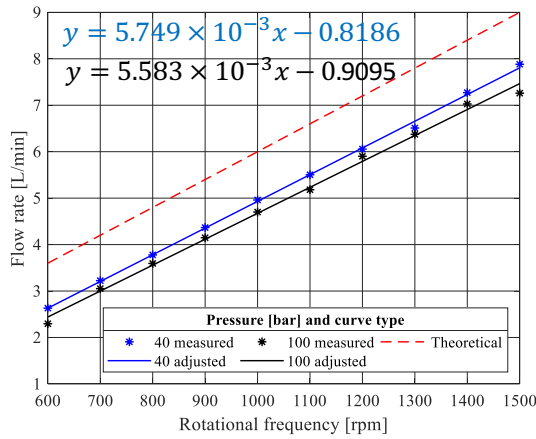
c)

Flow rate curves: a) pump P1: 2.5 cm³/rev, b) pump P2: 4 cm³/rev, and c) pump P3: 6 cm³/rev.
Source: Author.

Figure 6.6 – Power and Torque.
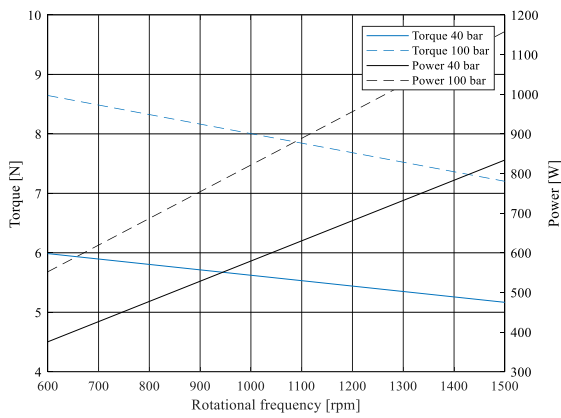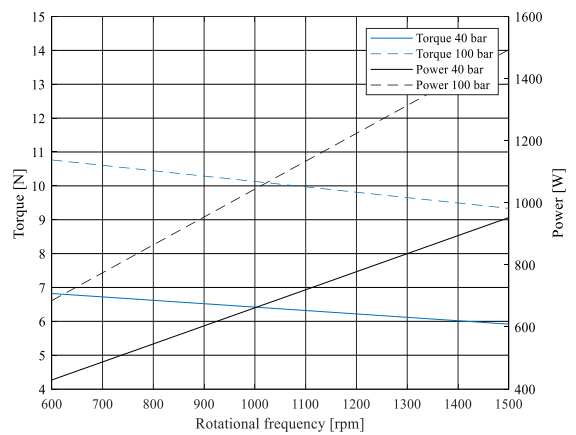
a)   b)
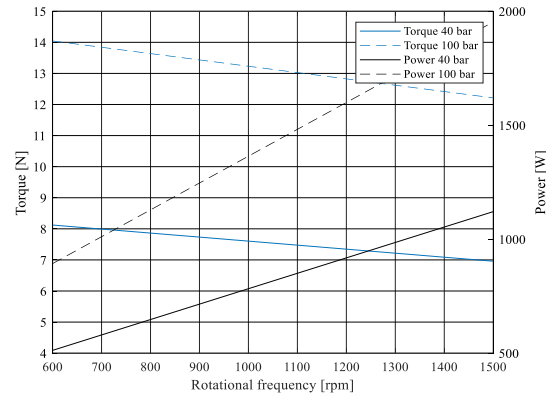
c)

Electrical power and torque curves: a) pump P1: 2.5 cm³/rev, b) pump P2: 4 cm³/rev, and c) pump P3: 6 cm³/rev.
Source: Author.

6.1.3 Maps of the digital hydraulic pump

The digital hydraulic pump maps used in the control strategy to select the pump unit combination and the rotational frequency for the electric motor were obtained applying the method proposed on the Chapter 4. In this case, as the digital hydraulic pump and the cylinder already existed, the method was applied from the Evaluation and Selection phase, to verify if DHP were able to be used following the proposed approach and to select the pump unit combination which gives the best efficiency for each working condition evaluated. Table 6.2 present the results obtained from the actuator sizing, where A_M is the cylinder average area to move forward and backward and p_{max} is the maximum pressure estimated to move the external load of 20 kN.

Table 6.2 – Actuator sizing verification.

Requirements		Results	
t_s [s]	1	v_{max} [m/s]	0.111
x_{max} [m]	0.05	q_{Vmax} [L/min]	15.79
ω_n [rad/s]	6	A_M [m²]	2.37×10^{-3}
		p_{max} [MPa]	9.367

Source: Author.

Based on the results obtained from the actuator sizing verification and from the pump the digital hydraulic pump characterization, it was concluded that the existed DHP is able to be used following the proposed approach, where the maximum flow rate required is within the flow rate range of the pump, considering the variable angular velocity of the electric motor.

Table 6.3 and Table 6.4 are the pump unit selection map and rotational frequency map, respectively. Together, both maps are the core of the system control strategy, used to select the pump unit combination and its rotational frequency in experimental and simulation conditions during the system working.

Table 6.3 – Pump unit selection map of the DHP.

Pressure [bar]	Flow rate [L/min]																
	0	1	2	3	4	5	6	7	8	9	10	11	12	13	14	15	16
20	0	1	3	5	6	7	7	7	7	6	7	7	7	7	7	7	7
30	0	1	2	3	6	7	7	7	6	6	7	7	7	7	7	7	7
40	0	1	2	3	6	6	6	6	6	6	7	7	7	6	6	7	7
50	0	1	3	3	3	6	6	6	6	6	6	6	6	6	6	7	7
60	0	1	3	3	3	3	6	6	6	6	6	6	6	6	6	7	7
70	0	1	3	3	3	3	6	6	6	6	6	6	6	6	7	7	7
80	0	1	3	3	3	3	6	3	6	6	6	6	6	6	7	7	7
90	0	1	3	3	3	3	3	3	6	5	5	6	6	7	7	7
100	0	1	3	3	3	3	3	3	5	5	6	6	6	7	7	7

Source: Author.

Table 6.4 – Rotational frequency map of the DHP.

Pressure [bar]	Flow rate [L/min]																
	0	1	2	3	4	5	6	7	8	9	10	11	12	13	14	15	16
20	0	685	502	504	536	516	599	683	766	1034	932	1015	1099	1182	1265	1348	1431
30	0	639	688	636	538	537	617	698	943	1044	939	1019	1100	1180	1260	1341	1421
40	0	658	696	521	556	658	760	861	963	1065	973	1057	1140	1471	1573	1390	1474
50	0	688	509	680	851	682	781	880	979	1077	994	1275	1374	1473	1572	1400	1481
60	0	732	526	693	859	1026	802	898	994	1090	1185	1281	1377	1473	1569	1402	1479
70	0	729	508	681	855	1029	1203	904	1007	1110	1213	1316	1419	1522	1370	1454	1539
80	0	728	508	682	857	1032	1207	902	1556	1114	1220	1326	1432	1538	1389	1477	1565
90	0	756	514	691	868	1044	1221	1398	1575	1138	1463	1589	1454	1560	1413	1496	1579
100	0	798	521	700	879	1058	1237	1417	1596	1360	1487	1376	1484	1593	1436	1522	1609

Values presented in rpm.
Source: Author.

The numbers shown in Table 6.3 refer to the combination of the pumping units used, where numbers 1, 2, and 3, mean pump P1, pump P2, and pump P3, respectively. The numbers 4, 5, 6 and 7, mean the combination of pumps P1+P2, P1+P3, P2+P3, and P1+P2+P3, respectively. Associated to the selection map and rotational frequency map are the overall efficiency map (Table 6.5) and torque map (Table 6.6) for each pump unit combination respectively.

Table 6.5 – Overall efficiency map of the DHP.

Pressure [bar]	Flow rate [L/min]																
	0	1	2	3	4	5	6	7	8	9	10	11	12	13	14	15	16
20	0	0.10	0.23	0.32	0.38	0.46	0.48	0.53	0.54	0.56	0.60	0.63	0.62	0.61	0.58	0.55	0.53
30	0	0.14	0.26	0.36	0.45	0.50	0.53	0.58	0.60	0.62	0.66	0.68	0.68	0.68	0.66	0.65	0.64
40	0	0.17	0.30	0.41	0.48	0.52	0.56	0.60	0.63	0.65	0.67	0.68	0.69	0.69	0.71	0.68	0.68
50	0	0.20	0.37	0.44	0.49	0.54	0.58	0.62	0.65	0.67	0.68	0.70	0.71	0.73	0.74	0.72	0.72
60	0	0.21	0.38	0.46	0.52	0.55	0.59	0.63	0.66	0.68	0.70	0.72	0.74	0.76	0.77	0.75	0.76
70	0	0.23	0.42	0.49	0.55	0.58	0.61	0.65	0.66	0.68	0.70	0.72	0.74	0.75	0.74	0.75	0.76
80	0	0.25	0.44	0.51	0.57	0.60	0.63	0.66	0.68	0.69	0.71	0.73	0.75	0.76	0.75	0.76	0.78
90	0	0.26	0.45	0.52	0.59	0.61	0.64	0.67	0.70	0.69	0.71	0.74	0.75	0.77	0.75	0.77	0.79
100	0	0.26	0.46	0.53	0.60	0.61	0.65	0.68	0.71	0.69	0.72	0.73	0.75	0.77	0.75	0.78	0.80

Source: Author.

Table 6.6 – Torque map of the DHP.

Pressure [bar]	Flow rate [L/min]																
	0	1	2	3	4	5	6	7	8	9	10	11	12	13	14	15	16
20	0	0.80	0.83	1.17	1.54	1.81	2.39	2.25	2.52	1.82	2.34	2.28	2.62	2.87	3.21	3.55	3.90
30	0	1.23	1.61	2.13	2.99	3.80	4.26	4.25	3.30	3.44	4.22	4.27	4.58	4.78	5.01	5.25	5.51
40	0	1.61	2.24	3.69	4.56	4.98	5.09	4.90	4.84	5.08	6.13	6.36	6.60	5.33	5.42	7.07	7.31
50	0	2.03	3.31	3.31	3.95	6.58	6.64	6.31	6.42	6.67	8.10	6.77	6.72	6.77	6.86	8.74	8.93
60	0	2.47	4.23	4.23	4.78	5.08	8.14	7.68	8.01	8.25	8.35	8.23	8.16	8.21	8.29	10.38	10.51
70	0	2.87	4.94	5.79	5.65	6.00	6.09	9.13	9.61	9.81	9.83	9.64	9.59	9.68	12.02	12.06	12.16
80	0	3.27	5.76	6.70	6.49	6.93	6.96	10.55	6.95	11.32	11.29	11.07	11.02	11.11	13.64	13.66	13.71
90	0	3.64	6.61	7.66	7.28	7.85	7.81	7.62	7.76	12.82	10.62	10.65	12.45	12.54	15.22	15.22	15.21
100	0	3.96	7.46	8.62	8.05	8.77	8.64	8.44	8.56	11.86	11.80	13.84	13.88	13.96	16.80	16.74	16.68

Values presented in N.m.
Source: Author.

To reduce the size, the maps presented here were reduced, showing the flow rate in steps of 1 L/min, from 0 to 16 L/min. However, in the experiments and simulations, the maps are refined in steps of 0.1 L/min. The refinement is important to observe the limit of the working area of each pumping unit combination and observe the presence of isolated pump unit combinations. The isolated pump unit combination occurs when a given pump unit combination appears in the map surrounded by different pumping unit combinations (Figure 6.7a). This occurs due two main factors:

Firstly, the rotational frequency for the evaluated point is only achieved by the pump unit selected, and the second is that the pump unit combination selected has a higher efficiency. However, as the process is totally numerical sometimes the difference of efficiency from two different combinations are very small. Therefore, when isolated pump unit combinations appears it is recommended to check if the predominant combination of the area is not able to

be used due to rotational frequency limitation or difference in efficiency, to avoid the number of consecutive changes in the pump unit combination in a short interval. As an example, observing Figure 6.7a, for a pressure coordinate of 40 bar and flow rate of 3 L/min the difference in efficiency between the pump unit combination number 3 and number 5 is small and can be neglected. In order to avoid two consecutive switching during a pressure fluctuation, the map can be adjusted to Figure 6.7b. The same process is used to evaluate other points by following the pressure and flow rate directions on the map.

The points were deeply analyzed and manually modified without significantly degrading system performance (Figure 6.7b). After the adjustment the average efficiency of the DHP changed from 54.85% to 54.84%, considering the full map. The rotational frequency, efficiency and torque maps were updated according to the selection map as well.

Figure 6.7 – Isolated pumping unit combinations.
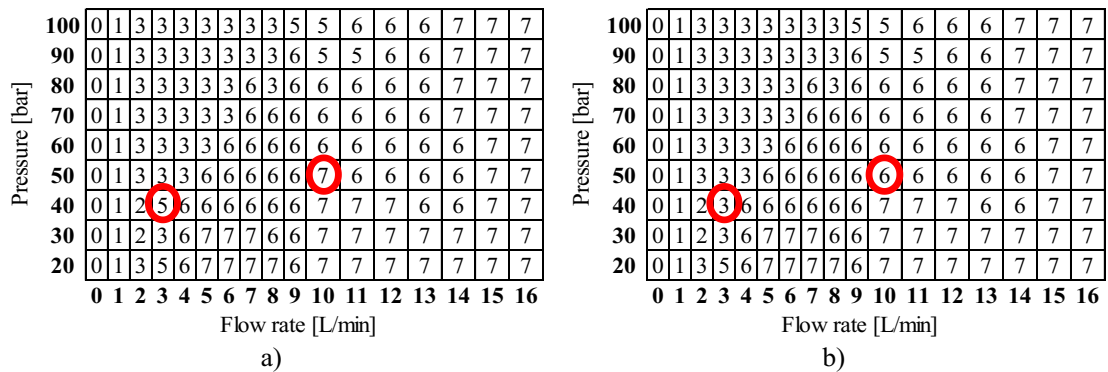
Original selection map (a), adjusted selection map (b).
Source: Author.

6.2 LIMITATION AND CONTROL UNIT

The valve manifold was first developed by Belan (2018) and a second version of the valve manifold was used by Nostrani (2021). The manifold comprises four hydraulic lines and sixteen on/off valves connecting each cylinder chamber with each hydraulic line. The manifold was developed to be multifunctional, allowing the implementation of different control strategies by using different hydraulic lines and valve combinations, thus obtaining a multimode system. For example, Belan (2018) has used three lines supplied by constant pressure, and Nostrani (2021) has used two lines for work and one for an anti-cavitation system (Figure 6.8).

In this thesis, all four supply lines of the valve manifold are used due to the adopted control strategy. The first line is used as a supply line. A second line is a normal return line to the reservoir. The third line is the return line used in the assisted load condition, which has a throttling valve, and the fourth line has a pressure relief valve for safety. However, the on/off valves, of the pressure relief line, are not used. The chambers are connected through check valves. Therefore, only 12 on/off valves are used to control the cylinder (valves numbers 5 to 16 in Figure 6.1). The on/off valves are able to operate under a pressure differential of 35 MPa, and present a flow rate of 20 L/min under a pressure differential of 2 MPa. Table 6.7 presents the list of components of the limitation and control unit.

Figure 6.8 – Valve manifold.
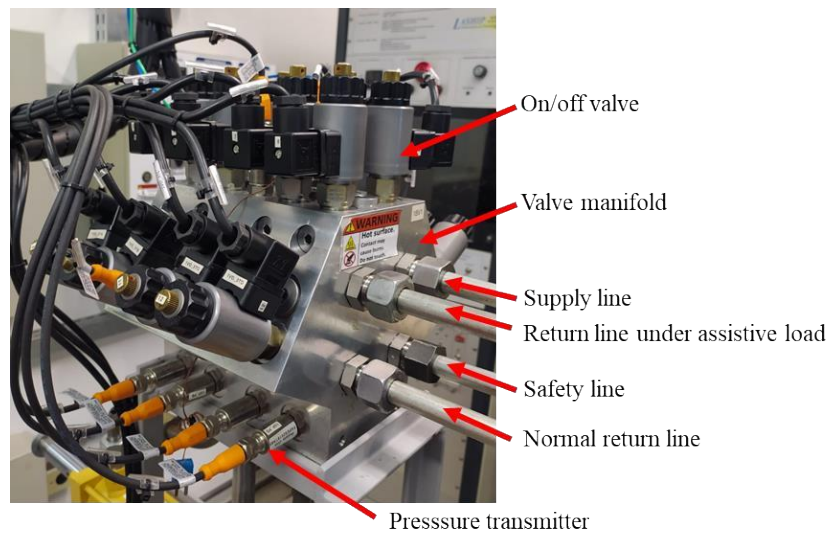
Source: Author.

Table 6.7 – Limitation and control unit component list.

Component	Label	Code
Check valve poppet type	$1VR_{xTA}$, $1VR_{xTB}$, $1VR_{xTC}$, $1VR_{xTD}$	Bosch Rexroth 04.31.20.00 56 Z 00
Directional on/off valves	$1VD_{xTA}$, $1VD_{xTB}$, $1VD_{xTC}$, $1VD_{xTD}$	Bosch Rexroth KSDER1NB/HN11V
Proportional solenoids	$1VD_{xTA}$, $1VD_{xTB}$, $1VD_{xTC}$, $1VD_{xTD}$	Bosch Rexroth Class H 37-X-RY-Y 00
Relief valve	1V13	Bosch Rexroth DBDH6 G 18/100
Throttling valve	1V12	Stauff
Pressure transmiters	$1SP_{PSx}$, $1SP_{PA}$, $1SP_{PB}$, $1SP_{PC}$, $1SP_{PD}$	IFM PU5401

x: Number of valve block line.
Source: Author.

6.2.1 Limitation and control unit characterization

The main components of the limitation and control unit are the directional on/off valves. They are used to control the cylinder movement and present a significant impact on the system behavior. The characterization of on/off valves consists of determining their flow coefficient and their dynamics.

Nostrani (2021) carried out the experimental characterization of the on/off valves used in the valve blocks. Different flow rates were applied to the on/off valve to obtain the valve pressure drop in both flow directions and calculate the flow coefficient. The average flow rate coefficient obtained for the valve port 1 to 2 was 2.790×10^{-9} m^3/(sPa$^{0.5}$) and for the port 2 to 1 was 2.691×10^{-9} m^3/(sPa$^{0.5}$) (NOSTRANI, 2021). Figure 6.9 presents the hydraulic diagram of the test bench used in the on/off valve characterization.

Figure 6.9 – Hydraulic diagram of the test bench.
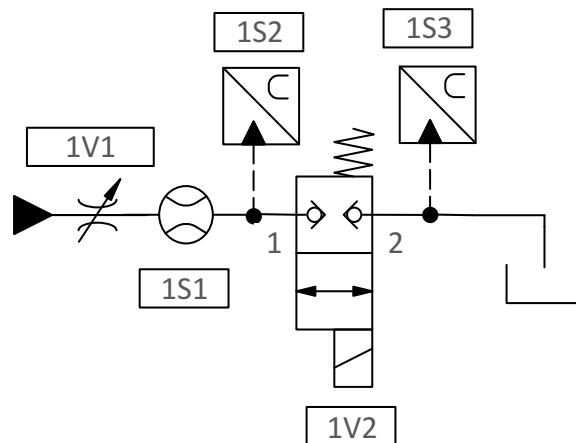
Source: Nostrani (2021).

The same test bench (Figure 6.9) was used to obtain the dynamics of the on/off valves. According to Breidi *et al.* (2014) and Nostrani (2021) the time delay in opening the valve (t_{sod}) is obtained in the period between the application of the signal (point A) and the time in which the pressure drops 10% of its value (point B) (Figure 6.10a). In a similar way, the valve closing time delay (t_{scd}) is obtained (Figure 6.10b). The valve opening response time (t_{sor}) and valve closing response time (t_{scr}) are estimated from the period of time between the pressure achieving 10% to 90% of the steady-state values, points B and C (NOSTRANI, 2021). Table 6.8 presents the estimated parameters of the normally closed valves used in the block of valves of the limitation and control unit and the estimated parameters of the normally closed valves used in the digital hydraulic pump.

In order to dissipate the extra external energy, the throttling valve was adjusted manually to obtain a flow coefficient of $1 \times 10^{-10} m^5/Ns$, based on simulation results.

Figure 6.10 – On/off valves response time characterization.

a)

b)
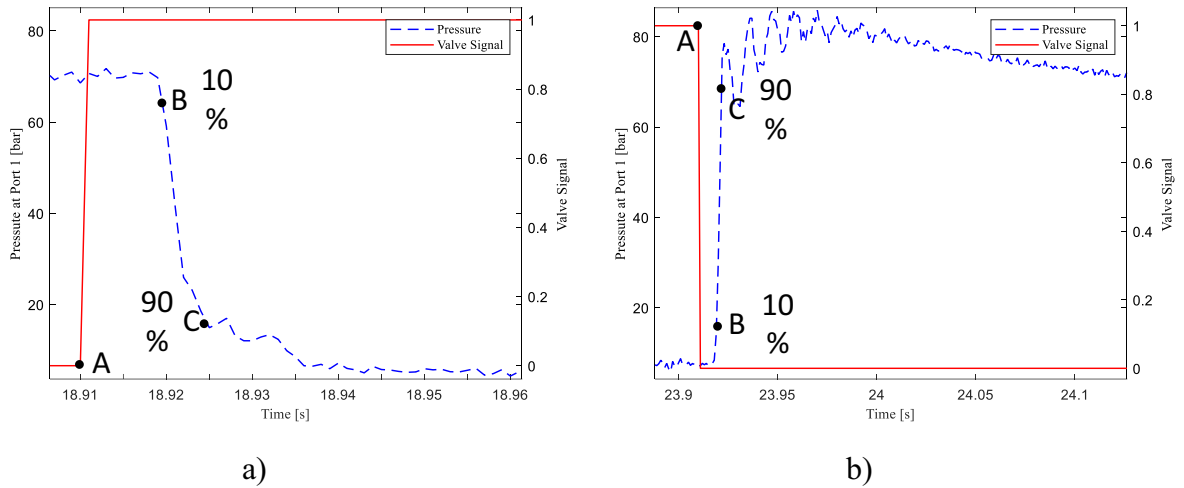
a) Valve opening, b) Valve closing.
Source: Nostrani (2021).

Table 6.8 – On/off valve parameters.

Parameter	Normally closed Value	Normally open	Unit
t_{sod}	0.01	0.067	s
t_{sor}	0.009	0.03	s
t_{scd}	0.004	0.029	s
t_{scr}	0.004	0.01	s
ω_{on}	2000	206.9	rad/s
ω_{off}	2000	600	rad/s
cd_{12} / cd_{21}	0.64 / 0.69	0.67	-
d	0.0063	0.0046	m
x_{vmax}	0.00045	0.001	m
f	1	1	-
ρ	870	870	kg/m³

Source: Adapted from Nostrani (2021).

6.3 SECONDARY CONVERSION UNIT

In this work, the secondary conversion unit is a four-chamber hydraulic cylinder with different areas (Table 6.9)(Figure 6.11), with maximum working pressure of 21 MPa (210 bar). The cylinder was developed and manufactured by WIPRO to be used as a Digital Hydraulic Actuator in Belan (2018). A position transmitter (label 1SL1), model BTL5-A11-M0200 from BALLUFF, is coupled to the four-chamber cylinder rod. A load cell (label 2FS1), model U2A from HBM, is used between the four chamber cylinder (label 1A1) and the external load cylinder (label 2A1) (Figure 6.1).

Table 6.9 – Cylinder parameters.

Cylinder parameters		
Parameter	Value	Unit
Area A	1.571×10^{-3}	m^2
Area B	1.119×10^{-3}	m^2
Area C	7.07×10^{-4}	m^2
Area D	1.347×10^{-3}	m^2
Stroke	0.2	m

Source: LASHIP DHA project documentation Wipro presentation.

Figure 6.11 – Four chamber cylinder.
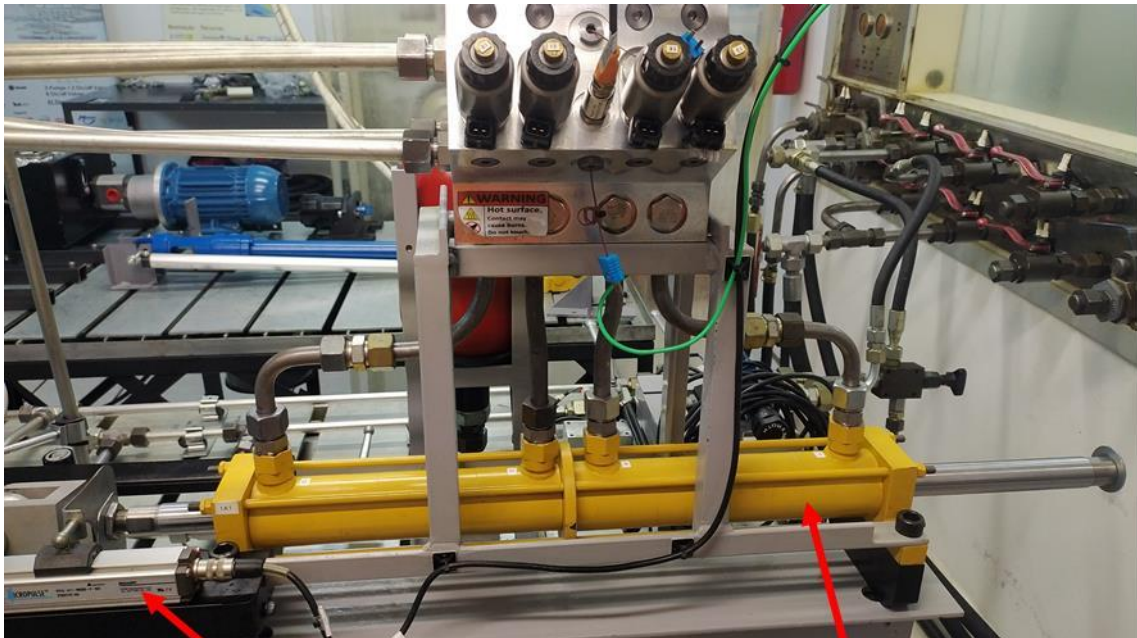
Position transmitter   Four chamber cylinder

Source: Author.

6.3.1 Secondary conversion unit characterization

Experiments were carried out to obtain the friction map of the four-chamber cylinder and calculate the parameters of the LuGre friction model. The digital hydraulic pump was used to control the flow rate to the cylinder and its velocity.

The equation of motion was used to estimate the frictional force during the steady-state condition using the measured values of the pressures in the cylinder chambers, given by

$$F_{fric} = p_A A_A - p_B A_B + p_c A_c - p_D A_D, \tag{6.1}$$

Figure 6.12 presents the experimental results obtained for positive and negative velocities. Table 6.10 presents the values used in the LuGre friction model. LuGre static parameters were estimated using the nonlinear least squares method to solve the equation given by

$$F_{fric} = F_c + (F_s - F_c)e^{-\left(\frac{v}{v_s}\right)^\alpha} \tag{6.2}$$

where F_C is the Coulomb friction force, F_s is the static friction force , v_s is the Stribeck velocity, v is the cylinder velocity, and α is the Stribeck coefficient.

The Stribeck coefficient was adjusted to fit the curve at the experimental data points. Bristle stiffness ($\sigma0$) and micro viscous coefficient of friction of bristles ($\sigma1$) were estimated using dynamic simulation due to the difficulty of measuring micro displacements (TEIXEIRA, 2015; VALDIERO, 2005). During the simulations, the value of $\sigma0$ was adjusted to obtain a microstrain value of the order of 1 to 50 μm (TEIXEIRA, 2015; VALDIERO, 2005).

According to Astrom & De Wit (2008), the parameter $\sigma1$ represents damping in the pre-displacement regime and the impact of this parameter on the ability of the model to accurately predict friction forces depends on the application. The same authors also mention that for mechanical applications, where the resolution and precision are within the millimeter scale, the impact of $\sigma1$ is smaller.

Tran *et al.* (2014), Valdiero (2005), and Yanada *et al.* (2010) used the LuGre friction model and its modified versions to model the friction force of hydraulic cylinders, where to ensure the passivity condition the authors found good agreement with a value of $\sigma1$ equal to

0.1. In this thesis, the same value for $\sigma 1$ was used and also showed a good relationship in the simulation results.

Figure 6.12 – Friction force map of the cylinder.
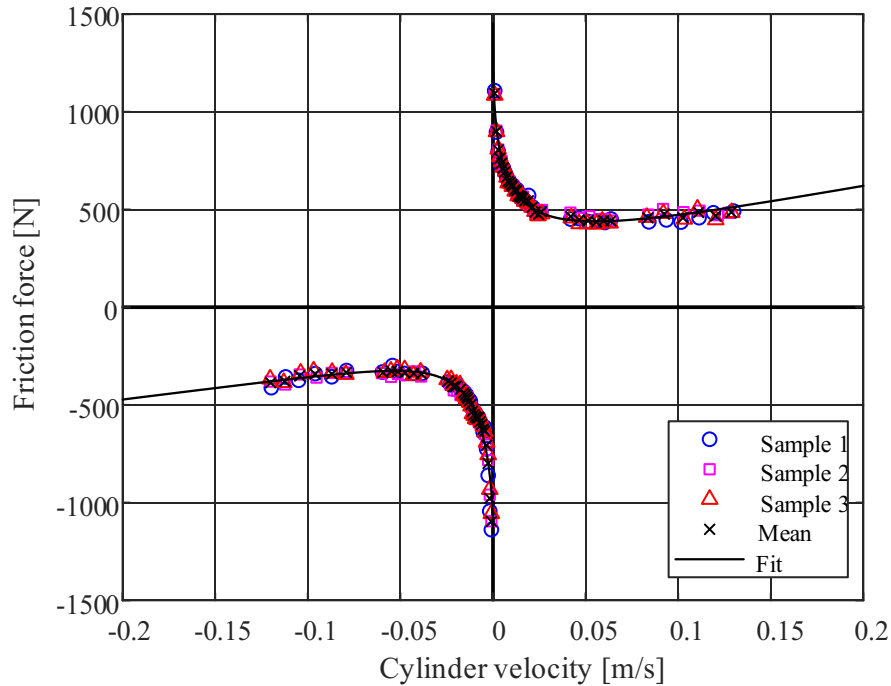
Source: Author.

Table 6.10 – LuGre parameters.

Parameter	Positive velocities	Negative velocities	Unit
Coulomb Force (F_c)	271.65	235.29	N
Static force (F_s)	1364.15	1124.50	N
Stribeck velocity (v_s)	0.006968	0.008257	m/s
Stiffness coefficient ($\sigma 0$)	5×10^6	2.5×10^6	N/m²
Damping coefficient ($\sigma 1$)	0.1	0.1	Ns/m
Viscous coefficient ($\sigma 2$)	1712.65	1183.28	Ns/m
α	0.48	0.67	

Source: Author.

6.4 EXTERNAL LOAD SYSTEM

Another hydraulic cylinder was coupled to the four-chamber cylinder to produce an external load (Figure 6.13). The system comprises an asymmetrical cylinder controlled by a

proportional pressure-reducing valve model Bosch DREBE 6x-10. A hydraulic power unit (IPÚ – LASHIP) is used to supply constant pressure (7.5 MPa / 75 bar) to the cylinder and valve (Figure 6.14). The valve controls the pressure of the chamber with the largest area. While the other chamber is supplied by constant pressure. A PID controller is used to control the force produced by the cylinder. The force feedback signal is obtained from the load cell coupled between both cylinder rods. Two pressure transmitters (IFM PU5401) are used to check the pressures in both cylinder chambers.

Figure 6.13 – External load system.

Hydraulic power unit

Load cell   Asymmetrical cylinder
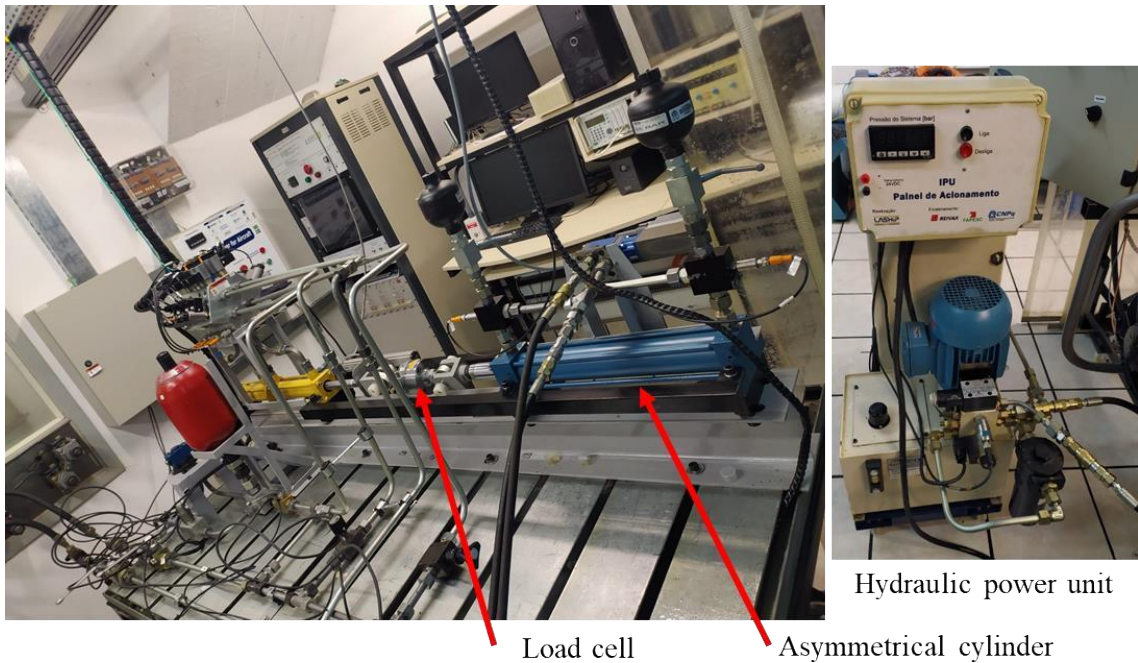
Source: Author.

Figure 6.14 – External load hydraulic system.
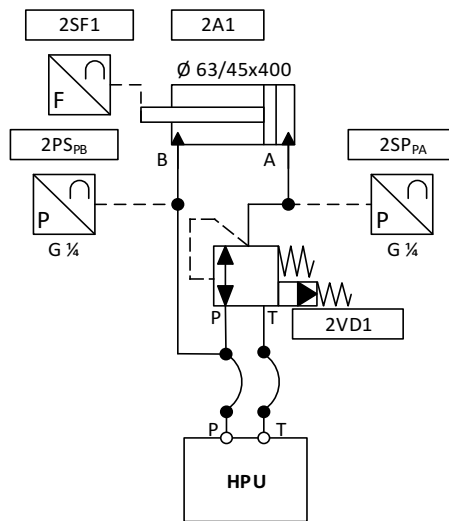
Source: Author.

6.5 DATA ACQUISITION AND SYSTEM CONTROL

Data acquisition and control are performed using a dSPACE DS PCC processor and a DS1103 controller board, which has multiple configurable digital and analog input and output ports. An Interface Homme Machine (IHM) was created in the Control desk software, which is used to monitor and command the test bench. The Control desk is used as a bridge to connect the control developed in MatLab/Simulink® to the dSPACE controller board. Figure 6.15 presents a diagram of the control signals and energy.

Figure 6.15 – Block diagram of the control signals, command and energy.
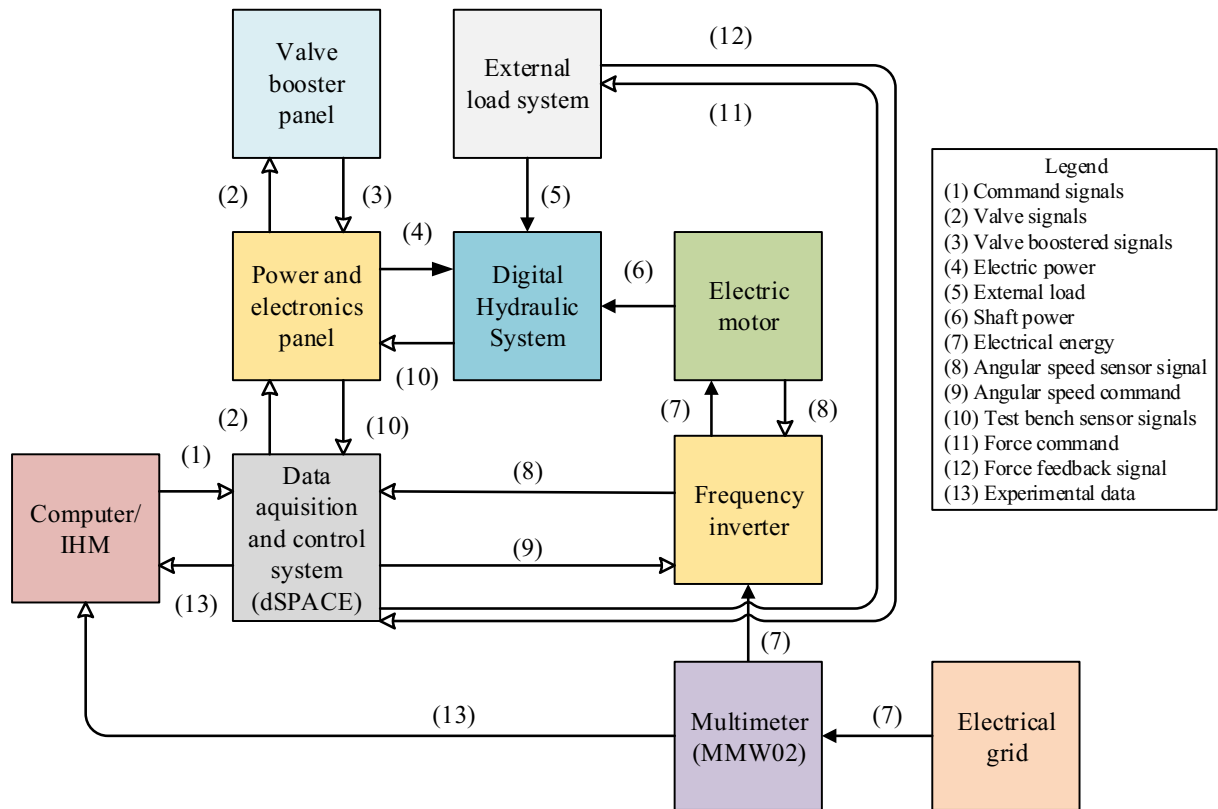
Source: Author.

As shown in Figure 6.15, the signals from the test bench sensors are sent to dSPACE and monitored in the virtual control panel. From the IHM, it is possible to send position commands to the test bench. The command is processed through the control developed in MatLab Simulink® to obtain the actuation signals of the valves and the electric motor. The signals are then processed by the dSpace board, which sends the valve signals to the power electronic panel, which comprises the power electronic of the system, such as power sources and switches (Figure 6.16).

Figure 6.16 – Power and electronics panels.
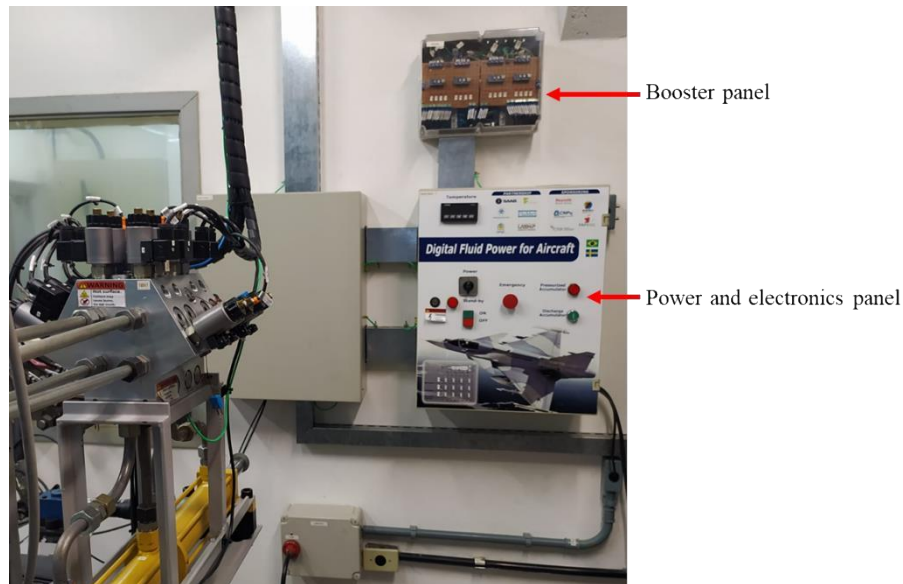
Source: Author.

The electronic panel sends the valve signals to open or close the valves to the valve booster panel. The booster was developed in LASHIP using the Peak-And-Hold technique, where a peak with voltage greater than the nominal one is applied to the valve solenoids to accelerate the activation or deactivation of the valve, in sequence the nominal voltage is used to maintain the valve opened (BREIDI *et al.*, 2014; MANTOVANI, 2019; NOSTRANI, 2021). The valve booster signal is sent back to the power and electronics panel which sends the correct voltage to the valve solenoids. In this case, the peak voltage used is 24V and the holding voltage is 5V. In parallel, the angular speed command goes to the frequency inverter, which uses an encoder signal as feedback to control the angular speed of the motor. The position transmitter closes the cylinder position control loop.

An electric multimeter WEG MMW02 was connected to the electrical grid lines before the frequency inverter to measure the power and energy consumption of the electric motor and the inverter (Figure 6.17). The currents were measured through current transformers (BHS model MTC320, 20/5A), while the voltages were connected directly to the multimeter. The data measured is sent to the computer using a Modbus protocol. The maximum sampling rate of the MMW02 is 1 Hz. This sampling rate is not ideal for dynamic systems where within a second the power can change significantly and not be measured.

Figure 6.17 – Frequency inverter and multimeter MMW02.
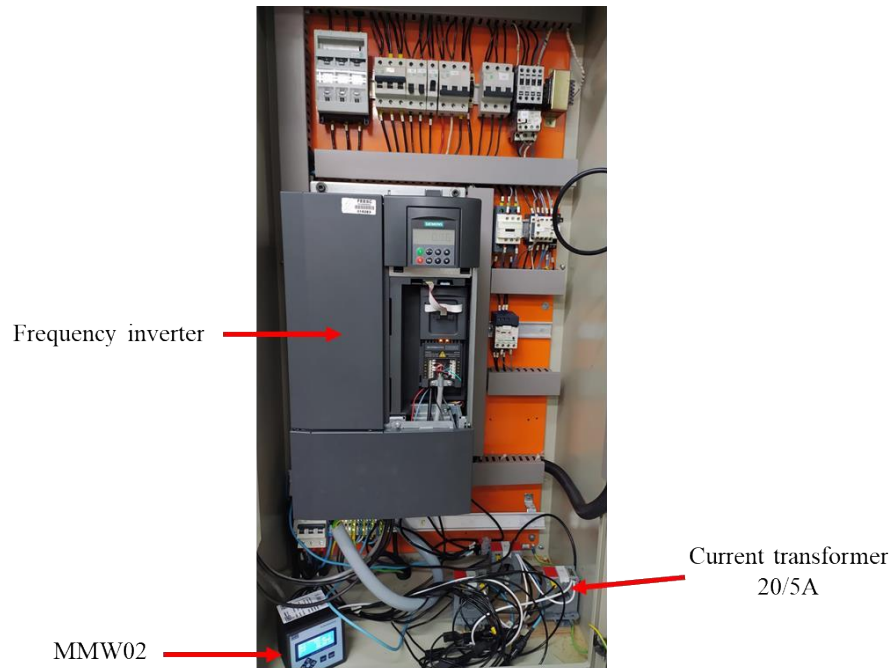
Source: Author.

7 SIMULATION AND EXPERIMENTAL RESULTS

7.1 POSITION CONTROL RESPONSES

A reference signal with different input commands was created to evaluate the position control of the Variable Speed Digital Electro-Hydraulic Actuator. An external compression load force of 1500 N was applied on the cylinder rod. The gains used in the Proportional Integral control of the VSDEHA were 1 and 0, respectively. In addition, a gain of $4.66 \times 10^{-3} \mathrm{m}^2/\mathrm{s}$ was used to convert the position reference of the controller to a flow rate reference. The delay time used for the minimum time to change a valve combination (dT_{min}) was 0.05 s, the delay time used to synchronize the valves of the limitation and control unit was 0.01 s, and the delay time to synchronize the valves of the DHP was 0.047s. Figure 7.1 presents the simulation results and the experimental results which presented a good response to the reference input commands.

Figure 7.1 – Response of position control.
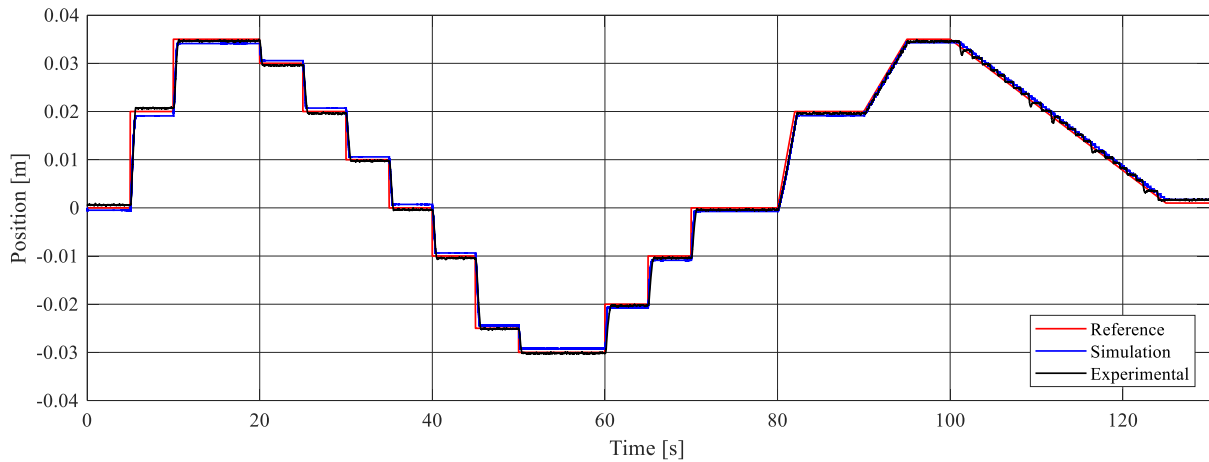
Source: Author.

Figure 7.2 details some of the step responses from Figure 7.1 and the response for the maximum designed step for the actuator. In the time of 5 s, the actuator receives a forward step input of 0.02 m (Figure 7.2a), the result of the simulation has presented a settling time of 0.64 s, while the experimental result has presented a settling time of 0.55 s. For both cases, there is a delay for the actuator start moving. This delay refers to the minimum time for changing the state of the valve. For this condition, the simulation result showed a faster response. However, it was noticed that the system has variable settling time, which can vary with the reference input signal.

In Figure 7.1, from 20 s to 50 s, there is a sequence of steps backward, where the largest one is 0.025 m, which occurs in 45 seconds (Figure 7.2b). The external load is compressing the cylinder rod and during the backward movements, the assistive load condition occurs. The Assistive Load block is used to identify the assistive load condition and activate the brake valve set, sending the flow rate through a metering valve, to dissipate the extra energy of the external load, improving the controllability of the actuator.

Figure 7.2c presents the response for the step of 0.05 m, used as reference to dimension the actuator. The simulation result showed a settling time of 0.875 s and the experimental result showed a settling time of 0.926 s. Both results are within the proposed actuator reference target, which is a response to a step of 0.05 m in the time of 1 s.

Figure 7.2 – Response to step inputs.

a)
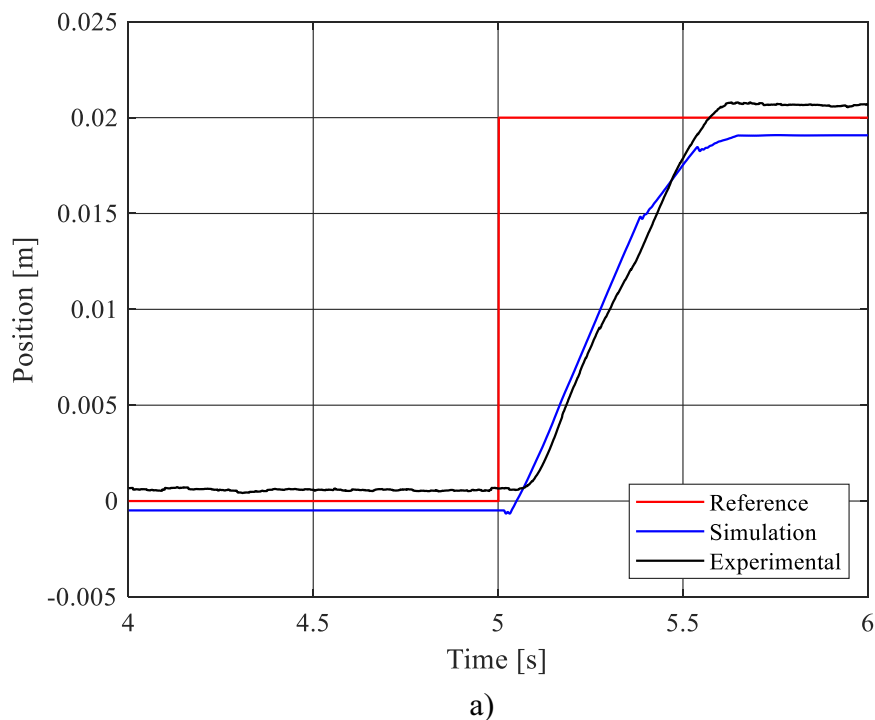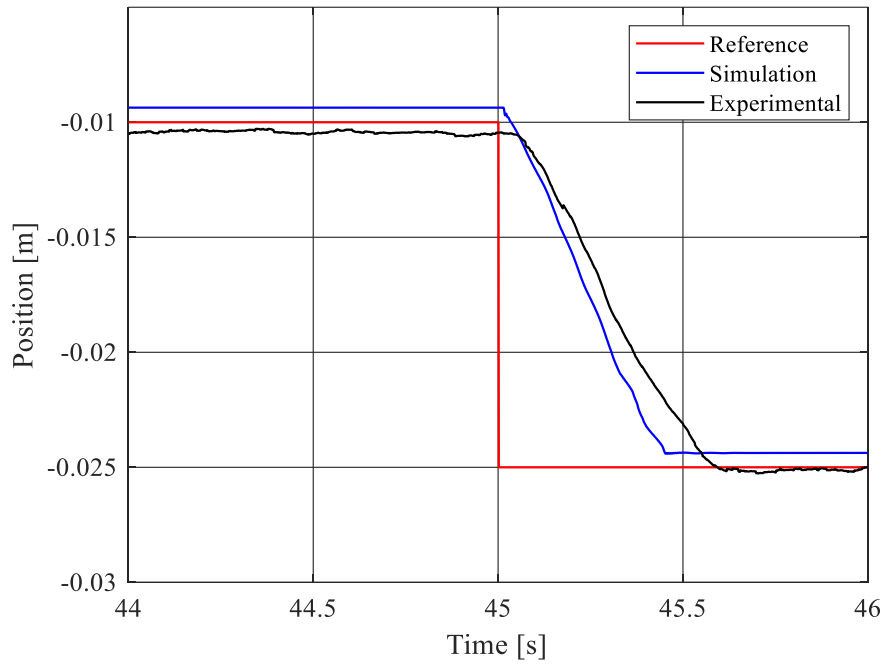
b)
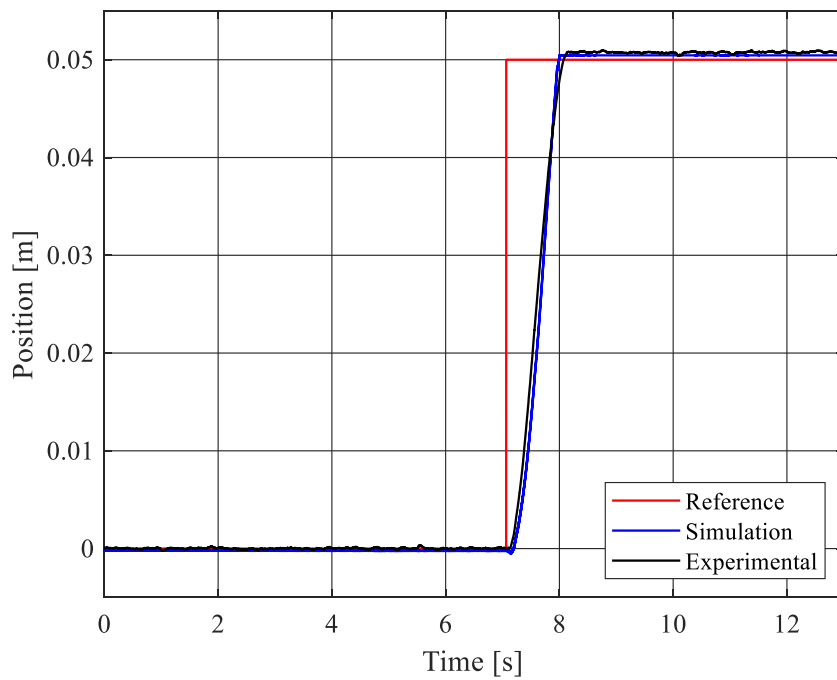
c)

a) Response to forward step of 0.02 m, b) Response to backward step of 0.025 m, and c) Response to forward step of 0.05.
Source: Author.

Figure 7.3 present the ramp inputs of Figure 7.1. In the review of digital hydraulics, it was noticed that one of characteristics of the digital hydraulic actuators is the discretized

movement, due to the discretized levels of flow rate or pressure used to control the actuator. One of the purposes of this thesis is to make the cylinder motion smoother as it can be observed in Figure 7.3a. During the ramp input signal, the controller holds one pump unit combination and controls the cylinder velocity using the electric motor to supply the necessary flow rate.

However, it was noticed that it is necessary that the input command has a minimum rate of change, which implies the minimum speed of the cylinder so that there is continuous movement. In case of the input has a rate of change below a minimum, the movement becomes discretized, which makes the DHP turns on and off to keep following the position (Figure 7.3b). The rate of change of the input ramps in Figure 7.3a and Figure 7.3b are 0.01 m/s and 0.003 m/s, respectively.

The developed model was able to predict the behavior of the system, presenting the continuous and discretized movements, as well as presented by the experimental results. Additional tests were performed to verify the minimum velocity necessary to keep the continuous movement. When it is considered that the VSDEHA is coupled to another cylinder used to produce the external load, it was defined that the minimum velocity must be at least 2.7 times the minimum theoretical velocity of the cylinder (0.0037 m/s), calculated by the minimum flow rate divided by the area of the cylinder. In this case, the minimum rate of change input to maintain continuous motion was a ramp at a rate of 0.01 m/s.

Figure 7.3c presents the most critical operating condition for the developed digital hydraulic actuator, a backward ramp with assistive load condition. In this case, it was noticed that the simulation was capable to predict the cylinder behavior, moving in a discretized way, with small steps. The discrete motion was confirmed during the experiments. However, in the experiments, the steps were larger than the steps predicted by the simulation and presented overshoots. For both cases, the metering valve used to dissipate external energy was adjusted for step conditions to avoid excessive throttling. For this condition, if it were possible to adjust the metering valve continuously to match the desired speed, a continuous movement without overshoot could be achieved, as occurs in servo hydraulic systems.

Figure 7.3 – Response to ramp inputs.

a)

b)
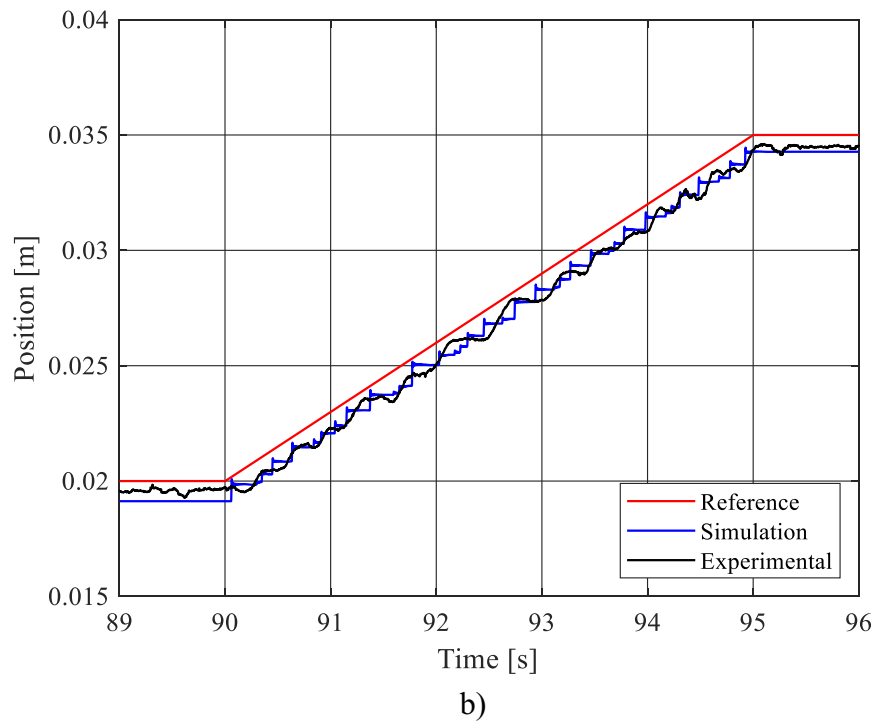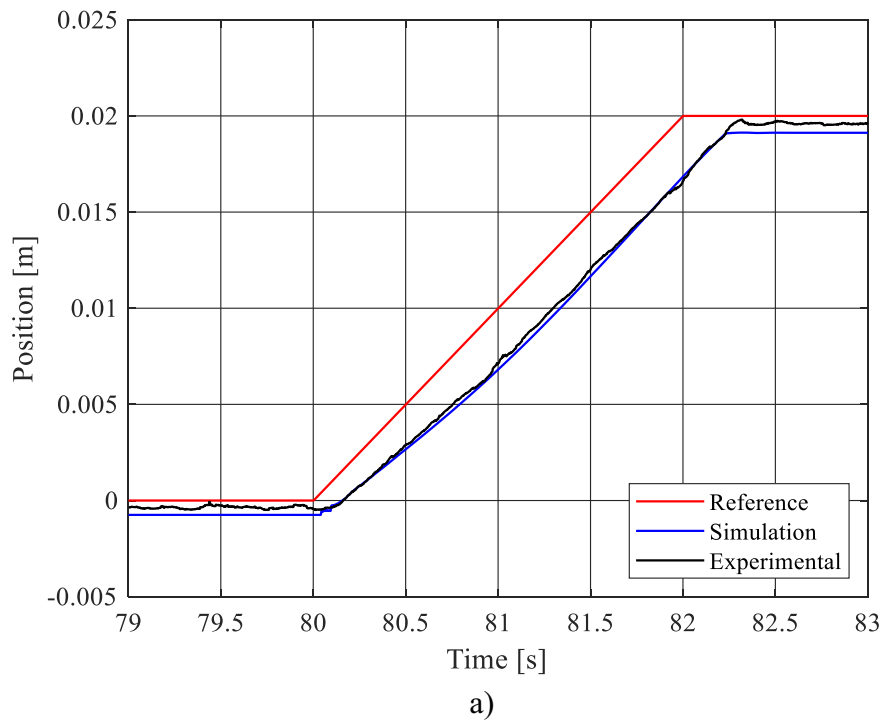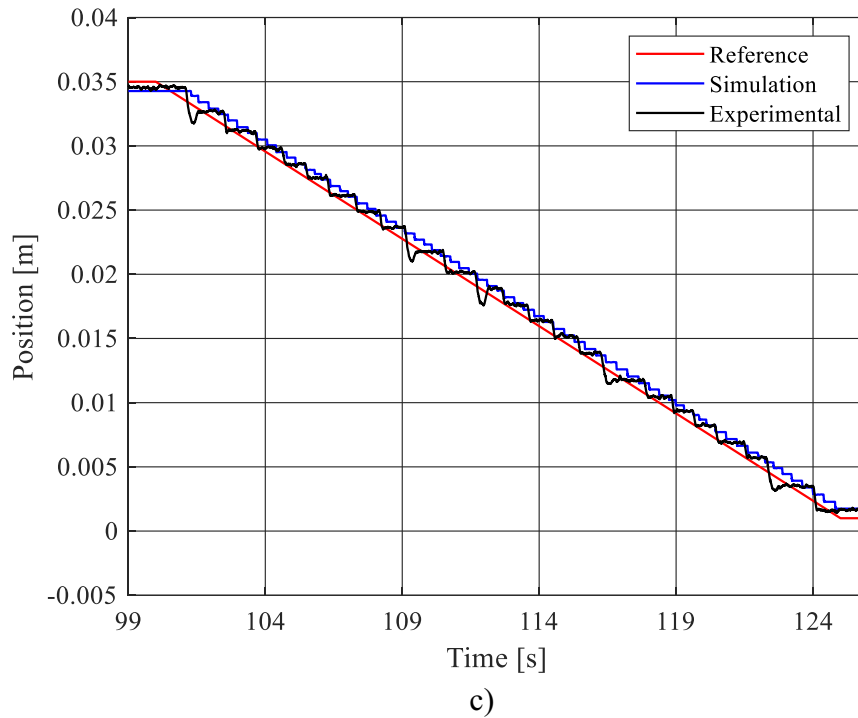
a) Response to ramp with continuous movement, b) Response to ramp with discretized movement, and c)
Response to ramp in assistive load condition.
Source: Author.

Analyzing Figure 7.2 and Figure 7.3, it is possible to notice small errors in the steady state. The error is considered in the control strategy and is an effect of the locker block, necessary to avoid the unwanted actuation of valves due to the high frequency noise present in the sensor signals. Both experimental and simulation results have the same locker block configuration of 0.001 m of tolerance. However, for the simulation case, as there is no noise effect, the locker is activated as soon as the error is within the tolerance, stopping the actuator before the reference position. Figure 7.4 presents the position error of the actuator.

Figure 7.4 – Position error of the controller.
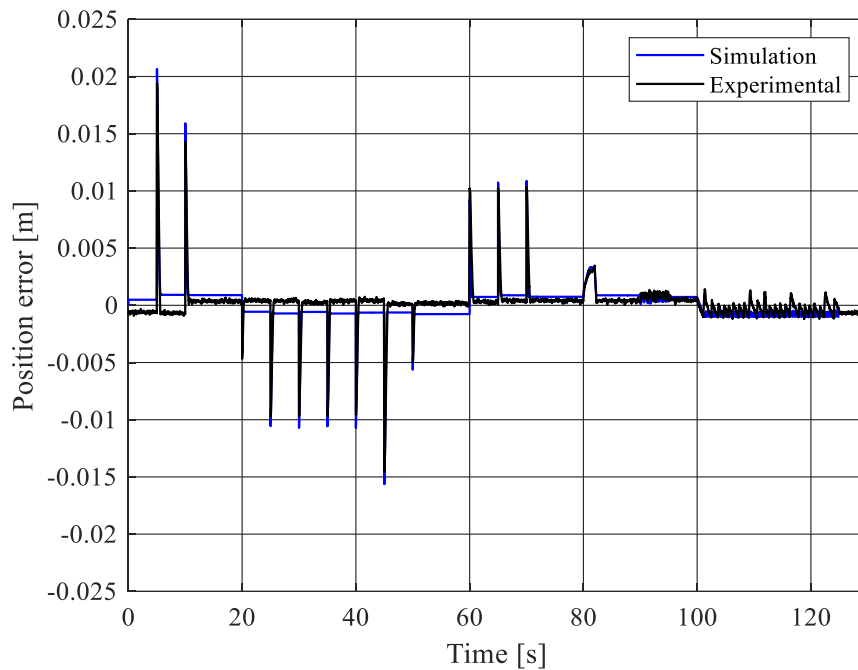
Source: Author.

Figure 7.5 presents the external compression load force applied to cylinder rod during the experiments. The same load is applied to obtain simulation results. Due to technical limitations, the load system was unable of applying a constant force during the cylinder movement. The load behavior also affects the actuator behavior and it could explain the overshoots in Figure 7.3c, where the fixed adjustment of the metering valve is not enough to dissipate the energy of load peaks.

The load fluctuation also justifies the use of Fuzzy logic to implement the assistive load block, used to identify the load direction, since the member functions are configured to accommodate the load fluctuation range, making decisions through the sum of conditions and its intensity.

Figure 7.5 – External load.
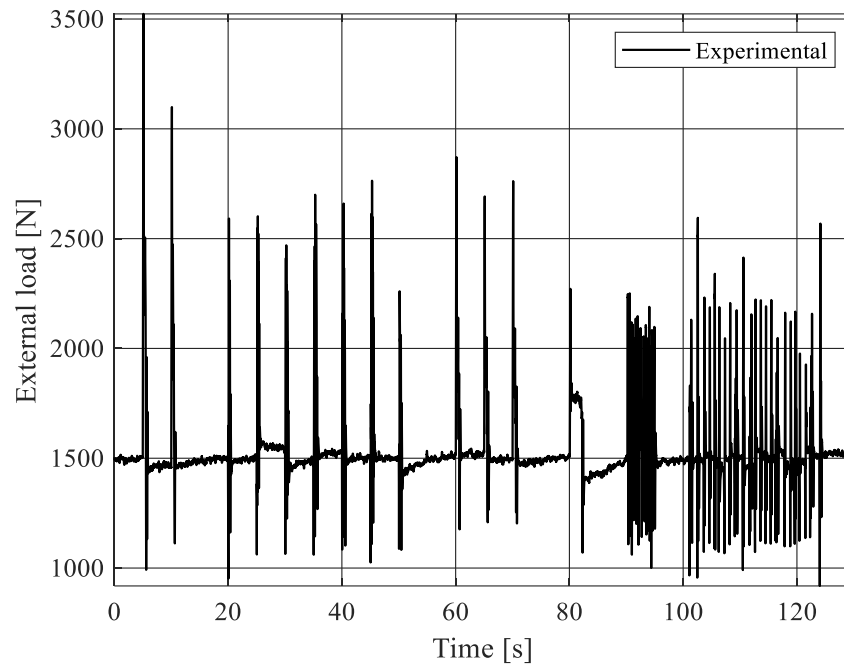
Source: Author.

Figure 7.6 presents the behavior of the pressures in the cylinder chambers, for the experimental and simulation results. There is a small difference between the pressure level obtained in the simulation and the pressure level from the experiments. However, the behavior of both results is quite similar. The differences are related to the nonlinearities of the system that are not fully represented by the models used, as the friction forces and its nonlinearities, which can vary with the pressure and temperature conditions.

Figure 7.7 presents the behavior of the pressures in the pumping units of the digital hydraulic pump for simulation and experimental results. As in the cylinder chambers, the pressures present the same behavior at different levels. Regarding the selection of the pumping unit, the pressure difference between the experiment and the simulation can change the selected pumping unit combination, as shown in Figure 7.7c. Between 60 and 70 s pump unit 3 was not activated in the experiment, while in the simulation, the pump unit 3 was activated to be combined with the pump unit 1 and 2 as shown in Figure 7.8.

Figure 7.6 – Pressures in the chambers of the cylinder.
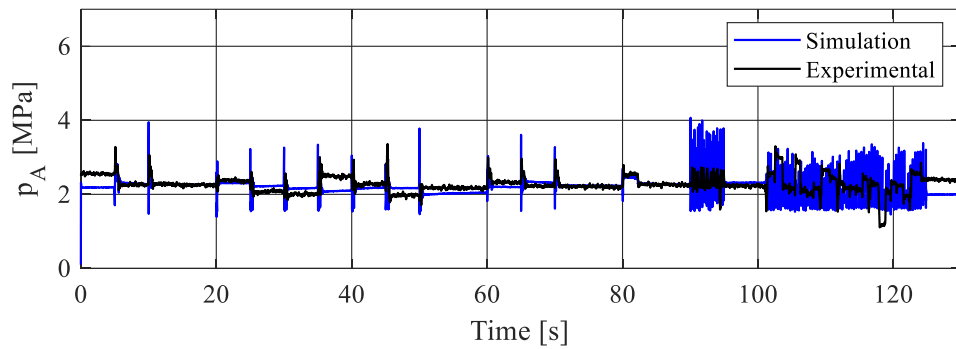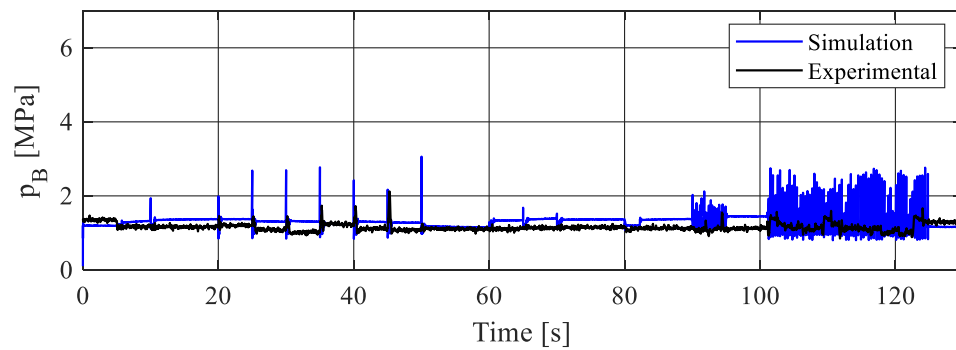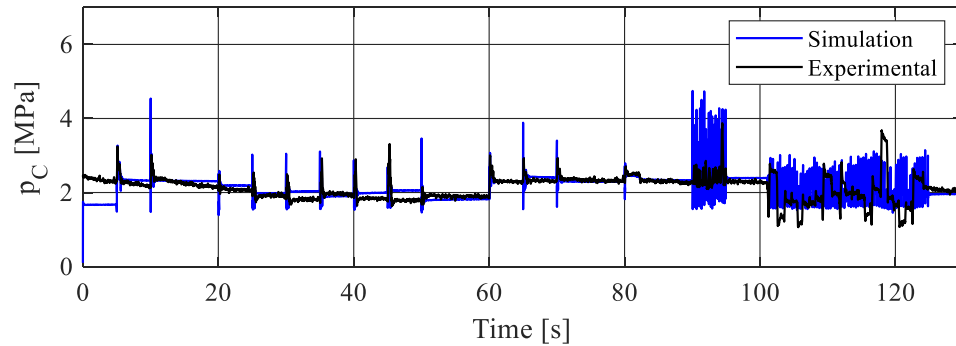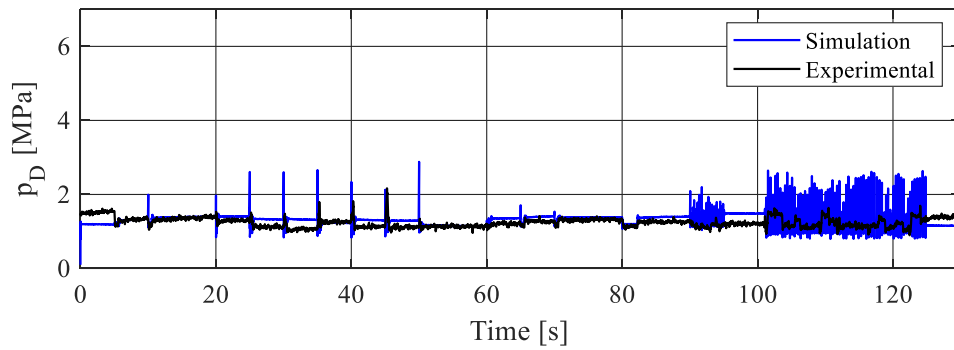
a) Cylinder chamber A, b) Cylinder chamber B, c) Cylinder chamber C, and d) Cylinder chamber D.
Source: Author.

Figure 7.7 – Pressures in the pumping units of the DHP.
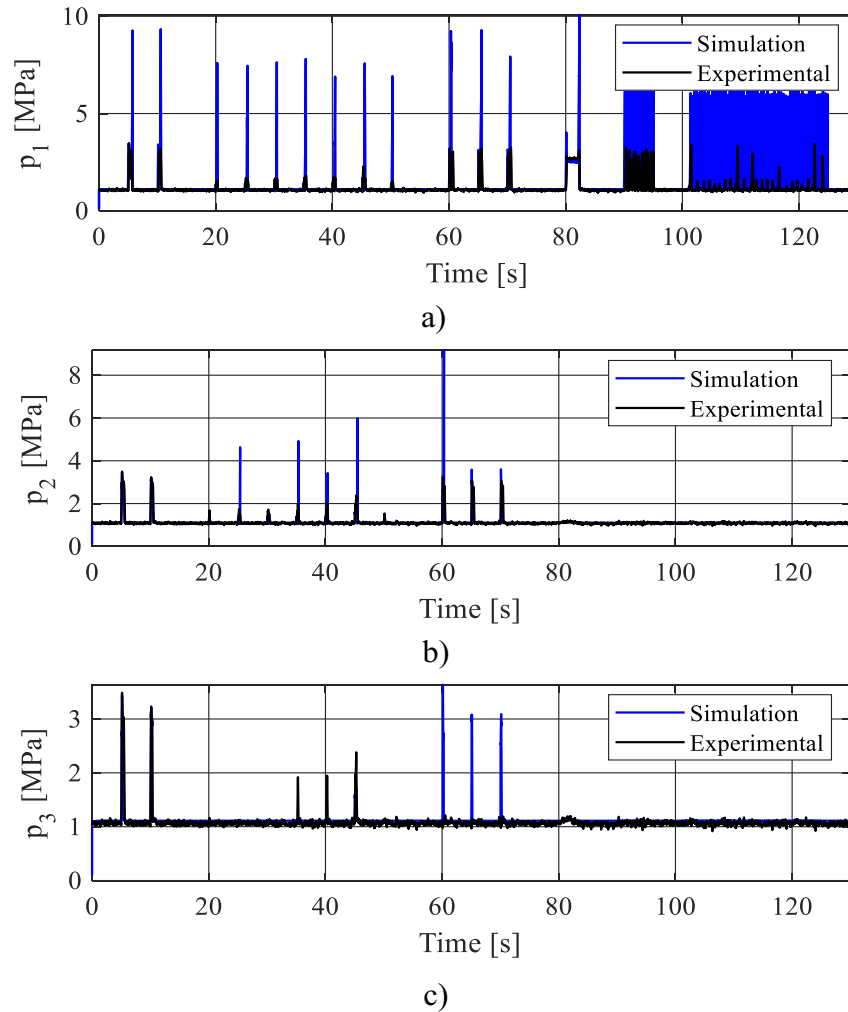
a) Pump unit 1, b) Pump unit 2, and c) Pump unit 3.
Source: Author.

Figure 7.8b presents the selected pump unit combinations in times between 59 and 71 s. In the simulation, the pump unit combinations 3 and 5 are used for a short period. However, in the experiment, the pump unit combination selected are 4 and 2, respectively. This may be related to the pressure level difference between simulation results and experimental results. In addition, in Figure 7.8b, it is possible to notice that, in the experiment, the time to deactivate the valve combination is a greater than in the simulation. This could be related to the time to the position signal and its noise fluctuation to be within the locker region, which justifies the behavior of the experiment, presenting a smaller error than the simulation, for the same error tolerance.

Figure 7.8 – Selected pump unit combinations.
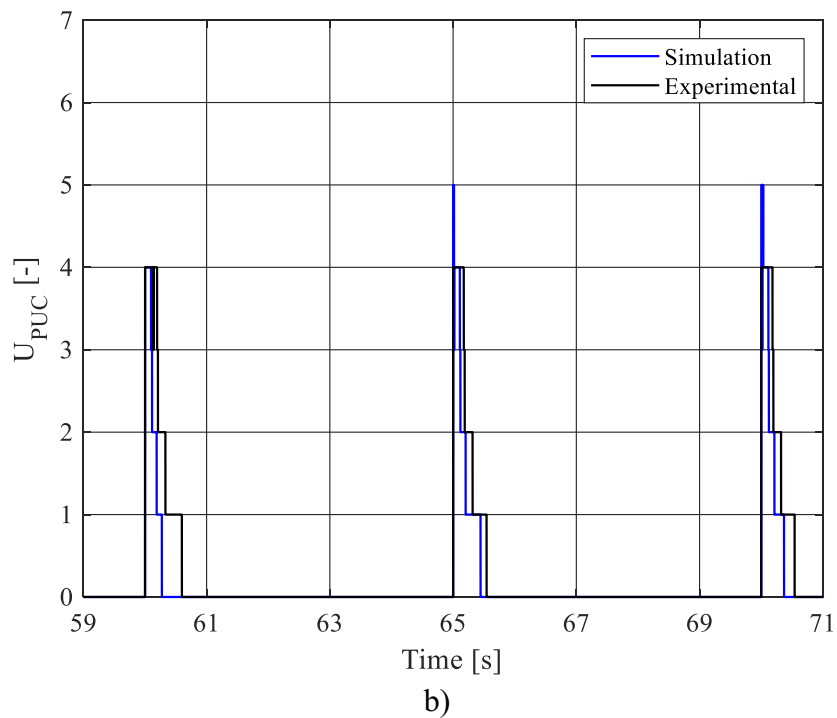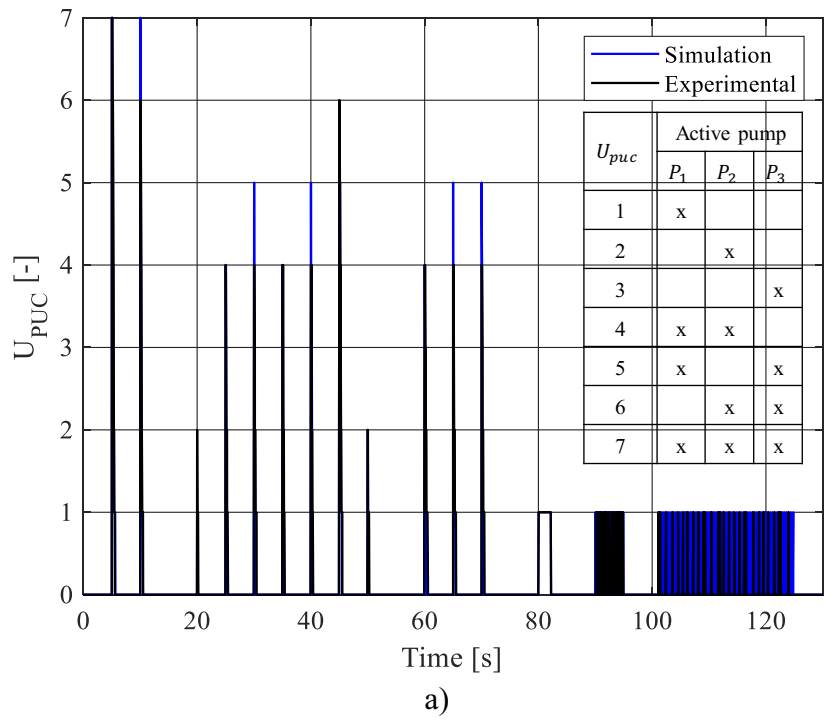
a) Pump unit combination, and b) Detailed pump unit combination.
Source: Author.

Figure 7.9 presents the signal commands for the valves of the cylinder manifold, where U_{PA}, U_{PB}, U_{PC}, and U_{PD} are the signals for the valves connecting the supply line to the cylinder chambers A, B, C and D, respectively. In the same way, the signals for the set of valves

connecting the return line with the cylinder chambers are U_{RA}, U_{RB}, U_{RC}, and U_{RD} (Figure 7.10), and the signals for the set of brake valves are U_{RAb}, U_{RBb}, U_{RCb}, and U_{RDb} (Figure 7.11), respectively.

In Figure 7.11, it is important to highlight that in the presence of assistive load, only the set of brake valves is activated, to dissipate the external energy. However, if the assistive load is not detected, both the normal return line and brake valves are activated as it can be seen in the period from 5 to 20 s. The use of the two sets of valves for the return line under resistive load conditions is due to the time to change the combination of valves. If, during movement, the external load becomes assistive, only the normal return valves are closed, keeping the brake valves open, instead of closing the return valves and opening the brake valves, reducing the response time of the system to a variation in the load direction.

Under assistive load conditions, only the brake valves are used to connect the cylinder chambers with the reservoir, as can be seen between 20 s and 50 s. When the cylinder is moving backward with an external compression load force, the valves in the normal return line of chambers A and C are kept closed (U_{VRA} and U_{VRD}) while the brake valves are used (U_{VRAb} and U_{VRDb}). As it can be seen in Figure 7.11 the simulation was able to represent the experimental results with good precision. The signal of the assistive load is presented in Figure 7.12, which turns on or off for each input command and during the movement if the load direction changes.

Figure 7.9 – Valve signals: supply line to cylinder chambers.
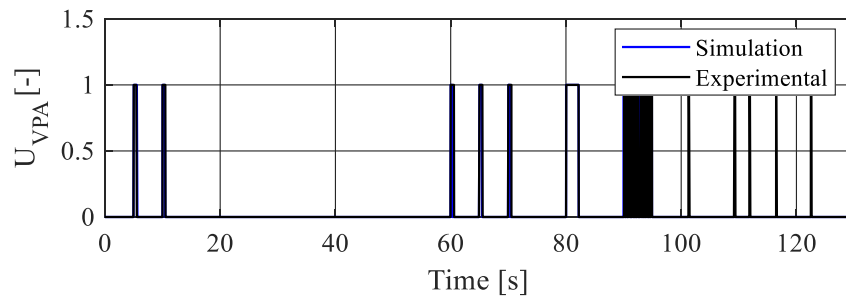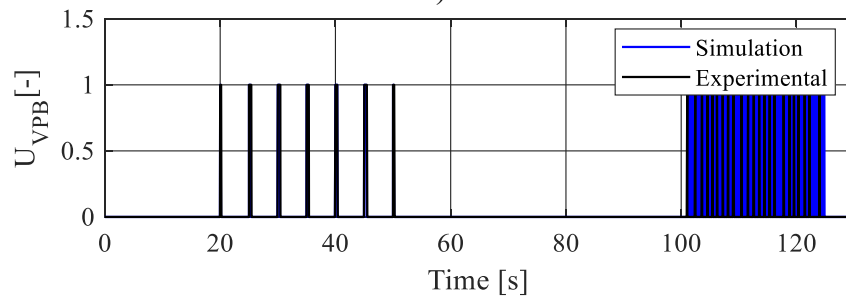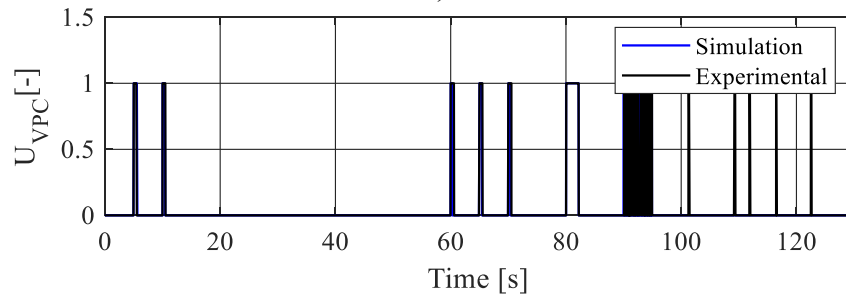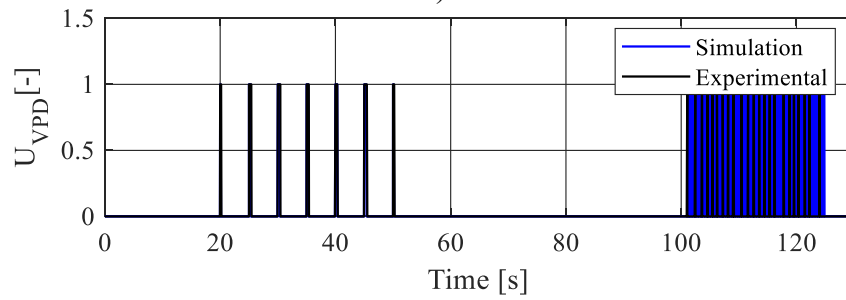
a) Cylinder chamber A, b) Cylinder chamber B, c) Cylinder chamber C, and d) Cylinder chamber D.
Source: Author.

Figure 7.10 – Valve signals: cylinder chambers to return line.
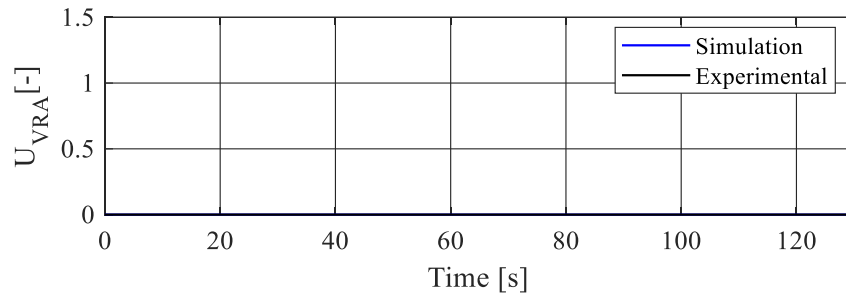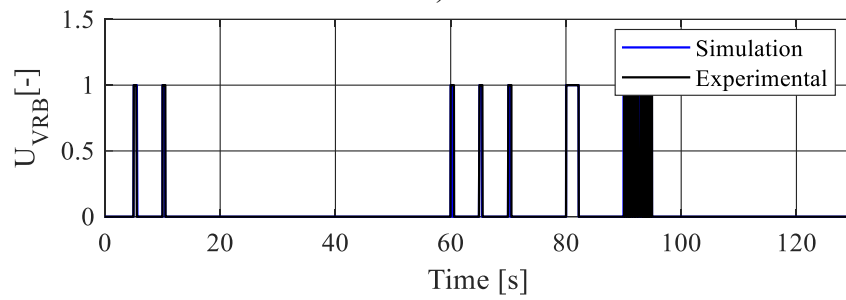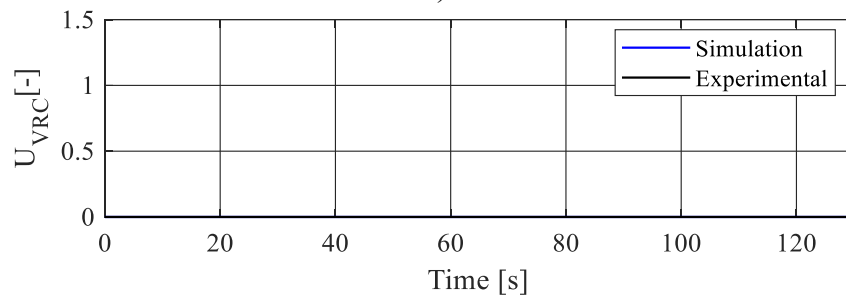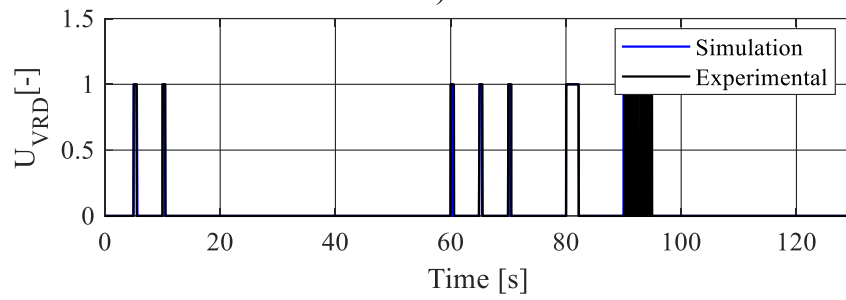
a) Cylinder chamber A, b) Cylinder chamber B, c) Cylinder chamber C, and d) Cylinder chamber D.
Source: Author.

Figure 7.11 – Valve signals: cylinder chambers to return line with brake valve.
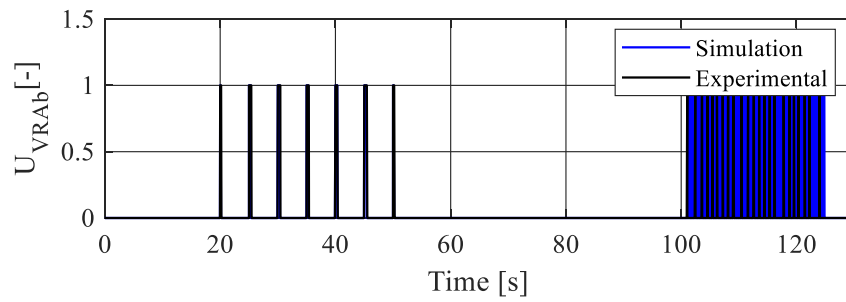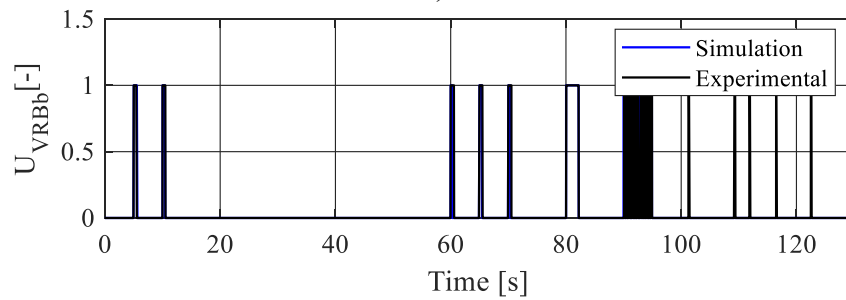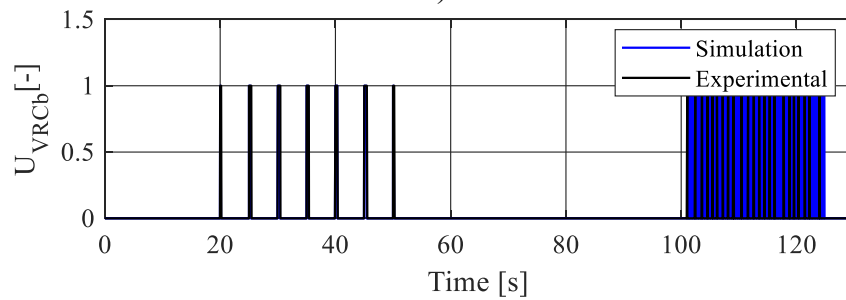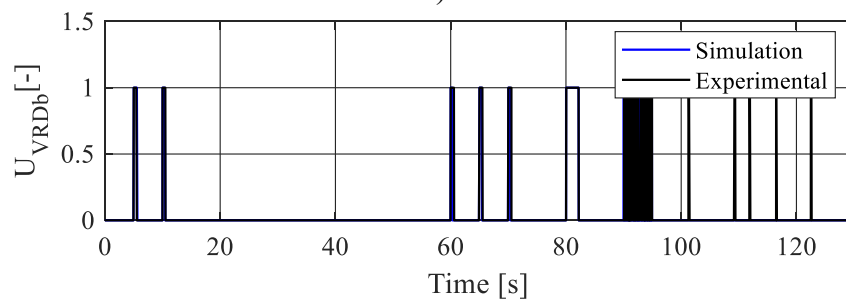
a) Cylinder chamber A, b) Cylinder chamber B, c) Cylinder chamber C, and d) Cylinder chamber D.
Source: Author.

Figure 7.12 – Assistive load signal.
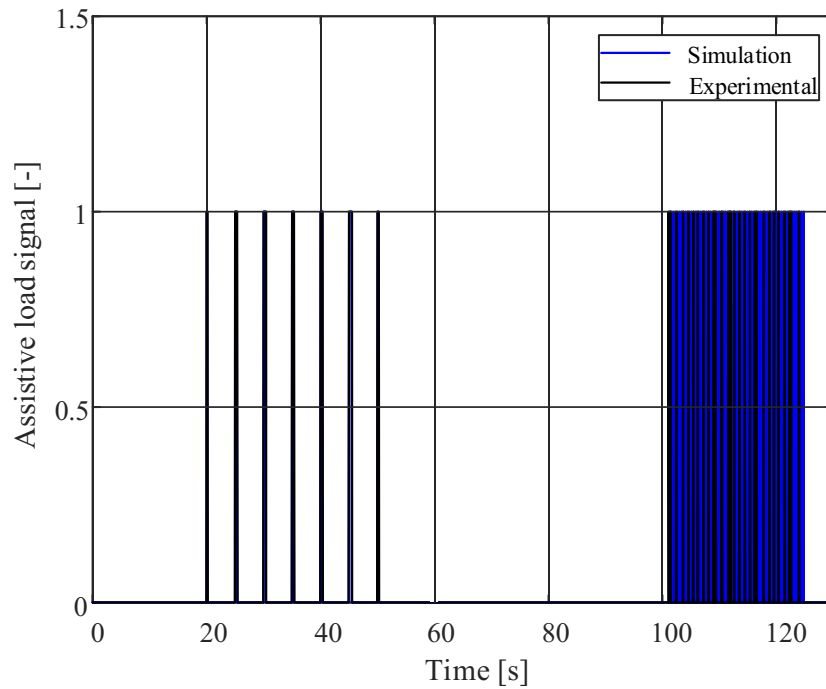
Figure 7.13 presents the locker activation, where it is possible to notice the locker working to keep the cylinder within the error tolerance. Without the use of the locker, the actuator would continue to follow the position variation caused by the position signal noise.

Figure 7.14 presents the response to position control when the assistive load sensor block is not active. In this case, it is possible to notice that, under assistive load conditions, the actuator presents overshoots during the movements with assistive load. This behavior is related to the characteristic of the digital hydraulics, where the valves used are totally opened or closed to avoid throttling control. In this condition, the external load increases the cylinder speed and the system, due to the valve dynamics, is not able to react to maintain the position reference. During the experiments, the overshoots were more aggressive than in the simulation, keeping the same external load conditions. In cases like these, the throttling control is welcome to dissipate external energy and improve the controllability of the actuator.

Figure 7.13 – Locker signal.
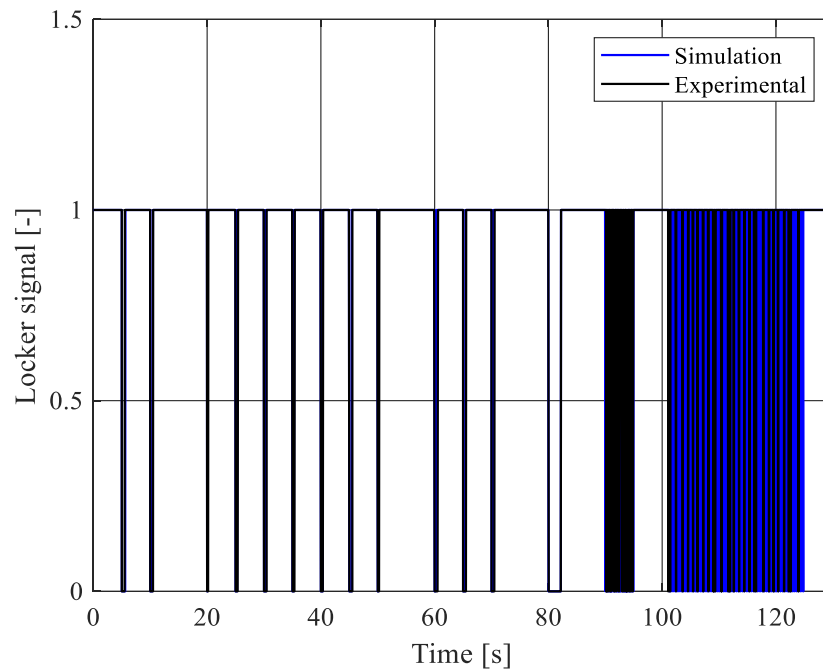
Source: Author.

Figure 7.14 – Position control without assistive load block.
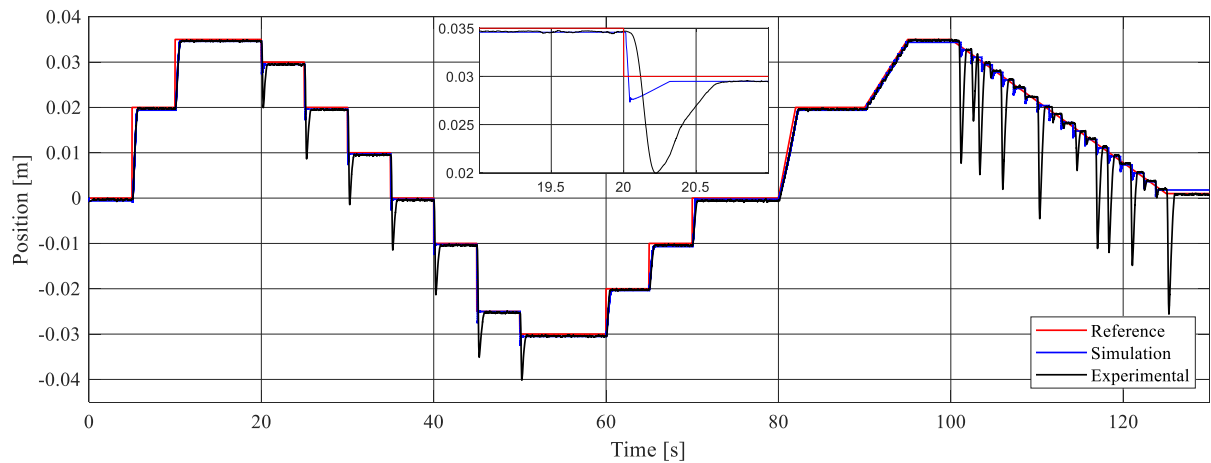
As mentioned earlier, due to computational constraints, it was not possible to run the model of the electrical motor and the model of the hydraulic system together. Instead, a second-order transfer function with a natural frequency of 4.18 rad/s and a damping ratio of 1 was used in the hydraulic system model to simulate the dynamics of the electric motor. The transfer function parameters were obtained by identifying the behavior of the electric motor coupled to the digital hydraulic pump on the test bench. The torque and the rotational frequency command

calculated from the hydraulic system model were used as input for the electric motor model, to obtain the dynamic behavior and power consumption of the electric motor. Figure 7.15 shows the behavior of the rotational frequency from the test bench, the transfer function of the hydraulic system model, the electrical motor model and the input rotational frequency command used in the simulations.

Figure 7.15b presents a detailed view of the rotational frequency during the cylinder ramp input (Figure 7.3a), where it is possible to notice the differences between the results from simulation models and test bench. The electric motor model showed a faster response to the input command. However, this behavior is not observed in the experiment, which is slower. This can be explained by the difficulty in obtaining precise parameters for the electric motor model such as the inertia of the entire system coupled to electric motor, the mechanical frictional forces, and also the electric parameters from the frequency inverter. Torque is calculated based on the working conditions of the digital hydraulic pump and the electric motor, during a steady state condition. To obtain a more representative model it would be necessary to use more sophisticated instruments, such as a dynamometer coupled between the digital hydraulic pump and the electric motor to measure the real torque during transient state.

Figure 7.15 – Comparison of experimental and simulated rotational frequency.

a)
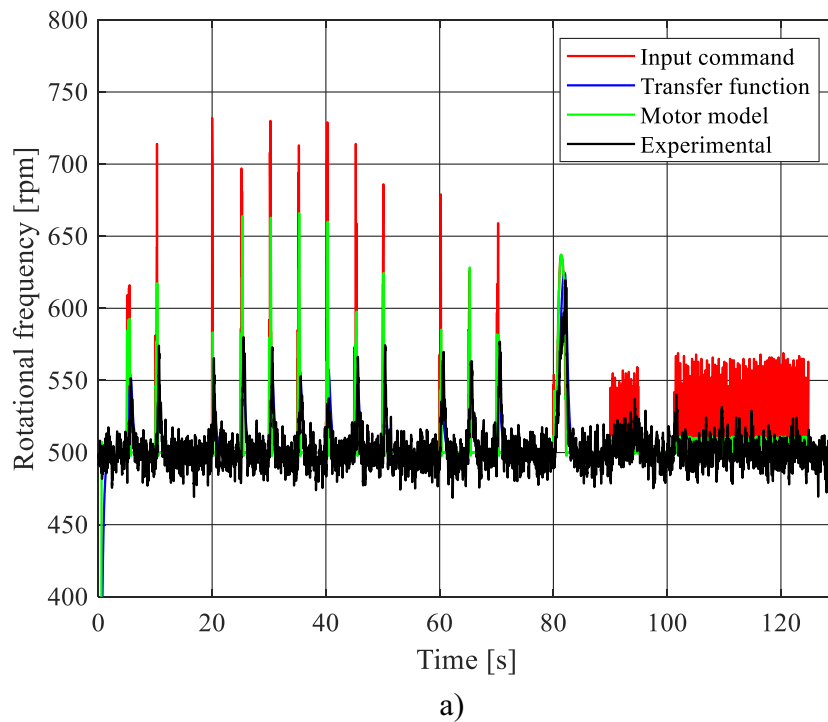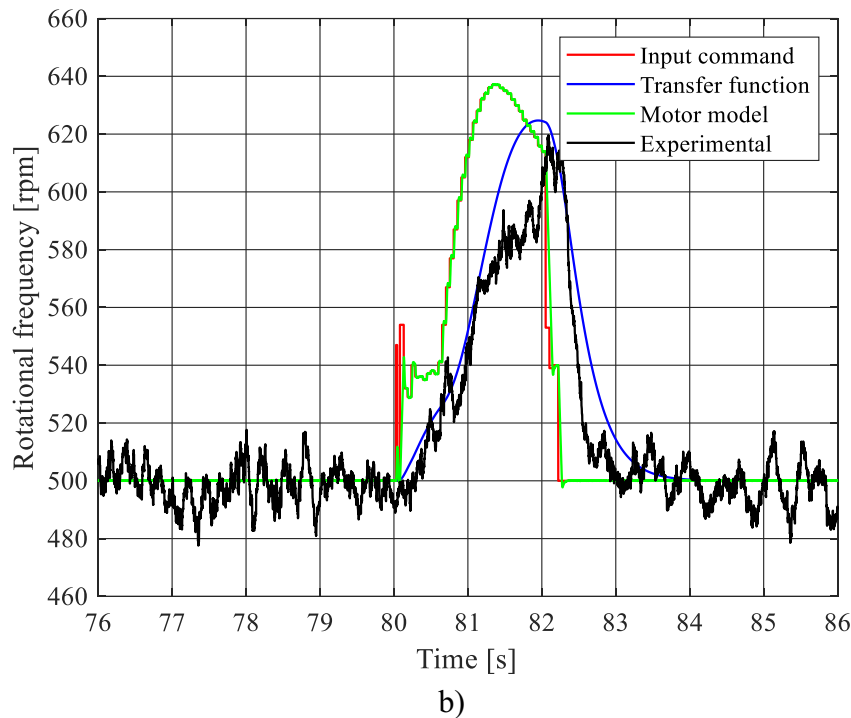
a) Rotational frequency behavior during the experimental and simulated cycle, b) Detailed behavior for ramp input in time 80 s.
Source: Author.

Analyzing Figure 7.15b, it is possible to observe the electromagnetic noise distorting the rotational frequency signal of the electric motor. As the output signal is affected by the noise, it is possible to infer that the reference signal used by the frequency inverter to control the rotational frequency is also affected causing fluctuations in the rotational frequency as observed in the average behavior of the experimental response.

During the experiments, it was observed that the main source of electromagnetic noise is the frequency inverter. Figure 7.16 shows an unfiltered signal from the position transmitter with the frequency inverter on standby and driving the electric motor. The frequency inverter is positioned around 10 m away from the sensors, while the electric motor is positioned around 2 m from the sensors. A transformer is used to isolate the electrical circuit used to supply the measurement system from the electrical circuit used to supply the frequency inverter. Sensor cables are shielded. A capacitor banks was connected to the electrical circuit that supply the sensors to try to attenuate the fluctuations but it was not effective.

In parallel, filters were implemented and tested in the Simulink to treat the signals. Fast Fourier Transform was used to try to identify the frequencies of the noise. However, the sampling rate of the dSPACE is 1000 samples per second, which according to Nyquist theorem,

the maximum frequency represented by this sample rate is 500 Hz. However, the switching frequency of typical IGBT frequency inverter topologies ranges from 20 to 50 kHz (ONSEMI, 2018). The 100-point moving average filter was the most cost-effective solution found and was used to filter the experimental test signals.

Figure 7.16 – Unfiltered position signal.
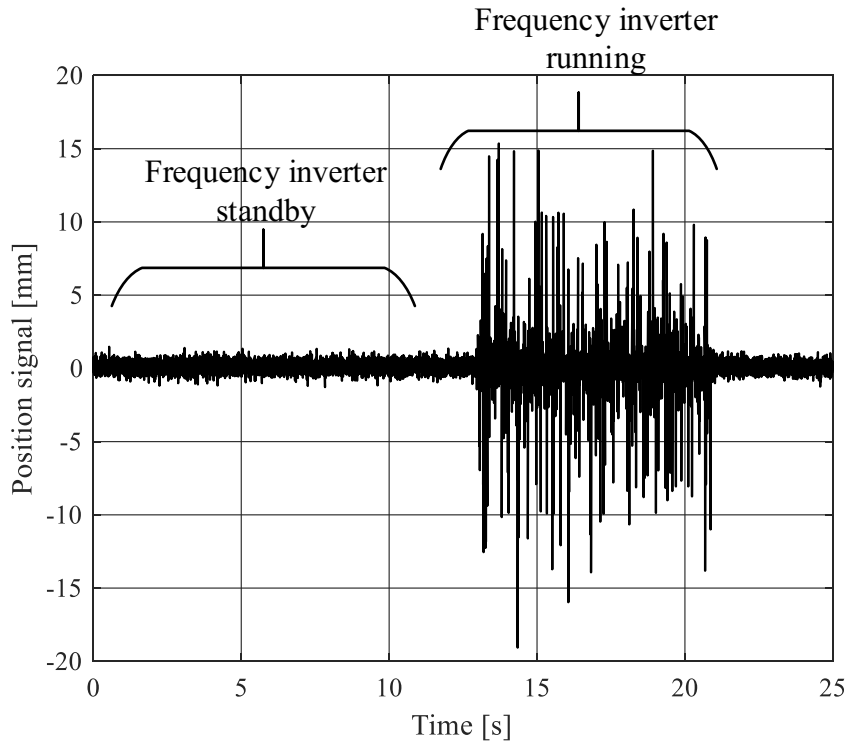
Source: Author.

Based on the results presented in this section, despite the difficulties presented, it is considered that the developed models presented good correlation and significant precision with the experimental test bench, and they can be used for further studies.

7.2 ENERGY ANALYSIS

7.2.1 Effect of the assistive load identifier on the energy consumption

According to Silva *et al.*, (2022) using the combination of throttling control with digital hydraulics in specific moments it is possible to improve the controllability and energy consumption of the digital hydraulic system. Figure 7.17 shows the electrical energy

consumption measured on the test bench for the system with the assistive load identifier active and inactive during the movement presented in Figure 7.14. When the assistive load identifier is inactive, there are some peaks in power consumption. The peaks are related to the power required to recover the cylinder position, mainly represented between the times 100 and 130 s. In the time 80 s, it is possible to notice that for both experiments the power behavior was the same, which is related to the ramp input with resistive load (Figure 7.3a).

Following the analysis of Figure 7.17, between the times 20 and 50 s the consumptions in both experiments are quite similar. In this case, it is assumed that the electric multimeter was not able to capture the fast variation in the power consumption. This is noticed also in the between 100 and 130 s where only few points have power consumption peaks, while the cylinder presented several overshoots in this region. The energy consumption for the experiments with assistive load identifier active and inactive were 0.012503624 and 0.012903214 kWh, respectively. To facilitate the comparison, the energy measured by the MMW02 was converted from kWh to Joule, being 45.013 kJ and 46.451 kJ, respectively. This result shows that the strategy adopting the throttling valve to avoid the overshoots of the cylinder requires about 3.2% less energy and presents better controllability.

Figure 7.17 – Electric power consumption comparison.
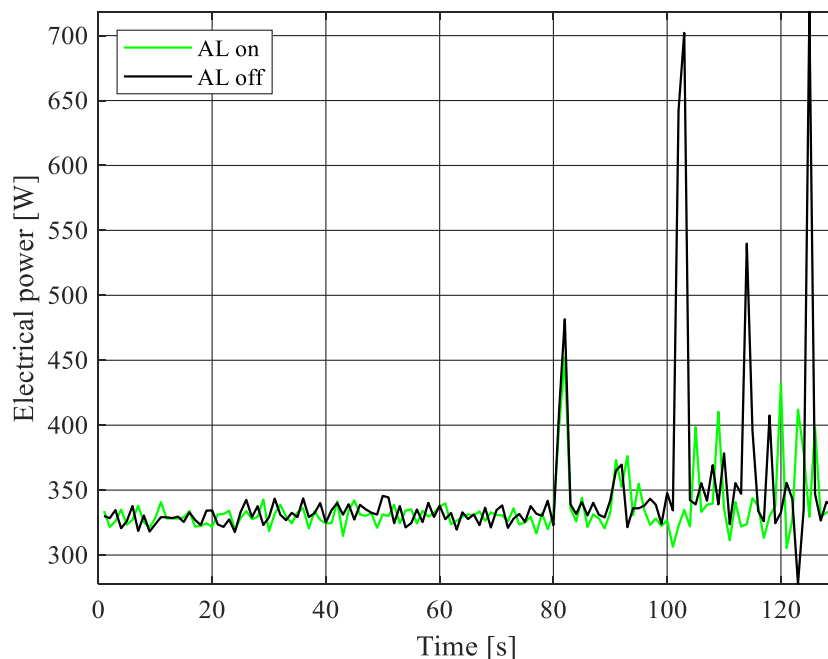
AL – Assistive load block.
Source: Author.

7.2.2 Test bench energy evaluation

The test bench was developed to work under conditions similar to those of an aircraft actuator. One of the concerns was how to obtain a pressurized reservoir since the pumps used in the DHP are not capable of withstanding high pressures on the suction side due to constructive restrictions. To overcome part of this issue, a second power unit was used to keep the return line at a pressure of 1 MPa. However, the pump suctions remained connected to an atmospheric pressure reservoir.

Therefore, analysis was performed comparing the input and output energies considering two configurations. The first configuration considers the experimental test bench in the real conditions, where the return line is kept pressurized by a second hydraulic power unit, and the DHP suction is not pressurized. This configuration is evaluated experimentally and simulation to verify the differences between the model and the experimental test rig and also to calculate the internal energy conversion, since some variables such as torque and flow rate are not accessed during the experiments.

The second configuration considers the DHP suction at same pressure level as the pressurized return line, which means that the system has a pressurized reservoir as in an aircraft. This configuration is evaluated by simulation only.

The electrical energy consumed by the electric motor and frequency inverter is considered the input energy of the actuator. Maximum instantaneous voltage (V_{max}) and Maximum instantaneous current (I_{max}) are measured by the MMW02 electric multimeter and the consumed energy is calculated by

$$E_{elec\_in} = \frac{3}{2} \int_0^t V_{max} I_{max}\, dt, \tag{7.1}$$

The mechanical energy output of the electric motor is given by

$$E_{mec\_shaft} = \int_0^t \omega_r T\, dt, \tag{7.2}$$

where ω_r is the angular velocity of the electric motor rotor and T is the torque load.

The hydraulic energy output of the DHP is given by

$$E_{hid\_DHP} = \int_0^t (\Delta p_1 q_{V1} + \Delta p_2 q_{V2} + \Delta p_3 q_{V3}) dt, \tag{7.3}$$

where Δp is the pressure differential on each pumping unit and q_V is the flow rate delivered by each pumping unit.

The hydraulic energy input to the cylinder can be calculated by

$$E_{hid\_cyl} = \int_0^t (p_A A_A - p_B A_B + p_C A_C - p_D A_D) v \, dt, \tag{7.4}$$

where p_A, p_B, p_C and p_D are the cylinder chamber pressures, A_A, A_B, A_C and A_D are the cylinder chamber areas, respectively, and v is the cylinder velocity.

The energy used to power the measurement system and valves is not considered. The output energy of the actuator is obtained from the mechanical power output during the movement presented in Figure 7.1, which is calculated using the information of force and velocity information of the cylinder given by

$$E_{out\_cyl} = \int_0^t f v \, dt, \tag{7.5}$$

where f is the force produced by the cylinder and v is the cylinder velocity.

However, to obtain the cylinder velocity it is necessary to derive the cylinder position signal. The derived signal is highly affected by fluctuations in the position signal, which is affected by noise even after filtered. Figure 7.18 presents the cylinder velocity calculated from the experimental position signal (Figure 7.1) and its filtered cylinder velocity, as it is considered that the main cause of the fluctuations is noise in the position signal and not cylinder acceleration. The low pass filter used was a second order transfer function with undamped frequency of 157.08 rad/s and a damping coefficient of 1.

Figure 7.18 – Cylinder velocity.
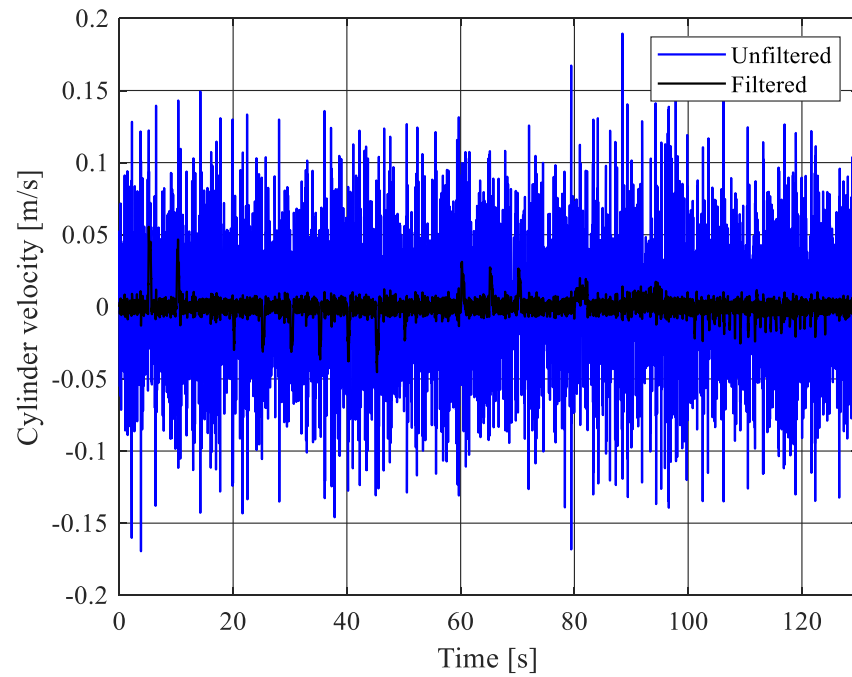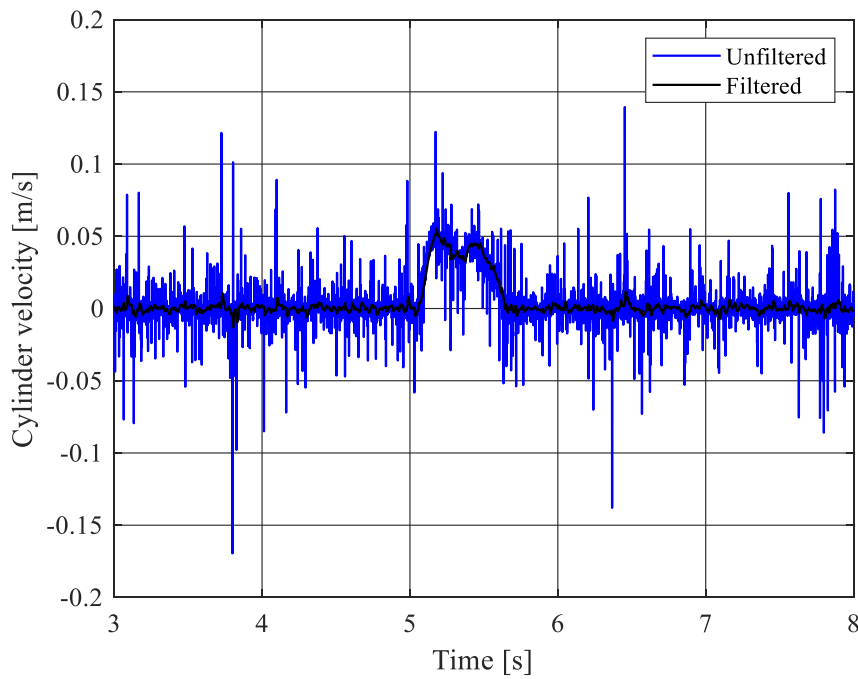
a) Cylinder velocity unfiltered and filtered, b) Detailed cylinder velocity filtered and unfiltered
Source: Author.

Energy results are calculated from the position control response in Figure 7.1. Figure 7.19 presents the experimental results of the electrical energy input and the mechanical energy output of the cylinder rod for the actual configuration of the test bench. The main losses are presented for each energy conversion.

Figure 7.19 – Experimental input and output energy.
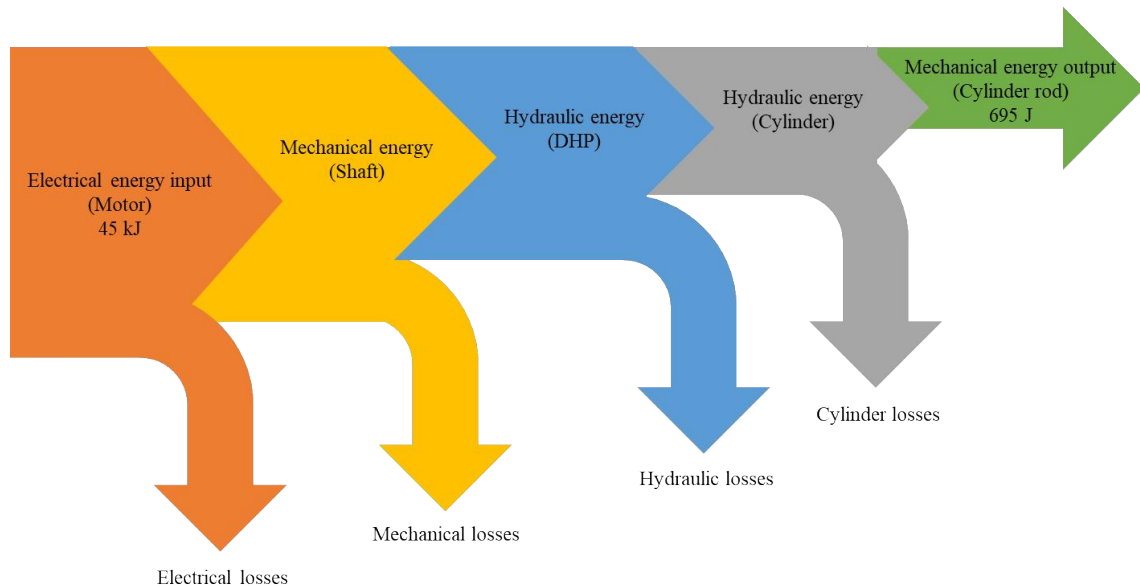
Source: Author.

Due to technical limitations, it was not possible to measure the energy conversions in all stages. However, it was possible using the simulation model (Figure 7.20). The electric motor model was used to calculate the electrical energy consumption according to the rotational frequency and torque demanded by the hydraulic system model. The model presented energy input about 8% higher compared with the experimental result. This could be related to the faster response of the electrical motor model (Figure 7.15), which requires more power to increase the rotational frequency. However, the difference is small when looking at the overall picture of the solution.

The higher losses presented in Figure 7.20 are related to the electro-mechanical conversion and hydraulic losses. The electromechanical conversion losses are explained by the region where the electric motor is used, which is at a low angular velocity where the motor has efficiency between 6% to 70% (ANNEX B – Electric motor report). This region of use of the electric motor is due to the size of the pumps that were not designed for the topology proposed in this thesis.

Figure 7.20 – Simulation results for energy input and output of the test bench.
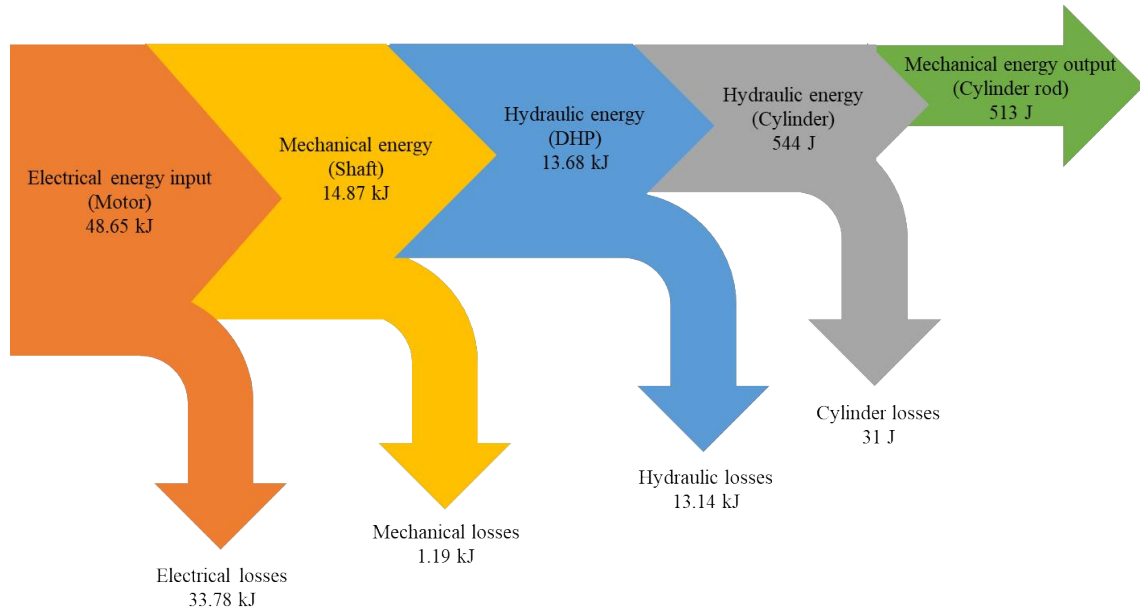
Source: Author.

Hydraulic losses are explained by the amount of energy produced and dissipated during the idle condition, which is when the DHP is sending the flow rate of all pumping units to the pressurized return line. In this specific case, to recirculate the hydraulic fluid, the pumps are suctioning fluid at 0 MPa and discharging it to a pressurized line at 1 MPa (10 bar). This pressure differential in the pumps also increases the torque needed to move them, increasing the electrical power consumption.

Figure 7.21 present the simulated energy results using the second configuration of the system, which considers a pressurized reservoir that was not possible to implement experimentally. The main difference in this working condition is related to the hydraulic energy losses. In this simulation, the DHP is suctioning and discharging the hydraulic fluid at a same pressure level (1 MPa). The energy losses are related to the internal friction and restrictions of hydraulic components of the hydraulic circuit. The low-pressure differential in the DHP reduces the torque needed to move it at idle, consequently reducing the electrical power consumption.

For the test bench, the average electrical power consumption of the DHP in idle condition, under a pressure differential of 1 MPa was 340 W. For a pressure differential of 0 MPa, it was 245W, which shows the difference when the reservoir and return line are in the same pressure.

In this second configuration, it is possible to analyze the energy consumption of the proposed digital hydraulic actuator. The work done by the cylinder is the same as the first

configuration, so the mechanical energy produced in the cylinder rod is the same. Likewise, the hydraulic energy to the cylinder. The efficiency of the energy conversion in the cylinder is 94.3 %. Cylinder losses are related to friction and internal leaks between cylinder chambers, which are the same for both simulations (Figure 7.20 and Figure 7.21).

The hydraulic energy in the cylinder came from the hydraulic energy generated in the DHP, where part of the energy is sent to the reservoir when the system is idle and another part of the energy is dissipated due internal component losses. The hydraulic losses significantly decreased compared to a higher pressure differential in the DHP. The ratio between the hydraulic energy used in the cylinder and the hydraulic energy produced by the DHP is 62.3%. This represents the control efficiency promoted by the use of digital hydraulics where the dissipative control is avoided.

The conversion of mechanical energy into hydraulic energy reflects the efficiency of the pump units used in the DHP, which presented an efficiency of 22%. As presented in Figure 6.5, during the tests to obtain the flow curves, it was noticed that the pumps have low volumetric efficiency, it is important to highlight that the pumps are prototypes.

The conversion of electrical energy into mechanical energy reflects the efficiency of the electric motor used in the system, as previously mentioned the motor is operating in a low-efficiency region. The low torque required to move the DHP reduces electrical energy consumption. However, in this case, the electric motor still works far from its best operating region, presenting an efficiency of 13%. This demonstrates the importance of designing a hydraulic system considering the operating range of the electric motor.

Figure 7.21 – Simulation results considering a pressurized reservoir.
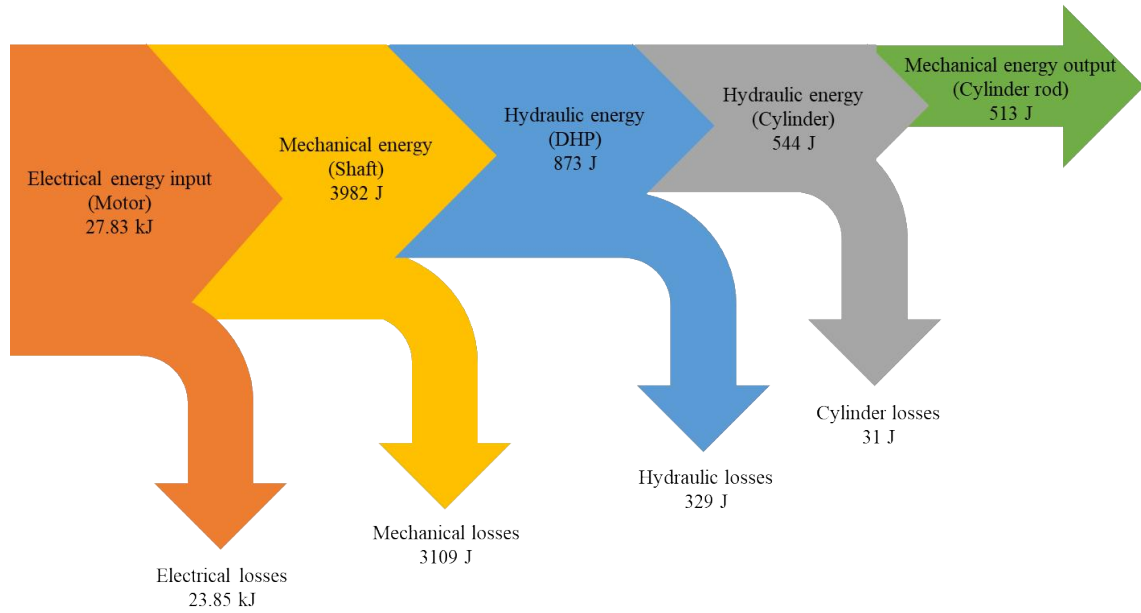
Source: Author.

Table 7.1 presents a resume of the energy efficiencies during the energy conversions in the system, the global efficiency of the system was around 1.8%, affected by the low efficiency of the pump units and the operating conditions of the electric motor. However, if the pumps with the best performance and the electric motor in its best operating region are considered, it is possible to increase the global efficiency to 44%, keeping the rest of the components.

Table 7.1 – Resume of energy efficiency.

Conversion	Efficiency simulated	Enhanced efficiency
Electrical to Mechanical	13%	87%
Mechanical to Hydraulic	22%	88%
Hydraulic to Hydraulic	62%	62%
Hydraulic to Mechanical	94%	94%
Global efficiency	1.8%	44%

Source: Author.

7.3 COMPARISON WITH AN ELECTRO HYDROSTATIC ACTUATOR

In this section, the proposed actuator (VSDEHA) is compared with an Electro Hydrostatic Actuator (EHA), modeled in APPENDIX A – Electro Hydraulic Actuator. For both

actuators, the design parameters are to be capable of moving a maximum load of 20kN in the maximum step of 0.05m, in a settling time of 1 s, the stroke was considered 0.1 m. The cylinder area of the VSDEHA was kept the same of the test bench. Applying the design method to sizing the actuator (Section 5.2), a maximum flow rate of 2.67×10^{-4} m³/s (16 L/min) is required. Applying the method presented in Section 4.2, resulted in a DHP with two pump units. The volumetric displacements of the pump units are 3 and 6 cm³/rev. The on/off valve parameters have also been optimized based on the currently available technology (LINJAMA *et al.*, 2015) and are shown in Table 7.2.

Table 7.2 – On/off valve parameters.

Parameter	Normally closed Value	Normally opened	Unit
t_{sod}	0.002	0.002	s
t_{scd}	0.002	0.002	s
ω_{on}	3000	3000	rad/s
ω_{off}	3000	3000	rad/s

Source: Author.

The actuators were simulated for different position steps in order to evaluate power consumption, energy consumption, and energy efficiency. A spring load, proportional to the cylinder displacement, is applied to the cylinder using a constant of 200kN/m.

Figure 7.22 presents the position references used to compare the EHA and VSDEHA. Step 1 is a step of 0.05 m, Step 2 is a step of 0.0225 m, and Step 3 is a step of 0.005 m. Both actuators presented a good response to the step inputs, achieving the target of 0.05 m. The settling time of the EHA for steps 1, 2 and 3 were 0.709 s, 0.508 s, and 0.625 s, respectively. The VSDEHA presented the settling time of 0.706 s, 0.649 s, and 0.634 s, respectively. During the movements of the VSDEHA, it is possible to notice some points where the movement changes suddenly, which is due to changes in the combination of pumping unit and the rotational frequency of the electric motor, in addition to other nonlinearities.

The simulation time of 3 s was used on purpose to evaluate the power consumption of both systems to move against a spring load in each different step. After the step, the actuators are kept on stand by holding the load. The electric motor model, developed for the test bench

simulation presented before, was used to evaluate the electrical power in both actuators (Figure 7.23).

Figure 7.22 – Reference inputs.
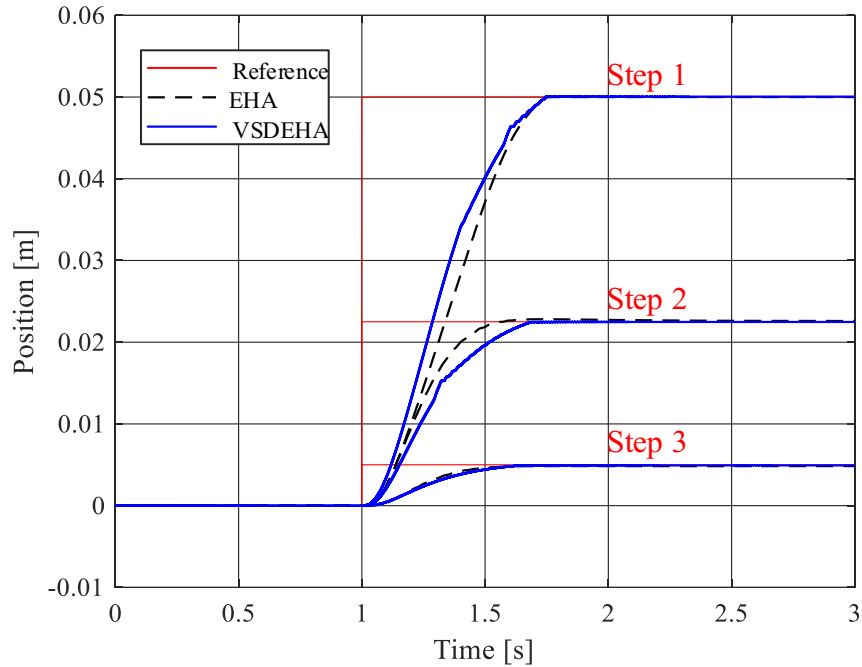
Source: Author.

Figure 7.23a presents the power consumption of the EHA. At the end of the step 1, the cylinder is maintaining position under a load of 10 kN. In the EHA, to maintain cylinder position, the pump must supply the necessary flow rate to reach a pressure level capable of balancing the external load and supplying internal leaks, which are proportional to the pressure differential on the pump. In this case, the pressure resulting from the external load has a direct effect on the pump, which requires a higher torque from the electric motor, increasing the power consumption. The average electric power needed to keep the position of the EHA in a steady state for step 1 is 1166 W. For steps 2 and 3, the external load acting in the pump is lower than the load in step 1 and the average electric power in steady state is 460 W and 420 W, respectively.

Figure 7.23 – Electric power consumption simulated.
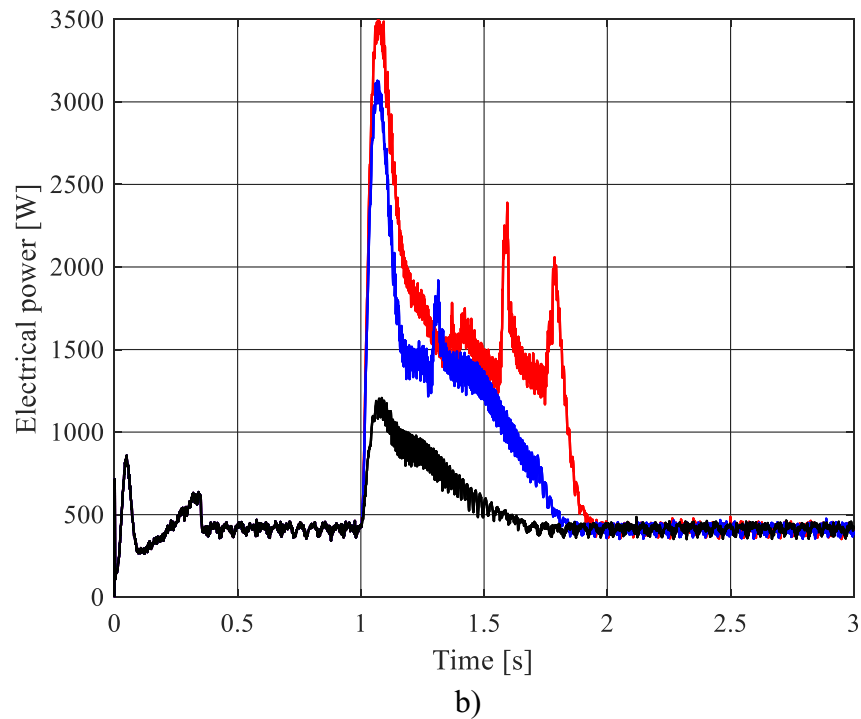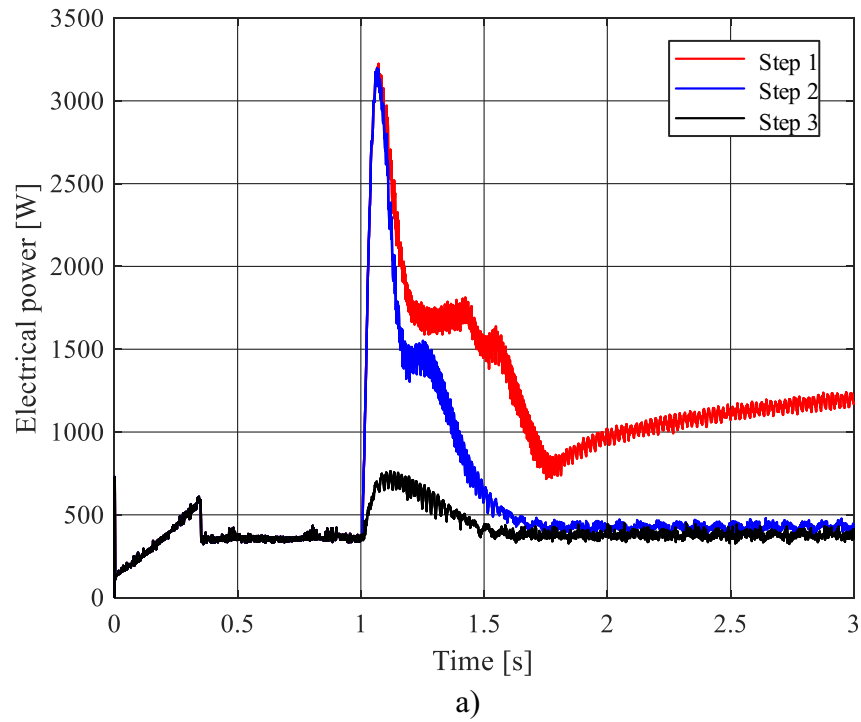
a) Electric power input for EHA, b) Electric power input for VSDEHA.
Source: Author.

In the VSDEHA, to maintain cylinder position, the on/off valves of the cylinder are closed and the pumps run at idle, sending the flow rate under a low-pressure differential to the

reservoir. The pressure resulting from the external load has no effect on the digital hydraulic pump, as the cylinder chambers are confined by the on/off valves. The DHP working at a low-pressure differential implies a low need for torque, which impacts the electrical power consumption necessary to run the DHP in idle (Figure 7.23b). However, in this case, it was observed that the electrical power consumption of the DHP is almost the same of the EHA in steps 2 and 3. This is explained by the rotational frequency of the DHP at idle (100 rpm) and the minimum necessary power to keep the electric motor speed, where even without torque, it is necessary an electric power between the range of 260 to 525 W, depending on the rotational frequency (ANNEX B – Electric motor report).

Table 7.3 presents a summary of the energy evaluation of the actuators during the simulated steps. For both actuators, the energy consumption of step 1 was higher than for the other steps due to the work to move against a higher external load, which is proportional to the cylinder displacement. Analyzing the mechanical energy available in the shaft and comparing it with the cylinder output mechanical energy, the efficiency of the EHA, for the steps 1, 2, and 3, was 33%, 45% and 15%, respectively. While the VSDEHA has presented an efficiency of 66%, 51%, and 16%, for the same steps, respectively. This efficiency cares about the hydro mechanical energy conversion inside the hydraulic circuit. For this case, the EHA has presented a low energy efficiency to maintain position under high load (step 1), mainly due to internal leakages.

For step 2 both actuators presented good efficiency, and the EHA presented a better response to the step input. In the step 3, the actuators have presented an efficiency of around 15%, which is related to the low-efficiency region of the pumps running at a low rotational frequency to reach the reference. In the case of the VSDEHA, the smaller pump is used at a higher rotational speed to achieve the position which improves the efficiency.

Due to the lack of information in the literature to obtain reliable parameters of electric motors of a similar amount of power, the electric motor model and its parameters are the same as the test bench, as the configuration of the actuators is similar. In this case, when the energy efficiency is calculated considering the electrical energy input related to the cylinder energy output, the energy efficiency drops drastically. Due to the size of the pumps used in the EHA and VSDEHA to achieve the design flow rate of 16 L/min. The motor is kept at a low rotational frequency most of the time, far from its best operating region.

Table 7.3 – Energy comparison.

Energy	Unit	EHA			VSDEHA		
		Step 1	Step 2	Step 3	Step 1	Step 2	Step 3
Electrical (Motor)	J	2896	1722	1183	2378	1992	1442
Mechanical (Shaft)	J	745.40	113.30	15.36	374.50	97.19	15.01
Hydraulic (DHP)	J	355.00	70.34	6.13	362.60	87.47	10.74
Hydraulic (Cylinder)	J	294.70	62.14	5.26	302.40	69.93	8.21
Mechanical (Cylinder)	J	250.10	51.06	2.34	249.70	50.32	2.42

Source: Author.

Therefore, the electrical results are used to obtain a quantitative value about the electrical energy used to move the actuators, as the same electric motor model is applied for both actuators. This result can be also compared with more efficient electric motor types in the future.

To evaluate the behavior of the EHA and VSDEHA, the actuators were positioned in 20%, 50% and 80% of the cylinder stroke and steps of 0.05 m, 0.0225 m, and 0.005 m were used to compare the settling time of the actuators. Figure 7.24 presents the results of this analysis where it is possible to notice that the solutions presented a similar settling time for the steps inputs and, due to the nonlinearities of the systems the settling times for each step are different, which means that the behavior of VSDEHA and EHA varies with the input amplitude and its position.

Figure 7.24 – Settling time of VSDEHA and EHA.
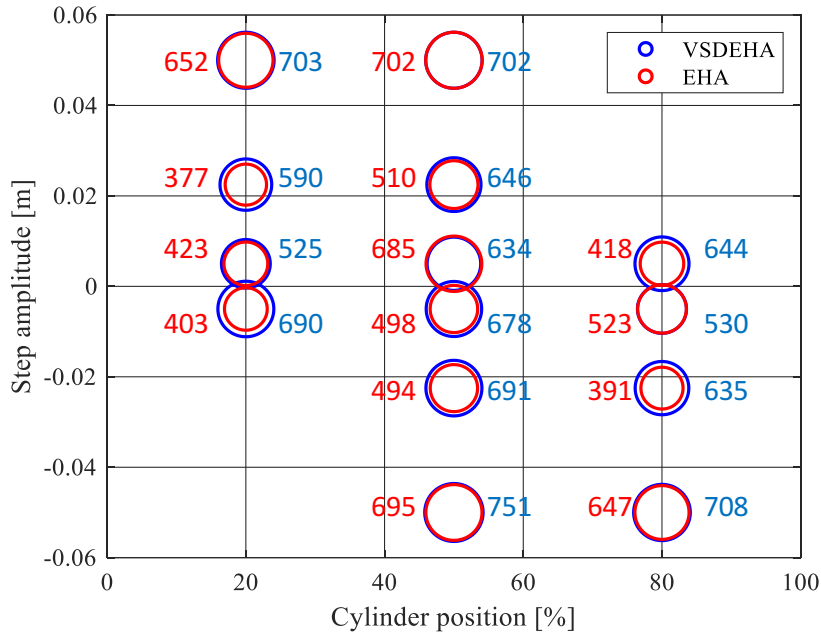
Source: Author.

7.4 CONSIDERATIONS ABOUT AIRCRAFT APPLICATION

The VSDEHA was developed to be used as a compact decentralized system, following the More Electric Aircraft and Power-by-Wire concepts to control the electric motor and pumps by wire, avoiding long hydraulic lines in the aircraft (Figure 5.1). As a compact system a small and pressurized reservoir is necessary, as in the EHA for aircraft. Since the test bench was developed using adaptations of standard components from the industry, evaluation about volume and weight is not possible to be performed at this moment.

In the VSDEHA, due to the control of the angular velocity of the electric motor, it is possible to reduce the number of valves used to control the cylinder, where it is possible to use only four on/off valves for a dual chamber cylinder configuration (Figure 5.1). A design using two pumps, as used in the comparison with the EHA, can be also used in order to obtain a compact solution.

In the VSDEHA, the angular velocity of the electric motor is always in the same direction, the cylinder direction is changed by valve commutation. There is no need to invert the angular velocity of the electric motor to change the cylinder direction. This is good from

the point of view of the pumps which can be optimized by manufacturers to run in only one direction.

About the reliability and redundancy, studies in the failure mode for digital hydraulics has been done and some results present that it is possible to keep a reasonable control of the system with valves in failure (LOPES JUNIOR, 2021; PETTERSSON, 2018). However, for this specific topology, a detailed study about the behavior of the system under failure was not carried out. The proposed redundancy for this system is the use of a similar system as backup, changing the main actuator to damping mode.

About the electric components, the actual components used to control the EHA, such as the inverter and sensors, can be also used to control the VSDEHA. The reduced number of on/off valves is an advantage of the VSDEHA if compared with other digital solutions. The use of less valves implies less power consumption of the electrical system of the aircraft.

As presented in the comparison with the EHA, to maintain position under high loads, the electric motor of the EHA must keep a high torque under low or zero rotational frequency, which increases the power consumption. As consequence, the electromagnetic torque needed to maintain the cylinder position is proportional to the current, as presented in the modelling of the induction motor (Section 5.3.5). According to Gundabattini *et al.* (2021), the temperature of the electric machine increases non-linearly with the load due to the losses in the motor, such as the stator cooper losses. The cooper losses are produced by the flux of current in the stator windings, which generates heat. These losses are dependent on the square of stator current (GUNDABATTINI *et al.*, 2021). The operating temperature of the components determines their service life and reliability, dissipate the heat is one of the challenges nowadays (MARÉ; FU, 2017).

In general, components developed for aeronautical applications must be of better quality and efficiency than industry standard components, due to the safety and reliability requirements that must be met for the component to obtain certification. For the proposed digital hydraulic actuator, better components can be developed in order to improve the behavior and efficiency of the system as all. The test bench was developed to be a proof of concept of the proposed actuator, achieving the Technology Readiness Level 3 (TRL3), showing a great potential to be developed, as the test bench does not reflect the maximum potential of the proposed system.

7.4.1 Simulation in aircraft environment

An aircraft model called Aero-Data Model in a Research Environment – ADMIRE was used to analyze the behavior of the VSDEHA in an aircraft environment. The ADMIRE is a software used to implement a Generic Aircraft Model (GAM) of a single seat delta canard unstable aircraft with 6 degrees of freedom, which includes the flight control systems (FCS), engine, actuators, and sensors (FORSSELL; NILSSON, 2005). The development of the ADMIRE started in 1997, using the GAM developed by Saab AB as basis, at Aeronautical Research Institute of Sweden (FFA) (FORSSELL; NILSSON, 2005). Since then, the model is used to develop studies in aircraft modelling and design of the control systems with aerodynamic data.

The adaptations of the ADMIRE to test the digital hydraulic solutions developed at LASHIP were carried out in Lopes Junior (2021). The results of the analysis using the VSDEHA were presented in the 33RD Congress of the International Council of the Aeronautical Sciences under the title of "A comparative analysis of innovative digital hydraulic actuators for primary flight control" (LOPES *et al.*, 2022) where the topologies of digital hydraulic actuators developed in LASHIP (DHA, DEHA, and VSDEHA) were compared against a SHA model, using the ADMIRE model as benchmark.

Figure 7.25 presents the deflection and the hinge moments for the control surfaces left inner elevon (LIE) and left outer elevon (LOE) during the roll-turn mission of the ADMIRE. In general, all actuators were able to accomplish the mission following the deflection reference presenting overshooting for different input signals. Figure 7.25a presents the overshoot comparison for the time between 5 and 5.5 s, where the overshoot for the SHA, DHA, DEHA and VSDEHA, were 5.3%, 13.8%, 4.8%, and 10.9%, respectively. For a displacement of -4.6°. Figure 7.25b the actuator response times were 0.168 s for the ADMIRE model, 0.197 s for the SHA, 0.241 s for the DHA and VSDEHA, and 0.351s for the DEHA (LOPES *et al.*, 2022).

Despite the oscillations presented by the digital hydraulic actuators, the hinge moment level was similar for all actuators (Figure 7.25c and Figure 7.25d). Oscillations and overshoots increase the workload of the actuators, increasing the output energy needed to follow the position reference, which impacts the final energy consumption. However, comparing with the energy input of the SHA the levels of energy consumption are completely different.

As previously mentioned, the SHA has to keep the system pressurized to compensate for internal leaks and during movement, part of the energy generated in the pump is dissipated

in the valve. In the DHA, the analysis does not consider the energy necessary to produce the constant pressure lines. In this solution, the combination of pressure lines and cylinder areas are used to move the cylinder. Due to the characteristics of the digital hydraulics, the force required to move the cylinder may be less than the force available in the cylinder, which causes the cylinder to spend more energy as it works with constant pressure sources.

Figure 7.25 – Flight surface responses.
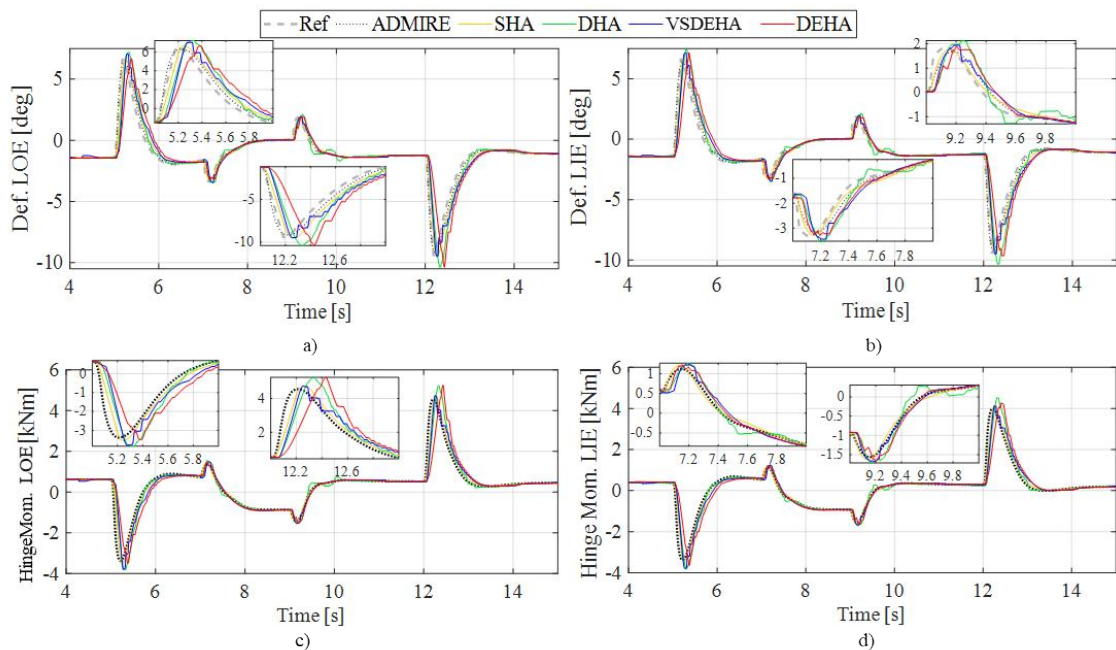
Source: Adapted from Lopes *et al.* (2022).

In the DEHA and VSDEHA, the actuators work using the concept of flow source, and the pressure is a consequence of the external load. This characteristic follows the power-on-demand concept, where the actuators work with a pressure proportional to the load. However, the DEHA has a limited number of discrete velocities, where it is not possible to meet velocities between two consecutive levels. Comparing the energy input of the digital solutions with the SHA, in the LOE during the roll-turn mission, it was noticed that the DHA presented an energy saving of 3.5 times, the DEHA present an energy saving of 9.5 times, and the VSDEHA presented an energy saving of 22 times (Figure 7.26).

As the third topology developed at LASHIP, the VSDEHA is a natural evolution of the DHA and DEHA, where the use of a different control strategy to control the on/off valves and electric motor presents improvements in the behavior and energy saving. Further studies involving an analysis of flight quality and handling of the aircraft, using the VSDEHA, have to

be developed to verify the effects of the overshooting deviation and the settling time during the flight mission. In addition, further studies involving redundancy, failure mode, and the use of different control strategies must be developed to evaluate the applicability for aircraft.

Figure 7.26 – Energy consumption of LIE and LOE.
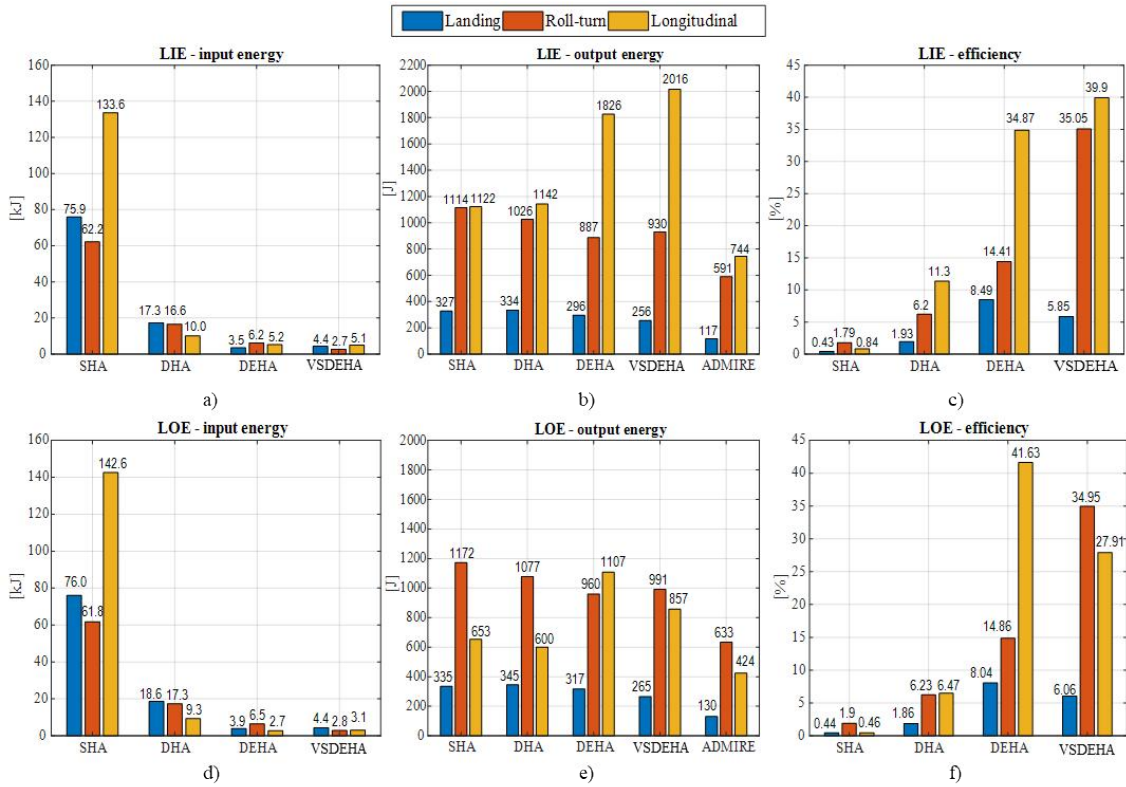
Source: Adapted from Lopes *et al.* (2022).

8 CONCLUSIONS

The main objective of the present thesis was the development of an actuator for aircraft applications using the digital hydraulics concept allied to the more electric aircraft and power by wire concepts to obtain an efficient and decentralized topology. The main idea came from the characteristics of the EHA combined with the use of digital hydraulics to develop a power on demand actuator aiming in to reduce the energy dissipation.

The topology was called as Variable Speed Digital Electro-Hydraulic Actuator (VSDEHA). In this topology, the digital hydraulics is used to direct the fluid of the DHP to the cylinder, controlling its movement without throttling the hydraulic power generated by the pump. The flow rate is controlled by the number of active pump units and by the angular velocity of the electric motor, which are chosen according to the flow rate level required and pressure conditions of the cylinder, aiming into use the combination of pump unit and angular velocity with best efficiency available.

A method to sizing a digital hydraulic pump with variable speed is proposed. Based in the requirements of maximum and minimum flow rate, maximum working pressure, and maximum and minimum angular speed available, different configurations of digital hydraulic pumps can be created varying the number of pump units and their volumetric displacement sizes. Configured DHPs are compared against each other to get the most efficient configuration. In addition, the results of the method are used in the control strategy to improve energy efficiency. A method to sizing the cylinder and defines the flow rate is used and combined with the proposed method to sizing a DHP can be used together as a guideline to sizing a digital hydraulic actuator.

The component models are presented, including the electric motor model which can be used to simulate the electrical power consumption. The MatLab/Simulink® and Hopsan play an important role into the implementation of the models used. The parameters used were obtained from experiments carried out during the development of this thesis or obtained from other works developed at LASHIP. The models and parameters can be useful for future works as some parameters as the electric motor parameters and LuGre friction parameters are difficulty to obtain.

In the control strategy, an assistive load identifier using Fuzzy logic was proposed to select specific valves to dissipate the extra external load energy. This strategy presented good results in simulation and experiments, improving the cylinder controllability and energy consumption, where the energy saving in the experiments with the assistive load identifier was

about 3%. With the use of the variable speed, it was also possible to obtain a smooth and continuous movement due to the fine flow rate control.

The energy saving is one of the main goals in to use digital hydraulics, which aims to avoid the use of throttling control in the hydraulic power produced by the pump. The results using the validated model of the digital hydraulic pump to calculate the efficiency of the conversion of the hydraulic energy from DHP to cylinder output energy, considering a pressurized reservoir, was about 58%. This value cold be improved with the use of more efficient pump units.

The electric motor used, has presented a maximum efficiency point of 85.7% running at 1800 rpm with a torque load of 30.38 Nm in the indirect field vector control. However, due to the volumetric displacement size of the pump units used, the angular velocity range during the experiments was between 500 to 900 rpm, which is a low efficiency region of the electric motor (6 to 70%), decreasing the global efficiency of the test bench. This approach crossing the borders of the electro mechanical and hydraulic areas is interesting from the design perspective, as the knowledge about the cause effect relationship between system variables have to be used to improve the global efficiency of the solution.

A comparison with an EHA model was performed at equal work conditions. The VSDEHA presented a dynamic behavior similar to the EHA and hydro mechanical efficiency of 66% while the EHA presented an efficiency of 33%, mainly due to the internal leakages. A comparison published by LASHIP, including the author of this thesis, was used to compare the models of the digital hydraulic solutions developed in LASHIP and a SHA model, inside an aircraft model environment. The VSDEHA also presented a better average energy saving and was able to accomplish the roll-turn mission used to compare the models.

The topology presented is in early stages of development, the validated model and the test bench results can be considered as development in a Technology Readiness Level 3, where the proof of concept was achieved. Further studies evaluating the solution from other perspectives are necessary in order to gain maturity for aircraft applications due to the high level of safety and reliability required in this area. Besides, technological improvements in components are necessary to achieve the full potential of the solution.

Finally, VSDEHA showed good results and can be easily directed to other application areas, such as mobile heavy machinery and industry, due to the use of cheaper, simpler, and more robust components, in order to reduce implementation and maintenance costs. The

research and results contribute to development and dissemination of digital hydraulics in Brazil, where LASHIP is a pioneer in this topic of research.

8.1 PROPOSALS FOR FUTURE STUDIES

Different areas of knowledge were approached in the development of the thesis. Due to the limited time and the focus on the objective of developing a new actuator, it was not possible to deepen the studies in all the areas addressed. Therefore, the following topics are suggested for future work.

- Develop a study about how to evaluate the dynamic response for digital hydraulic actuators considering the nonlinearities and the intrinsic behavior of the digital solutions;
- Develop a study about the relationship of the volumetric displacement of the pumps and electric motor angular speed to improve the use of the best operating region of the electric motor;
- Develop an electric motor model of a Permanent Magnet Synchronous Machine to analyze the energy efficiency of the system;
- Develop a study using Fuzzy logic and Neural Networks to control the on/off valves;
- Develop a study of a digital hydraulic actuator in a closed circuit with pressurized reservoir;
- Develop a study to improve control strategies to obtain better energy efficiency;
- Develop a study about the redundancy and failure modes for this topology.

REFERENCES

ACHTEN, P. **Convicted to Innovation in Fluid Power.** Proceedings of the Institution of Mechanical Engineers, Part I: Journal of Systems and Control Engineering, v. 224, n. 6, p. 619–621, 2010.

ALLE, N.; HIREMATH, S. S.; MAKARAM, S.; SUBRAMANIAM, K.; TALUKDAR, A. **Review on electro hydrostatic actuator for flight control**. International Journal of Fluid Power, v. 17, n. 2, p. 125–145, 2016.

ARGO HYTOS. **Datasheet GL HA0060**. , 2019.

ASTROM, K. J.; DE-WIT, C. C. **Revisiting the LuGre friction model**. IEEE Control Systems, v. 28, n. 6, p. 101–114, dez. 2008.

AWREJCEWICZ, J.; OLEJNIK, P. **Analysis of dynamic systems with various friction laws**. Applied Mechanics Reviews, v. 58, n. 1–6, p. 389–410, 2005.

BELAN, H. C. **Sistemas de atuação hidráulicos digitais para aviões com foco em eficiência energética**. Tese de Doutorado, Universidade Federal de Santa Catarina, Centro Tecnológico, Programa de Pós Graduação em Engenharia Mecânica, Florianópolis, 2018.

BELAN, H. C.; LOCATELI, C. C.; DE PIERI, E. R.; DE NEGRI, V. J. **Aumento da eficiência energética em sistemas hidráulicos utilizando hidráulica digital**. Anais do 20° Congresso Brasileiro de Automática- CBA. Belo Horizonte - MG, Brasil: 2014.

BENNETT, J. W.; ATKINSON, G. J.; MECROW, B. C.; ATKINSON, D. J. **Fault-Tolerant Design Considerations and Control Strategies for Aerospace Drives.** IEEE Transactions on Industrial Electronics, v. 59, n. 5, p. 2049–2058, maio 2012.

BIM, E. **Máquinas Elétricas e Acionamento**. 2° ed. Rio de Janeiro: Elsevier, 2012.

BOGLIETTI, A.; CAVAGNINO, A.; TENCONI, A.; VASCHETTO, S. **The safety critical electric machines and drives in the more electric aircraft**: A survey. IECON Proceedings (Industrial Electronics Conference), p. 2587–2594, 2009.

BOLOGNANI, S.; ZORDAN, M.; ZIGLIOTTO, M. **Experimental fault-tolerant control of a PMSM drive.** IEEE Transactions on Industrial Electronics, v. 47, n. 5, p. 1134–1141, 2000.

BOSCH REXROTH, G. **External gear pump Series B**. , 2013. Disponível em: <https://md.boschrexroth.com/modules/BRMV2PDFDownload-internet.dll/re10088_2013-09.pdf?db=brmv2&lvid=1175079&mvid=13786&clid=20&sid=ED93D565FC2AE32532173 62E17E8EB70.borex-tc&sch=M&id=13786,20,1175079>

BOSCH REXROTH, G. **External gear pump Standard performance AZPW**. , 2016.

BOSE, B. K. **Modern Power Electronics and AC Drives**. [s.l.] Prentice Hall, 2002.

BOSTANCI, E.; MOALLEM, M.; PARSAPOUR, A.; FAHIMI, B. **Opportunities and Challenges of Switched Reluctance Motor Drives for Electric Propulsion**: A Comparative Study. IEEE Transactions on Transportation Electrification, v. 3, n. 1, p. 58–75, 2017.

BRAUN, R.; KRUS, P. **Tool-Independent Distributed Simulations using Transmission Line Elements and the Functional Mock-up Interface**. SNE Simulation Notes Europe, v. 24, n. 3–4, p. 149–154, 2014.

BREIDI, F.; HELMUS, T.; HOLLAND, M.; LUMKES, J. **The impact of peak-and-hold and reverse current driving strategies on the dynamic performance of commercial**

cartridge valves. ASME/BATH 2014 Symposium on Fluid Power and Motion Control, FPMC 2014, p. 1–8, 2014.

CANALS CASALS, L.; MARTINEZ-LASERNA, E.; AMANTE GARCÍA, B.; NIETO, N. **Sustainability analysis of the electric vehicle use in Europe for CO2 emissions reduction**. Journal of Cleaner Production, v. 127, p. 425–437, 2016.

CAO, W.; MECROW, B. C.; ATKINSON, G. J.; BENNETT, J. W.; ATKINSON, D. J. **Overview of electric motor technologies used for more electric aircraft (MEA)**. IEEE Transactions on Industrial Electronics, v. 59, n. 9, p. 3523–3531, 2012.

CASSANDRAS, C. G.; LAFORTUNE, S. **Introduction to Discrete Event Systems**. Second ed. Boston, MA: Springer US, 2008.

CHAKRABORTY, I.; JACKSON, D.; TRAWICK, D. R.; MAVRIS, D. **Development of a Sizing and Analysis Tool for Electrohydrostatic and Electromechanical Actuators for the More Electric Aircraft**. 2013 Aviation Technology, Integration, and Operations Conference. Reston, Virginia: American Institute of Aeronautics and Astronautics, 12 ago. 2013a. Disponível em: <https://arc.aiaa.org/doi/10.2514/6.2013-4282>

CHAKRABORTY, I.; TRAWICK, D. R.; JACKSON, D.; MAVRIS, D. **Electric Control Surface Actuator Design Optimization and Allocation for the More Electric Aircraft**. 2013 Aviation Technology, Integration, and Operations Conference. Reston, Virginia: American Institute of Aeronautics and Astronautics, 12 ago. 2013b. Disponível em: <https://arc.aiaa.org/doi/10.2514/6.2013-4283>

COSTA, G. K.; SEPEHRI, N. **Hydrostatic transmissions and actuators: operation, modelling and applications**. [s.l.] John Wiley & Sons, Ltd, 2015. v. 4

DE NEGRI, V. J.; RAMOS FILHO, J. R. B.; SOUZA, A. D. C. **A design method for hydraulic positioning systems**. Proceedings of USA: NFPA. Las Vegas, 2008.

DE NEGRI, V. J.; WANG, P.; PLUMMER, A.; JOHNSTON, D. N. **Behavioural prediction of hydraulic step-up switching converters**. International Journal of Fluid Power, v. 15, n. 1, p. 1–9, 2014.

DE WIT, C. C.; LISCHINSKY, P.; ÅSTRÖM, K. J.; OLSSON, H. **A New Model for Control of Systems with Friction**. IEEE Transactions on Automatic Control, v. 40, n. 3, p. 419–425, 1995.

DONKOV, V. H.; ANDERSEN, T. O.; LINJAMA, M.; EBBESEN, M. K. **Digital Hydraulic Technology for Linear Actuation**: A State of the Art Review. International Journal of Fluid Power, p. 263–304, 2020.

DUNKER, C.; POOLE, K.; THIELECKE, F. **Towards More-Efficient Aircraft Hydraulic Systems**: Conceptual Design of a Variable-Speed Fixed-Displacement Electric Motor Pump. SAE International, 2013.

ELBULUK, M. E.; KANKAM, M. D. **Motor drive technologies for the power-by-wire (PBW) program: options, trends and tradeoffs**. Proceedings of the IEEE 1995 National Aerospace and Electronics Conference. NAECON 1995. IEEE, 1995.

FORSSELL, L.; NILSSON, U. **ADMIRE The Aero-Data Model In a Research Environment Version 4.0**, Model Description. FOI-Totalforsvarets forskningsinstitut, 2005.

GARCIA, A.; CUSIDÓ, J.; ROSERO, J. A.; ORTEGA, J. A.; ROMERAL, L. **Reliable electro-mechanical actuators in aircraft.** IEEE Aerospace and Electronic Systems

Magazine, v. 23, n. 8, p. 19–25, 2008.

GRANOVSKII, M.; DINCER, I.; ROSEN, M. A. **Economic and environmental comparison of conventional, hybrid, electric and hydrogen fuel cell vehicles**. Journal of Power Sources, v. 159, n. 2, p. 1186–1193, 2006.

GUNDABATTINI, E.; KUPPAN, R.; SOLOMON, D. G.; KALAM, A.; KOTHARI, D. P.; ABU BAKAR, R. **A review on methods of finding losses and cooling methods to increase efficiency of electric machines**. Ain Shams Engineering Journal, v. 12, n. 1, p. 497–505, 2021.

HEIKKILA, M.; LINJAMA, M. **Hydraulic Energy Recovery in Displacement Controlled Digital Hydraulic System**. Proceedings from the 13th Scandinavian International Conference on Fluid Power, June 3-5, 2013, Linköping, Sweden. 2013. Disponível em: <https://ep.liu.se/en/conference-article.aspx?series=ecp&issue=92&Article_No=51>

HEIKKILÄ, M.; TAMMISTO, J.; HUOVA, M.; HUHTALA, A. K.; LINJAMA, M. **Experimental evaluation of a digital hydraulic power management system**. Third workshop on Digital Fluid Power. Tampere: 2010. Disponível em: <https://urn.fi/URN:NBN:fi:tty-201604253879>

HUGHES, A.; DRURY, B. **Electric motors and drives: fundamentals, types and applications**. 4. ed. [s.l.] Newnes, 2013. v. 82

ISHIKAWA, T.; DOHMEKI, H. **The Fundamental Design Technique of Switched Reluctance Motors, and Comparison with PMSM**. 2012 XXth International Conference on Electrical Machines. IEEE, 2012.

JACK, A. G.; MECROW, B. C.; HAYLOCK, J. A. **A comparative study of permanent magnet and switched reluctance motors for high-performance fault-tolerant applications**. IEEE Transactions on Industry Applications, v. 32, n. 4, p. 889–895, 1996.

JAISWAL, S.; SOPANEN, J.; MIKKOLA, A. **Efficiency comparison of various friction models of a hydraulic cylinder in the framework of multibody system dynamics**. Nonlinear Dynamics, v. 104, n. 4, p. 3497–3515, 2021.

JIAN, F.; MARÉ, J. C.; YONGLING, F. **Modelling and simulation of flight control electromechanical actuators with special focus on model architecting, multidisciplinary effects and power flows**. Chinese Journal of Aeronautics, v. 30, n. 1, p. 47–65, 2017.

KARAGÖZ, Y.; BALCI, Ö.; GEZER, O.; KALE, S.; KÖTEN, H. **Performance analysis of a hybrid lightweight vehicle with downsized engine**. Energy Sources, Part A: Recovery, Utilization and Environmental Effects, v. 42, n. 12, p. 1513–1525, 2020.

KRAUSE, P. C.; WASYNCZUK, O.; SUDHOF, S.; PEKAREK, S. **Analysis of Electric Machinery and Drive Systems**. Third Edit ed. [s.l.] John Wiley & Sons, 2013. v. 75

KRISHNAN, R. **Switched reluctance motor drives: modeling, simulation, analysis, design, and applications**. [s.l.] CRC press LLC, 2001.

LEE, W.; SCHUBERT, E.; LI, Y.; LI, S.; BOBBA, D.; SARLIOGLU, B. **Electrification of turbocharger and supercharger for downsized internal combustion engines and hybrid electric vehicles-benefits and challenges**. 2016 IEEE Transportation Electrification Conference and Expo, ITEC 2016, 2016.

LINJAMA, M. **Digital Fluid Power – State of the Art**. Proceedings of the 12th Scandinavian International Fluid Power Conference Vol3, p. 331– xx, 2011.

LINJAMA, M.; PALONIITTY, M.; TIAINEN, L.; HUHTALA, K. **Mechatronic Design of Digital Hydraulic Micro Valve Package**. Procedia Engineering, v. 106, p. 97–107, 2015.

LINJAMA, M.; SCHEIDL, R.; SCHMIDT, S. **Discussion: Is the future of fluid power digital?** Proceedings of the Institution of Mechanical Engineers. Part I: Journal of Systems and Control Engineering, v. 226, n. 6, p. 726–727, 2011.

LINSINGEN, I. VON. **Fundamentos de Sistemas Hidráulicos**. 4. ed. Revisada, Editora UFSC, Florianópolis, 2013.

LOPES JUNIOR, R. S. **Avaliação do desempenho dinâmico de um atuador hidráulico digital para aplicações aeronáuticas em condição de falha**. [s.l.] Dissertação de mestrado - Universidade Federal de Santa Catarina, Centro Tecnológico, Programa de Pós-Graduação em Engenharia mecânica, Florianópolis, 2021.

LOPES, R. S.; SILVA, D. O. E; NOSTRANI, M. P.; DELL'AMICO, A.; KRUS, P.; DE NEGRI, V. J. **A COMPARATIVE ANALYSIS OF INNOVATIVE DIGITAL HYDRAULIC ACTUATORS FOR PRIMARY FLIGHT CONTROL**. 33RD Congress of the International Council of the Aeronautica Sciences. Stockholm: 2022.

MANTOVANI, I. J. **Otimização dos chaveamentos entre válvulas ON/OFF em atuadores hidráulicos digitais**. Dissertação de mestrado - Universidade Federal de Santa Catarina, Centro Tecnológico, Programa de Pós-Graduação em Engenharia mecânica, Florianópolis, 2019.

MANTOVANI, I. J.; VIGOLO, V.; BELAN, H. C.; DE NEGRI, V. J. **Overview of the Digital Hydraulic Actuator (DHA) Concept for Aircraft**. Proceedings of the 4th Workshop on Innovative Engineering for Fluid Power, 2018. Disponível em: <https://ep.liu.se/en/conference-article.aspx?series=ecp&issue=156&Article_No=5>

MARÉ, J.-C. **Aerospace Actuators 1: Needs, Reliability and Hydraulic Power Solutions**. Hoboken, NJ, USA: John Wiley & Sons, Inc., 2016.

MARÉ, J.-C. **Aerospace Actuators 2: signal-by-wire and power-by-wire**. John Wiley & Sons, 2017.

MARÉ, J. C.; FU, J. **Review on signal-by-wire and power-by-wire actuation for more electric aircraft**. Chinese Journal of Aeronautics Chinese Society of Aeronautics and Astronautics, 2017.

MARQUES, F.; FLORES, P.; PIMENTA CLARO, J. C.; LANKARANI, H. M. **A survey and comparison of several friction force models for dynamic analysis of multibody mechanical systems**. Nonlinear Dynamics, v. 86, n. 3, p. 1407–1443, 2016.

MATHWORKS. **Three-Phase Asynchronous Drive with Sensor Control**. Disponível em: <www.mathworks.com/help/sps/ug/three-phase-asynchronous-drive-with-sensor-control.html>. Acesso em: 6 abr. 2022.

MATSUSE, K.; SAITO, S.; TADAKUMA, S.; BRUSSO, B. **History of motor drive technologies in Japan, Part 2**. IEEE Industry Applications Magazine, v. 20, n. 1, p. 8–15, 2013.

MOIR, I.; SEABRIDGE, A. **Aircraft Systems: Mechanical, electrical, and avionics subsystems integration**. Third ed. Chichester, UK: John Wiley & Sons, Ltd, 2008.

NAAYAGI, R. T. **A review of more electric aircraft technology**. **2**013 International Conference on Energy Efficient Technologies for Sustainability, ICEETS 2013, p. 750–753,

2013.

NANAKI, E. A.; KORONEOS, C. J. **Comparative economic and environmental analysis of conventional, hybrid and electric vehicles** - The case study of Greece. Journal of Cleaner Production, v. 53, p. 261–266, 2013.

NOSTRANI, M. P. **DEVELOPMENT OF A DIGITAL ELECTRO HYDROSTATIC ACTUATOR FOR APPLICATION IN AIRCRAFT FLIGHT CONTROL SURFACES**. Tese de doutorado - Universidade Federal de Santa Catarina, Centro Tecnológico, Programa de Pós-Graduação em Engenharia mecânica, Florianópolis, 2021.

NOSTRANI, M. P.; KRUS, P.; DE NEGRI, V. J.; DELL'AMICO, A. **An Aircraft Actuator Driven by Digital Hydraulic Pumps.** DINAME 2019 - Proceedings of the XV International Symposium on Dynamic Problems of Mechanics, M.A. Savi, T.G. Ritto and W.M. Bessa (Editors), ABCM, Buzios, RJ, Brazil, March 10th to 15th, 2019.

OBED, A. A.; KADHIM, A. K. Speed and Current Limiting Control Strategies for BLDC Motor Drive System: A Comparative Study. **International Journal of Advanced Engineering Research and Science**, v. 5, n. 2, p. 119–130, 2018.

ONSEMI. **IGBT Technologies and Applications Overview: How and When to Use an IGBT.** www.Onsemi.Com. [s.l: s.n.]. Disponível em: <https://www.onsemi.com/pub/Collateral/TND6235-D.PDF>.

PATEL, J. M.; HIRVANIYA, H. V; RATHOD, M. **Simulation and Analysis of Brushless DC Motor Based on Sinusoidal PWM Control**. Simulation v. 2, n. 3, p. 2004–2006, 2014.

PETTERSSON, R. **Safety analysis on digital hydraulics: Redundancy study for aviation applications**. [s.l.] Master Thesis, Division of Fluid and Mechatronic Systems, Linköping University, 2018.

QAZI, A.; HUSSAIN, F.; RAHIM, N. A. B. D.; HARDAKER, G.; ALGHAZZAWI, D.; SHABAN, K.; HARUNA, K. Towards Sustainable Energy: A Systematic Review of Renewable Energy Sources, Technologies, and Public Opinions. **IEEE Access**, v. 7, p. 63837–63851, 2019.

QIAO, G.; LIU, G.; SHI, Z.; WANG, Y.; MA, S.; LIM, T. C. **A review of electromechanical actuators for More/All Electric aircraft systems**. Proceedings of the Institution of Mechanical Engineers, Part C: Journal of Mechanical Engineering Science, v. 232, n. 22, p. 4128–4151, 2018.

RADUN, A. V. **High-Power Density Switched Reluctance Motor Drive for Aerospace Applications**. IEEE Transactions on Industry Applications, v. 28, n. 1, p. 113–119, 1992.

REZAEI, N.; COSSAR, C.; MEHRAN, K. **Modelling and Analysis of Indirect Field-Oriented Control of SVPWM-Driven Induction Motor Drive Based on a Voltage Source Inverter**. Canadian Conference on Electrical and Computer Engineering, v. 2018- May, p. 1–6, 2018.

RONGJIE, K.; ZONGXIA, J.; SHAOPING, W.; LISHA, C. **Design and Simulation of Electro-hydrostatic Actuator with a Built-in Power Regulator.** Chinese Journal of Aeronautics, v. 22, n. 6, p. 700–706, 2009.

ROSERO, J. A.; ORTEGA, J. A.; ALDABAS, E.; ROMERAL, L. **Moving towards a more electric aircraft**. IEEE Aerospace and Electronic Systems Magazine, v. 22, n. 3, p. 3–9, 2007.

ROSS, T. J. **Fuzzy Logic with Engineering Applications**. 3rd ed. John Wiley & Sons, 2010.

SARLIOGLU, B.; MORRIS, C. T. **More Electric Aircraft: Review, Challenges, and Opportunities for Commercial Transport Aircraft**. IEEE Transactions on Transportation Electrification, v. 1, n. 1, p. 54–64, 2015.

SCHÄFER, A. W.; BARRETT, S. R. H.; DOYME, K.; DRAY, L. M.; GNADT, A. R.; SELF, R.; O'SULLIVAN, A.; SYNODINOS, A. P.; TORIJA, A. J. **Technological, economic and environmental prospects of all-electric aircraft**. Nature Energy, v. 4, n. 2, p. 160–166, 2019.

SCHEIDL, R.; LINJAMA, M.; SCHMIDT, S. **Is the future of fluid power digital?** Proceedings of the Institution of Mechanical Engineers. Part I: Journal of Systems and Control Engineering, v. 226, n. 6, p. 721–723, 2012.

SILVA, D. O. E; CARVALHO, L. A. B.; DE NEGRI, V. J.; WALTRICH, G. **Digital Hydraulic Pump: an energy efficiency study**. Proceedings of the 26th International Congress of Mechanical Engineering. ABCM, 2021. Disponível em: <http://abcm.org.br/anais-de-eventos/COB2021/1613>

SILVA, D. O. E; NOSTRANI, M. P.; LOPES JUNIOR, R. S.; WALTRICH, G.; KRUS, P.; DE NEGRI, V. J. **Digital Electro Hydraulic Actuator with Variable Speed Digital Hydraulic Pump : A Design Overview**. 2022 IEEE Global Fluid Power Society PhD Symposium. Naples, Italy, 2022.

SIVANANDAM, S. N.; SUMATHI, S.; DEEPA, S. N. **Introduction to fuzzy logic using MATLAB**. Berlim. Springer, 2007.

TEIXEIRA, P. L. **Análise Teórico Experimental De Prensa Dobradeira Hidráulica Controlada Por Bomba-Motor Com Velocidade Variável**. Dissertação de mestrado - Universidade Federal de Santa Catarina, Centro Tecnológico, Programa de Pós-Graduação em Engenharia mecânica, Florianópolis, 2015.

TRAN, X. B.; HAFIZAH, N.; YANADA, H. **Modeling of dynamic friction behaviors of hydraulic cylinders**. Mechatronics, v. 22, n. 1, p. 65–75, 2012.

TRAN, X. B.; KHAING, W. H.; ENDO, H.; YANADA, H. **Effect of friction model on simulation of hydraulic actuator.** Proceedings of the Institution of Mechanical Engineers. Part I: Journal of Systems and Control Engineering, v. 228, n. 9, p. 690–698, 2014.

VALDIERO, A. C. **CONTROLE DE ROBÔS HIDRÁULICOS COM COMPENSAÇÃO DE ATRITO**. Tese de doutorado - Universidade Federal de Santa Catarina, Centro Tecnológico, Programa de Pós-Graduação em Engenharia mecânica, Florianópolis, 2005..

VAN DEN BOSSCHE, D. **The A380 Flight Control Electrohydrostatic Actuators, Achievements and Lessons Learnt**. 25Th International Congress of the Aeronautical Sciences. 2006.

WANG, S.; TOMOVIC, M.; LIU, H. **Commercial Aircraft Hydraulic Systems**. [Shanghai Jiao Tong University Press Aerospace Series. Academic Press, 2016.

WRÓBLEWSKA-KREPSZTUL, J.; RYDZKOWSKI, T.; BOROWSKI, G.; SZCZYPIŃSKI, M.; KLEPKA, T.; THAKUR, V. K. **Recent progress in biodegradable polymers and nanocomposite-based packaging materials for sustainable environment.** International Journal of Polymer Analysis and Characterization, v. 23, n. 4, p. 383–395, 2018.

YANADA, H.; TAKAHASHI, K.; MATSUI, A. **Identification of Dynamic Parameters of**

Modified LuGre Model and Application to Hydraulic actuator. JFPS International Journal of Fluid Power System, v. 3, n. 1, p. 1–8, 2010.

YANG, Z.; SHANG, F.; BROWN, I. P.; KRISHNAMURTHY, M. **Comparative study of interior permanent magnet, induction, and switched reluctance motor drives for EV and HEV applications**. IEEE Transactions on Transportation Electrification, v. 1, n. 3, p. 245–254, 2015.

ZAPOROZHETS, O.; ISAIENKO, V.; SYNYLO, K. **Trends on current and forecasted aircraft hybrid electric architectures and their impact on environment.** Energy, v. 211, p. 118814, 2020.

ZHANG, J.; YANG, M.; XU, B. **Design and experimental research of a miniature digital hydraulic valve**. Micromachines, v. 9, n. 6, p. 1–12, 2018.

ZHANG, L. W.; SOJOBI, A. O.; KODUR, V. K. R.; LIEW, K. M. **Effective utilization and recycling of mixed recycled aggregates for a greener environment**. Journal of Cleaner Production, v. 236, p. 117600, 2019.

ZHANG, Q.; KONG, X.; YU, B.; BA, K.; JIN, Z.; KANG, Y. **Review and Development Trend of Digital Hydraulic Technology**. Applied Sciences, v. 10, n. 2, p. 579, 13 jan. 2020.

ZUO, L.; WANG, C.; CORDER, G. D. **Strategic evaluation of recycling high-tech metals from urban mines in China**: An emerging industrial perspective. Journal of Cleaner Production, v. 208, p. 697–708, 2019.

APPENDIX A – ELECTRO HYDRAULIC ACTUATOR

The electro hydrostatic actuator was developed based on the same requirements used in the test bench, which are maximum force 20 kN, a settling time of 1 s, a maximum step of 0.05 m, a maximum pressure 21 MPa, and a stroke of 0.2 m. Aiming to develop an EHA similar to the test bench. The cylinder area of the EHA was considered the average area of the four-chamber cylinder used in the test bench ($A_{EHA} = 23.72 \times 10^{-4} \mathrm{m}^2$). Based on the requirements, the method proposed by De Negri *et al.* (2008) was used to determine the maximum flow rate ($2.63 \times 10^{-4} \mathrm{m}^3/\mathrm{s}$).

The method proposed in Chapter 4 was used to design and select a hydraulic pump for the EHA, the method was configured for only one pump. To evaluate the consumption of electrical energy, the angular speed of the pump was considered within the range of the electric motor on the test bench (0 to 167.55 rad/s).

In this case, the limitations of the pump such as minimum angular velocity and maximum pressure in the suction were ignored and it was considered that the pump is able to be used in an EHA. The pump selected was a 9 cm³/rev Figure A1. Following the method proposed in chapter 4 the flow rate and torque curves of the pump were used to obtain the flow rate map, torque map, and angular velocity map. Since only one pump is used, the selection map was not needed.

Figure A1 – Flow rate and torque curves.
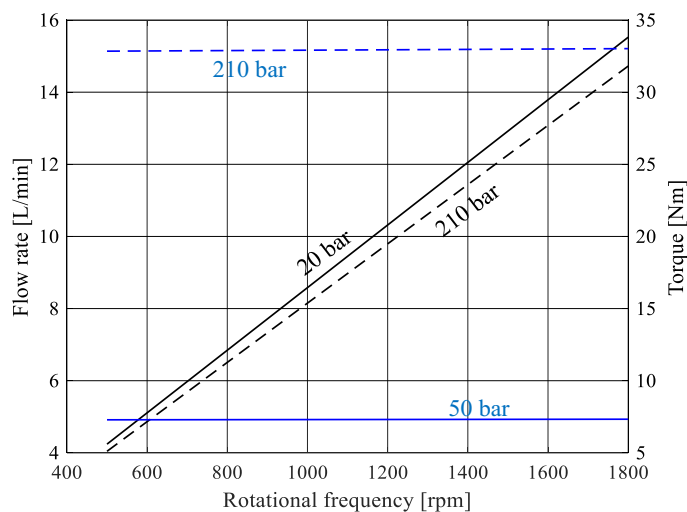
Source: Author.

The hydraulic circuit was based on a single pump circuit with a pressurized reservoir (COSTA; SEPEHRI, 2015; MARÉ, 2017). The software Hopsan was used to implement the EHA components Figure A2. The cylinder is modeled as a symmetric dual-chamber cylinder. The LuGre friction model was used adopting the same parameters obtained in the test bench of the VSDEHA. Two relief valves are used to connect the high and low pressure lines of the EHA, for safety. A pressurized reservoir is used to represent a refeed system, which is connected by two check valves to the lines of the EHA to avoid cavitation. The pump is modeled with internal leakage calculated in real time simulation and a drain with a fixed flow rate coefficient. The equations used to model the EHA components are the same ones presented in Section 5.3, with respective adjustments for the case.

Figure A2 – EHA implemented in Hopsan.
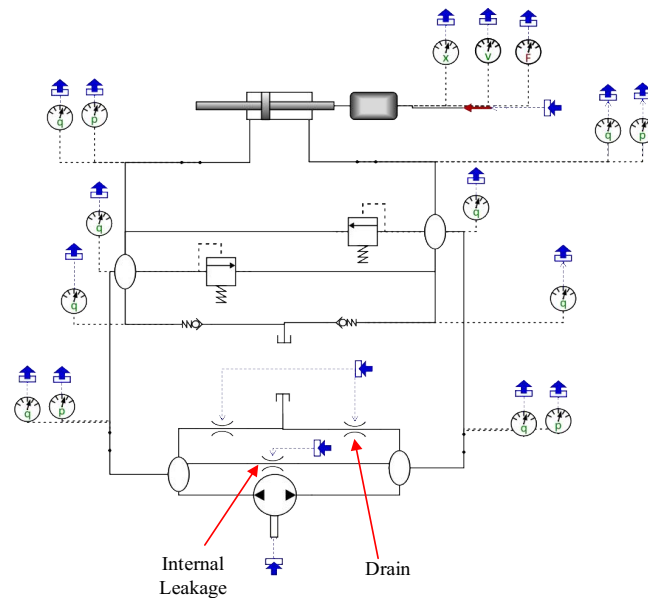
Source: Author.

A PI controller is used to control the movement of the actuator, the proportional gain used is 2.2 and the integral gain used is 0.3. In addition, a gain of $5.33 \times 10^{-3} \mathrm{m}^2/\mathrm{s}$ is used to convert the position error in to flow rate required to the flow rate map. Like in the VSDEHA the rotational frequency of the electric motor is controlled using the maps of the pump to supply the demanded flow rate. Table A1 presents other parameters necessary to implement the model in Hopsan.

Table A1 – Parameters of the EHA model.

Parameters	Unit	Value
Bulk Modulus	Pa	1.3×10^9
Check valve restriction coef.		7.5×10^{-7}
Check valve crack pressure	Pa	1×10^5
Cylinder Area	m^2	2.372×10^{-3}
Cylinder Stroke	m	0.1
Cylinder dead volume	m^3	3×10^{-5}
Cylinder leakage coef.		1×10^{-14}
Drain pressure flow coef.	m^5/Ns	2.5×10^{-12}
Mass moved	kg	100
Relief valve opening pressure	Pa	1.5×10^7
Relief valve Nominal flow rate	m^3/s	1.667×10^{-3}
Reservoir pressure	Pa	1×10^6
Reservoir drain pressure	Pa	0
Volume lines	m^3	1×10^{-3}

Source: Author.

APPENDIX B – DESIGN OF DHP AN EXAMPLE OF APPLICATION

In order to apply the proposed method, the following example is presented, where the requirements of Phase 1 is a digital hydraulic pump that must provide a flow rate range from 1.6×10^{-5} to 2.6×10^{-4} m³/s (1 to 16 L/min), the maximum pressure is 20 MPa (200 bar), the angular velocity range is 83.77 to 188.49 rad/s (800 rev/min to 1800 rev/min). The estimated volumetric efficiencies at the minimum and maximum flow rate are 0.7. The pumps of the database used was shown in Figure 4.5. Seven DHPs were configured and the number of pump units and the numerical pattern used were: 2 equal pump units, 2 pump units in a power of two, 2 pump units in a power of three, 3 equal pump units, 3 pump units in a power of two, 3 pump units in a power of three, and 3 pump units with their volumetric displacements distributed in Fibonacci sequence.

The results of the DHPs evaluated in Phase 2 are presented in Table B1. Where in the Volumetric Displacement column are the values obtained from the Optimization process and the values available in the Database obtained from the manufacturer's datasheet. Appling Phase 3, the table also shows the rank of the average overall efficiency of the DHPs configured.

Table B1 – Ranking of the available pump solutions.

Rank	Number of Pumps / Numerical Pattern	Volumetric Displacement		Average Overall Efficiency
		Optimization	Database	
1	3 / power of 3	0.98 / 2.94 / 8.82	1.2/ 4/ 8	0.63
2	3 / power of 2	1.82 / 3.64 / 7.29	2/ 4/ 8	0.59
3	3 / Fibonacci	2.22 / 2.22 / 4.44	2 / 2 / 4	0.46
4	2 / power of 3	2.22 / 6.66	2 / 5.5	0.40
5	3 / equals	2.22 / 2.22 / 2.22	2 / 2 / 2	0.38
6	2 / power of 2	2.22 / 4.44	2 / 4	0.31
7	2 / equals	2.22 / 2.22	2 / 2	0.23

Source: Author.

The pump in the first position of the rank will be referred to from now as DHP1. Table B2 shows the selection map of the DHP1, where the pump unit combinations that have the best overall efficiency are presented. Numbers 1 through 7 in the table represent the pump unit combination selected to be used. Similar tables are obtained for the other digital hydraulic pumps in the rank.

Table B2 – DHP1: Selection map.

Pressure	Flow rate [L/min]																
[bar]	0	1	2	3	4	5	6	7	8	9	10	11	12	13	14	15	16
20	0	1	1	2	4	4	4	3	5	5	6	7	7	7	7	7	7
40	0	1	1	2	4	4	4	3	5	5	7	7	7	7	7	7	7
60	0	1	1	2	4	4	4	3	3	6	6	6	7	7	7	7	7
80	0	1	1	2	4	4	4	3	3	6	6	6	6	6	7	7	7
100	0	1	1	2	2	4	4	3	3	3	3	3	6	6	6	7	7

Source: Author.

The DHP1 was able to meet design constraints for a minimum and maximum flow rate within the angular velocity and pressure range. As shown in Table B2, the DHP1 uses the pump unit combination 1, which in this case has the smallest volumetric displacement, to meet the lower flow rate demand and increases the number of pump units to meet the higher flow rate demand.

For flow rates above 2×10^{-4} m³/s (12 L/min), it is possible to notice that combination number 7 is dominant, as combination 7 is the combination using all 3 pumps, which theoretically is able to supply a flow rate of 3.96×10^{-4} m³/s (23.8 L/min), considering the maximum angular velocity.

The efficiency map of the DHP1 is presented in Table B3. The map is useful for estimating the overall efficiency of the digital hydraulic pump during a given operating cycle, which can be used to compare different solutions.

Table B3 – DHP1: Efficiency map.

Pressure	Flow rate [L/min]																
[bar]	0	1	2	3	4	5	6	7	8	9	10	11	12	13	14	15	16
20	0	0.31	0.26	0.49	0.52	0.50	0.49	0.63	0.64	0.63	0.68	0.68	0.68	0.67	0.67	0.66	0.66
40	0	0.38	0.34	0.59	0.61	0.60	0.59	0.73	0.73	0.72	0.76	0.76	0.75	0.75	0.75	0.75	0.74
60	0	0.43	0.39	0.64	0.65	0.64	0.64	0.77	0.77	0.78	0.78	0.78	0.78	0.77	0.77	0.77	0.77
80	0	0.47	0.43	0.67	0.66	0.66	0.66	0.79	0.79	0.79	0.79	0.79	0.78	0.78	0.78	0.78	0.78
100	0	0.50	0.47	0.68	0.67	0.67	0.66	0.81	0.80	0.80	0.79	0.79	0.79	0.78	0.78	0.78	0.78

Source: Author.

Table B4 presents the rotational frequency map of DHP1, which is the rotational frequency required by the DHP1 to meet the flow rate for each operating point. It is possible to notice that in some regions, the digital hydraulic pump is able to increase or decrease the flow

rate without changing the pump unit combination (Table B2), allowing the implementation of a continuous control of the angular velocity source.

Table B4 – DHP1: Angular velocity map [rev/min].

Pressure	Flow rate [L/min]																
[bar]	0	1	2	3	4	5	6	7	8	9	10	11	12	13	14	15	16
20	0	938	1750	815	847	1046	1245	892	899	1009	867	874	952	1029	1107	1184	1262
40	0	946	1757	829	866	1069	1272	898	908	1018	809	887	966	1044	1123	1201	1280
60	0	953	1764	844	885	1092	1299	903	1032	805	893	982	979	1059	1138	1218	1298
80	0	960	1771	858	905	1115	1325	909	1038	817	906	996	1086	1175	1154	1235	1315
100	0	967	1777	872	1154	1138	1352	914	1045	1175	1305	1436	1101	1192	1283	1252	1333

Source: Author.

Table B5 presents the torque map of DHP1, which can be used combined with the angular velocity map to assist the designer in the task of estimating and selecting the power source for the DHP. The maximum torque calculated to the DHP1 was 22.24 Nm when running at 134.45 rad/s (1283 rev/min), and the power calculated at the same point was about of 2.98 kW.

Table B5 – DHP1: Torque map [Nm].

Pressure	Flow rate [L/min]																
[bar]	0	1	2	3	4	5	6	7	8	9	10	11	12	13	14	15	16
20	0	2.20	2.75	2.95	3.37	3.50	3.63	4.25	4.65	4.73	5.47	4.20	4.20	4.20	4.20	4.20	4.20
40	0	2.64	3.21	4.32	5.18	5.33	5.47	7.02	7.86	7.94	8.40	8.40	8.40	8.40	8.40	8.40	8.40
60	0	3.09	3.67	5.70	7.01	7.15	7.30	9.78	9.86	13.68	13.73	13.79	12.61	12.61	12.61	12.61	12.61
80	0	3.54	4.14	7.08	8.83	8.98	9.13	12.54	12.63	17.81	17.87	17.93	17.98	18.04	16.81	16.81	16.81
100	0	3.98	4.60	8.45	8.63	10.81	10.97	15.30	15.39	15.47	15.56	15.64	22.12	22.18	22.24	21.01	21.01

Source: Author.

The results and analyses presented above belong to the post-processing phase of the proposed method, where it is important to highlight that the overall efficiency is just one of the variables that must be evaluated to select the configuration of the digital hydraulic pump. With the torque and angular velocity information, it is possible to estimate the power and size of the electric motor needed to move the DHP. As design criteria depend on the application, more requirements can be used in the final evaluation to compare the DHPs.

Another advantage of applying this method to the design of the digital hydraulic pump is the possibility of using the pump unit selection map and angular velocity map of the DHP within an intelligent control strategy. Where the required pressure and flow rate conditions can

be used as inputs to the maps to obtain the pump unit combination and the angular velocity, which can be used to control the on/off valves and the angular velocity source, to achieve the flow rate required.

ANNEX A – LUGRE MODEL

The LuGre model was proposed by De Wit *et al.* (1995), which according to the same authors the model is based on the average deflection of the bristles modeled by

$$\frac{dz}{dt} = v - \frac{|v|}{g(v)}z \qquad (A.1)$$

where z is the bristle average deflection, v is the relative velocity between two surfaces, and $g(v)$ is a positive function which depends on several parameters such as temperature, lubrication, and properties of material in contact (Figure A.1).

Figure A.1 – Friction interface between two surfaces.
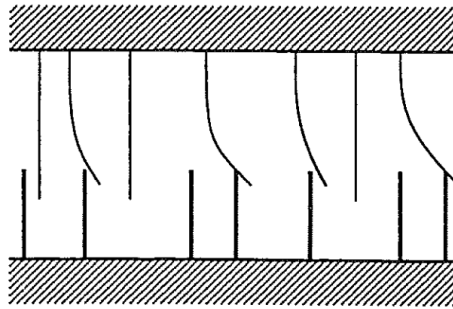
Source: de Wit *et al.* (1995).

In steady state the equation A.1 becomes

$$z = g(v)sgn(v) \qquad (A.2)$$

According to De Wit *et al.* (1995) the friction force generate from the bending of the bristles can be described as

$$F = \sigma_0 z + \sigma_1 \frac{dz}{dt} + \sigma_2 v \qquad (A.2)$$

where σ_0 is the stiffness of the bristles, σ_1 is the micro-viscous friction coefficient for bristles, and σ_2 is a viscous coefficient.

The Stribeck effect can be described as

$$\sigma_0 g(v) = F_C + (F_S - F_C)e^{-\left(\frac{v}{v_s}\right)^2} \tag{A.3}$$

where F_C is the Coulomb friction force, F_s is the static friction force , v_s is the Stribeck velocity, and v is the cylinder velocity (DE WIT *et al.*, 1995).

In steady state motion the relation between velocity and friction force is given by

$$F(v) = F_C sgn(v) + (F_S - F_C)e^{-\left(\frac{v}{v_s}\right)^2} sgn(v) + \sigma_2 v \tag{A.4}$$

The equation A.4 can be rewritten for positive and negative velocities, considering asymmetric friction forces (VALDIERO, 2005).

$$F(v) = \begin{cases} F_{Cp} + \left(F_{Sp} - F_{Cp}\right)e^{-\left(\frac{v}{v_{sp}}\right)^2} + \sigma_{2p}v, & \text{for } v > 0 \\ F_{Cn} + (F_{Sn} - F_{Cn})e^{-\left(\frac{v}{v_{sn}}\right)^2} + \sigma_{2n}v, & \text{for } v < 0 \end{cases} \tag{A.5}$$

According to Astrom & Canudas-de-Wit (2008) the parameter σ_1 represent the damping in the pre displacement regime and for mechanical systems it is possible to consider $\sigma_1 = 2\xi\sqrt{\sigma_0 m} - \sigma_2$, with $\xi = 1$, critical damped, where m is the moved mass. Belan (2018) quotes that a 0.1 Ns/m is a good value for σ_1.

ANNEX B – ELECTRIC MOTOR REPORT

UNIVERSIDADE FEDERAL DE SANTA CATARINA

GRUCAD
Grupo de Concepção e Análise de
Dispositivos Eletromagnéticos

Relatório de ensaio - Determinação de rendimento e de perdas

Data	25/08/2022
Elaboração	Técnico Cristian F. Mazzola e Prof. Carlos A. C. Wengerkievicz
Supervisão	Prof. Nelson Jhoe Batistela
Contato	cristian.mazzola@ufsc.br, c.a.correa@ufsc.br, jhoe.batistela@ufsc.br

Dados do motor

Identificação	Nova 7,5 cv 4 polos 60 Hz		
Potência (kW)	5.5	Tensão (V)	380
Corrente (A)	12.1	Frequência (Hz)	60
Rotação (rpm)	1755	Cos fi	0.76
Polos	4	Torque (N.m)	29.9

Dados do inversor

Identificação	Siemens MicroMaster 440

Ensaios realizados

1. Ensaio de carga para medição das perdas totais do conjunto motor + inversor com controle vetorial
2. Ensaio de carga para medição das perdas totais do conjunto motor + inversor com controle V/f
3. Ensaio de carga para medição das perdas no motor alimentado por inversor com controle vetorial
4. Ensaio de carga para medição das perdas no motor alimentado por inversor com controle V/f
5. Ensaios de segregação de perdas no motor sob alimentação senoidal (IEEE Std. 112 método B)

Relatório de ensaio
Motor Nova 7,5 cv + Inversor Siemens
Bancada de ensaios
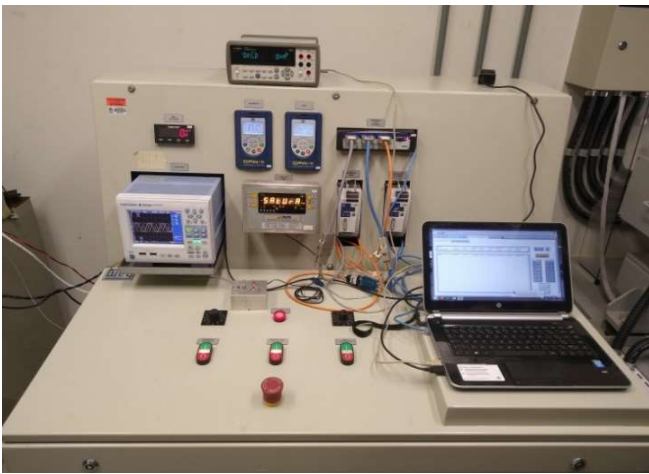
Medição de grandezas elétricas (V, I, P, f): Analisador Yokogawa WT500 com 3 TCs 50:5 A

Medição de grandezas mecânicas: Transdutor HBM TB40D, MX460 e software em Labview

Medição de resistência do estator: Multímetro de bancada Agilent 34401A, a 4 fios, com comutador a reles

Medição de temperatura: Data logger Yokogawa GP10 com termopar entre carcaça e pacote

Alimentação senoidal: Fonte eletrônica Supplier FCATH-3000-38-50 + banco trifásico de transformadores

Carga: Motor de indução de 30 cv controlado por inversor sem regeneração de energia

Bancada de ensaios

1. Perdas totais com controle vetorial

Configuração experimental

Perdas totais

Rede
380 V
60 Hz

Inversor
(vetorial)

Motor

Dinamô-
metro

Tensão
Corrente
Potência

Torque
Velocidade
angular

1. Perdas totais - vetorial
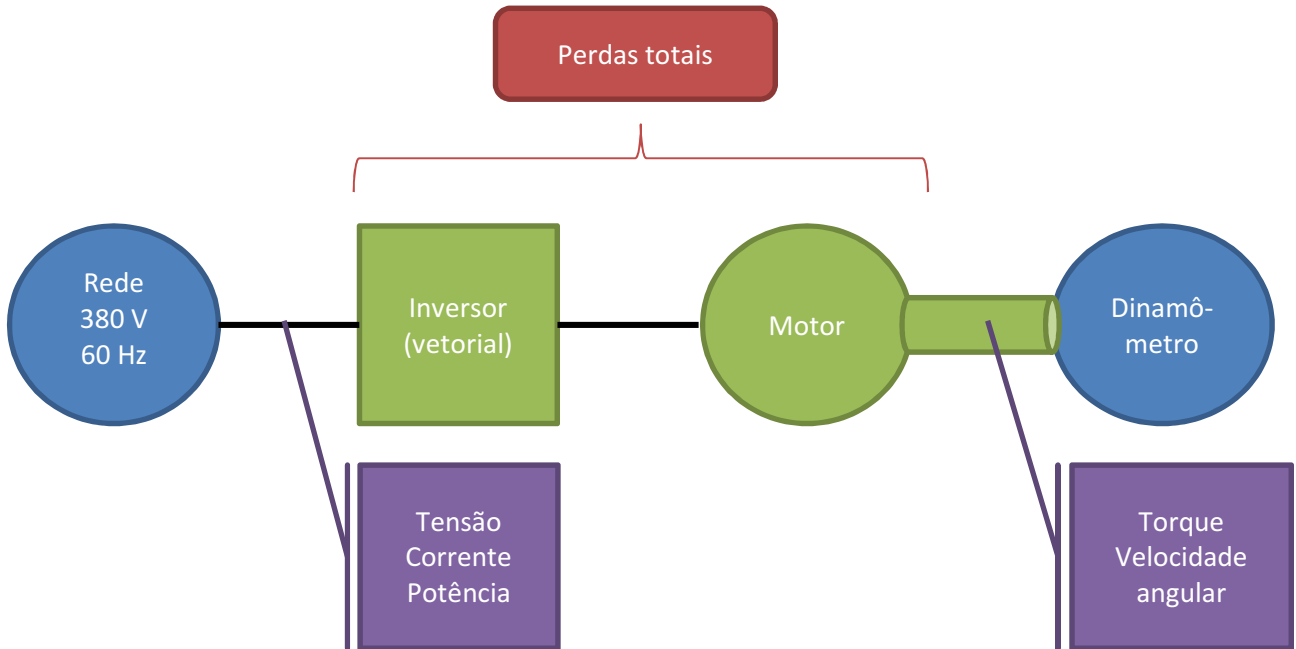
Relatório de ensaio
Motor Nova 7,5 cv + Inversor Siemens

Resultados

1800 rpm   Temperatura do ensaio (°C):   82.1

Urms (V)	Irms (A)	Pin (W)	F(Hz)	T (N.m)	N (rpm)	Peixo (W)	Perdas (W)	Rend. (%)
391.98	19.182	9489.4	59.957	42.639	1800.1	8039.4	1450.1	84.7
393.13	16.232	7880.0	59.996	35.696	1800.0	6726.0	1154.1	85.4
393.60	14.001	6689.9	59.995	30.389	1800.1	5733.1	956.8	85.7
394.53	10.681	4918.7	60.014	22.039	1800.1	4154.4	764.3	84.5
395.22	7.924	3507.8	60.059	15.267	1800.1	2874.9	632.9	82.0
395.67	4.839	2000.8	60.017	7.899	1800.1	1487.9	513.0	74.4
396.79	1.511	525.8	60.008	0.419	1800.1	79.1	446.7	15.0

1350 rpm   Temperatura do ensaio (°C):   82.4

Urms (V)	Irms (A)	Pin (W)	F(Hz)	T (N.m)	N (rpm)	Peixo (W)	Perdas (W)	Rend. (%)
393.18	15.600	7553.6	59.993	44.189	1350.0	6249.5	1304.1	82.7
393.66	13.254	6273.8	59.985	36.755	1350.0	5204.3	1069.4	83.0
394.05	11.113	5146.8	59.983	30.170	1350.0	4254.5	892.3	82.7
394.86	8.452	3786.7	59.980	21.985	1350.1	3110.7	676.0	82.1
395.29	6.457	2785.8	59.966	15.750	1350.0	2225.7	560.0	79.9
395.95	4.046	1629.6	59.982	8.311	1350.1	1175.2	454.4	72.1
396.35	1.297	439.2	59.964	0.359	1350.1	51.2	388.0	11.7

900 rpm   Temperatura do ensaio (°C):   82.2

Urms (V)	Irms (A)	Pin (W)	F(Hz)	T (N.m)	N (rpm)	Peixo (W)	Perdas (W)	Rend. (%)
393.98	11.487	5360.9	59.933	44.094	900.0	4156.4	1204.5	77.5
394.35	9.781	4488.9	59.922	37.125	900.0	3500.3	988.6	78.0
394.84	8.197	3669.5	59.930	30.377	900.1	2867.7	801.9	78.1
394.96	6.376	2756.7	59.959	22.641	900.1	2134.8	621.9	77.4
395.26	4.704	1951.5	59.922	15.572	900.0	1467.8	483.6	75.2
395.69	3.053	1191.0	59.931	8.569	900.0	808.5	382.5	67.9
395.92	1.077	356.5	59.945	0.361	900.1	33.9	322.5	9.5

450 rpm   Temperatura do ensaio (°C):   80.4

Urms (V)	Irms (A)	Pin (W)	F(Hz)	T (N.m)	N (rpm)	Peixo (W)	Perdas (W)	Rend. (%)
394.39	7.247	3176.8	59.969	44.468	450.1	2092.2	1084.6	65.9
394.67	6.171	2640.0	59.951	36.670	450.0	1727.8	912.2	65.4
394.85	5.095	2121.8	59.978	29.378	450.0	1385.3	736.5	65.3
395.13	3.901	1563.5	59.971	21.407	450.0	1008.7	554.8	64.5
395.35	2.887	1114.1	59.973	14.491	450.0	683.4	430.7	61.3
395.51	1.976	711.7	59.979	7.708	450.0	362.9	348.8	51.0
395.48	0.842	264.1	59.959	0.385	449.8	16.3	247.8	6.2
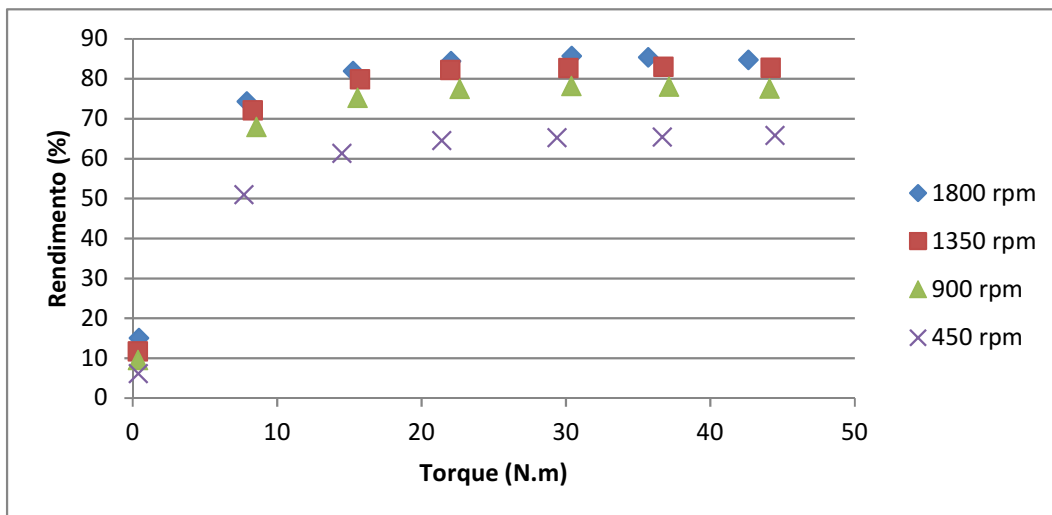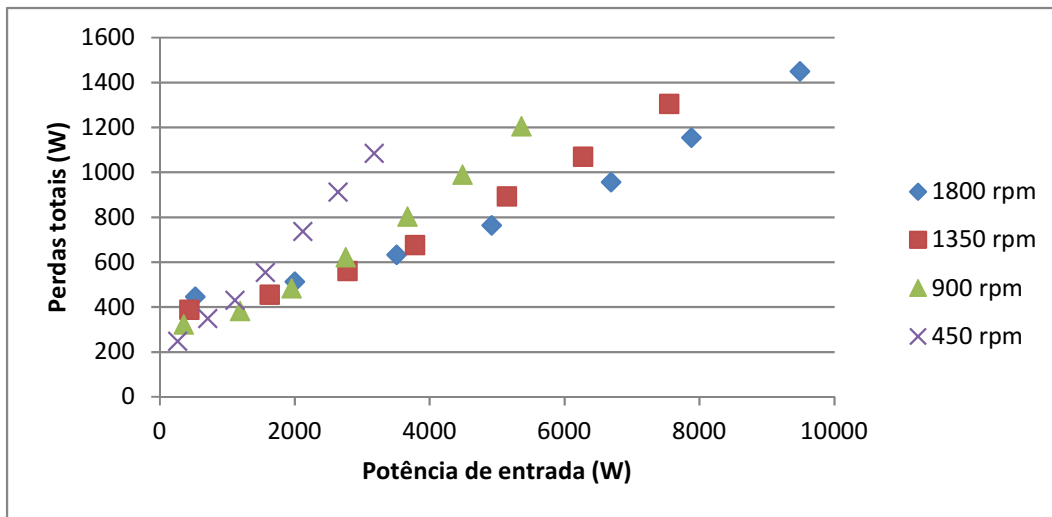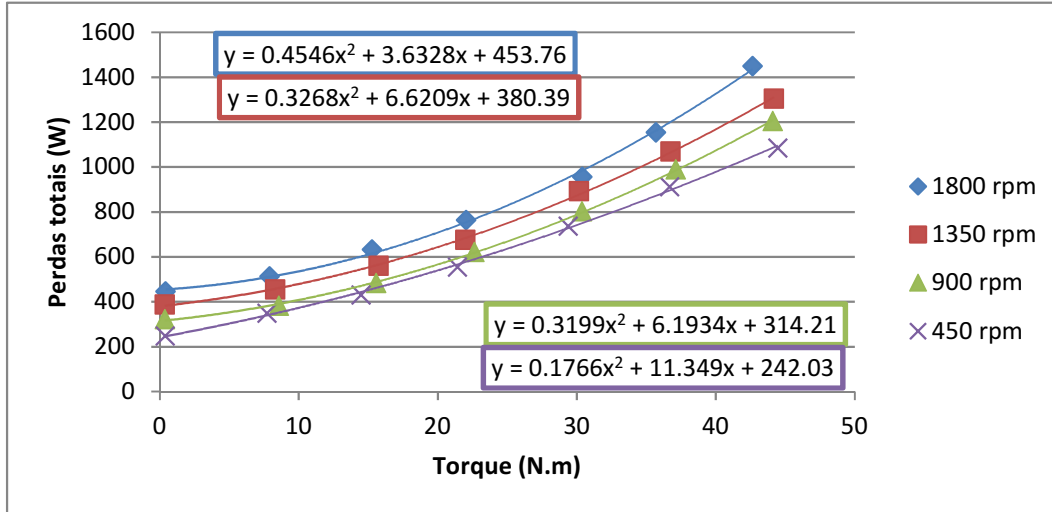
1. Perdas totais - vetorial

Curvas

1. Perdas totais - vetorial

Total loss [motor and drive] - Vectorial control

Total loss [motor and drive] - Vectorial control

1. Perdas totais - vetorial

2. Perdas totais com controle V/f

Configuração experimental

```
                          ┌─────────────────┐
                          │  Perdas totais  │
                          └─────────────────┘

  ┌──────────┐   ┌──────────────┐   ┌──────────┐   ┌──────────────┐
  │  Rede    │   │              │   │          │   │  Dinamô-     │
  │  380 V   │───│ Inversor (V/f)│──│  Motor   │───│  metro       │
  │  60 Hz   │   │              │   │          │   │              │
  └──────────┘   └──────────────┘   └──────────┘   └──────────────┘

               ┌──────────────┐              ┌──────────────┐
               │  Tensão      │              │  Torque      │
               │  Corrente    │              │  Velocidade  │
               │  Potência    │              │  angular     │
               └──────────────┘              └──────────────┘
```
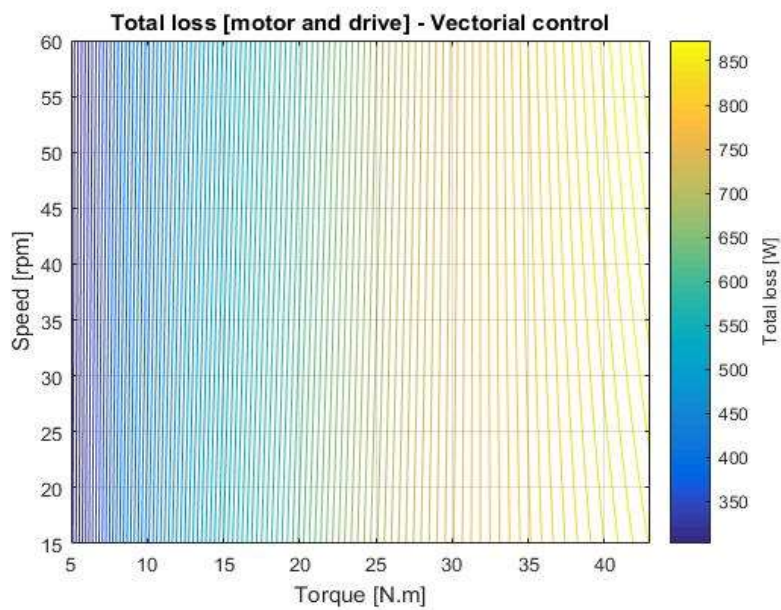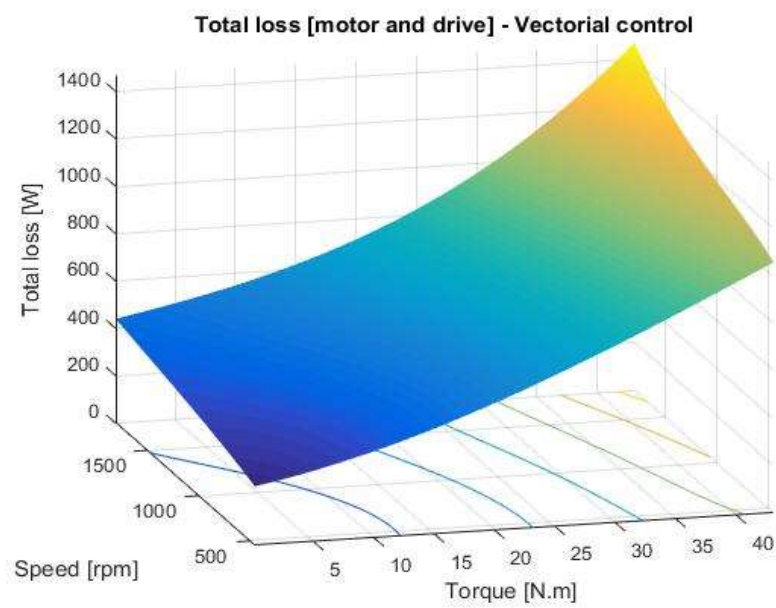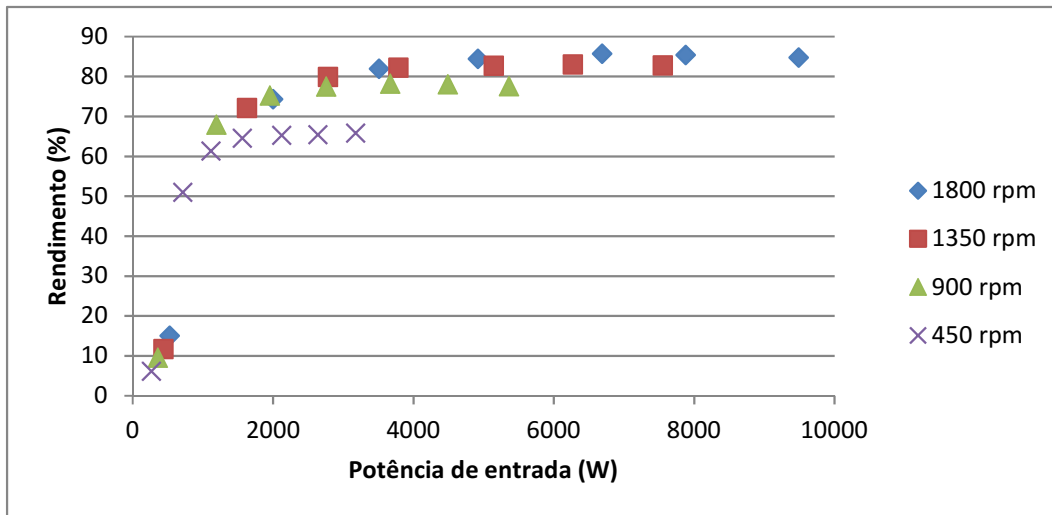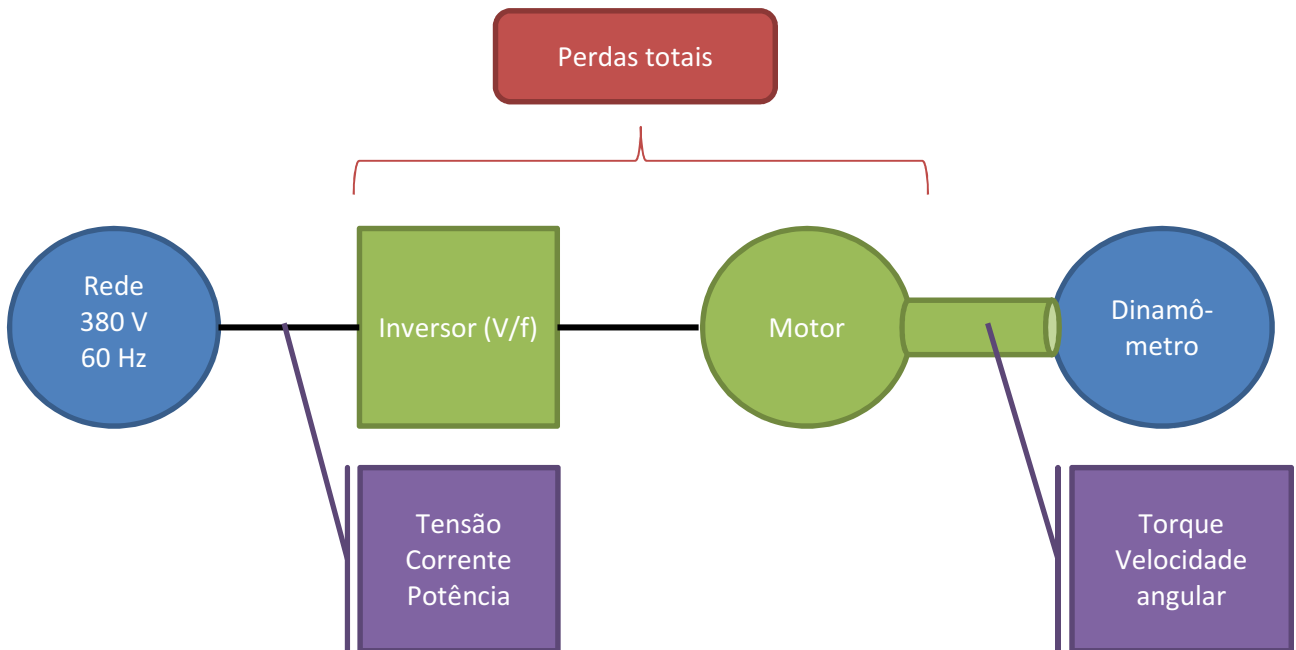
Relatório de ensaio
Motor Nova 7,5 cv + Inversor Siemens

Resultados

60 Hz 380 V   Temperatura do ensaio (°C):   83.0

Urms (V)	Irms (A)	Pin (W)	F(Hz)	T (N.m)	N (rpm)	Peixo (W)	Perdas (W)	Rend. (%)
388.50	19.311	9471.3	60.006	44.561	1721.2	8032.7	1438.6	84.8
389.14	16.395	7885.8	59.987	37.027	1735.6	6730.1	1155.8	85.3
389.74	13.931	6571.7	59.982	30.735	1747.4	5625.0	946.7	85.6
390.42	10.636	4838.2	59.981	22.263	1762.6	4110.7	727.5	85.0
391.09	7.898	3452.9	59.969	15.337	1774.5	2849.3	603.6	82.5
391.64	4.781	1950.9	59.968	7.656	1787.1	1433.1	517.8	73.5
392.19	1.614	560.8	59.985	0.426	1798.2	80.2	480.7	14.3

45 Hz 285 V   Temperatura do ensaio (°C):   85.6

Urms (V)	Irms (A)	Pin (W)	F(Hz)	T (N.m)	N (rpm)	Peixo (W)	Perdas (W)	Rend. (%)
389.01	15.259	7256.7	59.997	44.389	1269.7	5901.3	1355.4	81.3
389.42	13.077	6100.9	59.982	37.309	1283.8	5018.1	1082.7	82.3
390.02	10.818	4927.7	60.004	30.057	1298.2	4086.0	841.7	82.9
390.63	8.472	3753.1	59.976	22.499	1312.1	3090.9	662.2	82.4
391.14	6.064	2564.9	59.984	14.718	1325.8	2043.9	521.0	79.7
391.90	4.051	1623.4	59.988	8.348	1336.1	1167.3	456.1	71.9
392.45	1.387	471.5	59.989	0.349	1348.4	49.0	422.5	10.4

30 Hz 190 V   Temperatura do ensaio (°C):   78.7

Urms (V)	Irms (A)	Pin (W)	F(Hz)	T (N.m)	N (rpm)	Peixo (W)	Perdas (W)	Rend. (%)
390.27	11.152	5127.3	59.976	44.698	812.3	3802.8	1324.5	74.2
390.77	9.522	4282.2	59.971	37.544	829.0	3258.6	1023.7	76.1
391.23	7.863	3452.7	59.991	30.285	845.0	2679.3	773.3	77.6
391.65	6.069	2578.1	60.001	22.236	861.3	2004.4	573.7	77.7
392.09	4.589	1873.0	60.006	15.479	873.7	1416.6	456.4	75.6
392.76	2.979	1143.5	59.994	8.192	886.2	758.8	384.6	66.4
393.01	1.174	390.6	60.005	0.329	898.5	31.2	359.5	8.0

15 Hz 95 V   Temperatura do ensaio (°C):   81.1

Urms (V)	Irms (A)	Pin (W)	F(Hz)	T (N.m)	N (rpm)	Peixo (W)	Perdas (W)	Rend. (%)
391.73	7.099	3079.4	59.973	44.459	331.7	1544.9	1534.5	50.2
391.95	5.861	2467.5	59.970	37.087	362.2	1406.5	1061.0	57.0
391.96	4.798	1958.4	59.948	30.017	385.4	1212.8	745.5	61.9
392.15	3.729	1470.3	59.951	22.459	406.0	954.3	516.0	64.9
392.39	2.759	1039.4	59.944	15.075	422.9	665.3	374.0	64.0
392.48	1.944	687.2	59.937	8.226	435.7	375.2	312.0	54.6
392.73	1.000	316.8	59.964	0.317	448.3	14.8	302.0	4.7
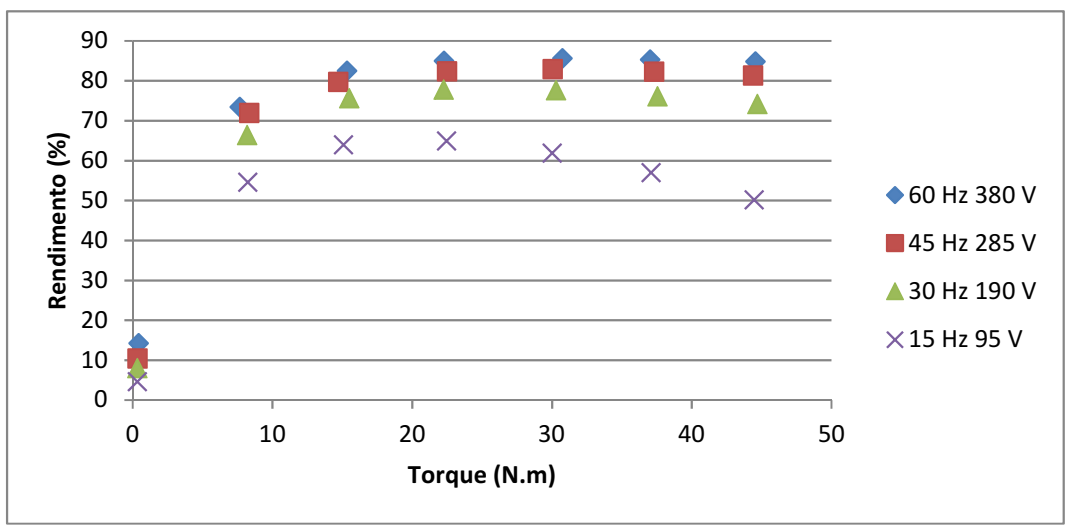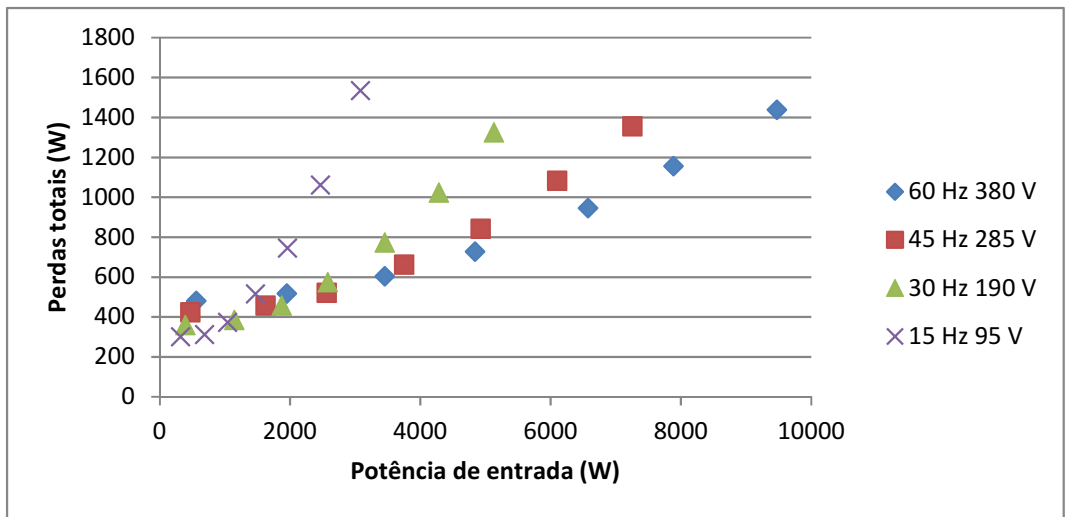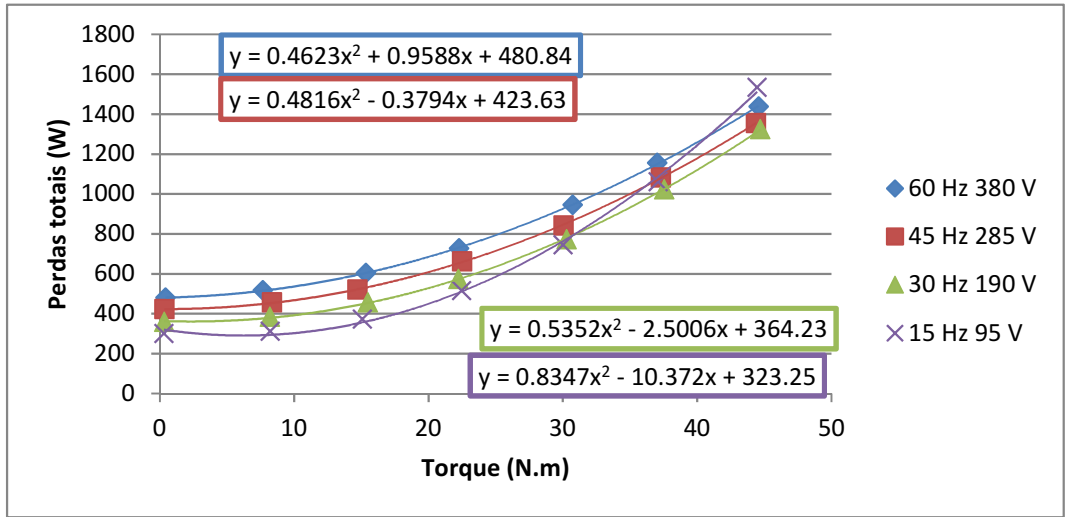
2. Perdas totais - Vf

Curvas

Gráfico — Perdas totais (W) × Torque (N.m)

$y = 0.4623x^2 + 0.9588x + 480.84$

$y = 0.4816x^2 - 0.3794x + 423.63$

$y = 0.5352x^2 - 2.5006x + 364.23$

$y = 0.8347x^2 - 10.372x + 323.25$

Legenda:
- 60 Hz 380 V
- 45 Hz 285 V
- 30 Hz 190 V
- 15 Hz 95 V

Gráfico — Perdas totais (W) × Potência de entrada (W)

Legenda:
- 60 Hz 380 V
- 45 Hz 285 V
- 30 Hz 190 V
- 15 Hz 95 V

Gráfico — Rendimento (%) × Torque (N.m)

Legenda:
- 60 Hz 380 V
- 45 Hz 285 V
- 30 Hz 190 V
- 15 Hz 95 V

2. Perdas totais - Vf

Relatório de ensaio
Motor Nova 7,5 cv + Inversor Siemens

Legend:
- 60 Hz 380 V
- 45 Hz 285 V
- 30 Hz 190 V
- 15 Hz 95 V

(Eixos: Rendimento (%) vs. Potência de entrada (W))

Total loss [motor and drive] - V/f control

Total loss [motor and drive] - V/f control

2. Perdas totais - Vf
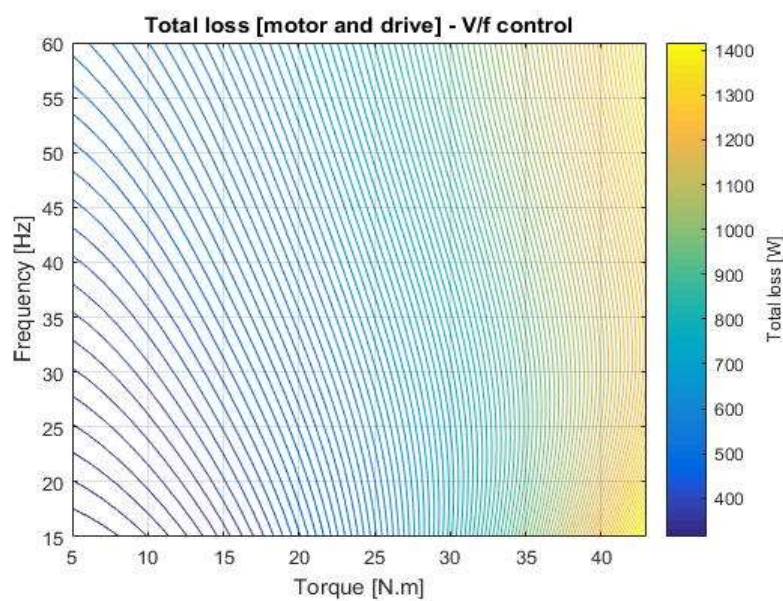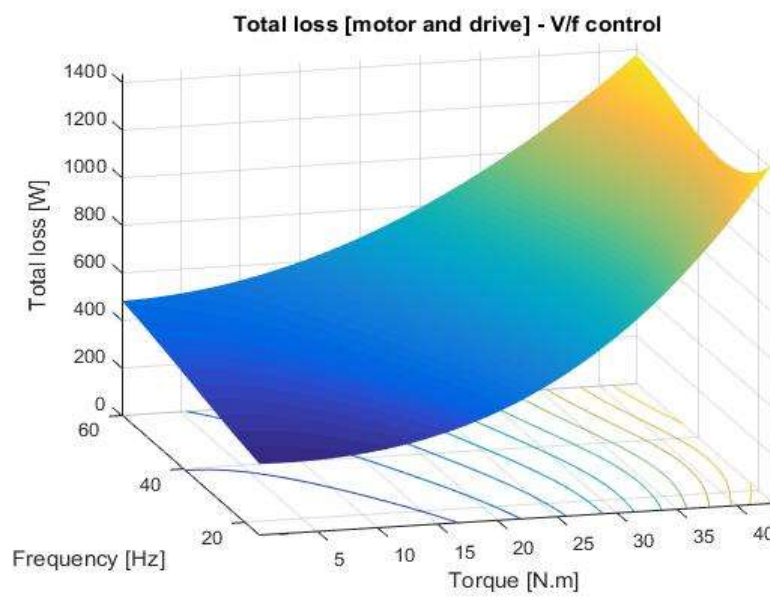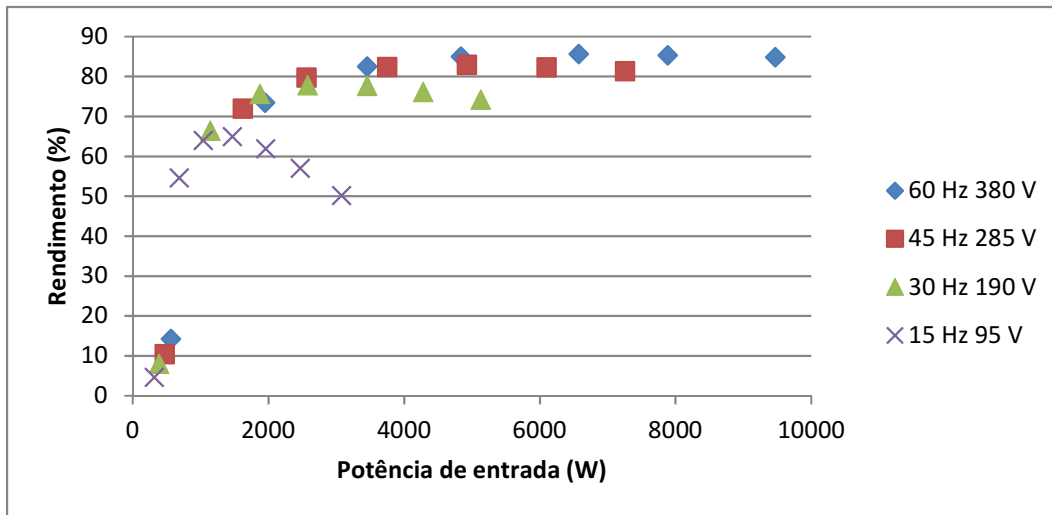
3. Perdas no motor com controle vetorial

Configuração experimental
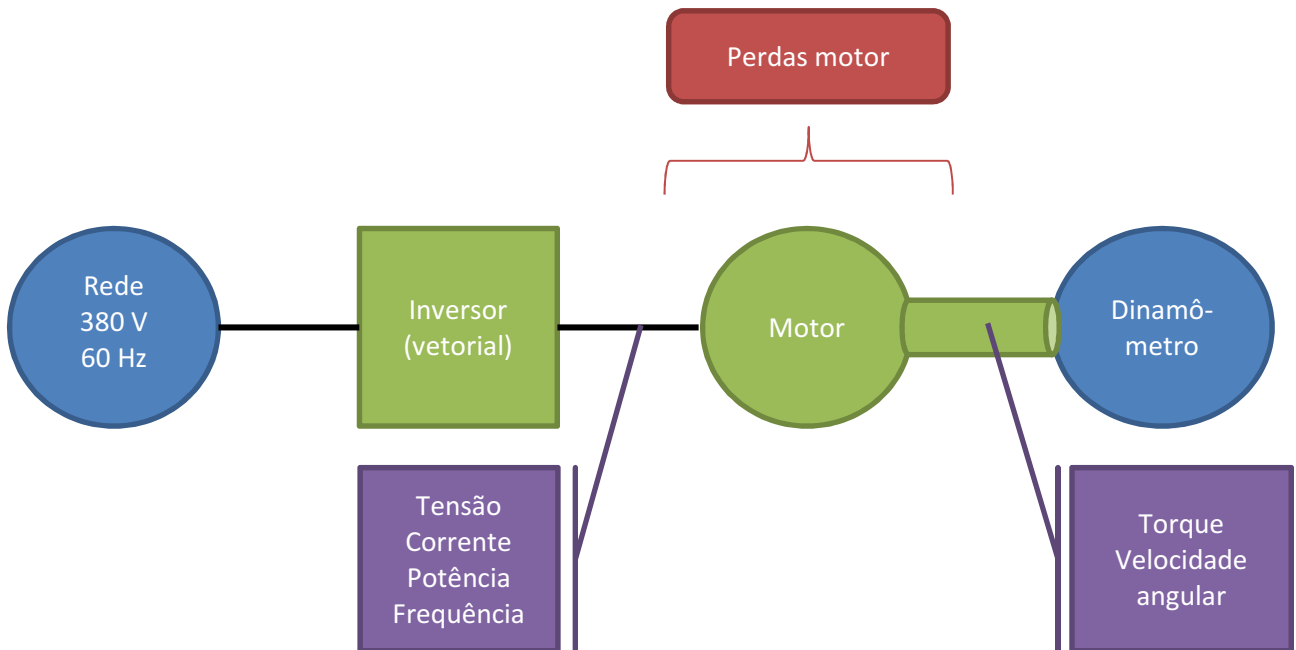
Resultados

1800 rpm   Temperatura do ensaio (°C):   79.6

Urms (V)	Irms (A)	Pin (W)	F(Hz)	T (N.m)	N (rpm)	Peixo (W)	Perdas (W)	Rend. (%)
415.63	17.049	9133.7	63.814	41.669	1800.3	7848.8	1285.0	85.9
419.84	14.819	7827.6	63.032	36.076	1800.1	6798.1	1029.5	86.8
422.12	12.758	6475.3	63.888	30.014	1800.2	5649.4	825.9	87.2
425.72	10.567	4856.5	63.108	22.400	1800.1	4226.4	630.1	87.0
426.68	8.812	3329.0	60.880	14.930	1800.1	2809.7	519.3	84.4
423.87	7.440	1985.5	60.501	8.235	1800.1	1546.2	439.4	77.9
420.21	6.417	458.8	60.073	0.451	1800.1	83.0	375.8	18.1

1350 rpm   Temperatura do ensaio (°C):   78.4

Urms (V)	Irms (A)	Pin (W)	F(Hz)	T (N.m)	N (rpm)	Peixo (W)	Perdas (W)	Rend. (%)
396.21	16.899	7470.1	47.135	44.776	1350.0	6337.8	1132.3	84.8
392.11	14.881	6228.7	46.846	37.454	1350.1	5285.7	943.0	84.9
386.48	12.815	4979.9	49.092	30.177	1350.0	4269.7	710.2	85.7
380.40	10.842	3806.4	48.364	22.964	1350.1	3251.0	555.4	85.4
376.09	9.004	2671.6	45.896	15.832	1350.1	2240.7	430.9	83.9
371.09	7.429	1569.9	45.526	8.666	1350.1	1222.1	347.8	77.8
366.73	6.353	339.7	45.063	0.368	1350.1	52.1	287.6	15.3

900 rpm   Temperatura do ensaio (°C):   88.7

Urms (V)	Irms (A)	Pin (W)	F(Hz)	T (N.m)	N (rpm)	Peixo (W)	Perdas (W)	Rend. (%)
332.26	16.791	5230.3	68.881	44.712	900.1	4216.1	1014.3	80.6
327.02	14.532	4236.3	56.089	36.626	900.0	3451.5	784.8	81.5
321.48	12.610	3411.5	47.017	29.686	900.0	2799.0	612.5	82.0
314.47	10.417	2487.4	44.494	21.712	900.0	2045.9	441.5	82.3
309.17	8.734	1760.3	40.130	15.120	900.0	1427.2	333.2	81.1
303.99	7.276	1056.9	32.621	8.513	900.0	805.5	251.4	76.2
298.64	6.252	237.7	30.054	0.351	900.0	33.6	204.1	14.2

450 rpm   Temperatura do ensaio (°C):   92.0

Urms (V)	Irms (A)	Pin (W)	F(Hz)	T (N.m)	N (rpm)	Peixo (W)	Perdas (W)	Rend. (%)
252.76	16.424	2917.7	113.350	43.740	450.0	2060.6	857.1	70.6
246.74	14.343	2360.7	89.208	36.102	450.0	1702.7	658.0	72.1
241.08	12.694	1933.0	68.594	30.108	450.0	1419.5	513.4	73.4
234.15	10.725	1451.3	57.279	22.943	450.0	1081.6	369.6	74.5
226.12	8.722	964.2	37.739	15.243	450.0	718.0	246.2	74.5
218.80	7.187	570.2	36.252	8.493	449.9	400.8	169.4	70.3
209.99	6.039	137.7	15.047	0.320	450.0	14.8	122.9	10.8
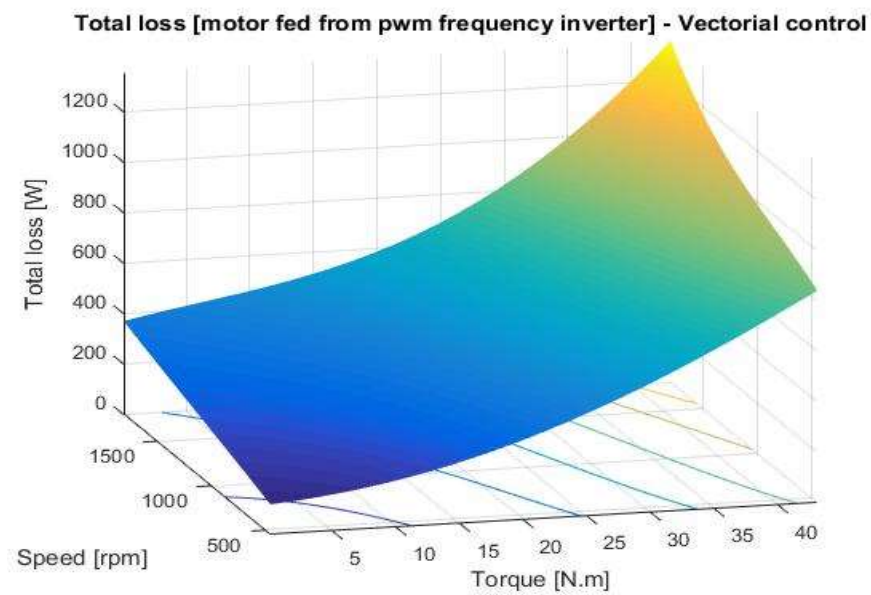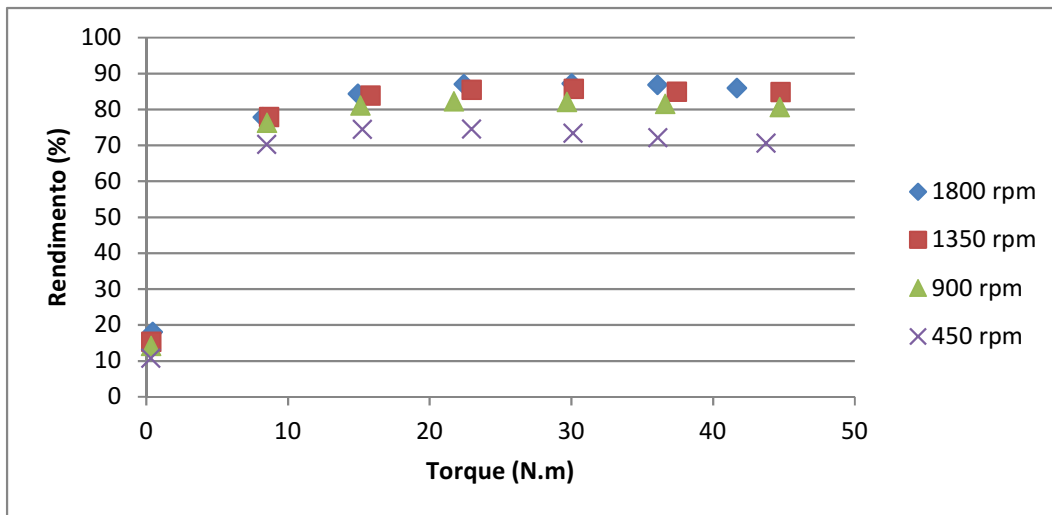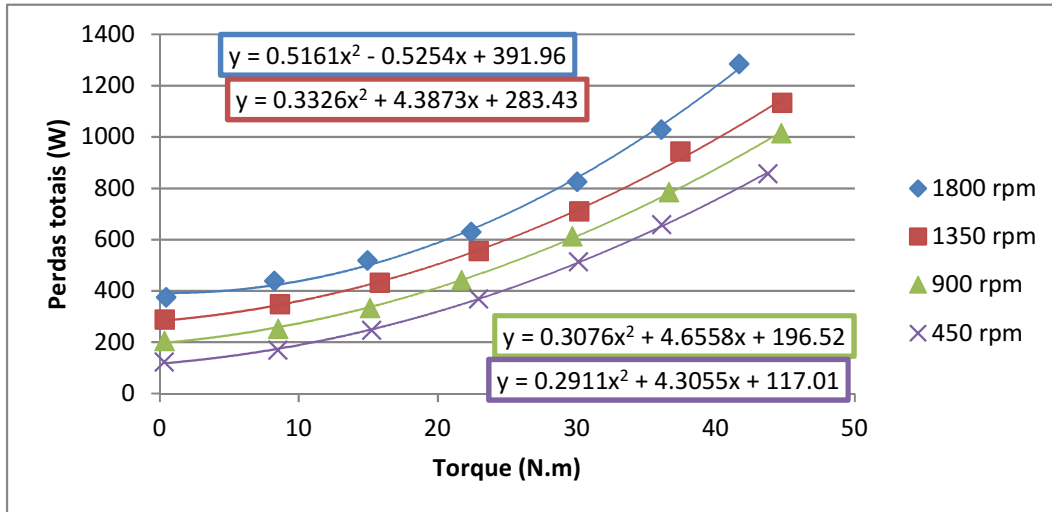
3. Perdas no motor - vetorial

Curvas

Total loss [motor fed from pwm frequency inverter] - Vectorial control

3. Perdas no motor - vetorial

Total loss [motor fed from pwm frequency inverter] - Vectorial control

3. Perdas no motor - vetorial

4. Perdas no motor com controle V/f

Configuração experimental

Perdas motor

Rede
380 V
60 Hz

Inversor (V/f)

Motor

Dinamô-
metro

Tensão
Corrente
Potência
Frequência

Torque
Velocidade
angular
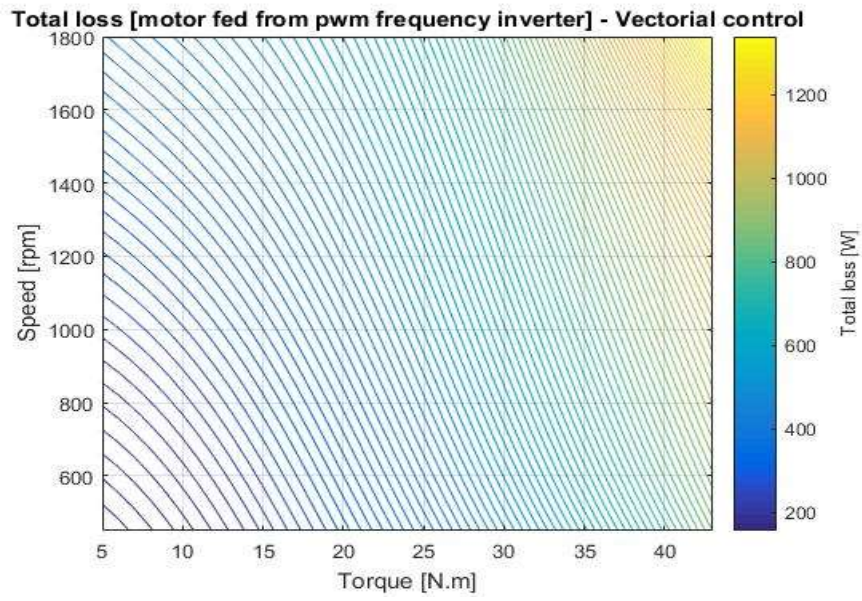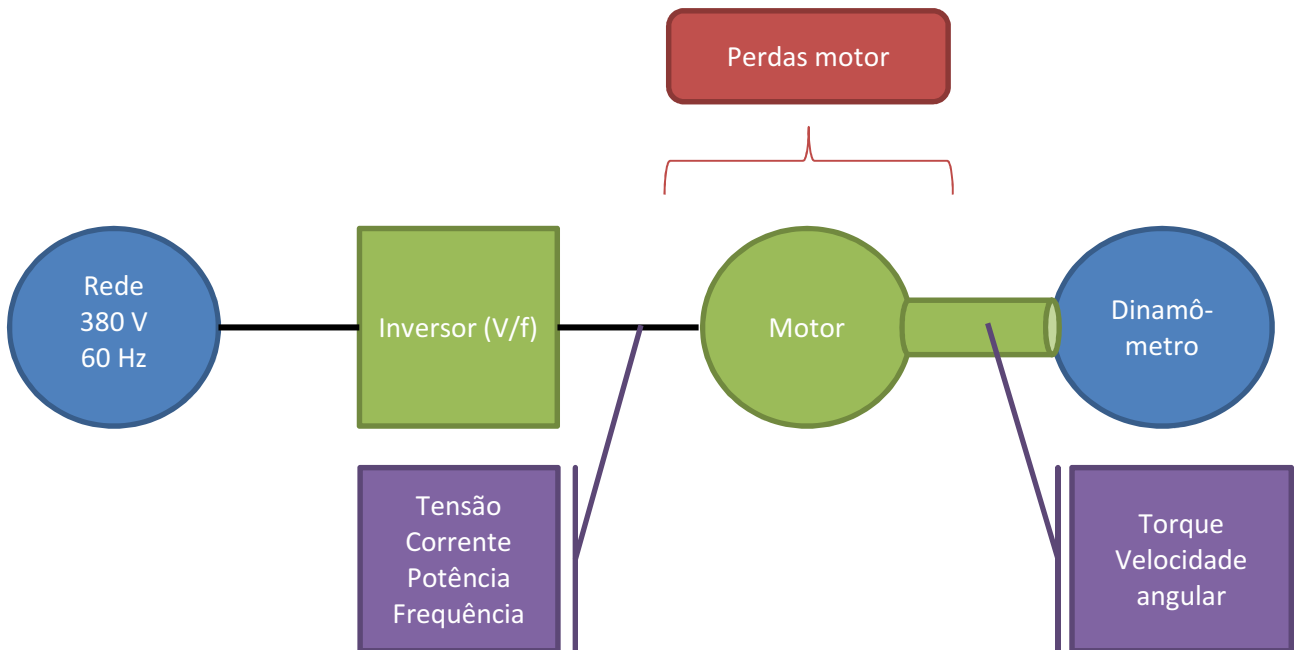
Relatório de ensaio
Motor Nova 7,5 cv + Inversor Siemens

Resultados

60 Hz 380 V   Temperatura do ensaio (°C):   93.6

Urms (V)	Irms (A)	Pin (W)	F(Hz)	T (N.m)	N (rpm)	Peixo (W)	Perdas (W)	Rend. (%)
418.03	17.493	9306.7	62.435	44.556	1716.9	8010.0	1296.7	86.1
419.57	15.091	7825.1	60.211	37.502	1731.4	6800.0	1025.1	86.9
421.62	12.630	6217.6	59.991	29.745	1746.9	5440.3	777.3	87.5
423.43	10.622	4785.0	59.990	22.575	1760.2	4161.6	623.4	87.0
425.78	8.911	3362.2	62.221	15.411	1773.1	2861.7	500.5	85.1
428.73	7.621	1885.7	59.988	7.785	1786.0	1455.6	430.0	77.2
432.70	7.127	486.2	59.991	0.456	1797.8	85.8	400.4	17.6

45 Hz 285 V   Temperatura do ensaio (°C):   84.0

Urms (V)	Irms (A)	Pin (W)	F(Hz)	T (N.m)	N (rpm)	Peixo (W)	Perdas (W)	Rend. (%)
362.08	17.761	7127.7	81.677	44.715	1262.2	5909.1	1218.6	82.9
363.33	15.080	5908.7	80.559	37.226	1279.0	4984.4	924.3	84.4
364.90	12.597	4713.4	62.326	29.625	1295.0	4018.3	695.1	85.3
366.83	10.561	3642.2	54.429	22.706	1309.0	3111.9	530.3	85.4
368.92	8.749	2523.7	49.726	15.264	1322.9	2115.0	408.6	83.8
371.71	7.474	1391.4	51.909	7.528	1336.4	1053.4	338.0	75.7
375.07	7.072	368.4	45.001	0.375	1348.0	53.0	315.5	14.4

30 Hz 190 V   Temperatura do ensaio (°C):   79.3

Urms (V)	Irms (A)	Pin (W)	F(Hz)	T (N.m)	N (rpm)	Peixo (W)	Perdas (W)	Rend. (%)
297.05	18.218	4946.7	43.644	44.675	804.4	3764.9	1181.7	76.1
298.05	15.252	4060.2	54.312	37.083	824.4	3201.1	859.1	78.8
299.38	12.628	3229.8	73.230	29.737	842.4	2623.9	605.9	81.2
300.68	10.359	2440.3	39.995	22.261	858.6	2002.5	437.8	82.1
302.50	8.516	1669.5	34.458	14.772	873.4	1351.6	317.9	81.0
304.79	7.394	962.2	38.345	7.562	886.4	702.9	259.3	73.1
307.42	7.103	274.9	30.630	0.347	898.2	32.9	241.9	12.0

15 Hz 95 V   Temperatura do ensaio (°C):   80.0

Urms (V)	Irms (A)	Pin (W)	F(Hz)	T (N.m)	N (rpm)	Peixo (W)	Perdas (W)	Rend. (%)
210.96	22.216	3046.0	424.256	45.283	297.4	1409.9	1636.1	46.3
211.92	16.647	2279.8	27.801	36.902	350.2	1353.2	926.6	59.4
212.58	13.238	1774.2	55.029	29.922	378.7	1186.9	587.3	66.9
213.66	10.240	1284.9	77.496	22.074	403.4	932.7	352.3	72.6
214.88	8.232	880.5	29.978	14.795	421.4	653.4	227.1	74.2
217.00	7.176	516.6	27.592	7.589	436.1	347.6	169.0	67.3
219.06	7.180	180.1	20.563	0.330	448.5	15.4	164.7	8.5

* Inconsistente

4. Perdas no motor - Vf

Curvas

Graph: Perdas totais (W) vs Torque (N.m)

$y = 0.4772x^2 - 1.3524x + 405.89$

$y = 0.4863x^2 - 1.713x + 319.37$

$y = 0.5562x^2 - 4.1557x + 251.12$

$y = 1.0686x^2 - 18.166x + 213.41$

- 60 Hz 380 V
- 45 Hz 285 V
- 30 Hz 190 V
- 15 Hz 95 V

Graph: Rendimento (%) vs Torque (N.m)

- 60 Hz 380 V
- 45 Hz 285 V
- 30 Hz 190 V
- 15 Hz 95 V

Total loss [motor fed from pwm frequency inverter] - V/f control

4. Perdas no motor - Vf

Total loss [motor fed from pwm frequency inverter] - V/f control
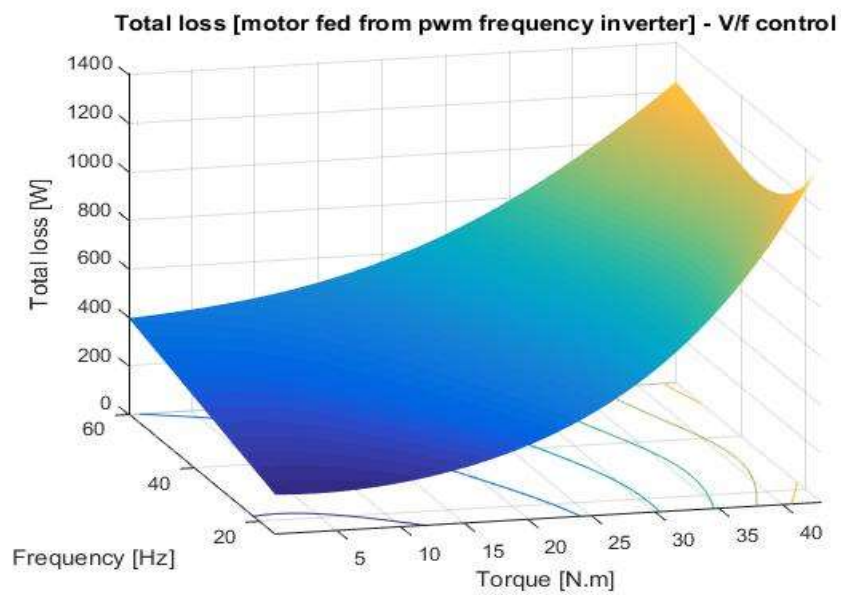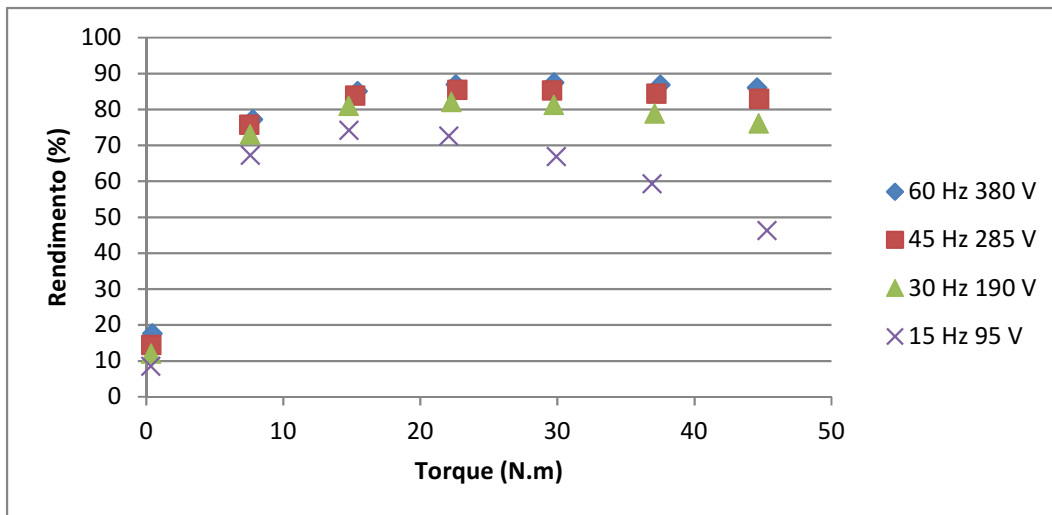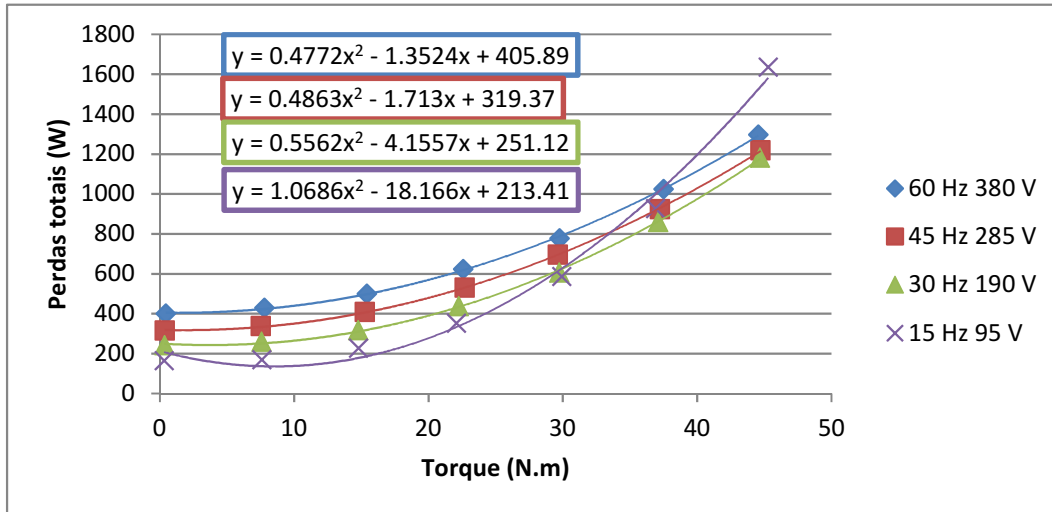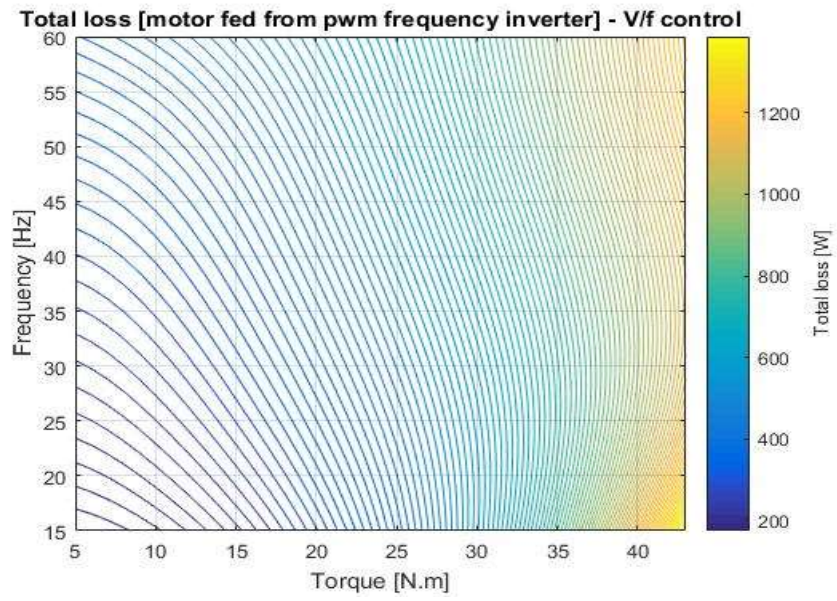
5. Perdas no motor com alimentação senoidal

Configuração experimental
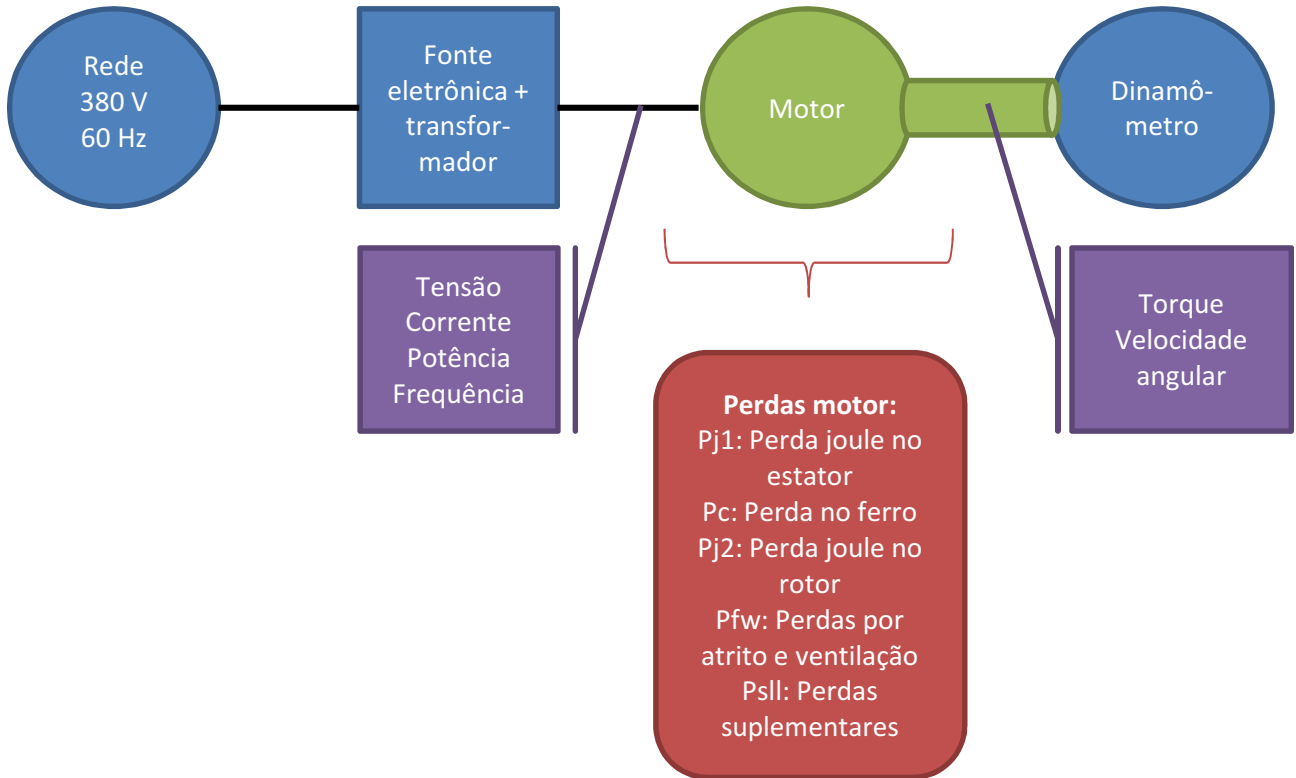
Rede 380 V 60 Hz

Fonte eletrônica + transformador

Motor

Dinamô-metro

Tensão
Corrente
Potência
Frequência

Torque
Velocidade
angular

Perdas motor:
Pj1: Perda joule no estator
Pc: Perda no ferro
Pj2: Perda joule no rotor
Pfw: Perdas por atrito e ventilação
Psll: Perdas suplementares

Relatório de ensaio
Motor Nova 7,5 cv + Inversor Siemens

Resultados

60 Hz 380 V   Temperatura do ensaio (°C):   87.6

Urms (V)	Irms (A)	Pin (W)	F(Hz)	T (N.m)	N (rpm)	Peixo (W)	Perdas (W)	Rend. (%)
376.39	17.066	9263.0	59.995	44.688	1724.2	8062.2	1200.8	87.0
378.15	14.814	7750.0	59.994	37.429	1738.1	6808.1	941.9	87.8
379.82	12.796	6286.3	59.995	30.337	1751.2	5546.2	740.1	88.2
381.42	10.948	4777.7	59.994	22.752	1764.2	4197.0	580.6	87.8
382.96	9.462	3291.3	59.995	15.145	1776.4	2819.9	471.4	85.7
384.19	8.602	2072.0	59.993	8.871	1786.1	1655.7	416.3	79.9
385.76	8.161	487.3	59.995	0.522	1798.2	96.4	390.9	19.8

s (pu)	Pj1 (W)	Pc (W)	Pj2 (W)	Pfw (W)	Psll (W)
0.04200	490.0	175.5	361.1	81.1	93.1
0.03428	369.2	179.4	246.9	81.1	65.3
0.02703	275.5	183.1	157.5	81.1	42.9
0.01978	201.6	186.9	86.8	81.1	24.1
0.01301	150.6	190.6	38.4	81.1	10.7
0.00762	124.5	193.6	13.4	81.1	3.7
0.00090	112.1	197.5	0.2	81.1	0.0

45 Hz 285 V   Temperatura do ensaio (°C):   87.6

Urms (V)	Irms (A)	Pin (W)	F(Hz)	T (N.m)	N (rpm)	Peixo (W)	Perdas (W)	Rend. (%)
282.27	16.537	6762.4	44.995	43.020	1276.5	5741.3	1021.2	84.9
283.68	14.654	5806.3	44.996	37.051	1288.6	4987.6	818.7	85.9
285.22	12.684	4727.6	44.997	30.158	1301.5	4094.5	633.1	86.6
286.85	10.816	3561.7	44.996	22.399	1315.0	3081.2	480.5	86.5
288.32	9.424	2480.1	44.997	15.105	1327.0	2096.9	383.2	84.5
289.73	8.544	1430.6	44.994	7.930	1337.8	1101.9	328.7	77.0
291.13	8.277	368.6	44.995	0.413	1348.6	56.1	312.6	15.2

s (pu)	Pj1 (W)	Pc (W)	Pj2 (W)	Pfw (W)	Psll (W)
0.05434	460.1	122.2	335.8	54.9	48.1
0.04540	361.3	125.3	241.5	54.9	35.7
0.03586	270.7	128.7	155.2	54.9	23.6
0.02581	196.8	132.3	83.4	54.9	13.0
0.01699	149.4	135.7	37.3	54.9	5.9
0.00889	122.8	139.0	10.4	54.9	1.6
0.00093	115.3	142.3	0.1	54.9	0.0

30 Hz 190 V   Temperatura do ensaio (°C):   87.6

Urms (V)	Irms (A)	Pin (W)	F(Hz)	T (N.m)	N (rpm)	Peixo (W)	Perdas (W)	Rend. (%)
189.36	16.362	4580.6	29.999	42.447	826.4	3670.3	910.3	80.1
189.67	14.543	3952.1	29.999	36.880	837.9	3228.5	723.6	81.7
189.98	12.528	3210.8	30.000	29.906	851.1	2669.5	541.4	83.1
190.38	10.412	2332.5	29.999	21.579	866.1	1953.1	379.3	83.7
190.63	9.325	1787.7	29.999	16.149	875.2	1480.1	307.5	82.8
190.98	8.250	1023.0	30.000	8.426	887.2	778.4	244.6	76.1
191.34	7.893	266.4	29.999	0.451	898.8	41.6	224.8	15.6

5. Perdas no motor - senoidal

s (pu)	Pj1 (W)	Pc (W)	Pj2 (W)	Pfw (W)	Psll (W)
0.08174	450.4	74.7	331.5	32.3	21.4
0.06897	355.8	76.5	242.8	32.3	16.2
0.05429	264.1	78.7	155.7	32.3	10.6
0.03762	182.4	81.3	77.8	32.3	5.5
0.02753	146.3	82.9	42.9	32.3	3.1
0.01418	114.5	85.2	11.7	32.3	0.8
0.00130	104.8	87.6	0.1	32.3	0.0

15 Hz 95 V   Temperatura do ensaio (°C):   87.6

Urms (V)	Irms (A)	Pin (W)	F(Hz)	T (N.m)	N (rpm)	Peixo (W)	Perdas (W)	Rend. (%)
90.69	18.418	2640.8	15.000	42.450	345.4	1529.1	1111.7	57.9
93.07	15.027	2143.0	14.999	36.268	374.0	1407.7	735.3	65.7
94.82	12.647	1743.6	14.998	30.254	393.7	1234.4	509.2	70.8
96.94	10.323	1263.3	15.003	22.053	413.9	942.0	321.4	74.6
98.58	9.079	868.9	15.000	14.520	428.5	639.9	229.0	73.6
99.92	8.691	544.4	15.000	7.776	439.0	350.1	194.3	64.3
101.21	8.987	217.3	15.000	0.434	449.0	21.2	196.1	9.8

s (pu)	Pj1 (W)	Pc (W)	Pj2 (W)	Pfw (W)	Psll (W)
0.23253	570.7	26.1	475.3	12.9	26.6
0.16892	379.9	30.3	292.7	12.9	19.4
0.12492	269.1	33.7	180.0	12.9	13.5
0.08039	179.3	37.9	84.1	12.9	7.2
0.04790	138.7	41.3	33.0	12.9	3.1
0.02446	127.1	44.3	9.1	12.9	0.9
0.00216	135.9	47.2	0.1	12.9	0.0

Curvas

$y = 0.4468x^2 - 2.0381x + 395.57$

$y = 0.4358x^2 - 2.5022x + 317.41$

$y = 0.4289x^2 - 2.2771x + 229.2$

$y = 0.7833x^2 - 13.35x + 228.19$

- ♦ 60 Hz 380 V
- ■ 45 Hz 285 V
- ▲ 30 Hz 190 V
- ✕ 15 Hz 95 V

Perdas totais (W) / Torque (N.m)

5. Perdas no motor - senoidal

Relatório de ensaio
Motor Nova 7,5 cv + Inversor Siemens

Legend:
- 60 Hz 380 V
- 45 Hz 285 V
- 30 Hz 190 V
- 15 Hz 95 V

Total loss [Motor fed from sinusoidal voltage supply]

Total loss [Motor fed from sinusoidal voltage supply]

5. Perdas no motor - senoidal
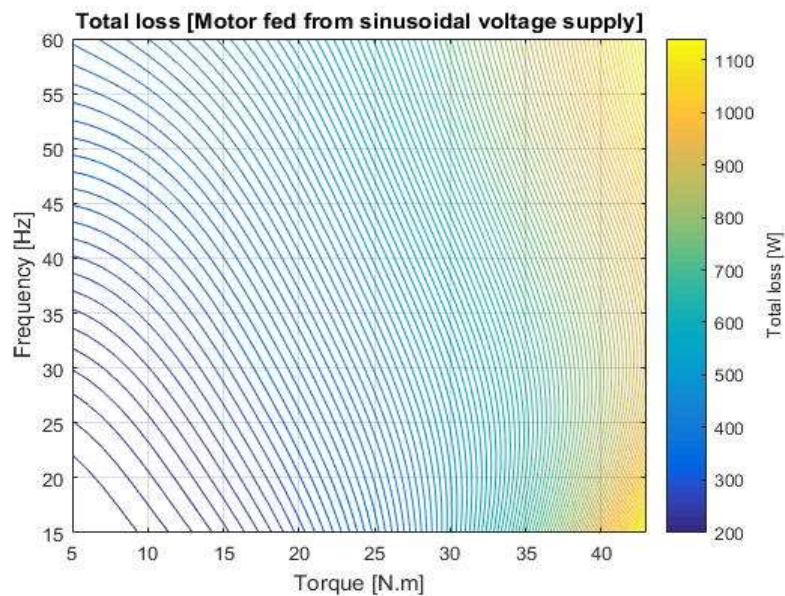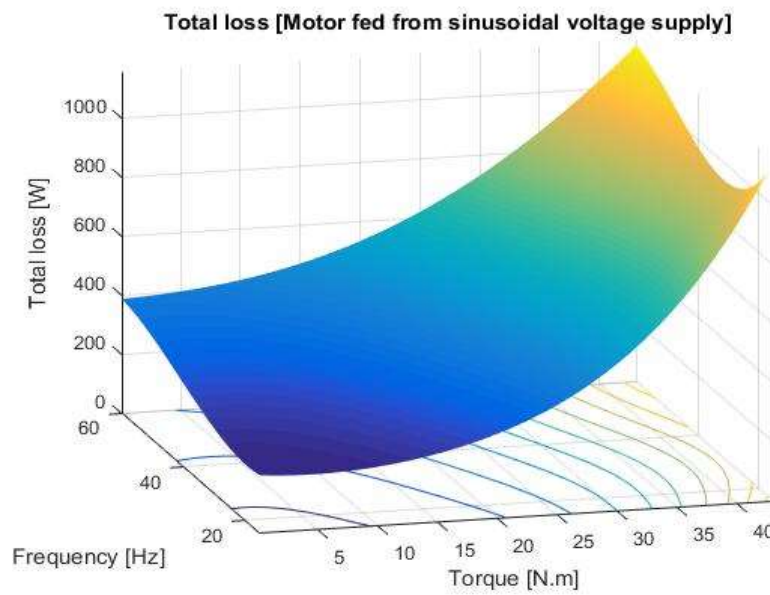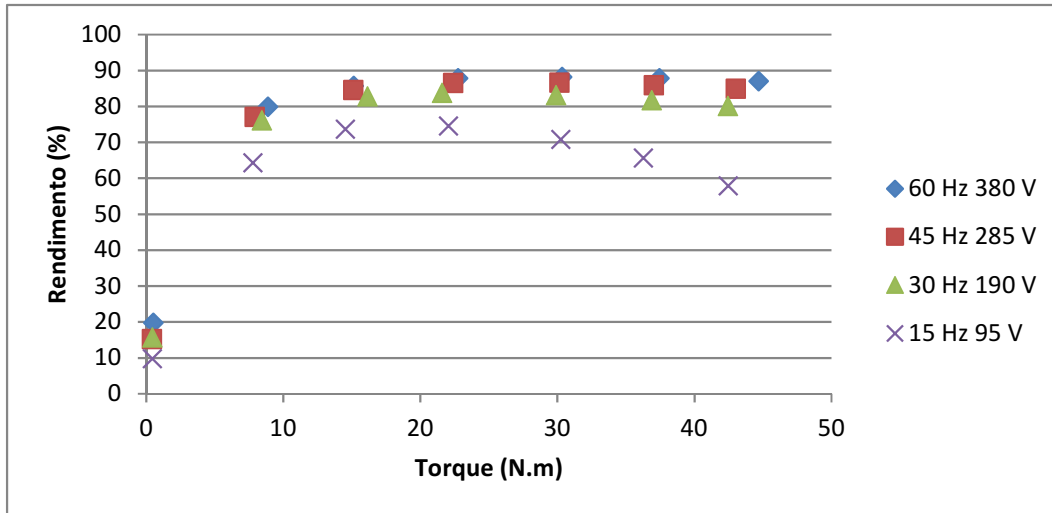
6. Perdas no inversor - Controle vetorial

Configuração experimental

Perdas totais interpoladas - Perdas no motor interpoladas

Resultados

Perdas no inversor

Rotação		1800 rpm	1350 rpm	900 rpm	450 rpm
	0	61.8	97.0	117.7	125.0
	5	81.1	108.0	125.7	157.4
	10	97.2	118.7	134.3	184.0
	15	110.3	129.2	143.5	204.9
Torque	20	120.4	139.3	153.4	220.1
(N.m)	25	127.3	149.2	163.8	229.6
	30	131.2	158.7	174.9	233.3
	35	132.0	168.0	186.5	231.3
	40	129.7	177.0	198.8	223.6
	45	124.3	185.7	211.7	210.2

Perdas totais

Rotação		1800 rpm	1350 rpm	900 rpm	450 rpm
	0	453.8	380.4	314.2	242.0
	5	483.3	421.7	353.2	303.2
	10	535.5	479.3	408.1	373.2
	15	610.5	553.2	479.1	452.0
Torque	20	708.3	643.5	566.0	539.6
(N.m)	25	828.7	750.2	669.0	636.1
	30	971.9	873.1	787.9	741.4
	35	1137.8	1012.4	922.8	855.6
	40	1326.4	1168.1	1073.7	978.5
	45	1537.8	1340.1	1240.6	1110.3

Perdas no motor

Rotação		1800 rpm	1350 rpm	900 rpm	450 rpm
	0	392.0	283.4	196.5	117.0
	5	402.2	313.7	227.5	145.8
	10	438.3	360.6	273.8	189.2
	15	500.2	424.1	335.6	247.1
Torque	20	587.9	504.2	412.7	319.5
(N.m)	25	701.4	601.0	505.2	406.6
	30	840.7	714.4	613.0	508.1
	35	1005.8	844.4	736.3	624.3
	40	1196.7	991.1	874.9	754.9
	45	1413.5	1154.4	1028.9	900.2

6. Perdas no inversor - Vetor.

Relatório de ensaio
Motor Nova 7,5 cv + Inversor Siemens
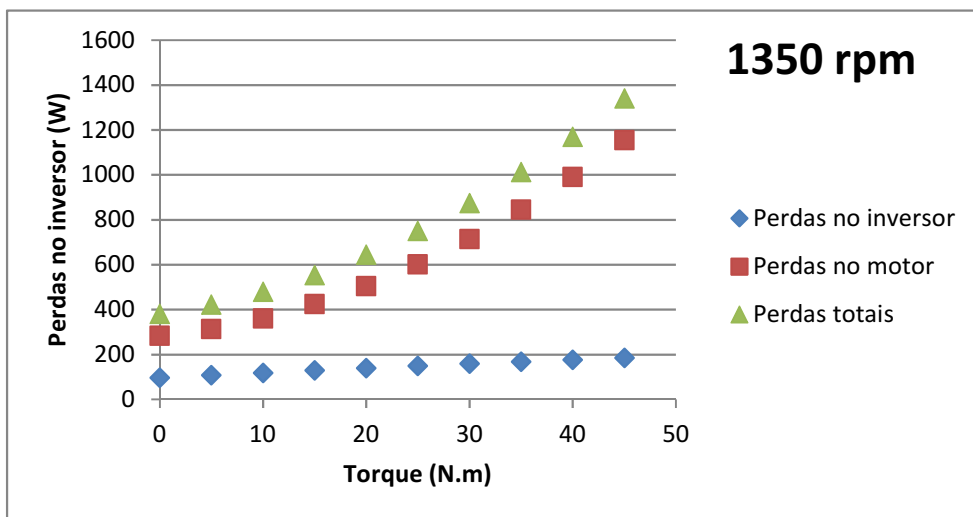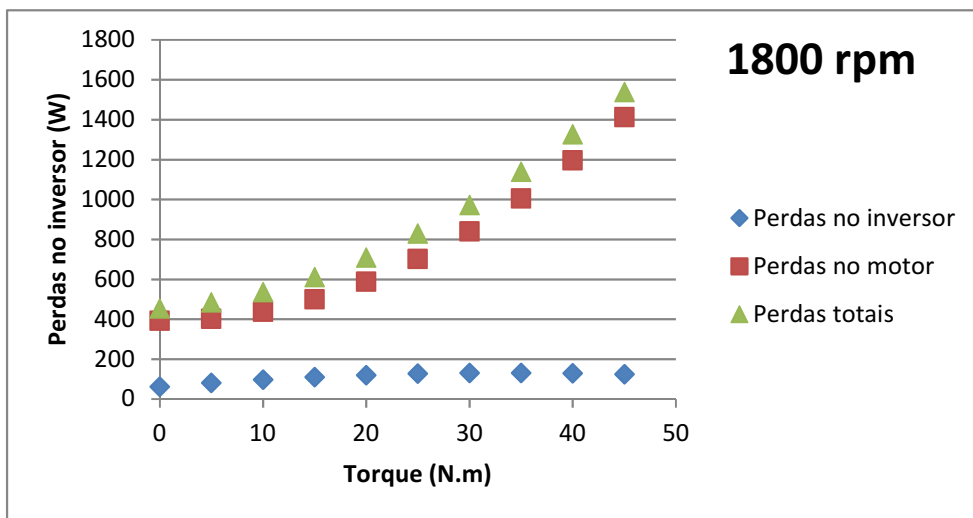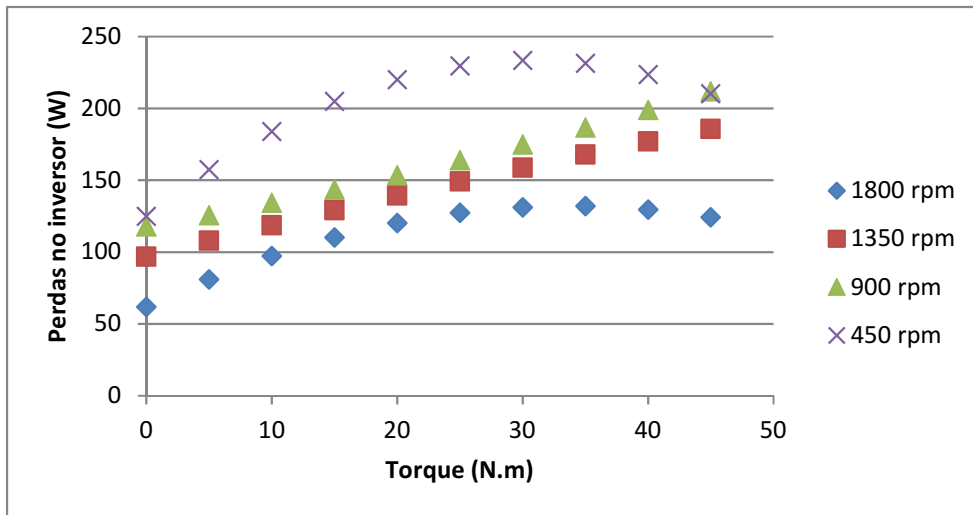
6. Perdas no inversor - Vetor.
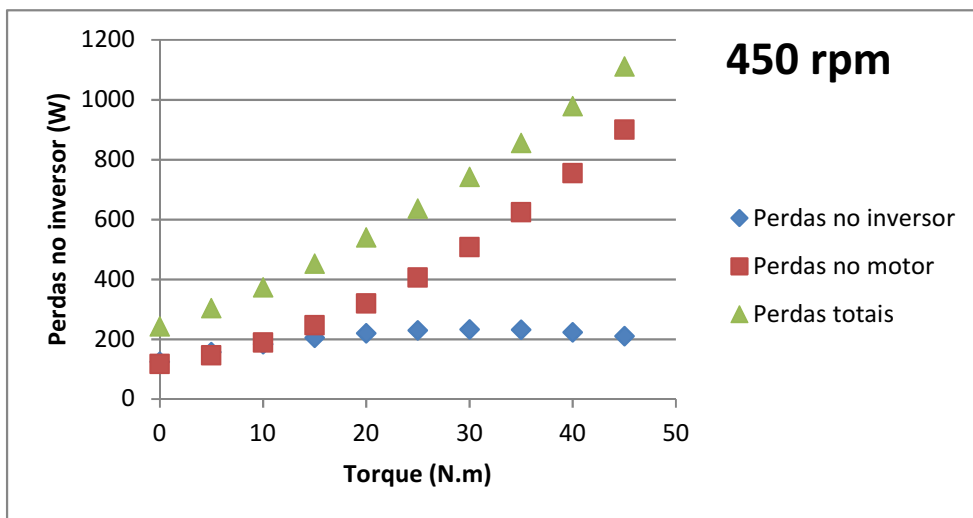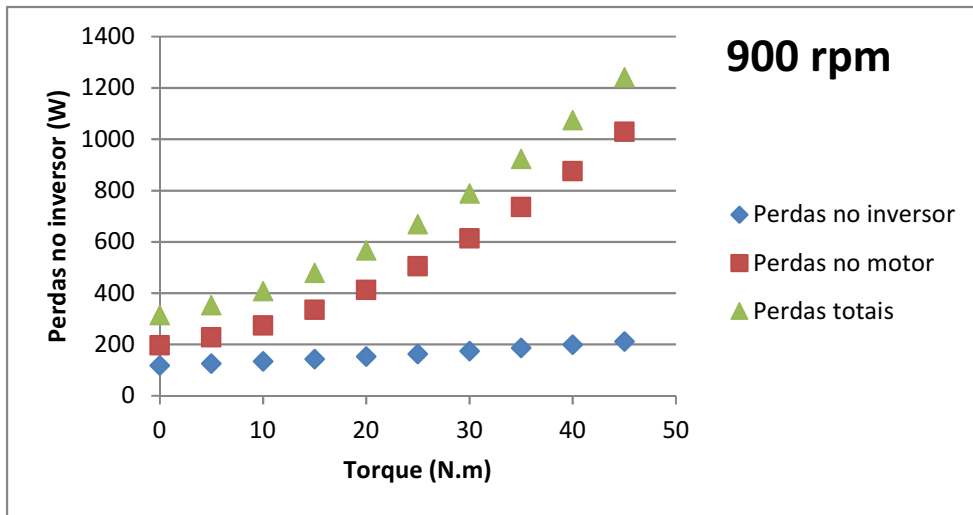
7. Perdas no inversor - Controle V/f

Configuração experimental

Perdas totais interpoladas - Perdas no motor interpoladas

Resultados

		Perdas no inversor			
Frequência		60 Hz	45 Hz	30 Hz	15 Hz *
	0	74.9	104.3	113.1	109.8
	5	86.1	110.8	120.9	143.0
	10	96.6	117.1	127.5	164.4
	15	106.3	123.2	133.2	174.1
Torque	20	115.2	129.1	137.8	172.2
(N.m)	25	123.4	134.7	141.3	158.5
	30	130.9	140.1	143.8	133.1
	35	137.6	145.2	145.2	96.1
	40	143.5	150.1	145.6	47.3

		Perdas totais			
Frequência		60 Hz	45 Hz	30 Hz	15 Hz
	0	480.8	423.6	364.2	323.3
	5	497.2	433.8	365.1	292.3
	10	536.7	468.0	392.7	303.0
	15	599.2	526.3	447.1	355.5
Torque	20	684.9	608.7	528.3	449.7
(N.m)	25	793.7	715.1	636.2	585.6
	30	925.6	845.7	770.8	763.3
	35	1080.7	1000.3	932.3	982.7
	40	1258.8	1179.0	1120.4	1243.9

		Perdas no motor			
Frequência		60 Hz	45 Hz	30 Hz	15 Hz
	0	405.9	319.4	251.1	213.4
	5	411.1	323.0	244.3	149.3
	10	440.1	350.9	265.2	138.6
	15	493.0	403.1	313.9	181.4
Torque	20	569.7	479.6	390.5	277.5
(N.m)	25	670.3	580.5	494.9	427.1
	30	794.8	705.6	627.1	630.2
	35	943.1	855.1	787.0	886.6
	40	1115.3	1028.9	974.8	1196.5

* Em 15 Hz, devido ao escorregamento excessivo, a regressão de perdas do motor pode não ser precisa o suficiente para permitir o cálculo das perdas no inversor

30 Hz

- ◆ Perdas no inversor
- ■ Perdas no motor
- ▲ Perdas totais

15 Hz *

- ◆ Perdas no inversor
- ■ Perdas no motor
- ▲ Perdas totais

7. Perdas no inversor - Vf
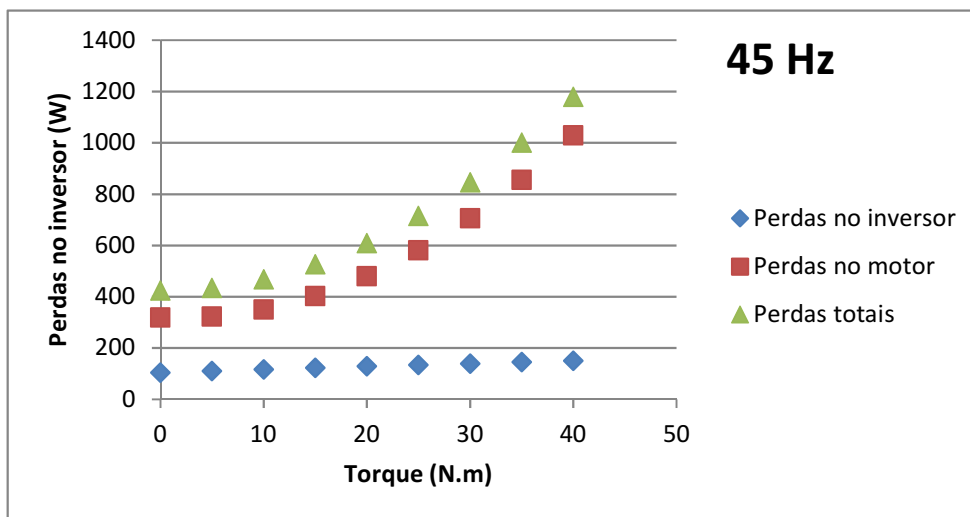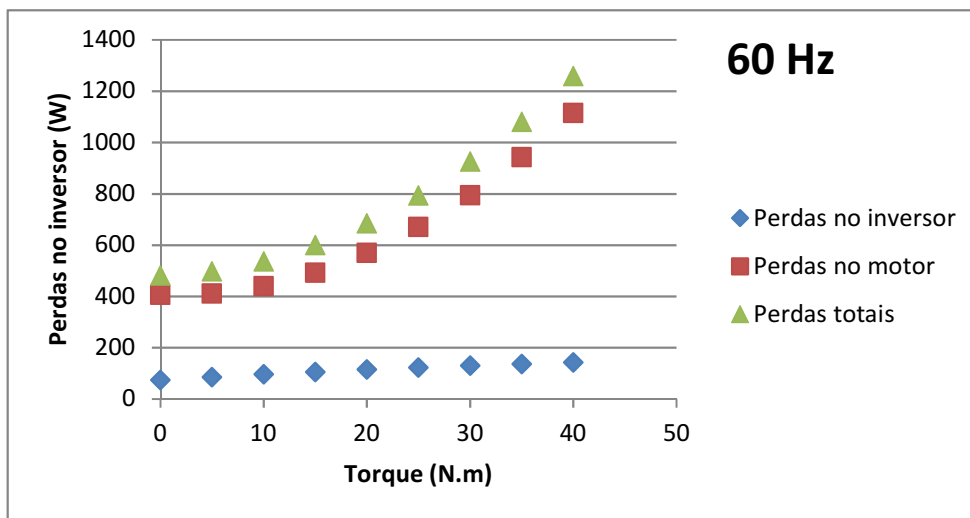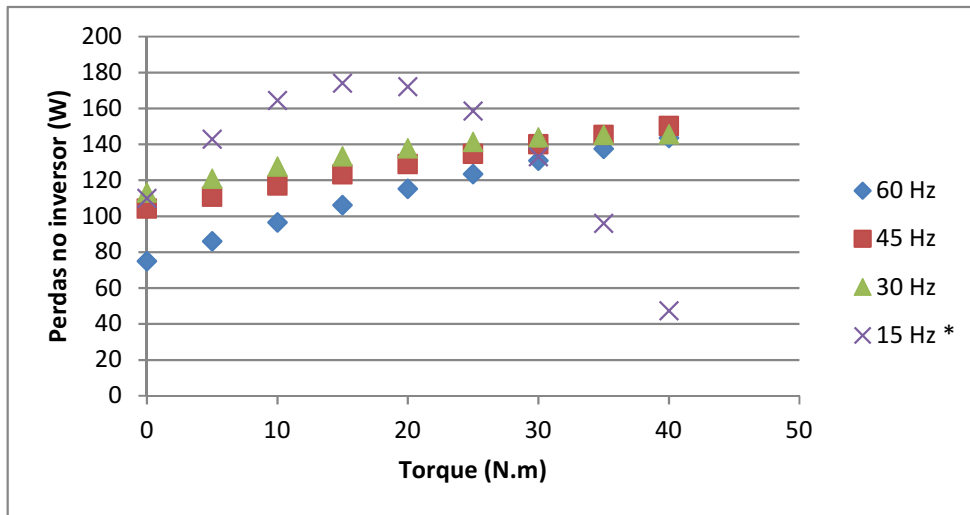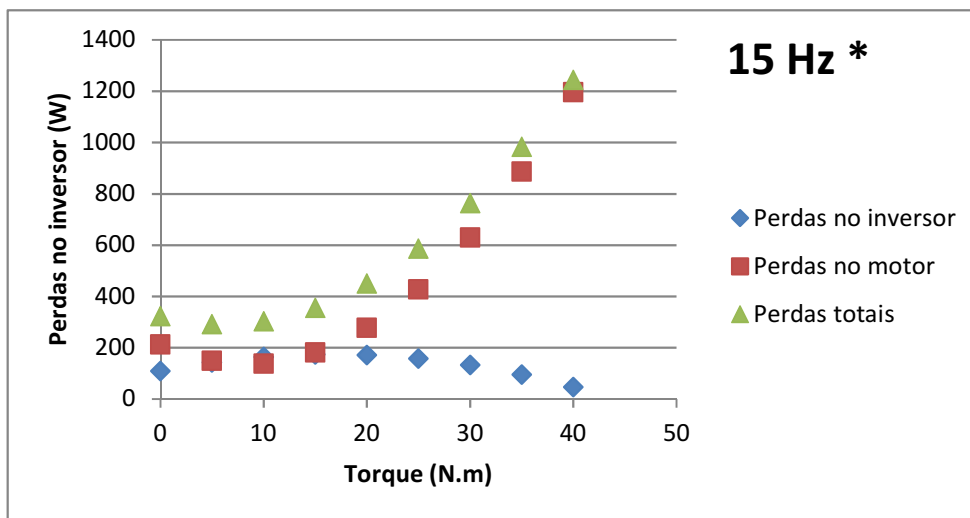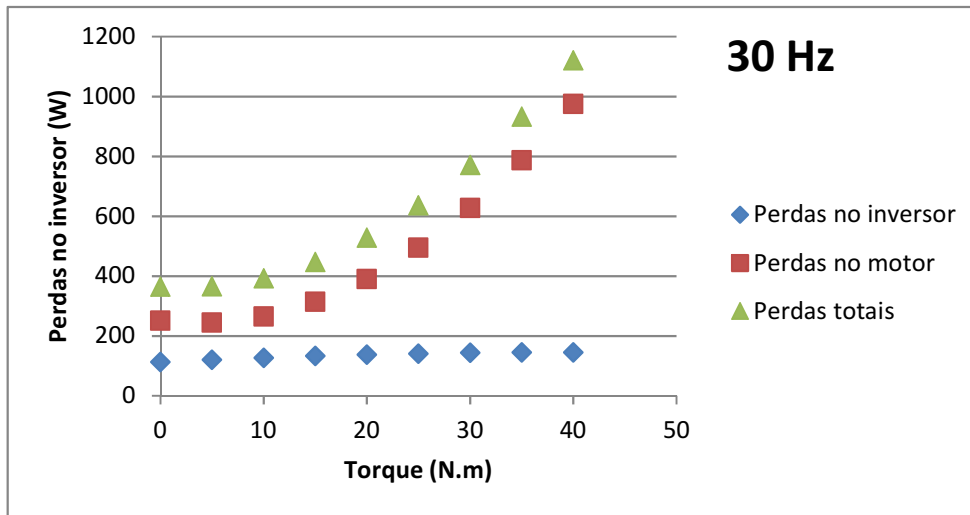
8. Parâmetros do circuito equivalente

Metodologia

Norma IEEE 112, método F com ensaio de impedância em escorregamento nominal

Parâmetros em 60 Hz

R1	X1	R2	X2	Rc*	Xm		X1/w	X2/w	Xm/w
0.5538	0.8572	0.5842	1.261	676.9	26.58		2.274E-03	3.345E-03	7.051E-02
Ω	Ω	Ω	Ω	Ω	Ω		H	H	H

Parâmetros em 45 Hz

R1	X1	R2	X2	Rc*	Xm		X1/w	X2/w	Xm/w
0.5538	0.6323	0.5767	0.9299	531.4	20.01		2.236E-03	3.289E-03	7.077E-02
Ω	Ω	Ω	Ω	Ω	Ω		H	H	H

Parâmetros em 30 Hz

R1	X1	R2	X2	Rc*	Xm		X1/w	X2/w	Xm/w
0.5538	0.3853	0.5753	0.5666	371.5	13.75		2.044E-03	3.006E-03	7.295E-02
Ω	Ω	Ω	Ω	Ω	Ω		H	H	H

Parâmetros em 15 Hz

R1	X1	R2	X2	Rc*	Xm		X1/w	X2/w	Xm/w
0.5538	0.1895	0.5895	0.2787	192.9	7.055		2.011E-03	2.957E-03	7.486E-02
Ω	Ω	Ω	Ω	Ω	Ω		H	H	H

*Rc corresponde às perdas no ferro e não é incluído no modelo do Krause.

Pode ser ignorado para fins de controle